The Objective Motion Cueing Test (OMCT) refers to a way to measure motion characteristics of a simulation objectively, by constructing so-called frequency response functions of the cueing system. Research in recent years has applied the OMCT to a number of fixed-wing research simulators. However, the effect of aircraft dynamics on predicted motion fidelity of the OMCT is poorly understood. The goal of this research therefore is to increase the understanding of the OMCT, by applying it to helicopter simulations.
From literature, it was found that abstractions on the input signals of the OMCT may affect the representativity of predicted motion characteristics. As a first step in this thesis, the effect of these assumptions on the predicted motion characteristics of the OMCT was studied. It was seen that the current OMCT has a set of input signals which may be representative for heave motion, but might not be representative for pitch and surge motion characteristics.
Therefore it was investigated whether a potentially superior OMCT, better representing helicopter motion, can be defined. An OMCT was tailored to longitudinal helicopter motion. Notable differences in pitch and surge motion characteristics were found.
However, for pilot-in-the-loop training, the aircraft motion does not only depend on the dynamics of the aircraft model, but also on pilot input. Therefore, using pilot-in-the-loop simulation data, the effect of manual pilot control behaviour on the proposed methodology was studied. It was seen that, although differences were identified, the main trend of the frequency response functions was determined by the dynamics of the helicopter model, not the pilot input.
Further research is recommended to evaluate the current set of input signals of the OMCT for a variety of models, also incorporating lateral motion, and tasks using a similar method presented in this thesis.

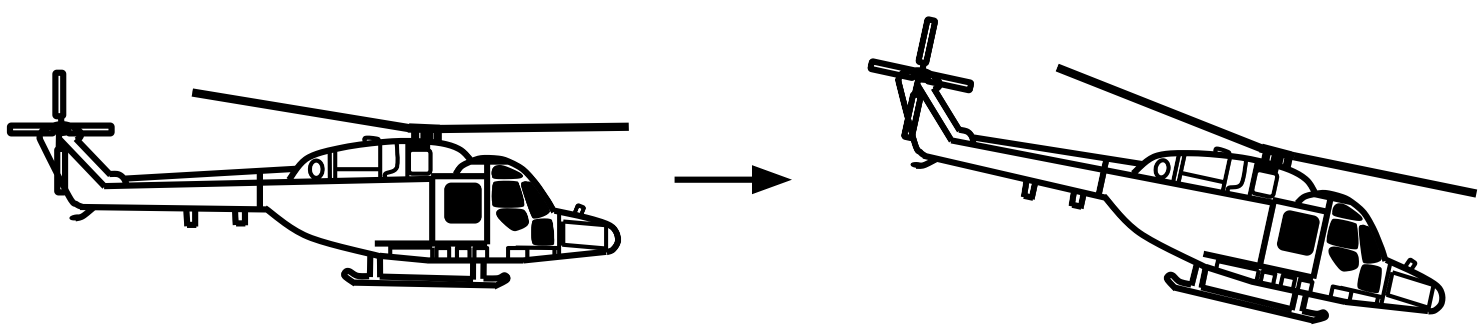

MSc. Thesis W.H. Dalmeijer - Motion Fidelity Assessment for Helicopter Simulations

TUDelft

Faculty of Aerospace Engineering

Delft University of Technology

Motion Fidelity Assessment for Helicopter Simulations

Extending the Objective Motion Cueing Test to Measure Rotorcraft Simulator Motion Characteristics

W.H. Dalmeijer

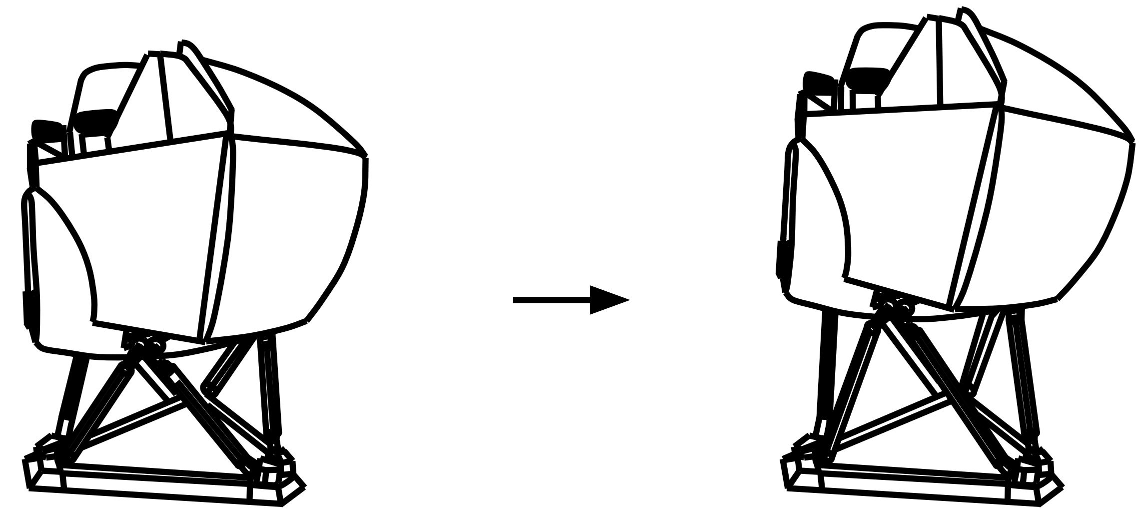

TUDelft

Faculty of Aerospace Engineering

Delft University of Technology

Motion Fidelity Assessment for Helicopter Simulations

Extending the Objective Motion Cueing Test to Measure Rotorcraft Simulator Motion Characteristics

Master of Science Thesis

For obtaining the degree of Master of Science in Aerospace Engineering
at Delft University of Technology

W.H. Dalmeijer

December 8, 2016

Faculty of Aerospace Engineering · Delft University of Technology

TU Delft

Delft University of Technology

Delft University Of Technology
Department Of
Control and Simulation

The undersigned hereby certify that they have read and recommend to the Faculty of Aerospace Engineering for acceptance a thesis entitled **"Motion Fidelity Assessment for Helicopter Simulations"** by **W.H. Dalmeijer** in partial fulfillment of the requirements for the degree of **Master of Science**.

Dated: December 8, 2016

Readers:

prof.dr.ir. M. Mulder

dr. ir. M. Pavel

dr. ir. M. Voskuijl

ir. O. Stroosma

ir. I. Miletović

Abstract

The Objective Motion Cueing Test (OMCT) refers to a way to measure motion characteristics of a simulation objectively, by constructing so-called frequency response functions of the cueing system. Research in recent years has applied the OMCT to a number of fixed-wing research simulators. However, the effect of aircraft dynamics on predicted motion fidelity of the OMCT is poorly understood. The goal of this research therefore is to increase the understanding of the OMCT, by applying it to helicopter simulations.

From literature, it was found that abstractions on the input signals of the OMCT may affect the representativity of predicted motion characteristics. As a first step in this thesis, the effect of these assumptions on the predicted motion characteristics of the OMCT was studied. It was seen that the current OMCT has a set of input signals which may be representative for heave motion, but might not be representative for pitch and surge motion characteristics.

Therefore it was investigated whether a potentially superior OMCT, better representing helicopter motion, can be defined. An OMCT was tailored to longitudinal helicopter motion. Notable differences in pitch and surge motion characteristics were found.

However, for pilot-in-the-loop training, the aircraft motion does not only depend on the dynamics of the aircraft model, but also on pilot input. Therefore, using pilot-in-the-loop simulation data, the effect of manual pilot control behaviour on the proposed methodology was studied. It was seen that, although differences were identified, the main trend of the frequency response functions was determined by the dynamics of the helicopter model, not the pilot input.

Further research is recommended to evaluate the current set of input signals of the OMCT for a variety of models, also incorporating lateral motion, and tasks using a similar method presented in this thesis.

Contents

List of Figures

List of Tables

Nomenclature

List of Abbreviations

AC	Advisory Circular
AFCS	Automatic Flight Control System
BEM	Blade Element Method
CS	Certification Specification
DOF	Degree of Freedom
DRA	Defense Research Agency
EASA	European Aviation Safety Agency
FBP	Free Body Diagram
FFS	Full Flight Simulator
FFT	Fast Fourier Transform
FNPT	Flight Navigation Procedures Trainer
FSTD	Flight Simulator Training Device
GLA	Glauert
HP	High Pass
HPS	Helicopter Pilot Station
HQR	Handling Quality Rating scale
ICAO	International Civil Aviation Organization
IFR	Instrument Flight Rules
IMU	Inertial Measurement Unit
JAXA	Japan Aerospace Exploration Agency
LGP	Lower Gimbal Point
LGS	Lower Gimbal Spacing
LP	Low Pass filter
MCS	Motion Cueing System
MDA	Motion Drive Algorithm
MFR	Motion Fidelity Rating scale
MTE	Mission Task Element
NLR	National Aerospace Center
OMCT	Objective Motion Cueing Test
OTO	Otolith
RAE	Royal Aircraft Establishment

RPM	Rotations per Minute
SCC	Semi-Circular Canals
SFR	Simulation Fidelity Rating scale
SRS	Simona Research Simulator
TF	Transfer Function
ToT	Transfer of Training
TsAGI	Central Aerohydrodynamic Institute
UGP	Upper Gimbal Point
UGS	Upper Gimbal Spacing

List of Symbols

Greek		
α_c	[rad]	Angle of Attack of the Control Plane
α_d	[rad]	Disk Incidence Angle
β	[rad]	Flapping angle
γ	[-]	Lock Number
δ_3	[rad]	Pitch-flap coupling angle
ϵ	[rad]	Angle of attack
θ_c **or** θ_{1c}	[rad]	Longitudinal cyclic input
θ_c	[rad]	Simulator pitch angle
θ_f	[rad]	Pitch angle of the helicopter body
θ_0	[rad]	Collective input
λ_c	[-]	Non-dimensional inflow velocity cause by the flight velocity
λ_i	[-]	Non-dimensional inflow velocity of the main rotor
μ	[-]	Non-dimensional aircraft velocity
ρ	$[kg/m^3]$	Air density.
σ	[-]	Rotor solidity
σ_{ug}	[-]	Turbulence intensity in x-direction
σ_{wg}	[-]	Turbulence intensity in z-direction
ϕ_f	[rad]	Roll angle of the helicopter body
ψ_f	[rad]	Yaw angle of the helicopter body
Ω	[rad/s]	Rotational velocity of the main rotor
Roman		
a_0	[rad]	Coning Angle, solution to the flapping equation
a_1	[rad]	Longitudinal tilt of the rotor with respect to the control plane
b_1	[rad]	Longitudinal tilt of the rotor with respect to the control plane
C_T	[-]	Thrust coefficient
C_D	[-]	Drag coefficient
c	[m]	Chord
D	[N]	Drag
EI	$[Nm^2]$	Blade Stiffness
f_{sp}	$[m/s^2]$	Specific Force
g	$[m/s^2]$	Gravitational acceleration
H	[N]	Force on the rotor disk as a result of profile drag forces and

induced velocities		
h_r	[m]	Distance from the c.g. to the main rotor hub
$I_x x$	$[kgm^4]$	Moment of Inertia around X_B axis
$I_y y$	$[kgm^4]$	Moment of Inertia around Y_B axis
$I_z z$	$[kgm^4]$	Moment of Inertia around Z_B axis
K_β	$[Nm^2]$	Spring Stiffness
L	[N]	Lift
L_g	[-]	Turbulence scale length
M_a **or** m	[kg]	Helicopter mass
p	[rad/s]	Roll rate
$\dot{p}$	$[rad/s^2]$	Roll acceleration
q	[rad/s]	Pitch rate
$\dot{q}$	$[rad/s^2]$	Pitch acceleration
R	[rad/s]	Rotor Radius
r	[rad/s]	Yaw acceleration
$\dot{r}$	$[rad/s^2]$	Yaw acceleration
S	$[m^2]$	Surface of the main rotor disk
T	[N]	Thrust
$\lvert T_i \rvert$	[-]	Magnitude of a transfer function for test i of an OMCT
$\angle T_i$	[-]	Phase of a transfer function for test i of an OMCT
u	[m/s]	Velocity on the X_B axis
$\dot{u}$	$[m/s^2]$	Acceleration on the X_B axis
$\bar{u}$	[-]	Input vector
V	[m/s]	Velocity vector
V_{dryden}	[m/s]	Turbulence velocity
v	[m/s]	Velocity on the Y_B axis
W	[N]	Weight
w	[m/s]	Velocity on the Z_B axis
X	[N]	Sum of forces in X_B direction
$\bar{x}$	[-]	State Vector
$\dot{\bar{x}}$	[-]	Differentiated State Vector
Y	[N]	Sum of forces in Y_B direction
$\bar{y}$	[-]	Output Vector
Z	[N]	Sum of forces in Z_B direction
Indices		
BEM	[-]	Blade Element Method
GLA	[-]	Method of Glauert
AP	[-]	Aircraft Position
SP	[-]	Simulator Position

Chapter 1

Introduction

Research Context

For the training of flight crews, the general aviation sector has come to rely heavily on flight simulator training devices and even full flight simulators, [1]. This is because the advantages of simulators are apparent. Firstly they offer a safe environment for the student develop his skills before he takes control of the real aircraft. Secondly, they are a cheaper alternative to performing all flight training in the air. And thirdly, situations and flight conditions can be practiced that would be too dangerous for an aircraft to perform in real life.

Besides education, simulators are used widely for their research purposes. In this field the simulator can be used to develop and asses new flight control systems. When testing a new flight control system for example, it is convenient that the designers can first test such a system on the ground. The simulator is than used as a pilot-in-the-loop testing station. Also for off-line testing, the simulator can be used. Secondly simulators provide a more controlled (and cheaper) environment to perform research in human factors, [1].

From the above it may be concluded that the industry is aided with simulators that simulate pilot sensory input as close as possible to the real aircraft. The hypothesis here is that pilot sensory input more closely resembling the real aircraft will result in better training of aspirant pilots. With the development of computer technology and the easy access to cheap computing power, especially the visual part of the simulator has improved tremendously, [2].

Also the motion cueing system has improved over the last few decades. In the 1970's, the 6 degrees of freedom hexapod motion system, like the one used for the SIMONA Research Simolator (SRS), was introduced. With this system, due to the concept of washout filters, it is possible to convey aircraft motion to the human vestibular system in a convincing way. However with the introduction of this new technology came the need to certify and control the standards of the simulator industry and in 1983, the FAA published the first version of an objective standard for flight simulator testing [3].

Nowadays simulator certification is conducted based on a series of objective tests, consisting of dimensional requirements for the motion cueing system and time-domain response characteristics. However, the integrated performance of motion cueing systems is evaluated using subjective pilot assessment, according to ICAO guidelines, [4]. For simulator certification, This means that before a simulator can be used for training, an experienced test pilot evaluates its performance. Based on his feedback, engineers modify the settings of the Motion Cueing Algorithm (MCA). A disadvantage of subjective assessment however, is that the results are often hard to repeat, that is, different pilots may assess the same motion cueing system differently, [5].

Recently, a new method for objective evaluation of integrated motion performance of simulators has been developed by Advani and Hosman, [5]. Whereas standard objective evaluation methods rely on requirements in the time domain, the OMCT looks at the frequency domain of the motion spectrum.

Relevant Literature

Similarly to Sinacori in [6], the OMCT studies the gain and phase shift of the MCA. However, whereas Sinacori only studies the frequency response at 1 $[rad/s]$, the OMCT evaluates cueing performance by constructing so-called frequency response functions of the motion system, by exciting the motion system with a sinusoidal input signal at 12 predefined frequencies. Each of the six axes is excited separately, resulting in 6 direct frequency response functions. Furthermore, to study inter-axes coupling, four extra tests are included to study pitch-surge and roll-sway coupling. The OMCT was added as an amendment to ICAO document 9625 in [4] in 2009.

An effort has been made to combine the OMCT with a criterium for motion fidelity. A criterium for motion fidelity was proposed by Advani and Hosman in 2007, given in [7], but was not adopted. In 2013, a practice of industries best standards was given by Hosman in [8]. At this point, the OMCT is therefore a useful tool to investigate the motion characteristics and have meaningful discussion about the relative motion fidelity between different cueing settings. Unfortunately the OMCT is not (yet) a stand-alone method to evaluate the absolute motion fidelity of the cueing system.

Practical implementation of the OMCT was described in [8] in 2013. On the limitations of the OMCT, Stroosma concludes that due to uncoupled input axes and assumed linearity of the input spectrum the OMCT may give an incomplete picture of motion characteristics:
"Input signals may have abstracted away some characteristics of the aircraft motions that play an important role in operational use. An example is the fact that for large [fixed-wing] aircraft a yaw motion is usually also accompanied by a sway specific force due to the distance of the pilot station to the center of gravity." [9]

Furthermore, Seehof concluded in 2014 the following on general applicability of the OMCT for all aircraft and training purposes in [10]:

- The OMCT uses a simplified set of input signals. For example, during take-off, in surge direction, the accelerations of the aircraft might be larger than 1 $[m/s^2]$, which is the amplitude prescribed by the OMCT. Results of the OMCT therefore may not be representative for this particular maneuver.
- The training purpose of the simulation may vary to a large extend. Up to now, no helicopter simulation has been investigated with respect to the OMCT.

From previous research into the practical implementation of the OMCT, it can be concluded that there exist doubts about the representativity of the input signals of the OMCT. To date, no studies have been conducted into the representativity of the OMCT for different aircraft dynamics. Therefore the effect of aircraft dynamics on predicted objective motion fidelity is poorly understood. This report aims to improve the understanding of the OMCT by studying the effect of aircraft dynamics on predicted objective motion fidelity.

Investigating the Representativity of the OMCT in the Helicopter Domain

One way to evaluate the effect of aircraft dynamics on predicted motion characteristics is by applying the OMCT to a fundamentally different aircraft model. Since the input signals of the OMCT were developed with fixed-wing aircraft in mind, [5], it hypothesized that an application into the rotorcraft domain might yield different predicted motion characteristics. The following question was therefore posed.

> To what extend is the set of input signals of the OMCT representative for helicopter motion and how do deviations from this set affect the predicted motion characteristics of the simulator in the longitudinal plane?

This question consists of two parts. Firstly, the current set of input signals needs to be compared to helicopter motion. Secondly it important to see which deviations from this set of input signals might affect the motion cueing algorithm and therefore the predicted motion fidelity of the simulation.

Furthermore it can be seen that this research is narrowed down to the longitudinal plane. Due to time constraints an analysis with 6 degrees-of-freedom is considered outside the scope of this project.

To answer this question, the following research objectives were set for this project.

1. Identify the state-of-the-art in motion fidelity assessment techniques for simulators, by performing a literature study.
2. Study the motion characteristics of helicopters by finding or simulating representative motion and converting relevant time-traces to the frequency domain.
3. Study the motion characteristics of a classical washout algorithm on a 6DOF hexapod motion cueing system, by performing a OMCT sensitivity analysis to changes in the input signals set.

The result from these objectives will be a qualitative analysis of the representativity of the OMCT in the helicopter domain. It is possible that the OMCT is found to be representative, either because the current set of input signals resembles helicopter motion well, or due to the the fact that identified misrepresentation from this set do not affect the MCA. In that case, this research will serve to support the OMCT in its current form.

A Better OMCT?

However, since previous research has already identified potential misrepresentations by the OMCT for fixed-wing aircraft motion, it is hypothesized that potential misrepresentations in the helicopter domain can be identified. If it is found that the OMCT might not be representative for particular motion characteristics, a logical next step would be to attempt to design a better OMCT. By doing so an answer is sought to the following research question.

Is it possible to define a potential superior set of OMCT input signal, that better represents helicopter motion in the longitudinal plane?

To this end, the following research objective was identified.

4. Design a tailored OMCT, better representing helicopter motion, using knowledge from the first three research objectives.

If it is found to be possible to construct a test with a different set of input signals than the current OMCT, it is interesting to see the predicted motion characteristics from such a test. If predicted motion characteristics differ from the original OMCT, this result will serve as a support for the findings from the first research question.

Helicopter motion is not only influenced by the dynamics of the aircraft, but also by atmospheric disturbances and pilot control input. It is therefore hypothesized that the answers to the research questions described here are influenced by pilot control strategy.

Investigating the Influence of Pilot Control Strategy

A logical next would therefore be to investigate the influence of pilot input to the preceding analysis. Therefore there can be distinguished a third part to this research project. The research question to be answered here is the following.

What is the influence of pilot control behavior on the frequency response functions computed by means of a tailored OMCT?

Whereas atmospheric turbulence is standardized and easily implemented in off-line simulations, models for pilot control strategy are often complex and difficult to implement. Pilot control strategy was therefore taken into account by performing a pilot-in-the-loop experiment on the SIMONA Research Simulator (SRS). This resulted in a final objective for this research project.

5. Study the effect of pilot control behaviour on the predicted motion characteristics of a tailored OMCT, by performing a pilot-in-the-loop experiment on the SRS.

A secondary purpose of the pilot-in-the-loop experiment is to validate identified differences in predicted motion fidelity between a tailored OMCT and the original OMCT by means of subjective assessment of different motion conditions. In this report, this final research objective will therefore be referred to as *validation experiment*.

Thesis Roadmap

Figure 1-1 links proposed research objectives for this research project in a roadmap. Figure 1-1 indicates objectives described by the preliminary analysis with a blue dotted line. A validation experiment in the SRS is indicated by a red dotted line.

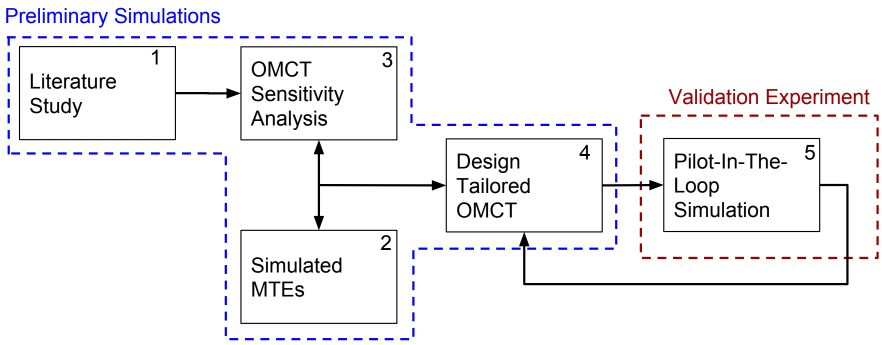

Figure 1-1: Roadmap linking different objectives for this research project.

Results from the pilot-in-the-loop simulation will be used for redesign of the tailored OMCT, hence the feedback structure depicted in Figure 1-1.

Report Structure

This final report consists of four parts. The first part is an article written for intended publication on the 73rd annual forum of the American Helicopter Society in may 2017, Part I. This article entails the results of all research objectives presented in this introduction, and can be read as a stand-alone document. For readers with little time, it is recommended to focus on the first part of this thesis.

In the second part the results of preliminary simulations are presented, that is, all results from research objectives that could be achieved off-line, without the need for pilot-in-the-loop simulation. After several addenda and errata were found in the original published preliminary report, [11], it was decided to create a revised version of several chapters for this document, Part II. Table 1-1 links the revised chapters from [11] to the research objectives as were identified in this introduction.

Table 1-1: Report Structure, allocating research objectives to appropriate chapters.

Research Objective	Chapter
1. Literature Study	chapter 2
2. Simulate Helicopter Motion	chapter 3
3. OMCT Sensitivity Analysis	chapter 4
4. Design Tailored OMCT	chapter 5
5. Pilot-in-the-loop Simulation	-

It can be seen that, for a description of the validation experiment, the reader is not referred to the Part II, but to the paper, Part I.

Subsequently, in Part III, revised appendices to the preliminary simulations are given. These appendices are presented in the order to which they are referred to in chapters 2 to 5 and contain background information and specific results for the off-line analysis. In Table 1-2 the contents of these appendices is explained.

Table 1-2: Structure of the revised appendices to the preliminary report.

Appendix	**Contents**
Appendix A	**Derivation of a Flapping Equation** - In this appendix, background information will be given about helicopter dynamics. A form of the flapping equation will be derived without the influence of forward flight velocity. Readers with limited knowledge about helicopter dynamics and its symbol conventions are recommended to read this appendix.
Appendix B	**The DRA (RAE) Research Lynx, ZD559** - A schematic side, top and front view, and numerical values used in the mathematical helicopter model will be given here, [12].
Appendix C	**MTE Description and Performance Standards** - A description and performance standards for the take-off and abort and hover MTEs from ADS-33, [13], will be given here.
Appendix D	**OMCT Verification** - The results from an off-line Objective Motion Cueing Test will be presented together with results from an on-line implementation on the SRS by Stroosma, [9]. Furthermore, the shapes of the frequencies response functions will be explained with reference to the classical washout algorithm. Readers that are new to the OMCT are encouraged to read this appendix.
Appendix E	**OMCT Sensitivity to MCA Settings** - Sensitivity of the frequency response functions of the OMCT was investigated in the longitudinal plane by means of a parametric study. Results are presented here.
Appendix F	**SRS Geometry** - This appendix presents the lay-out of the SRS, together with some key parameters, taken from [14].
Appendix G	**OMCT Sensitivity to MCA Settings: Tuning** - Frequency-domain information from the Mission Task Elements is combined with the results from Appendix E.
Appendix H	**OMCT Sensitivity to Input signals** - In this appendix, a sensitivity analysis of the OMCT with respect to the amplitude of the input signals is presented. The OMCT structure, including cross-tests is maintained.
Appendix I	**Tailored OMCT Sensitivity to MDA Settings** - Results from a sensitivity analysis conducted in a similar fashion as in Appendix E are given here. Two sets of input signals are considered: firstly a set based on a take-off and abort MTE and secondly a set based on the hover MTE.

Finally, appendices to the paper are presented in Part IV. Here the results from the validation experiment on the SRS are given in 6 chapters. Table 1-3 gives the contents of these appendices.

Table 1-3: Structure of the appendices to the validation experiment.

Appendix	**Contents**
Appendix J	**Time-Domain Data** - Firstly, the performance in terms of the longitudinal and vertical position of six runs from the validation experiment is presented here. Three runs correspond to the take-off and abort MTE and three runs correspond to the hover MTE. For each MTE, an example of a run with good performance, average and bad performance is given. Secondly, corresponding time-traces of the specific forces and pitch rotational accelerations are given.
Appendix K	**Frequency-Domain Data** - The amplitude and phase spectra of the six example runs from Appendix J is given in this appendix. Also the least-squares fit for the pitch, surge and heave motion characteristics is given.
Appendix L	**Tailored OMCT Input signals** - This appendix gives the tailored input signals for a tailored OMCT based on each run of the validation experiment, together with a mean and standard deviation of the phase and amplitude.
Appendix M	**Tailored OMCTs** - In this appendix gives the frequency response functions based on all runs of the validation experiment, including a mean and standard deviation of the phase and gain.
Appendix N	**Analysis of Pilot Control Input** - Pilot input was studied in the frequencies domain. In this appendix frequency-domain characteristics of the collective and cyclic pitch are presented.
Appendix O	**Pilot feedback** - Finally, in this appendix the pilot feedback in terms of a simulation fidelity metric and verbal comments is given for all three pilots.

W.H. Dalmeijer
Delft, December 2016

Part I

Paper for the 73rd Annual Forum of the American Helicopter Society

Extending the Objective Motion Cueing Test to Measure Rotorcraft Simulator Motion Characteristics

Wouter Dalmeijer
MSc Student
Delft University of Technology
Delft, Netherlands

Ivan Miletović
PhD Student
Delft University of Technology
Delft, Netherlands

Olaf Stroosma
Researcher
Delft University of Technology
Delft, Netherlands

Marilena Pavel
Assistant Professor
Delft University of Technology
Delft, Netherlands

ABSTRACT

In search of a more objective way to evaluate motion cueing fidelity, the Objective Motion Cueing Test (OMCT) was proposed by Advani and Hosman in 2006. However, an application of this test for rotorcraft has not yet been studied. The objectives of this paper are therefore (1) to investigate the extent to which the OMCT is representative for rotorcraft, (2) to investigate whether a potentially superior OMCT, better representing helicopter motion, can be defined and (3) to validate potential differences in the prediction of motion characteristics between an OMCT based on the helicopter motion, and the current OMCT, with a pilot-in-the-loop experiment on the SIMONA Research Simulator (SRS). It was found that the current OMCT has a set of input signals which is representative for helicopter heave motion, but might not be representative for pitch and surge motion characteristics. Using an OMCT tailored to longitudinal helicopter motion, notable differences in helicopter pitch and surge motion characteristics were found. Using pilot-in-the-loop simulation data, the effect of pilot control behaviour on the proposed methodology was studied. It was seen that, although differences were identified, the main trend of the frequency response functions was determined by the dynamics of the helicopter model. It is recommended to evaluate the current set of input signals of the OMCT for a variety of models, also incorporating lateral motion, and tasks using a similar method presented in this article.

INTRODUCTION

For simulator certification, the integrated performance of motion cueing systems is evaluated using subjective pilot assessment, according to ICAO guidelines in Ref. 1. This means that before a simulator can be used for training, an experienced test pilot evaluates its performance. Based on his feedback, engineers then modify the settings of the Motion Cueing Algorithm (MCA). A disadvantage of subjective assessment however, is that the results are often hard to repeat, that is, different pilots may assess the same motion cueing system differently, as was stated in Ref. 2.

In search for a method to more objectively evaluate simulator performance the Objective Motion Cueing Test (OMCT) was proposed by Advani and Hosman in Ref. 3 in 2006. Similarly to Sinacori in Ref. 4, the OMCT studies the gain and phase shift of the MCA. However, whereas Sinacori only studies the frequency response at 1 $[rad/s]$, the OMCT evaluates cueing performance by constructing so-called frequency response functions of the motion system, by exciting the motion system with a sinusoidal input signal at 12 predefined frequencies. Each of the six axes is excited separately, resulting in six direct frequency response functions. Furthermore, to study inter-axes coupling, four extra tests are included to study pitch-surge and roll-sway coupling. Table 1 gives a matrix containing the input and output axes for longitudinal tests. The OMCT was added as an amendment to ICAO document 9625 in Ref. 1 in 2009.

Table 1: Longitudinal OMCT test numbers, according to Ref. 3.

Input Axis	Output Axis		
	Pitch	Surge	Heave
Pitch	1	2	-
Surge	7	6	-
Heave	-	-	10

An effort has been made to combine the OMCT with a criterium for motion fidelity. A criterium for motion fidelity was proposed by Advani and Hosman in 2007, given in Ref. 5, but was not adopted. In 2013, a practice of industries best standards was given by Hosman in Ref. 6 and again in 2016 in Ref. 7. At this point, a fidelity criterium does not exist. the OMCT is therefore a useful tool to investigate motion characteristics of different cueing settings, but unfortunately not

To be presented at the AHS 73rd Annual Forum, Forth Worth, Texas, May 9–11, 2017.

(yet) a stand-alone method to evaluate the motion fidelity.

Practical implementation of the OMCT was described in Ref. 8 in 2013. On the limitations of the OMCT, Stroosma concludes that due to uncoupled input axes and assumed linearity of the input spectrum the OMCT may give an incomplete picture of motion characteristics:
"Input signals may have abstracted away some characteristics of the aircraft motions that play an important role in operational use. An example is the fact that for large [fixed-wing] aircraft a yaw motion is usually also accompanied by a sway specific force due to the distance of the pilot station to the center of gravity." Ref. 8

In the time domain, these abstractions become apparent. Figure 1 shows the motion output of a helicopter model during 10 [s] of hover in a longitudinal pilot-in-the-loop simulation, together with the input signal of an OMCT for a pitch frequency response function. For this particular test, the OMCT excites the MCA with $A_i sin\omega_i t$ on the pitch rotational channel. However, since it is assumed that aircraft pitch-surge motion is uncoordinated, also a term $gsin\theta$ is put on the surge channel. In this case, θ is the aircraft pitch angle. Heave motion is not excited.

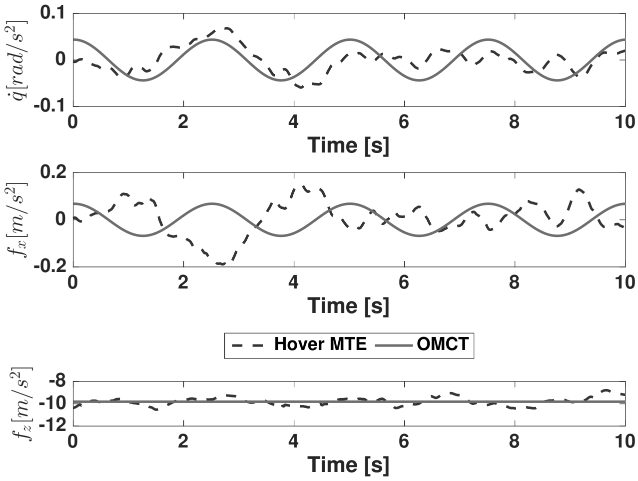

Fig. 1: Typical motion input to the MCA for a helicopter during hover, plotted together with the seventh input signal for the pitch frequency response function, OMCT test 1, ($\omega_7 = 1.585[rad/s]$).

It can firstly be seen that the OMCT excites only pitch and surge axes, whereas during a hover simulation all three longitudinal degrees-of-freedom are excited. Secondly it can be seen that the OMCT input signals are not of the same phase as those of the hover task. Looking at the specific force in surge direction, f_x, from 1 to 5 [s], it can be seen that the OMCT excites this axis at roughly 180 [deg] phase difference with the helicopter motion, whereas at the same time the pitch axis, $\dot{q}$, is excited with a similar phase, 0 [deg].

Furthermore, Seehof concluded in 2014 the following on general applicability of the OMCT for all aircraft and training purposes in Ref. 9:

- The OMCT uses a simplified set of input signals. For example, during take-off, in surge direction, the accelerations of the aircraft might be larger than 1 [m/s^2], which is the amplitude prescribed by the OMCT. Results of the OMCT therefore may not be representative for this particular maneuver.
- The training purpose of the simulation may vary to a large extent. Up to now, no helicopter simulation has been investigated with respect to the OMCT.

For a representative test in the case of figure 1, the addition of all 12 OMCT input signals should result in a signal with similar characteristics as the hover task of figure 1. However it can be seen that the amplitude of for example the surge input is similar to that of the hover task, already for just one frequency. A reconstruction of all 12 frequencies would likely result in a signal with too large amplitude for this task.

From previous research it can be thus be concluded that doubts exist about the extent to which the OMCT is representative in the helicopter domain. Underlying assumptions of the OMCT about the motion of fixed-wing aircraft may not be fully transferable. The first objective of this paper is therefore to investigate the extent to which the OMCT is representative for rotorcraft. A second objective is to investigate whether a potentially superior set of input signals better representing helicopter motion can be defined. A third objective is to validate potential differences in the prediction of motion characteristics between an OMCT based on the helicopter motion and the current OMCT with a pilot-in-the-loop experiment on the SIMONA Research Simulator (SRS).

EFFECT OF OMCT ASSUMPTIONS ON THE FREQUENCY RESPONSE FUNCTIONS

From literature two main assumptions of OMCT input signals on helicopter motion were identified: an uncoupled input and a linearity of the input spectra. However, what is the influence of these assumptions on the evaluation of motion characteristic of a classical washout algorithm in the longitudinal plane?

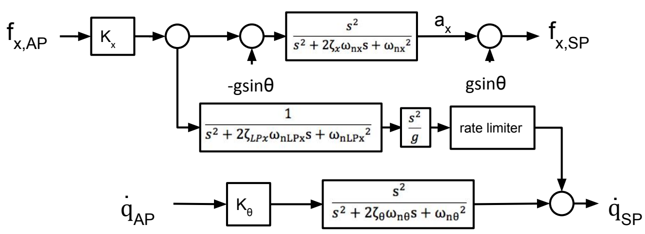

Fig. 2: Schematic representation of a cueing algorithm for pitch and surge in the longitudinal plane.

Figure 2 shows a schematic representation of a classical washout algorithm based on Reid an Nahon, Ref. 10, but for pitch acceleration and surge acceleration only. In figure 2, surge and pitch acceleration from the mathematical model are indicated with indices *AP* and the outgoing motion to the simulator is indicated with indices *SP*. Two main channels can be distinguished: a translational channel and a rotational channel. Furthermore, sustained accelerations are simulated by means of tilt coordination channel. Figure 3 shows a schematic representation of a classical washout algorithm for heave.

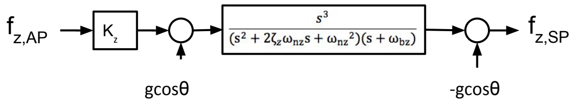

Fig. 3: Schematic representation of a cueing algorithm for heave in the longitudinal plane.

Note that all frequency response functions presented in this paper were obtained using a classical washout algorithm according to figure 2 and figure 3. Parameters were set according to table 2, unless specifically specified otherwise.

Table 2: Longitudinal settings for the classical washout algorithm.

	K	ω_n	ζ	ω_b	ω_{LP}
	$[-]$	$[rad/s]$	$[-]$	$[rad/s]$	$[rad/s]$
Pitch	0.7	0.8	1.0	0.0	-
Surge	0.7	1.0	1.0	0.0	2.0
Heave	0.5	2.5	1.0	0.2	-

Coupling of Input Signals

Crosstalk from Surge to Pitch The most important coupling in the cueing algorithm is crosstalk from surge to pitch. Sustained surge motion is simulated by tilting the simulator through a low-pass filter in the tilt coordination channel. This form of crosstalk is studied by the OMCT in 2 tests. Firstly in test 7 the surge axis is excited and the output on the pitch axis is measured, resulting in a pitch frequency response function due to an input on surge. Figure 4 shows the gain, $|H_7|$, and phase, $\angle H_7$ of test 7 for different cueing settings.

It should be noted that the simulator pitch angle was taken as output for this test, as was done by Hosman in Ref. 7, as opposed to the simulator pitch acceleration, as was done by Stroosma in Ref. 8. Since test 7 is essentially a frequency response function of the low-pass filter in the tilt coordination channel, such a representation can be more intuitively related to the MCA.

A typical tuning purpose of this test would be to determine the low-pass break frequency of the tilt coordination channel. As can be seen from figure 4, a higher break frequency will result in more cross coupling from surge to pitch, since the gain is larger for higher break frequencies. However, it is hard tune the algorithm based on this figure alone. It is is not clear which combination of gain and phase results in a simulation with a high predicted motion fidelity. Crosstalk from surge to pitch is a false cue, but due to the presence of tilt coordination

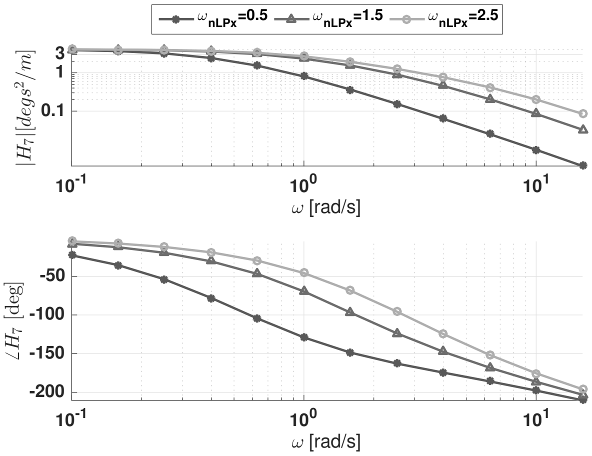

Fig. 4: Pitch frequency response function for a surge input, test 7 of the OMCT.

unavoidable. The gain of test 7 should not be as low as possible. However, a too large gain might result in unwanted pitch acceleration.

A solution to this problem might be to compare the results from test 7 with vestibular thresholds, such as obtained in Ref. 11. The hypothesis here is that if the frequency response function stays below thresholds of the semi-circular canals, the crosstalk from surge to pitch is acceptable. However, it could be that the characteristics of the crosstalk are sub-threshold in the frequency-domain, but are super-threshold in the time domain. Secondly motion cues presented to the pilot do not only depend on the cueing system, but also on the motion of the aircraft, which is not taken into account with such an approach. Another way to get a more complete picture of the pitch motion characteristics is to combine test 7 with a direct pitch frequency response function, test 1.

Test 1 studies crosstalk from surge to pitch in a pitch frequency response function using both surge and pitch input. Since for fixed-wing aircraft it is assumed that there is an uncoordinated motion between pitch and surge, also a signal is fed into the simulator on surge: $f_x = gsin(\theta)$. These signals were visualized in the time domain in figure 1. The frequency-domain response is visualized in figure 5.

In figure 5 three situations are depicted. Firstly a frequency response function from the current OMCT is depicted, indicated by $f_x = gsin(\theta)$. Helicopter motion is mostly coordinated, which is a common assumption for helicopter dynamics in simulator fidelity research, used for example in Ref. 12 and Ref. 13. This is an indication that during a regular helicopter task, $f_x = \dot{u} - gsin(\theta) \cong 0$. In figure 5 this scenario is represented by $f_x = 0$. Thirdly a test is shown were instead of $f_x = gsin(\theta)$, $f_x = -gsin(\theta)$ is cued. This is corresponding to the findings from figure 1, where it was seen that the relative phase difference between pitch and surge was roughly 180 $[deg]$ between 1 and 5 $[s]$.

It can be seen that the choice of input on the surge channel significantly influences pitch motion characteristics, especially at low frequencies.

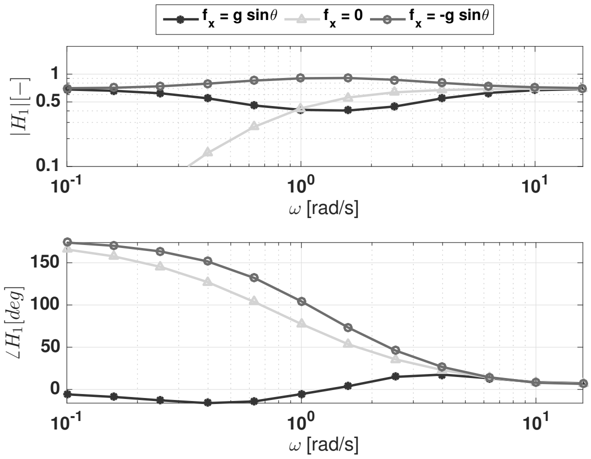

Fig. 5: Pitch frequency response computed with an input on pitch and surge axes, test 1 of the OMCT

Crosstalk from Pitch to Surge Crosstalk from pitch to surge originates from the transformation between the aircraft body frame of reference and the simulator inertial frame, indicated by $-gsin\theta$ in figure 3 and the transformation from the inertial frame of reference of the simulator to the simulator body frame, indicated by $gsin\theta$. θ in this case is the filtered pitch angle of the simulator. The OMCT studies this crosstalk by means of test number 2. Figure 6 shows a surge frequency response function due to an input on the pitch and surge channels.

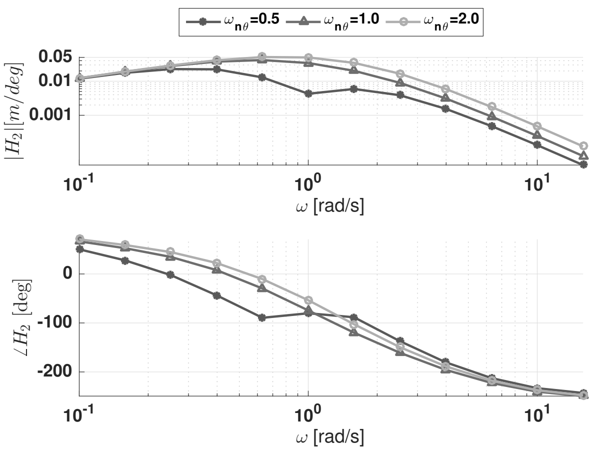

Fig. 6: Surge frequency response function due to pitch input, test 2 of the OMCT.

A typical tuning purpose of this test would be to determine the high-pass break frequency of the pitch channel. As can be seen from figure 6, a higher break frequency will result in more cross coupling from pitch to surge. However, as was the case for figure 4, the results from figure 6 are hard to interpret.

- As for test 1 displayed in figure 5, both an input on pitch axis and on the surge axis is used for this test. Therefore, not only is pitch-surge coupling included, but also surge-pitch coupling.
- Furthermore, surge acceleration a_x, not specific force f_x is taken as the output for this test.
- Cross talk from pitch to surge is a false cue but, like surge-pitch crosstalk not entirely unavoidable, as was discussed in Ref. 12. Similar to figure 4, it is therefore hard to judge surge motion characteristics based on test 2 alone. For a more complete picture of surge motion fidelity, test 2 should therefore be combined with a direct surge frequency response function, test 6 of the OMCT.

Linearity of Input Signals

From figure 1, it was seen that the amplitude of the surge input for an OMCT for pitch motion characteristics is larger than the actual input on the surge axis during pilot-in-the-loop hover simulation. The difference in amplitude might affect the OMCT for all non-linear elements in the motion cueing algorithm. Looking at figure 2 and figure 3, it can be seen that the most important non-linear element in the filter is the rate limiter in the tilt coordination channel. This limiter is present in the MCA to ensure that rotational rates from the tilt coordination channel are below perception thresholds. OMCT sensitivity to rate limiting was studied by Advani and Hosman in Ref. 7.

The effect of this non-linearity is illustrated by looking at test 6 with different amplitudes of the input spectrum, given in figure 7.

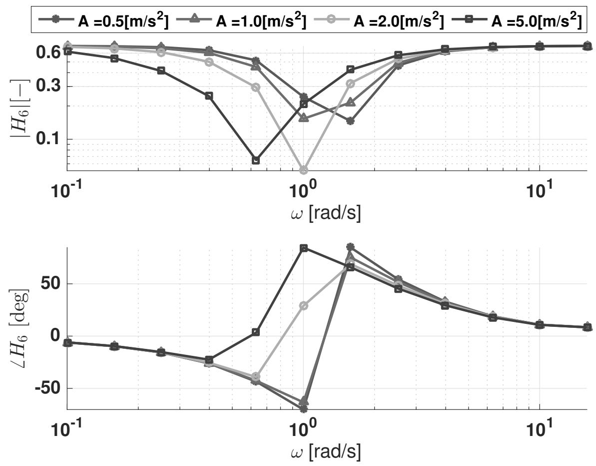

Fig. 7: Surge frequency response function computed using an input signal on the surge axis, $f_x = Asin(\omega t)$, with different amplitudes, test 6 of the OMCT.

It can be seen that for this particular motion setting, the frequency response at the Sinacori frequency of 1 $[rad/s]$ ranges from a modulus from 0.05 to 0.3. In practice this means that this cueing setting can have an OMCT gain varying with a factor 6 depending on the method of evaluation.

Issues with a possible implementation of the OMCT in the helicopter domain can be summarized essentially in three categories. Firstly surge-pitch coupling is represented incorrectly in the direct pitch frequency response function, figure 5. Secondly the results from cross coupling tests 2 and 7, given by figure 6 and figure 4 respectively, are hard to interpret. Finally there is a large sensitivity to rate limiting in the tilt coordination channel.

These issues boil down to to the fact that the OMCT might not incorporate knowledge about the physical motion of the helicopter sufficiently. Therefore, to find a more representative set of input signals for the OMCT, helicopter motion in the longitudinal plane needs to be studied in the frequency domain.

A BETTER OMCT?

An off-line simulation using a helicopter model and a non-human controller was conducted. Time traces of this simulation were thereafter transformed to the frequency domain and used to tailor a set of input signals, and subsequently an OMCT, to the motion of the off-line simulation.

Setting Up an Off-line Simulation

A reference task is needed for the set-up, yielding a reference trajectory that is representative for regular helicopter simulator training operations. Secondly it should be standardized, such that any results from this analysis can be compared to other research. A third requirement would be that the trajectory should sufficiently excite the dynamics of the aircraft on the frequency range of the OMCT.

Considering these requirements it was decided to use a Mission Task Element (MTE) from ADS-33, Ref. 14, a military design standard for handling qualities requirements. The resulting off-line simulation is schematically represented in figure 8.

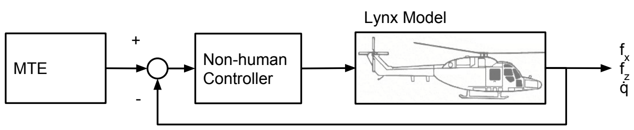

Fig. 8: Schematic flow chart of the off-line simulation.

A longitudinal MTE which is frequently used in simulator training, is an aborted take-off, referred to from now on as a take-off and abort. This task is initiated during hover at 35 $[ft]$ wheel height. The helicopter is accelerated to 40-50 $[kts]$, keeping the altitude constant as much as possible, at which point the take-off is aborted and the helicopter is decelerated back to hover again. Figure 9 shows the velocity profile of the take-off and abort MTE.

The goal of this MTE is to perform the maneuver in as little time as possible. The maneuver should be stopped if the helicopter is stabilized in hover at 800 [ft] from the starting point of the task. Figure 3 gives the desired and adequate performance for this task.

As can be seen from figure 9, the take-off and abort task is maneuver containing mainly low-frequency signals. To excite the higher frequencies on the OMCT spectrum, it was

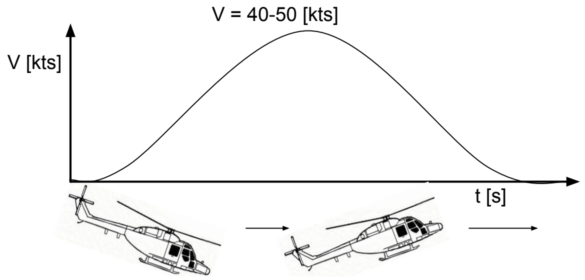

Fig. 9: Schematic of the Take-Off and Abort Mission Task Element.

Table 3: Adequate and desired longitudinal performance for a take-off and abort Mission Task Element.

	Adequate	Desired
Altitude $[ft]$	< 75	< 50
Time to complete $[s]$	< 30	< 25

therefore decided to also study a hover MTE using turbulence, since this task is more precise and requires higher frequency inputs from the controller.

A hover MTE is started at a small forward velocity of 6-10 $[kts]$. It is the goal of the pilot to stabilize the helicopter in hover at a specific location and remain in stabilized hover for 30 $[s]$. Figure 10 shows the velocity profile of a hover MTE.

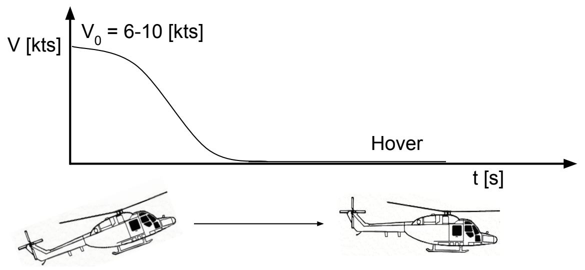

Fig. 10: Schematic of the Hover Mission Task Element.

Figure 3 gives the desired and adequate performance for this task.

To control the aircraft during these two MTEs, a controller consisting of two parts was designed and implemented. Firstly there is a PD controller, controlling the collective to keep the altitude constant throughout the maneuver. Secondly there is a PID controller computing a desired cyclic pitch to follow a velocity trajectory, according to the specific Mission Task Element.

A 3 Degrees-Of-Freedom, non-linear, longitudinal helicopter model was implemented, with numerical values taken from a DRA Research Lynx, Ref. 15. Equations of motion are given in appendix A. The following assumptions made on the dynamics and on the main rotor blades have particular influence on a tailored set of OMCT input signals.

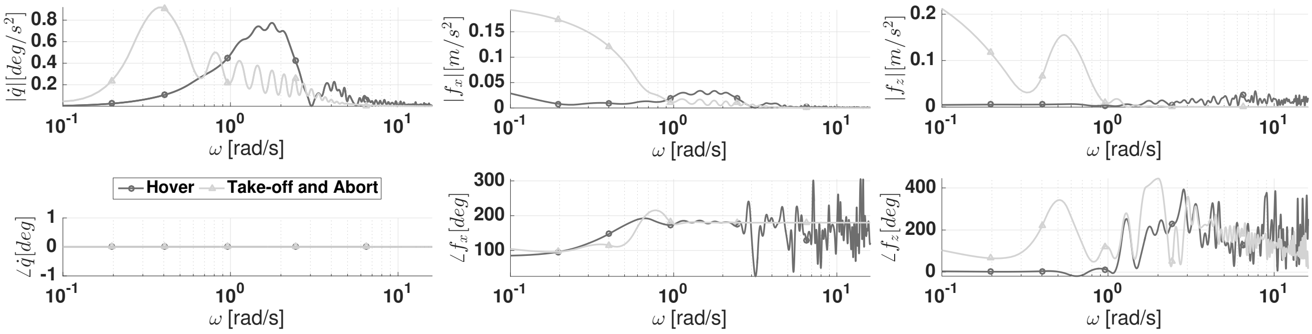

(a) Pitch. **(b) Surge.** **(c) Heave.**

Fig. 11: Amplitude and relative phase spectra used for a tailored OMCT.

Table 4: Adequate and desired longitudinal performance for a hover Mission Task Element.

	Adequate	Desired
Time to stabilize $[s]$	< 8	< 3
Longitudinal position $[ft]$	$+/-6$	$+/-3$
Altitude$[ft]$	$+/-2$	$+/-5$

- Fuselage drag was estimated by $D = C_D \frac{1}{2}\rho V^2 S$, with $C_D = 0.08[-]$ taken from Ref. 15. All other aerodynamic forces on the fuselage were neglected.
- A non-eccentric, spring-less flapping hinge and no drag forces on the main rotor were assumed. The effect of this assumption is that there are no moments or drag acting on the main rotor hub. Since these forces are small compared to the thrust force, as was stated in Ref. 16, this is considered a valid assumption for the purposes of this research.
- Quasi-steady inflow velocity and flapping dynamics are assumed.
- The engine is assumed to deliver the power required without delay, resulting in a constant RPM.

The result of these assumptions is that the only contributions to the specific forces in surge and heave direction are the main rotor thrust and the fuselage drag force. Furthermore, any pitch rotational acceleration is due to the main rotor thrust force.

To excite the higher frequencies on the OMCT spectrum, a turbulence model was implemented during the hover MTE. This turbulence model set a deviation from the body velocities u and w are using a Dryden spectrum according to Ref. 17. No rotational component in the turbulence was used.

Time traces of specific forces f_x and f_z and pitch acceleration $\dot{q}$ were computed for both MTEs. These time traces were subsequently converted to the frequency domain by means of the Fast Fourier Transform (FFT). This process results in 2 sets of 3 Power Spectral Densities (PSDs).

Tailoring the Input Signals

The amplitude from the PSDs can be used to make an estimate of a tailored amplitude spectrum directly. However, it is of importance to capture the relative phase between degrees of freedom. From figure 5 it was seen for example, that an OMCT pitch frequency response function is influenced significantly by the input of the surge axis. If the surge axis is excited by $gsin\theta$, the pitch motion characteristics at lower frequencies seem favourable. However, if the surge axis is excited by an input with 180 $[deg]$ relative phase difference, or $-gsin\theta$, there is a 180 $[deg]$ phase shift in the response function at low frequencies.

Following this reasoning it was decided to use both the amplitude and *phase* information from the PSDs. The absolute phase of the pitch axis was therefore set to zero and the *relative* phase for surge and heave was computed according to:

$$\angle f_x = \angle \dot{q} - \angle f_x \tag{1a}$$
$$\angle f_z = \angle \dot{q} - \angle f_z \tag{1b}$$
$$\angle \dot{q} = 0 \tag{1c}$$

However, due to the characteristics of the FFT, not on every OMCT frequency there is an estimate of the amplitude and phase. Therefore a model was made based on univariate splines to estimate amplitude and phase on OMCT frequencies. One set of input signals for the take-off and abort task and one set for the hover MTE were determined. Figure 11 shows the amplitude and relative phase models for pitch-surge and heave respectively.

Several interesting observations can be made from figure 11.

- Firstly it can be seen that amplitude at most points is a factor 50 times smaller than 1 $[m/s^2]$, which is the amplitude used for the current OMCT according to Ref. 1. This indicates that the signals going into the classical washout algorithm are over-sized in the original OMCT for this specific MTE and helicopter model.

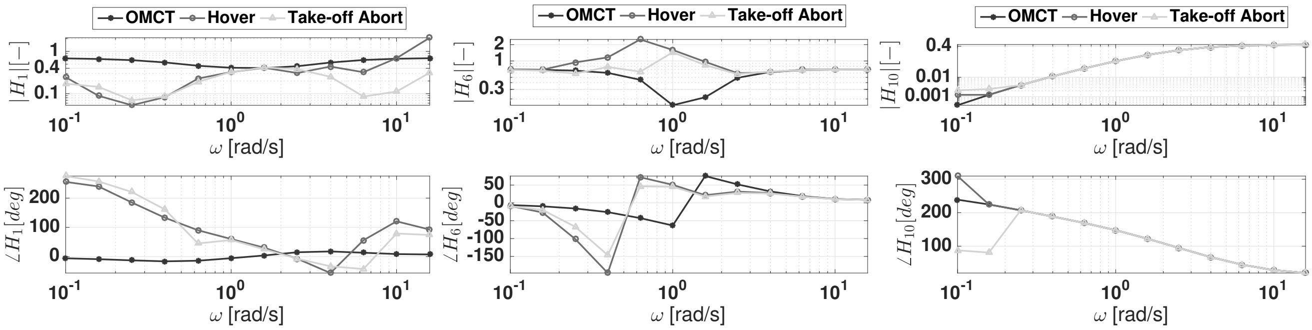

(a) Pitch. **(b) Surge.** **(c) Heave.**

Fig. 12: Comparison between two tailored OMCTs and the original OMCT.

- Secondly it can be seen that noise is present in the signals for frequencies above 2 $[rad/s]$. This noise due to a combination of the effect of atmospheric turbulence for the hover task and windowing from the FFT.
- Thirdly, the relative phase in figure 11b shows that the relative phase between pitch and surge is about 100 $[deg]$ for low frequencies and about 180 $[deg]$ for $\omega > 0.7[rad/s]$. A positive pitch motion therefore means a negative surge acceleration and vice versa.

A mathematical explanation for the last observation can be sought in the equations of motions that were used for the helicopter model. The expression for the specific force in surge direction is given by:

$$f_x = -\frac{D}{m}\cos\theta_f - \frac{T}{m}\sin(\theta_{1c} - \alpha_1) \tag{2}$$

In this expression, θ_f is the pitch angle of the helicopter, θ_{1c} is the angle of the control plane and α_1 is the longitudinal flapping angle. However, since pitch acceleration is solely caused by the thrust force, the second term in equation 2 can be substituted, resulting in the following expression,

$$f_x = -\frac{D}{m}\cos\theta_f - \frac{I_{yy}}{mh_R}\dot{q} \tag{3}$$

where I_{yy} is the moment of inertia of the helicopter body and h_R is the distance between the c.g. and the rotor hub.

To evaluate the relative phase between f_x and $\dot{q}$, it is important to note that angular acceleration is the double derivative of the helicopter pitch angle, $\dot{q} = \ddot{\theta}_f$. If it is assumed that $q \doteq \sin(\omega t)$ then $\theta_f = -\frac{1}{\omega^2}\sin(\omega t) = -\frac{1}{\omega^2}\dot{q}$. Substituted into equation 3 this gives:

$$f_x = -\frac{D}{m}\cos(-\frac{1}{\omega^2}\dot{q}) - \frac{I_{yy}}{mh_R}\dot{q} \tag{4}$$

It can be seen that for high frequencies, $-\frac{1}{\omega^2}\dot{q}$ becomes small, and f_x is only influenced by $-\frac{I_{yy}}{mh_R}\dot{q}$, meaning that the relative phase between pitch and surge for high frequencies is that of $-\frac{I_{yy}}{mh_R}$ or 180 $[deg]$.

Tailoring the OMCT

During pilot-in-the-loop simulation, different DOFs are excited simultaneously. Therefore it was decided to use the tailored input signals to excite different DOFs *simultaneously*.

A classical washout algorithm as was given in figure 2 and figure 3 with a parameter set equal to that of table 2 was excited on pitch, surge and heave *simultaneously*. The result is presented in figure 12, where the tailored OMCT is compared to the original OMCT. Figure 12a, figure 12b and figure 12c show the frequency response functions of the pitch channel, the surge channel and the heave channel respectively.

It was chosen to tailor the OMCT using the same 12 prescribed OMCT frequencies ranging from 0.1 to 15.8 $[rad/s]$, since a larger amount of frequencies would hinder any practical implementation of a tailored test in the future. Since all axes are excited simultaneously, the cross tests for the original OCMT lose their significance and are no longer performed.

The following observations can be made from the comparison between the original and tailored OMCT.

- At low frequencies for the pitch frequency response function, the current OMCT predicts favorable motion characteristics, with a gain of close to 1 and a phase close to 0 $[deg]$. However, both the tailored OMCT based on the hover task and on the take-off and abort task predict poor motion characteristics with a low gain and a phase around 200 $[deg]$ lead. This is an indication pitch-surge motion in this case is more coordinated, corresponding to the case of $f_x = 0$ in figure 5. At high frequencies upswing is present in the hover task. For the take-off and abort task, the gain is lower than the current OMCT. These phenomena are the result of crosstalk from the surge to the pitch axis. Similarly to figure 4, in figure 13 the low-pass break frequency on the tilt coordination channel was varied.
  From figure 13 it can be seen that when tuned such that little coupling is expected from surge to pitch, the pitch frequency response function resembles a high-pass filter.
- From figure 12b it can be seen that the surge frequency response function for the original OMCT predicts a 'gap'

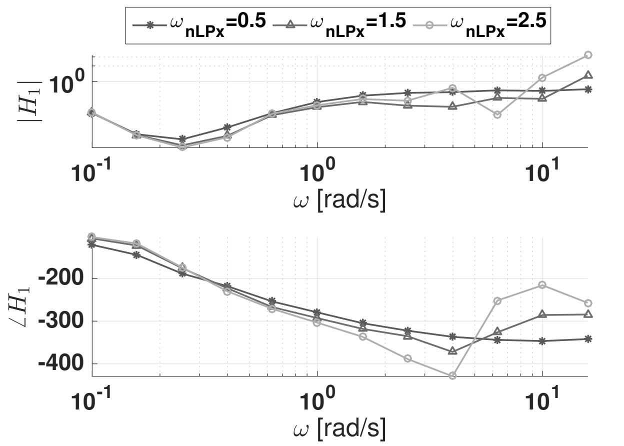

Fig. 13: Pitch frequency response function tailored to a Hover MTE.

in motion characteristics between the tilt coordination filter and the surge translational channel. However, for the tailored OMCTs, surge motion is cued *more* than in actual helicopter flight. From figure 12b it can be seen that the magnitude becomes larger than 1, for some frequencies. This effect is due to crosstalk from pitch to surge. Similarly to figure 6, in figure 14 the high-pass break frequency on the pitch channel was varied.

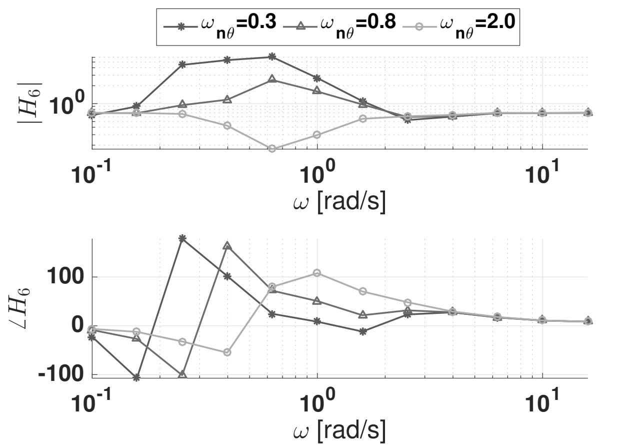

Fig. 14: Surge frequency response function tailored to a Hover MTE.

It can be seen that by tuning the classical washout algorithm such that little coupling is expected from pitch to surge, the surge frequency response function resembles the original OMCT.

- There is little difference between the frequency response function for heave for the original OMCT and a tailored OMCT. This is an indication that in the classical washout filter, heave is mostly uncoupled with other DOFs.

With this methodology, notable differences in the motion cueing characteristics were identified for the pitch and surge axes. Most importantly it was seen that coupling between pitch and surge are directly visible in the frequency response plots figure 12a and figure 12b, as an addition to frequency response functions from the original OMCT.

For actual pilot-in-the-loop simulation, the human controller will influence the control input of the model and therefore the characteristics of the helicopter motion. A limitation of the preceding analysis is therefore that the amplitude and relative phase of different degrees of freedom are not only influenced by the dynamics and Mission Task Element, but also by pilot control behavior.

VALIDATION EXPERIMENT

Identified differences in the prediction of motion characteristics between a tailored OMCT and the current OMCT were validated with a pilot-in-the-loop experiment. The primary objective of this experiment is to study the influence of pilot control behavior on a tailored OMCT. Secondly, it interesting to see if upswing on the surge axis due to pitch-surge coupling has any influence of pilot fidelity ratings. Figure 15 shows a schematic representation of the experimental set-up.

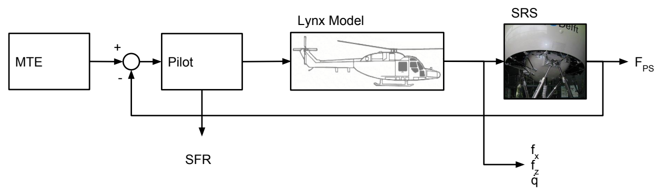

Fig. 15: Schematic flowchart of a pilot-in-the-loop simulation.

Experimental Set-up

For the validation experiment, the SIMONA Research Simulator (SRS) at Delft University of Technology, figure 16, was used. The SRS is a 6 Degree-Of-Freedom simulator developed for human-machine interface and handling qualities research. The motion system is hydraulic, consisting of 6 actuators. Figure 16 shows the exterior and the interior of the SRS.

(a) Exterior. **(b) Interior.**

Fig. 16: SIMONA Research Simulation (SRS).

The SRS is equipped with an 180 by 40 [*deg*] field of view collimated outside visual display, which together with a high quality scene detail and an update rate of 120 Hz results in high fidelity visual cues provided to the pilot. The visual cues are synchronized with the motion cues to within 10 [ms].

Control was provided to the pilot by means of a collective and a the longitudinal cyclic only. A basic 6 instrument set-up was provided digitally on the center Multi-Function Display (MFD) of the SRS

For this experiment, a non-linear 3-DOF mathematical model equal to that of the off-line analysis was implemented in the simulation architecture of SRS.

Mission Task Elements Similarly to the off-line analysis two MTEs were flown. Firstly a take-off and abort task was performed. Table 3 depicts desired and accurate performance according to Ref. 14 for this task. Dedicated visual cues for this task were implemented in the SRS visual display and are illustrated by figure 17.

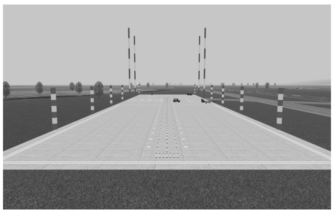

Fig. 17: Front view of the take-off and abort symbology.

Secondly a hover MTE was performed. Table 4 depicts desired and accurate performance according to Ref. 14 for this task. Figure 18a and figure 18b show dedicated visual cues implemented in the SRS visual display.

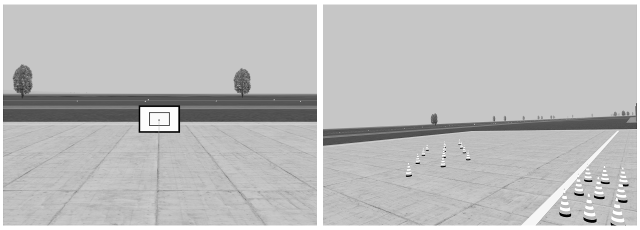

(a) Front. **(b) Diagonal.**

Fig. 18: View of the hover symbology.

Motion Cueing Settings Besides the MTEs, a second independent variable for this experiment was considered. In the off-line simulation, the most notable difference in motion characteristics between the tailored OMCT and the current OMCT was the upswing on the surge frequency response. This upswing was due to crosstalk from pitch to surge, influenced mostly by the high-pass break frequency on the pitch channel. It is therefore interesting to see the influence of this parameter on pilot fidelity ratings. To this end, four different motion cueing conditions were presented to the pilot. The high-pass pitch break frequency was varied, $\omega_{n_\theta} = 0.5$, 0.8, 1.2 and $1.5[rad/s]$. Other parameters were set similarly to the off-line simulation, given in table 2.

Experimental Procedure Three experienced helicopter pilots participated in this experiment. Credentials are presented in figure 5.

Table 5: Participants.

No.	Flight Hours	Type	Last Flight	Pilot Type
1	1000	CH47D-F	active	Military
2	1000	CH47D-F	active	Military
3	Over 4000	Alouette III, Cougar	2014	Military

Pilots were instructed to fly the simulator with a similar control strategy as they would fly the aircraft. They were also requested specifically to strive for desired performance as much as possible. After a familiarization period in which pilots were presented with all test conditions and were allowed to practice until a stable performance for both tasks was achieved, 8 test conditions were presented to the participant. Each test condition was flown until 3 consecutive runs with a stable performance were achieved. Thereafter the participant was asked to award a fidelity metric for that particular condition. To avoid any additional learning between runs, different motion settings were varied between conditions according to table 6.

Table 6: Test matrix for three participants.

Condition	Task	ω_{n_θ} s1	ω_{n_θ} s2	ω_{n_θ} s3
1	Hover	0.5	1.2	0.8
2	Hover	1.2	0.8	1.5
3	Hover	0.8	1.5	1.2
4	Hover	1.5	0.5	0.5
5	TO-A	1.2	1.2	1.5
6	TO-A	0.5	1.5	0.8
7	TO-A	1.5	0.8	0.5
8	TO-A	0.8	0.5	1.2

The motion output of the flight model was recorded. With these time-traces, tailored OMCTs were conducted. Secondly, the fidelity of the different motion settings of the classical washout algorithm will be assessed using the Simulation Fidelity Rating (SFR) scale, given in appendix B, as was proposed by Perfect and Timson in Ref. 18. The SFR assumes a high fidelity simulation when the attainable performance of the simulation is similar to the performance in the real helicopter with minimal task strategy adaptation. Although numerical values for the mathematical model were taken from a Lynx reference helicopter, model fidelity permits a direct comparison between simulator and helicopter performance. Performance will therefore be judged based on the experience of the participants.

Hypotheses

Since the model outcome is influenced by pilot control behaviour, it is expected that tailored OMCTs based on the experimental data will show differences with the off-line analysis. Moreover, since pilots will not fly every run with a similar performance, it is expected that the experimental data will show variance on both the gain and phase of the OMCT predictions.

A secondary purpose of this experiment is to validate the pitch-surge coupling subjectively by means of the SFR scale. Since upswing is present in the frequency response function for surge at low values of ω_{n_θ}, it is expected that the pilot with rate these simulations will a higher SFR, indicating a lower total fidelity of the simulation. It is hypothesized that participants will rate the simulation with a lower SFR for higher values of ω_{n_θ}, indicating a higher total fidelity of the simulation.

RESULTS

Objective Metrics - Time Domain

The performance of both MTEs is presented in figure 19 and figure 20 respectively, in terms of longitudinal position and altitude. Also visualized are desired and adequate performance according to Ref. 14.

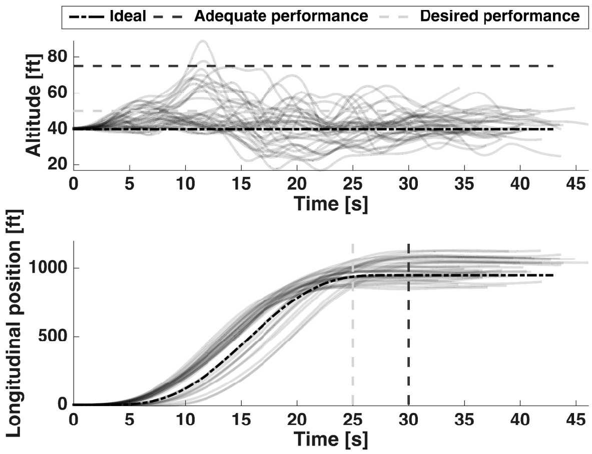

Fig. 19: Altitude and longitudinal position for the Take-Off and Abort MTE.

From figure 19 it can be seen that the take-off and abort maneuver was performed with adequate performance. However, during the experiment it was noticed that participants had trouble identifying the endpoint of the maneuver. This resulted in an overshoot or undershoot of the desired end location of the task. As was identified by Atencio in 1993, Ref. 19, due to a limited field-of-view, lateral and longitudinal drift is known problem for rotorcraft simulations.

Figure 20 shows the performance for the hover task. It can be seen that for most runs adequate performance was achieved. However, also for this task, difficulty to maintain longitudinal position was identified. Furthermore it can be seen that for the first participant the initial altitude of the maneuver was set too high, at 20 [ft]. This was corrected for the subsequent participants. This was considered acceptable, since the participant corrected the altitude within 5 [s].

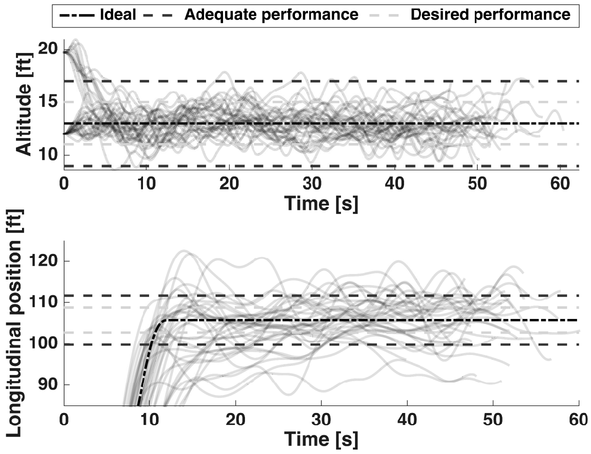

Fig. 20: Altitude and longitudinal position for the hover MTE.

Objective Metrics - Tailored Input Signals

The time traces of specific forces and rotational accelerations from the experiment were converted to the frequency domain and the relative phases were computed, according to the methodology proposed in the off-line analysis. Figure 21 and figure 22 show the amplitude and relative phase for the take-off and abort and hover task, respectively.

The following observations were made.

- The highest amplitude for the pitch input signals is around $1[rad/s]$.
- For surge input signals, the amplitude is higher for low frequencies than the off-line analysis, for the take-off and abort task. Furthermore, it can be seen that a large variance is present in the relative phase for low frequencies for the hover task.
- The amplitude in heave is larger as compared to the off-line analysis. The controller is better capable to keep the aircraft at a constant altitude than a human operator. The relative phase for both tasks does not show a clear trend, not unlike the off-line analysis.

Objective Metrics - Tailored OMCT

A tailored OMCT was computed by using a tailored set of input signal for each test run. Result will be displayed here using a parameter set given in table 2. figure 24a and figure 23a show the pitch frequency response functions for the tailored OMCTs, together with the off-line analysis and the original OMCT. The mean and standard deviation in the form of an error bar are shown for all participants and all test conditions.

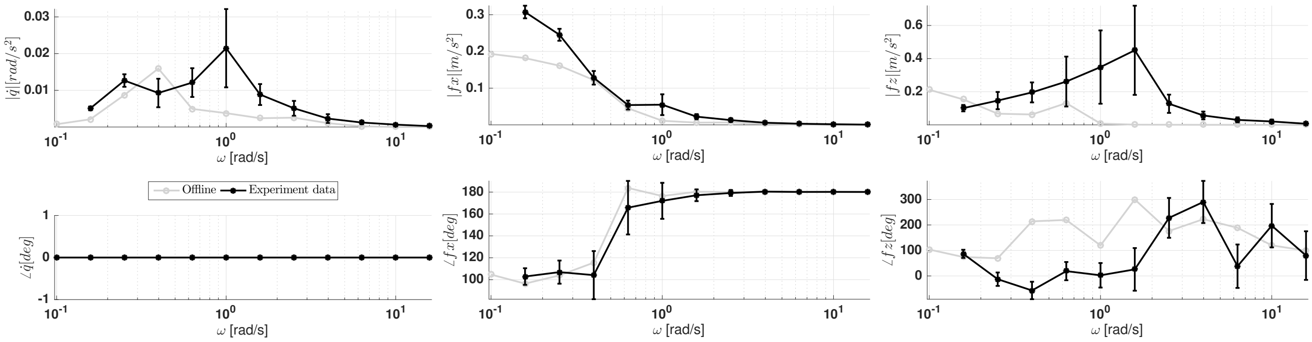

(a) Pitch. **(b) Surge.** **(c) Heave.**

Fig. 21: Amplitude and phase spectrum for a tailored OMCT based on experimental data for a take-off and abort MTE.

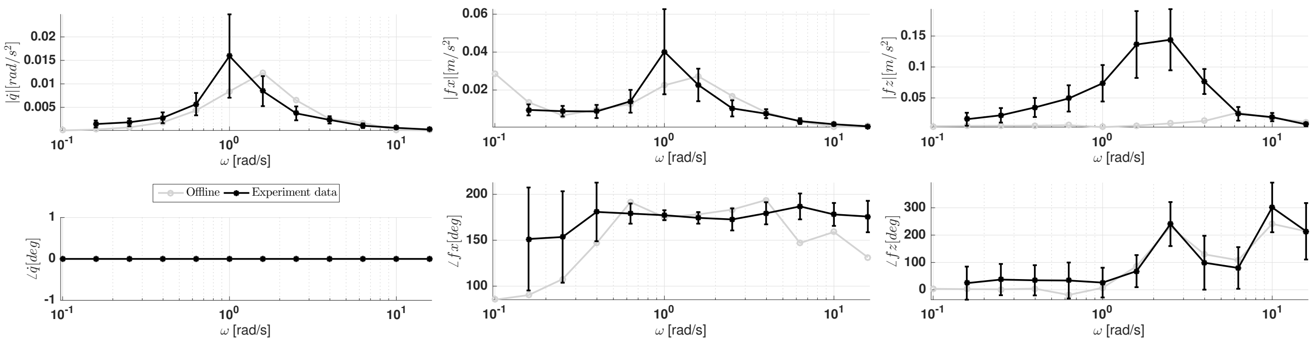

(a) Pitch. **(b) Surge.** **(c) Heave.**

Fig. 22: Amplitude and phase spectrum for a tailored OMCT based on experimental data for a hover MTE.

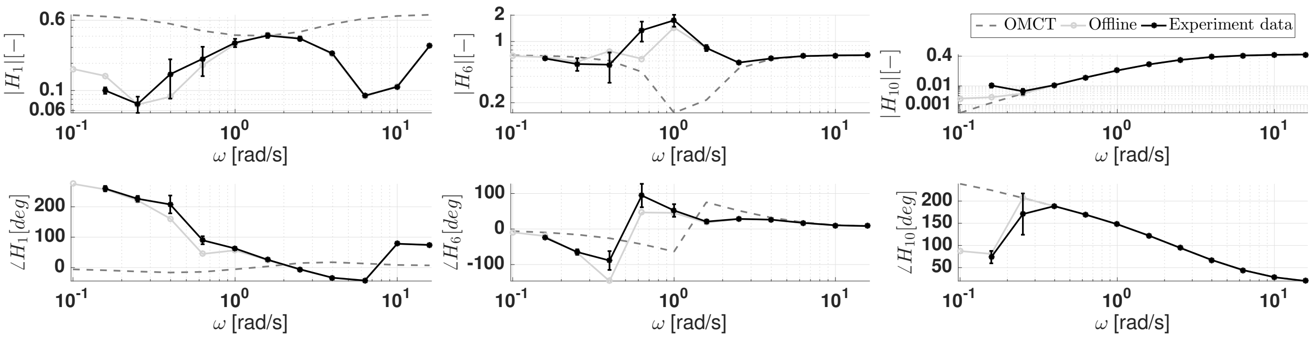

(a) Pitch. **(b) Surge.** **(c) Heave.**

Fig. 23: Frequency response functions for the take-off and abort MTE.

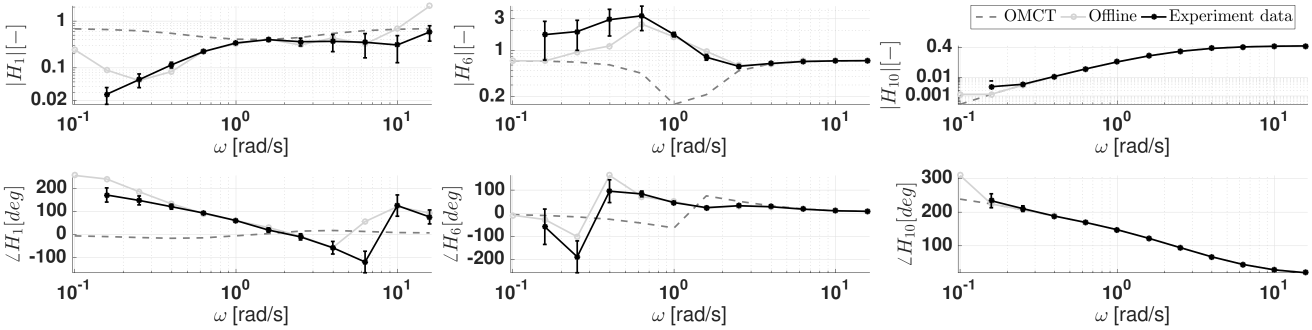

(a) Pitch. **(b) Surge.** **(c) Heave.**

Fig. 24: Frequency response functions for the hover MTE.

From figure 24a it can be seen that the experimental data follows the same trend as the off-line analysis. It can be seen that no data point exists for the lowest OMCT frequency point, $\omega = 0.1[rad/s]$. This is because the tasks do not provide sufficient measuring time for the lower frequencies of the OMCT. Furthermore there is variance on the amplitude and phase for frequencies below 0.3 and above 2 $[rad/s]$ for the hover MTE. This is an indication that a combination of pilot input and turbulence has an effect on the motion characteristics. Variance above 2 $[rad/s]$ is thought to originate from turbulence, since no variation is present in the take-off and abort task. Furthermore there is a large variance present at lower frequencies of the take-off and abort MTE, according to figure 23a.

Figure 24b and figure 23b show the surge frequency response function for the tailored OMCT. Again, experimental data is compared to the original OMCT and the off-line analysis. It can be seen that for the hover MTE, upswing on the surge axis at low frequencies is higher for the experimental data as compared to the off-line analysis. Furthermore, it can be seen that there is large variance at the low frequency response points. Secondly it can be seen that for the take-off and abort task indicated upswing is also present. However, variance exists on frequency point 0.4, 0.6 and 1.0 $[rad/s]$ of the OMCT.

Finally, figure 24c and figure 23c show the heave frequency response function for the tailored OMCT, for both MTEs. It can be seen that there is little difference between a tailored OMCT and the original OMCT, both for the off-line simulation and the experimental data. However at low frequencies, both the off-line and the experimental data predict a higher amplitude than the original OMCT.

Crosstalk from Pitch to Surge For the secondary objective of this experiment a tailored OMCT was performed for every test run on the motion cueing settings of that particular test run. Figure 25 shows the mean of the surge frequency response functions for the 4 different motion conditions, for the hover task. It can be seen that a similar trend is visible as was seen during the off-line analysis, presented in figure 14. For low values of the high-pass break frequency on the pitch channel, there is an upswing in the surge specific force at low frequencies.

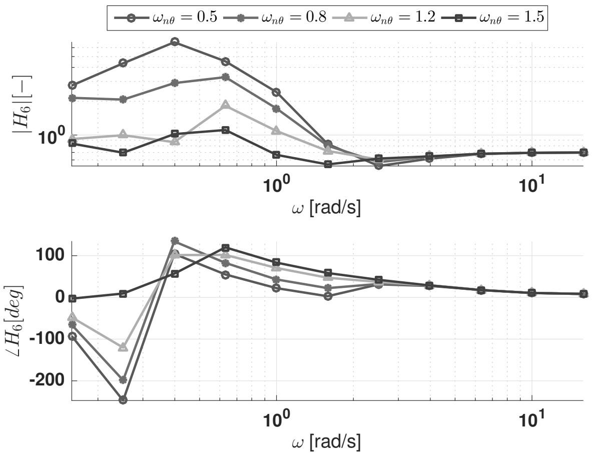

Fig. 25: Frequency response function for surge motion characteristics for 4 motion conditions, hover.

A similar result was obtained from the take-off and abort MTE, presented in figure 26, where the surge frequency response functions for the take-off and abort task are presented.

Subjective Metrics - SFR

Pilot ratings have been summarized for the different test conditions in figure 27. Similar motion conditions are rated with a different SFR, but in some cases also with a different fidelity level. It can be seen that condition 2 is awarded the lowest fidelity ratings for the hover MTE. For the take-off and abort MTE, condition 3 seems of the lowest fidelity. From discussion about the ratings during the experiment, participants gave the following explanations.

- Participant 1 rated all conditions equally, with an SFR of 2, indicating all simulations were of fidelity level 1. As explanation he gave: *"we are trained to not trust the motion of the helicopter, but rely on instruments as much as possible"*.
- Participant 2 indicated for the second test condition in hover: *"turbulence interfered with motion"*. Further-

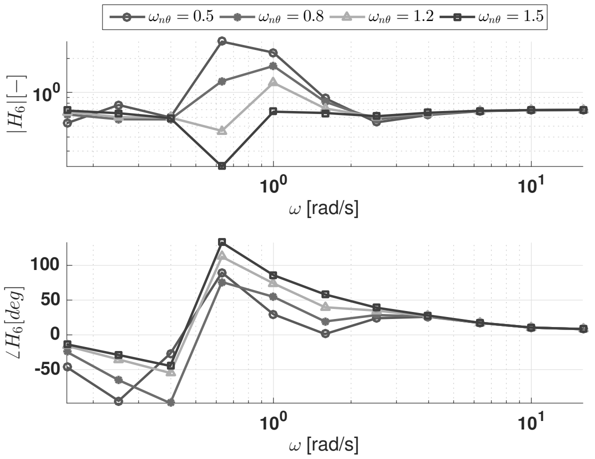

Fig. 26: Frequency response function for surge motion characteristics for 4 motion conditions, take-off and abort.

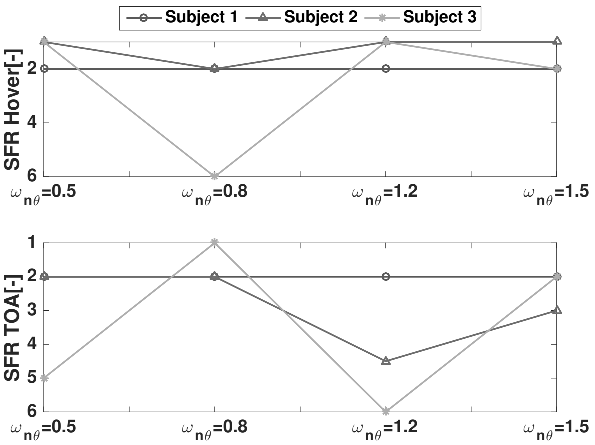

Fig. 27: Awarded SFR rating per test condition for both the Hover and Take-off and Abort MTEs.

more, he indicated for the third test condition in the take-off and abort task *"I miss the motion cue for longitudinal acceleration"* and *"for this condition I relied more on my instruments."*

- Participant 3 indicated for the second test condition in hover: *"There is a delay in the response of the aircraft"*. Secondly, he indicated for the first test condition in the take-off and abort task: *"There was little difference in motion, but due to large travel in de cyclic stick, the simulation was less realistic."* Lastly he indicated for the third test condition in take-off and abort: *"The pitch movement for this condition was too large for my liking."*

DISCUSSION

In this paper the extent to which the current OMCT is representative for rotorcraft was studied. The effect of assumptions in the input signals on the frequency response functions was studied. It should be noted however, that this analysis is limited to the classical washout algorithm. Furthermore any effects of the cueing hardware on the frequency response functions were not taken into account.

A methodology was proposed to compute a set of input signals that potentially better represents motion of a specific helicopter model and two specific MTEs. This was done by modeling the amplitude and relative phase for the three longitudinal axes. The following advantages have been identified. The first advantage is that crosstalk between the degrees of freedom is now directly visible as an addition to the direct frequency response functions. This makes it possible to see the effect of a parameter in the classical washout algorithm on all axes simultaneously. For tuning purposes, the off-axis performance can therefore be assessed directly. For example, the influence of the high-pass break frequency on the surge axes directly be tested by varying $\omega_{n\theta}$ and computing the surge frequency response function, without the need for cross tests. Secondly, test duration is reduced significantly, since all response functions can be computed using only one sweep through the frequencies.

A downside of the proposed method is firstly that the tailored OMCT outcome is very sensitive to the signal-processing of the amplitude and relative phase spectra. Since there are often no exact estimates of the amplitude and phase form the FFT at the OMCT frequencies, a least-squares fit had to be made. It was seen that this fit is very sensitive to the degree and amount of splines used. Furthermore it was seen that the resulting signals often had an amplitude 50 times smaller than the current OMCT. This might give problems with the signal-to-noise ratio of sensors in practical implementation of such a test in the future. Thirdly the shape of the frequency response functions is less intuitively related to the classical washout algorithm.

Finally it should be noted that the model output is not only influenced by the dynamics of the helicopter, but also by the pilot control input. For any off-line analysis in the future, it might be considered to use a pilot model that better portrays pilot control behavior.

A validation experiment on the SRS was subsequently conducted. It was seen that pilot input did have a noticeable influence on the motion characteristics of the simulation, especially for surge and pitch. An explanation this can be sought in the fact that the relative phase of the surge input spectrum for both tasks varies largely depending on the run, as can be seen from figure 22b and figure 21b. Especially for hover, the relative phase varies between 100 and 200 $[deg]$. This in turn is due to the fact that the drag component in the specific force is unpredictable since it is influenced by pilot control input and due to turbulence present in the hover task. If the relative phase is close to 200 $[deg]$, specific force due to the pitch rotation will be canceled out by acceleration in surge direction of the helicopter body. The amplitude for the pitch frequency response plot will thus be lower. If the relative phase is close to 100 $[deg]$, surge due to pitch rotation will be canceled out less. The amplitude for the OMCT pitch frequency response function will higher.

Performing the analysis with a more complex mathematical model might influence the relative phase between pitch and surge and will therefore also influence the fidelity of a tailored OMCT. It would therefore be interesting to see the influence of a horizontal tail, the presence of a spring and/or drag forces on the main rotor on the relative phase between pitch and surge.

Finally a subjective analysis of four motion cueing settings was performed to see if pilot subjective opinion was is agreement with the objective metrics. No trend was found in accordance with the hypothesis that a low high pass pitch break frequency would results in a better SFR rating. An explanation can be sought in two aspects of the simulation.

- Firstly the model fidelity might have interfered with the SFR evaluation. Pilots indicated that they frequently encountered a pilot-induced-oscillation, especially in the training phase. This was due to the fact no augmentation was present in the model and pilots had to close the pitch feedback loop manually. Secondly pilots commented on the stick travel as being too large as compared to real helicopter flight. During the experiment, pilot were instructed to focus on the motion fidelity as much as possible. However, in one case the pilot reported still giving a bad fidelity metric, due to unusually large stick travel.
- Secondly performance was judged subjectively by the pilot and the experiment leader. There was implemented a display which plotted the velocity and altitude profile of the run real-time. However, the ADS-33 criteria were not included in this graph.

CONCLUSION

The objectives of this paper were (1) to investigate the extent to which the OMCT is representative for rotorcraft in the longitudinal plane, (2) to investigate whether a potentially superior set of input signals better representing helicopter motion can be defined and (3) to validate potential differences in the prediction of motion characteristics between an OMCT based on the helicopter motion and the current OMCT with a pilot-in-the-loop experiment.

The following conclusions can be drawn.

1. The current OMCT is representative for heave motion characteristics, but issues arise when looking at the pitch and surge motion characteristics. Firstly surge-pitch coupling is represented incorrectly in the direct pitch frequency response function. Secondly the results from the tests for pitch-surge and surge-pitch coupling are hard to interpret. Finally there is a large sensitivity to rate limiting in the tilt coordination channel.
2. Notable differences in the motion cueing characteristics were identified for the pitch and surge axes, when tailoring a set of input signals to a specific helicopter model and two Mission Task Elements.
3. From the validation experiment it was firstly concluded that, although pilot control behavior significantly affects pitch and surge motion characteristics according to a tailored OMCT, the main trend of the frequency response functions was determined by the dynamics of the helicopter model. Secondly it was concluded that the observed changes in motion characteristics due to different cueing settings were not accompanied by a reported loss of motion fidelity by the pilots.

RECOMMENDATION

The ultimate objective of an objective motion cueing evaluation is to find a set of input signals that incorporates all important characteristics of helicopter motion, such that it can be used to evaluate a variety of different simulators and tasks. To this end, it is recommended to evaluate the current set of input signals of the OMCT for a variety of models, also incorporating lateral motion, and mission task elements using a similar method presented in this article. Furthermore it is recommended to implement a pilot model in future off-line analysis, such that sensitivity of the OMCT to the pilot task strategy is mitigated.

An Objective Motion Cueing Test with input signals more closely resembling helicopter motion will enable simulator engineers to evaluate the motion cueing fidelity in a more representative way. This in turn could support the development and configuration of motion cueing algorithms, which are more suitable for the task at hand: the training of helicopter pilots.

Author contact: Wouter Dalmeijer, W.H.Dalmeijer@student.tudelft.nl;
Ivan Miletović, I.Miletovic@tudelft.nl;
Olaf Stroosma, O.Stroosma@tudelft.nl;
Marilena Pavel, M.D.Pavel@tudelft.nl.

APPENDIX A

The non-linear, longitudinal equations of motion used for this research were:

$$\dot{u} = -g\sin\theta_f - \frac{D}{m}\cos(\theta_f) + \frac{T}{m}\sin(\theta_{1c} - a_1) - qw \tag{5a}$$

$$\dot{w} = g\cos\theta_f - \frac{D}{m}\sin(\theta_f) - \frac{T}{m}\cos(\theta_{1c} - a_1) + qu \tag{5b}$$

$$\dot{q} = -\frac{Th_R}{I_{yy}}\sin(\theta_{1c} - a_1) \tag{5c}$$

$$\dot{\theta}_f = q \tag{5d}$$

Here $\dot{u}$ and $\dot{w}$ are the derivatives of the body velocities and $\dot{q}$ is the pitch rotational acceleration. Furthermore θ_f is the pitch angle of the helicopter, θ_{1c} is the longitudinal cyclic input and α_1 is the longitudinal flapping angle.

Drag D is computed only taking into account the drag of the fuselage. Thrust T is given by $T = C_T \frac{1}{2}\rho V^2 S$, where C_T is computed by means of iterative solving for the inflow velocity of the main rotor, λ_i, using the the Blade Element Method and Glauert, given here:.

$$CT_{BEM} = \frac{1}{4}a_0\sigma\Big(\frac{2}{3}\theta_0(1+\frac{3}{2}\mu^2) - (\lambda_c + \lambda_i)\Big) \tag{6a}$$

$$CT_{GLA} = 2\lambda_i\sqrt{\Big(\frac{V}{\Omega R}\cos(\alpha_c - a_1)\Big)^2 + \Big(\frac{V}{\Omega R}\sin(\alpha_c - a_1) + \lambda_i\Big)^2} \tag{6b}$$

In these expressions, a_0 is lift coefficient of a rotor blade, σ is the rotor solidity, θ_0 is the collective input, Ω is the rotational velocity of the main rotor and R the rotor radius. The longitudinal flapping coefficient a_1 was computed from:

$$a_1 = \frac{\frac{8}{3}\mu\theta_0 - 2\mu(\lambda_c + \lambda_i) - \frac{16}{\gamma}\frac{q}{\Omega}}{1 - \frac{1}{2}\mu^2} \tag{7}$$

Here the airspeed V, the angle of attack of the control plane α_c, the non-dimensional aircraft velocity μ and the inflow velocity of the main rotor due to the aircraft velocity λ_c were computed according to the following set of equations.

$$V = \sqrt{u^2 + w^2} \tag{8a}$$

$$\alpha_c = \theta_{1c} - \tan^{-1}\frac{w}{u} \tag{8b}$$

$$\mu = V\frac{\cos\alpha_c}{\Omega R} \tag{8c}$$

$$\lambda_c = V\frac{\sin\alpha_c}{\Omega R} \tag{8d}$$

APPENDIX B

REFERENCES

1 Anon, "Attachment F. Frequency-domain Motion Cueing System Performance Test," *Doc 9625, Manual of Criteria for the Qualification of Flight Simulators*, Vol. I - Aeropl, ICAO, third edition, 2009.

2 Hosman, R. J. A. W., Advani, S. K., and Takats, J., "Status of the ICAO Objective Motion Cueing Test," Flight Simulation Research, New Frontiers, Conference Proceedings, 2012.

3 Advani, S. K. and Hosman, R. J. A. W., "Revising Civil Simulator Standards - An Opportunity for Technological Pull," Proceedings of the Modeling and Simulation Technologies Conference, 2006.
doi: 10.2514/6.2006-6248

4 Sinacori, J. B., "The Determination of Some Requirements for a Helicopter Flight Research Simulation Facility," Technical report, NASA Ames Research Center, Moffet Field, CA, 1977.

5 Advani, S. K., Hosman, R. J. A. W., and Potter, M., "Objective Motion Fidelity Qualification in Flight Training Simulators," Proceedings of the Modeling and Simulation Technologies Conference, 2007.
doi: 10.2514/6.2007-6802

6 Hosman, R. J. A. W. and Advani, S. K., "Are Criteria for Motion Cueing and Time Delays Possible ? Part 2 . Manual of Criteria for the Qualification and Testing of Flight Simulation Training," Proceedings of the Modeling and Simulation Technologies Conference, 2013.

7 Hosman, R. J. A. W. and Advani, S. K., "Design and Evaluation of the Objective Motion Cueing Test and Criterion," *The Aeronautical Journal*, Vol. 120, (1227), 2016, pp. 873–891.

8 Stroosma, O., "Applying the Objective Motion Cueing Test to a Classical Washout Algorithm," Proceedings of the Modeling and Simulation Technologies Conference, 2013.
doi: 10.2514/6.2013-4834

9 Seehof, C., Durak, U., and Duda, H., "Objective Motion Cueing Test - Experiences of a New User," Proceedings of the Modeling and Simulation Technologies Conference, 2014.
doi: 10.2514/6.2014-2205

10 Reid, L. D. and Nahon, M. A., "Flight Simulation Motion-base Drive Algorithimns: Part 1-Developing and Testing the Equations," Technical Report 296, UTIAS, Toronto, 1985.

11 Meiry, R. L., "The Vestibular System and Human Dynamic Space Orientation," Technical report, Massachusetts Institute of Technology, Man-Vehicle Lab, Boston, MA, 1966.

12 Hodge, S. J. and White, M. D., "Challenges in Roll-Sway Motion Cueing Fidelity : A View from Academia," Royal Aeronautical Society Flight Simulation Group Conference on "Challenges in Flight Simulation", 2015.

13 Wiskemann, C. M., Drop, F. M., Pool, D. M., van Paassen, M. M., Mulder, M., and Bülthoff, H. H., "Subjective and Objective Metrics for the Evaluation of Motion Cueing Fidelity for a Roll-Lateral Reposition Maneuver," Proceedings of the 70th American Helicopter Society International Annual Forum, 2014.

14 Anon, *ADS-33E-PRF, Aeronautical Design Standard Performance Specification Handling Qualities Requirements for Military Rotorcraft*, United States Army, Redstone Arsenal, Alabama, 2000.

15 Padfield, G. D., *Helicopter Flight Dynamics : The Theory and Application of Flying Qualities and Simulation Modeling.*, John Wiley & Sons., Washington, DC, 2007.

16 Bramwell, A. S. R., "Rotor forces and choice of axes," *Bramwell's Helicopter Dynamics*, edited by G. Done and D. Balmford, Butterworth-Heinemann, second edition, 2001, pp. 26–28.

17 Hoblit, F. M., *Gust Loads on Aircraft: Concepts and Applications*, AIAA, Washington, DC, 1988, pp. 42–44.

18 Perfect, P., White, M. D., Padfield, G. D., Erdos, R., and Gubbels, A. W., "A Rating Scale for the Subjective Assessment of Simulation Fidelity," *The Aeronautical Journal*, Vol. 118, (1206), 2014, pp. 953–974.

19 Atencio, A. J., "Fidelity Assessment of a UH-60A Simulation on the NASA Ames Vertical Motion Simulator," Technical report, NASA Ames Research Center, Moffet Field, CA, 1993.

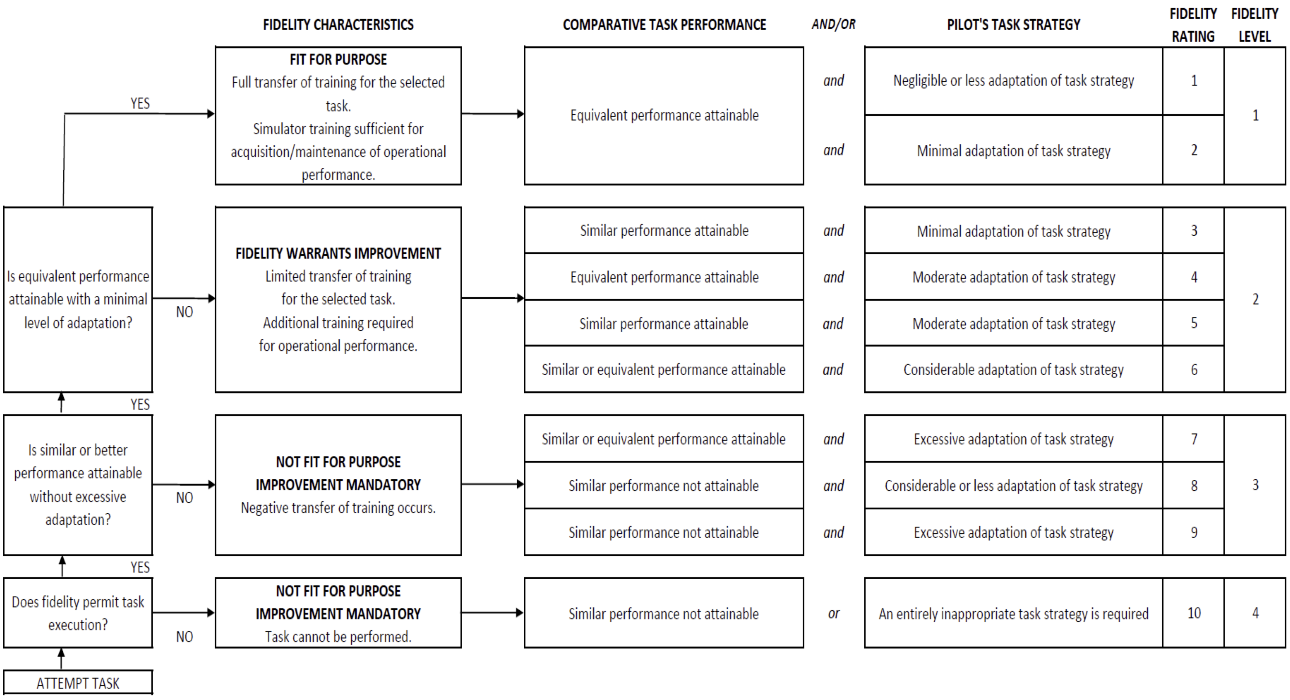

Fig. 28: Simulation Fidelity Rating scale, used for subjective evaluation of motion fidelity, taken from Ref. 20.

20 Beard, S. D., Reardon, S. E., Tobias, E. L., and Aponso, B. L., "Simulation System Fidelity Assessment at the Vertical Motion Simulator," Proceedings of the 69th American Helicopter Society International Annual Forum, 2013.

Part II

Revised Chapters from the Preliminary Report

Chapter 2

Literature Review on Simulation Fidelity

This first part of this preliminary report discusses different methods for evaluating motion fidelity. Its purpose is therefore to study the state of art the in the field of motion cueing fidelity research by means of a through literature review.

For this literature review, special attention is paid to the implementation of an objective motion cueing test in this field, especially for the use of evaluation helicopter simulations. The main question was identified as follows:

> What is the present state of research in the field of **simulator motion fidelity** and can an **Objective Motion Cueing Test** contribute to an improvement of simulator fidelity evaluation in the **helicopter domain?**

The proposed research question touches upon the concept of simulation fidelity, as well as different assessment methods. However, knowledge is needed of the motion cueing system to understand different assessment methods. Therefore, this literature review can be split into several different chapters. Firstly the concept of simulation fidelity will be explored in section 2-1. Thereafter, the characteristics of different motion cueing systems will be discussed in section 2-2. Thirdly, different evaluation methods will be discussed in section 2-3. Thereafter standard procedures in the industry will be discussed in section 2-4, where simulator certification will be treated.

Each subtopic for the proposed research question will begin with an introduction stating question for that particular topic. The literature survey will be concluded with a result and a conclusion section, to reflect on the research question.

2-1 Flight Simulation Fidelity

The concept of flight simulation fidelity is important in the discussion about motion cueing evaluation, since it narrows down the scope of this thesis. The subquestion that is to be

Figure 2-1: Air France Simulator of the A320, in use at the Air France training centre in Toulouse, France.

answered for this chapter is the following:

> What is the concept of simulation fidelity and how does it relate to fitness-for-purpose and simulator certification?

To relate fidelity to fit-for-purposes, it is important to know the functions of flight simulation and flight simulators. Therefore this will be discussed first, in subsection 2-1-1. Thereafter the main terms used in this thesis are stated in bold and subsequently explained in subsection 2-1-2.

2-1-1 The Use of Fight Simulation

The use of flight simulators was clear from the beginning of aviation. Flight simulators were made as far back as 1910, in the form of the early Link trainer, [1]. Apart from recreational purposes, there can be distinguished a number of uses for flight simulation and flight simulators. They boil down to four categories, as identified by [15]: 1. Training, 2. Systems and equipment design, development test and evaluation, 3. Research on human performance and 4., licensing and certification.

1. **Training**
   The very first flight simulators were developed for educational purposes, that is, the training of pilot students. It's primary objective is therefore the **Transfer of Training (ToT)**. Trainers were made from the beginning of aviation, as was stated in the preceding. However, only in the 1950's did large airlines kick start the industry by ordering simulator to train their pilots. The first simulators from this era did not have a visual system and were therefore primarily IFR training devices. The first visual system was a point-light source projection. This worked well for helicopter simulators, since their ground velocity was low. Later also the first motion platforms were introduced and by 1969, the first 6 DOF motion simulators were taken into service by the airlines. Nowadays, most training simulator use a dome-like structure to produce the visual, and a hexapod motion system to convey motion cues to the pilot. A good example of such a simulator is depicted in Figure 2-1
   The following advantageous of training simulators can be distinguished [2], [16].
   - Full Fight Simulators provide environment to train with a **reduced risk**. A student can practice basic piloting maneuvers without the risk of crashing the aircraft.

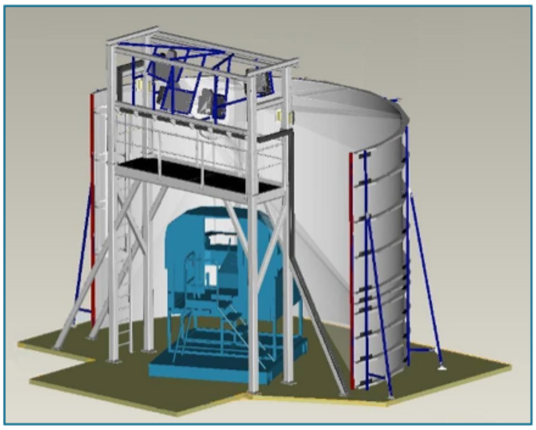

Figure 2-2: Illustration of the HPS at the Netherlands Aerospace Centre.

- It can readily be seen that conducting training in a simulator is **more cost efficient** than flying the actual aircraft. However, this difference in cost is less significant for helicopter simulators. The reason for this is twofold. First, there are simply less helicopter pilot students as the rotorcraft fleet is smaller. Furthermore, the difference in cost of a helicopter training and a simulator training is smaller than for a fixed-wing simulation, since the operating costs of a helicopter are less than for for example a passenger transport aircraft.
- The pilot student is able to **fly maneuvers that would not be allowed in the aircraft**. This means that they can explore area's of the flight envelope, that are not desirable to fly in under normal operational conditions, e.g. upset recovery training. It should be noted however, that the behavior of the aircraft is hard to validate for these kind of maneuvers. Upset recovery training not common in helicopter full flight simulators. For military pilots this means that they get a chance to practice flying close to terrain for example, when it is not desired by the public or that can threaten strategic and tactical secrecy [2].
- Furthermore, **training effectiveness** can be increased by to option to start the simulation anywhere in a particular the mission with the preferred weather conditions. Simulator can for example be used to train pilots for icing conditions, when they do not encounter them regularly. Furthermore, simulators allow the option to playback events to provide better feedback to the student on their piloting skills.
- Simulators **reduce carbon emissions and the noise footprint** of air traffic considerably.

2. **Design**
   The primary objective of a simulator used for the design, development and evaluation of e.g. cockpit instruments and Augmented Fight Control Systems (AFCS) is **reliable and valid data**. Most R&D simulators incorporate a motion system. However, if the design does not require evaluation using a pilot-in-the-loop experiment or if the pilot is not subject of interest, motion system are not always the obvious choice. An example of a R&D helicopter simulator is the Helicopter Pilot Station (HPS) at the Netherlands Aerospace Centre (NLR). This simulator is primarily used for the testing of new helicopter models or cockpit systems.
3. **Research on Human Performance**

Figure 2-3: Illustration of the Simona Research Simulator (SRS) at the faculty of aerospace engineering at Delft University of Technology (DUT).

The primary objective of a simulator used for research on human performance is also **reliable and valid data**. However, research has shown that experience pilots have a better performance when flying in motion-based simulators as opposed to fixed-base simulators,[17]. Therefore, for research in human performance, a motion system is a fundamental requirement. A good example of a research simulator designed for human-in-the-loop experiments in the Simona Research Simulator (SRS), shown in Figure 2-3

4. **Licensing and Certification**
   Lastly, simulators are used to fully certify pilots for a type of aircraft. This means that under current regulations it is possible for a pilot to obtain a type rating for a specific type of aircraft without ever having flown in that aircraft. Certification and licensing is typically done in the same simulators as described in item 1.

2-1-2 The Concept of Fidelity

There are numerous definitions about simulation fidelity used in literature. However, for this thesis the definition according to Pool is used:

The concept of fidelity, is the extend to which the simulation is capable of reproducing the the in-flight environment and experience.[18].

Fidelity therefore compares the simulation to the situation in the aircraft and it can be applied to every component of the flight simulator. However, the simulator and aircraft response are not only based on the dynamics of the aircraft, but also on the pilot and the sensors provided by the aircraft and the simulator. Fidelity can therefore be evaluated at different points in the pilot-in-the-loop structure. The basic structure of a human-machine interaction consists of three components, as in illustrated in Figure 2-4. Firstly there is the system, or here indicated as the aircraft response. Secondly there is the human operator, or in this case the pilot. Lastly there are the cueing system that rely information about the system to the operator. The resulting system forms a human-in-the-loop structure, as is indicated by the feedback loop in Figure 2-4.

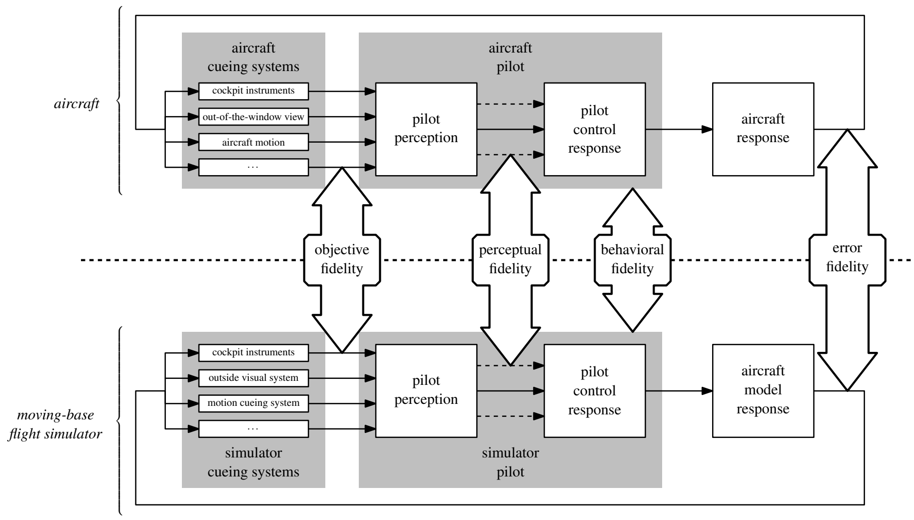

Figure 2-4: Four different types of fidelity as described in [18]

In this loop, fidelity can be measured at four different places. In the following these fidelity types are discussed, starting with the output of the sensors.

- **Objective Fidelity**
  Firstly there is objective fidelity. Objective fidelity refers to the extent to which the simulator resembles the aircraft by comparing parameters that can be objectively measured from the cueing systems.
- **Perceptual Fidelity**
  However, certification describes fidelity also from a perceptual point of view. Perceptual fidelity is the difference in perceived cues by the pilot in both the aircraft and the simulator. This type of fidelity is often measured subjectively and in therefore also referred to as **subjective fidelity**.
- **Behavioral Fidelity**
  Thirdly, it is also possible to study pilot behavior. This can be done by directly quantifying the control input. Secondly this can be done objectively by modeling the pilot.
- **Error Fidelity**
  Error fidelity compares the aircraft response to the simulator response directly after the system output. This type of fidelity specifically pertains to task performance. An exemple of error fidelity is the validation of mathematical models to describe the aircraft dynamics. However, model validation will not be the focus of this literature review, since it is not a pilot-in-the-loop process

Fidelity vs. Fitness-For-Purpose

The concept of motion fidelity is closely related to the concept of fit-for-puposeness. However, the two entities are often confused. Whereas fidelity deals with the accuracy with which the aircraft cues can be relayed to the pilot in the simulator, fitness-for-purpose describes the extend to which the simulator performs its job for which it was designed. Often, fitness-for-purpose and fidelity lead to similar design decisions. This is particularly true for the research simulator, where control performance is studied in human-in-the-loop experiments. It is of paramount importance here that the simulator represents the aircraft environment as well as possible, such that the results obtained in the simulator can be extrapolated to the real aircraft. However, for training simulators, the end goal is to prepare the pilot to make the correct control input in particular situation in the real aircraft. Therefore a full flight simulation is therefore not always desired, as it can distract the student from the task that is being taught. In those instances, the interests of fit-for-purposeless do not align with those of fidelity. It will be shown that in the fitness-for-purpose vs. fidelity discussion, especially the motion system is still a topic of debate.

2-2 Motion Cueing Systems

Before focus is put on the evaluation of the motion cueing system, it is relevant to discuss the characteristics of the motion cueing system first. The pilot perceives motion through a multitude of sensors.

- **Visually**
  Firstly the pilot can detect motion visually through either the instruments available in the cockpit to him, or changes in the outside view of the aircraft.
- **Vestibularly**
  Secondly, the pilot perceives motion through his vestibular organ, which consists of two parts. Firstly there are the otoliths, which are essentially a sensor for specific forces. Secondly there are the semicircular canals, which are a sensor for angular accelerations. This thesis focuses on the motion as perceived by the vestibular system.
- **Proprioceptively**
  Thirdly motion can be sensed by proprioceptively, that is by the contact forces and the change in contact forces on the body. For example, as the aircraft experiences high g-loads, the contact forces on the body of the pilot will also change.
- **Haptically**
  Lastly, motion can also be relaid to the pilot used haptical feedback on the control input devices in the cockpit.

The motion perception important to manual control, which is on a frequency range from 1-5 [rad/s], is mostly obtained though a combination of the visual organ and the vestibular organ. There has been a large discussion in the academic world about whether the input of the vestibular organ is needed for different simulator purposes. In the late 1990's and early 2000's, Burki-Cohen conducted many motion/no motion related experiments. However, a hard conclusion was not reached, [19], [20].

The need for motion depends on the simulator purpose and the task that is being simulated. McCauley concluded in 2006 that there is no hard scientific evidence to support the use of motion for training simulators, [16]. However McCauley concluded as well that motion is essential for pilot acceptance of the simulator. However, it can be stated that motion is essential when simulating a manual skill-based control task, [21].

Motion system can be divided into two categories. Firstly there are systems that move the whole simulator, of which the Stewart platform is the most commenly used example. For simulators used to simulate helicopter motion, a vibration platform is also sometimes used to

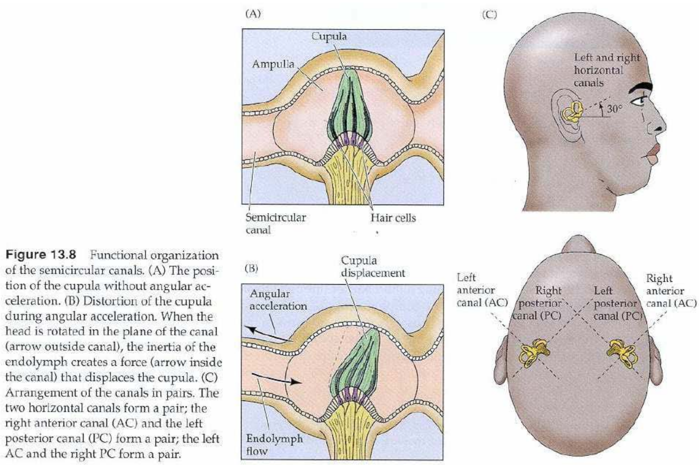

Figure 2-5: Position and working the semicircular canals, [22].

simulate higher frequency vibrations. These type of simulators rely motion proprioccepticaly and vestibularly. Secondly there are proprioceptive simulators, of which the g-seat is a good example. These simulate motion by changes the contact forces on the body of the pilot.

This chapter will discuss the characteristics of a hexapod Stewart platform motion cueing system, with the following research questions:

What are the characteristics of the motion cueing systems commonly used in the industry?

- How do motion cueing system make use of the limitations of the human vestibular system?
- What types of cueing algorithms are used?
- What are the major advantages/disadvantages of those cueing systems?

This chapter will be split into three sections. The design and cueing algorithm of the Stewart platform is based on the vestibular perception of motion. The vestibular system will therefore be discussed first in subsection 2-2-1. Thereafter the hexapod motion cueing system will be discussed in subsection 2-2-2. Finally, available cueing algorithms will be treated in Figure 2-10.

2-2-1 Vestibular System

As stated, the human vestibular system has two types of sensors, located at the inner ear. Firstly there are the semicircular canals, which give a cue for the rotational acceleration. Similarly to a gyroscope, each inner ear has three semicircular canals. There is one located horizontally inclined 30° to detect yaw, and two positioned vertically to detect pitch and roll acceleration. Figure 2-5 shows the positioning of the semicircular canals.

A semicircular canal is filled with fluid that is stagnant in rest and at constant rotational velocity. However, when the head experiences a rotational acceleration, the fluid start rotating and causes a little sensor, called the cupula to move in the direction of the velocity of the flow. This movement is converted to an electrical impulse to the brain.

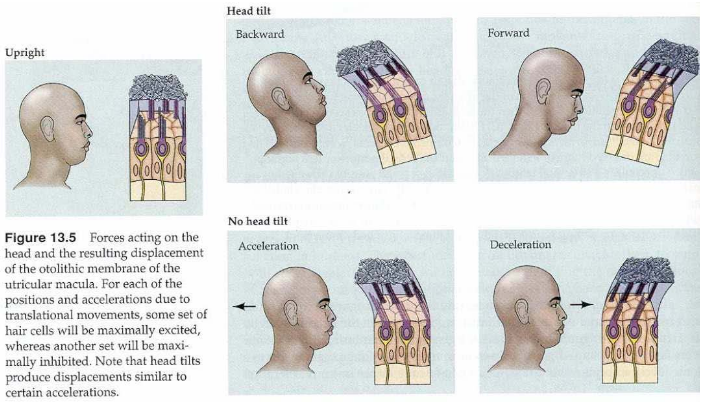

Figure 2-6: Working of the otoliths, [22].

Secondly, there are the otoliths, that measure specific force. Figure 2-6 shows the working principle an otolith. As can be seen an otolith consist of a membrane that moves independently form the cells located below the membrane. Haircell then measure the position of the membrane.

As can be seen from Figure 2-6, since the otolith measure specific force, there is essentially no difference between an acceleration and or a backwards rotation of the head, since the membrane behaves similarly in both cases. Linear acceleration or deceleration can therefore be simulated by tilting the pilot backwards and forwards respectively. This is an important result, that will be exploited in subsection 2-2-3.

Since both the otoliths and the semicircular canals are essentially sensors, a transfer function can be constructed to visualize their performance. It was found that the performance of the otoliths resembles Equation 2-1 and the performance of the semicircular canals resembles Equation 2-2.

$$H_{OTO} = \frac{1+s}{(1+0.5s)(1+0.016s)} \tag{2-1}$$

$$H_{SSC} = \frac{s(1+0.11s)}{(1+5.9s)(1+0.005s)} \tag{2-2}$$

At frequencies used for manual control (1-5 rad/s) the semicircular canals practically behave as a rate sensor, as can be seen from Figure 2-7a. However, at low frequencies an high frequencies, the bode plot resembles an acceleration sensor, as can be seen from the positive slope of the gain plot in Figure 2-7a at frequencies lower than 10^0 [rad/s] and higher than 10^1 [rad/s].

Figure 2-7b resembles a bode plot of the otoliths. Thresholds have been identified at $0.1°/s$ to $0.5°/s$ for angular velocities and $0.05m/s^2$ for the specific force.

2-2-2 Hexapod Motion System

The Hexapod Motion Cueing Platform is a special type of Steward platform, using 6 actuators to change the position of the simulator cockpit with respect to the ground. This type of system

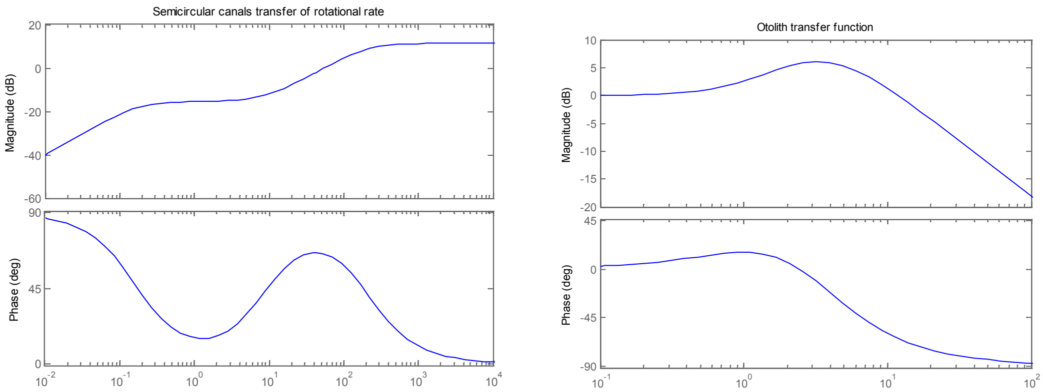

(a) Bode plot of the semicircular canals, [22]. **(b)** Bode plot of the otoliths, [22].

Figure 2-7: Transfer functions of the vestibular system.

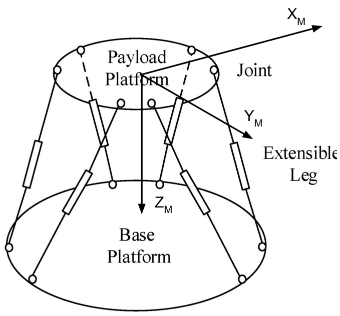

Figure 2-8: Schematic representation of a steward platform using 6 actuators.

is used for level D training simulators. Figure 2-8 shows a schematic representation of the hexapod system. With a system shown in Figure 2-8, motion in 6 degrees of freedom can be achieved. These degrees of freedom (DOFs) are characterized in a frame of reference fixed to the simulator platform, indicated here by the symbol M. The degrees of freedom are indicated as follows:

- Surge, motion in x-direction.
- Sway, motion in y-direction.
- Heave, motion in z-direction.
- The Euler angles ϕ, θ, ψ, similar to aircraft rotations

The geometry of the platform and the positioning of the points where the actuators attach, the upper gimbal points (UGPs) and lower gimbal points (LGPs), is determined by optimizing the motion space of the center of the upper gimbal circle. In robotics, an entire branch of research exists for the study of the geometry of steward platforms.

2-2-3 Classical Washout Algorithm

The motion of the aircraft cannot be fed directly into the platform, since there exists a limited amount of actuator space. An idea to cope with this is to scale the motion such that the position of the simulator rests within its motion space. However, the resulting accelerations

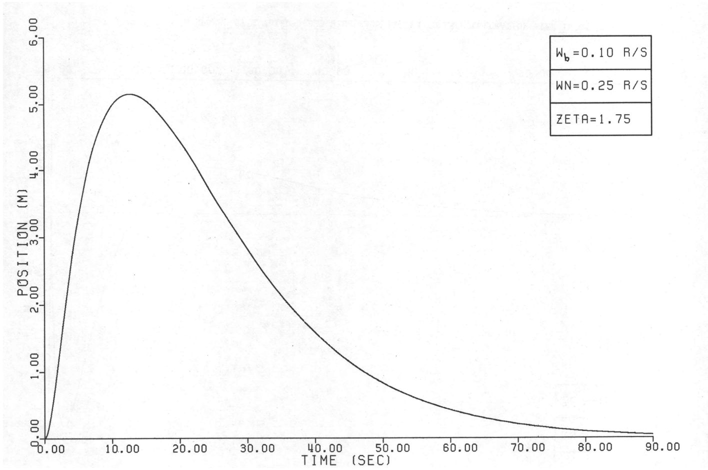

Figure 2-9: Example third order filter response to an acceleration step input, [23].

and specific forces would be far below the thresholds of the otoliths and the semicircular canals, such not yielding in a convincing simulation. Reid and Nahon, therefore came up with the idea to use both scaling and a washout filter to relay the motion, [23].

A washout filter is a third or second order high pass filter that steers back the position of the simulator to its original value, thereby optimizing the use of it workspace. A washout filter has a structure according to Equation 2-3.

$$TF = \frac{s^3}{(s^2 + 2\zeta\omega_n s + \omega_n^2)(s + \omega_b)} \tag{2-3}$$

If such a filter is applied to a step input in acceleration, the response is according to Figure 2-9.

Applying such a filter to each degree of freedom results in a set of three filters for the translational channel and a set of three filters for the rotational channel. Taking into account that the input are scaled first, this yields a classical washout filter, illustrated by the flowchart in Figure 2-10.

For sustained acceleration the platform makes use of the fact the the specific force measured by the otoliths can also be simulated by a rotation. This results in a third channel. By means of a low pass filter, sustained translational accelerations are converted to a suitable "tilt angle" of the simulator. The resulting scheme has three channels and uses both scaling a set of filter to modify the input for the simulator. The filters are in practice second order instead of third order. This is because of the presence of the tilt coordination channel.

2-3 Motion Fidelity Assessment Techniques

This section gives an overview of different simulator fidelity assessment techniques, related to the different types of fidelity, as describe in [18]. The question to be answered is therefore:

Which techniques are identified in literature to evaluate simulator fidelity and what are their benefits and drawbacks?

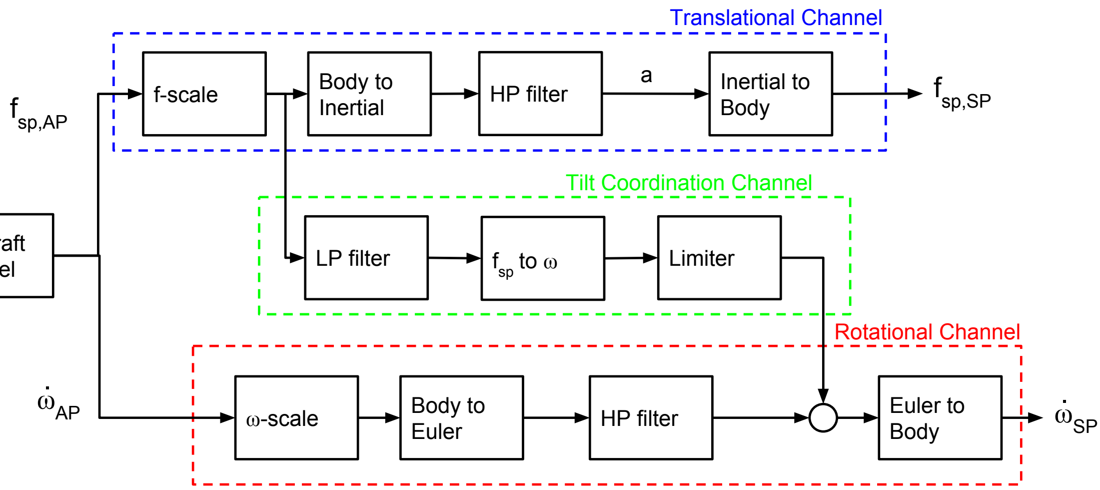

Figure 2-10: Classical washout algorithm as implemented in the Simona, adapted from Reid and Nahon, [23].

This chapter gives an overview of fidelity assessment techniques identified by literature, structured according to Figure 2-11. Figure 2-11 shows the same figure as was presented in section 2-1, but with different types of fidelity assessment techniques. Methods are divided in objective assessment, indicated in red, and subjective assessment, indicated in blue.

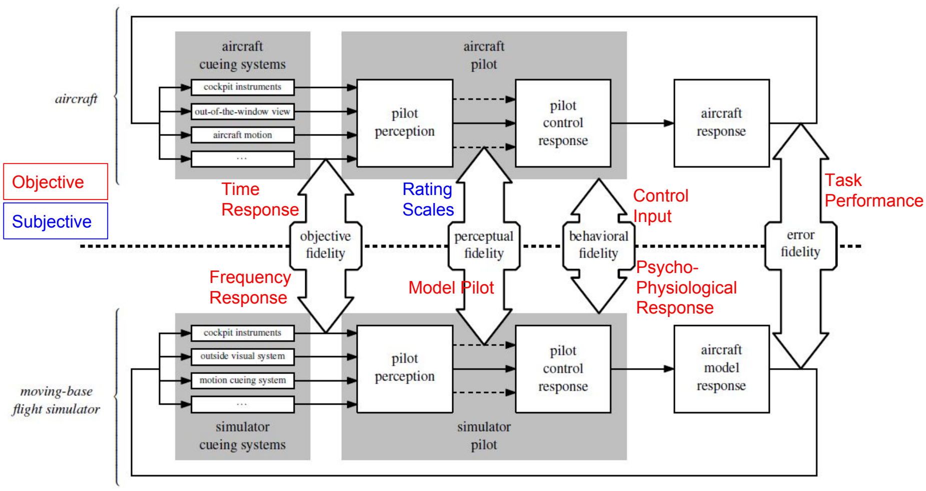

Figure 2-11: Four different types of fidelity as described in [18], connected to different methods of assessment.

As can be seen from Figure 2-11, different methods of assessing fidelity have been linked to the appropriate type of fidelity. subsection 2-3-1 and subsection 2-3-2 discuss the main methods testing the objective fidelity by treating the Sinacori-Schroeder Criterion and the OMCT respectively. In subsection 2-3-5 and subsection 2-3-3 perceptual fidelity is investigated by looking at modeling the pilot and pilot rating scales. Thirdly, the control input will be discussed in subsection 2-3-4 and task performance will be discussed insubsection 2-3-6. Assessment methods are indicated in **bold**.

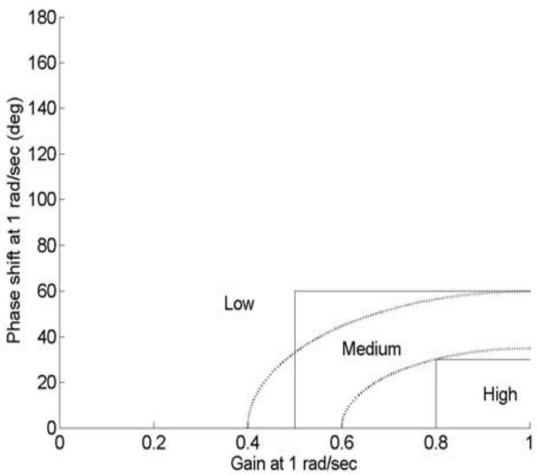

Figure 2-12: Sinacori criteria for motion fidelity, given by the square regions, together with the Schroeder criteria, given by the elliptical regions. Figure modified from [26].

2-3-1 Sinacori-Schroeder Criterion

To study the difference between the motion of the aircraft and the motion simulator directly, either a comparison can be made in the time-domain or in the frequency domain. The main topic of this thesis, the Objective Motion Cueing Test is objective assessment method for objective fidelity in the frequency domain. Most certification is based on the technique presented in this section. For the time-domain, **physical limits** such as maximum deflections and rates, have been defined in the certification specification FSTD(H), [24] and will be discussed in more detail in section 2-4.

However, most fidelity metrics are based on fidelity assessment methods in the frequency domain and have to do with the phase delay and bandwidth of the motion base. Historically filters were tuned using subjective pilot input. However, Sinacori recognized in 1977, [6], that if the simulator response has a gain of 1 and 0 phase delay, the motion of the simulator is identical to the aircraft and the motion fidelity is therefore of high quality. He defined therefore regions for the phase delay and motion gain, that give high, medium and low fidelity, with a maximum phase and gain limit for a specific level of fidelity, Figure 2-12.

Schroeder expanded upon the research of Sinacori by modifying the criteria somewhat in 1999, [25], resulting in the **Sinacori-Schroeder criteria**, shown in Figure 2-12. In Figure 2-12, the motion base gain at a frequency of 1 rad/s on the x-axis and the phase delay at 1 rad/s is on the y-axis is shown. 1 rad/s was chosen, since the human operator is mostly active around that frequency area.

Figure 2-12 defines three regions of fidelity. Table 2-1 gives the definition for the low, medium and high fidelity regions respectively.

Tuning can be simplified by connecting the phase and gain limits defined by Sinacori-Schroeder to the available motion space. Gouverneur performed tuning on the SRS, using these available motion space boundaries,[26]. Figure 2-13 shows the design space that results, where each point in blue is a specific combination of break frequency and gain of the motion filters.

Table 2-1: Definitions for three fidelity regions according to [25]

Fidelity Rating	Definition
Low	Motion sensations are noticeably different from flight, and objectionable.
Medium	Motion sensations are noticeably different from flight, but not objectionable.
High	Motion sensations are like those of flight.

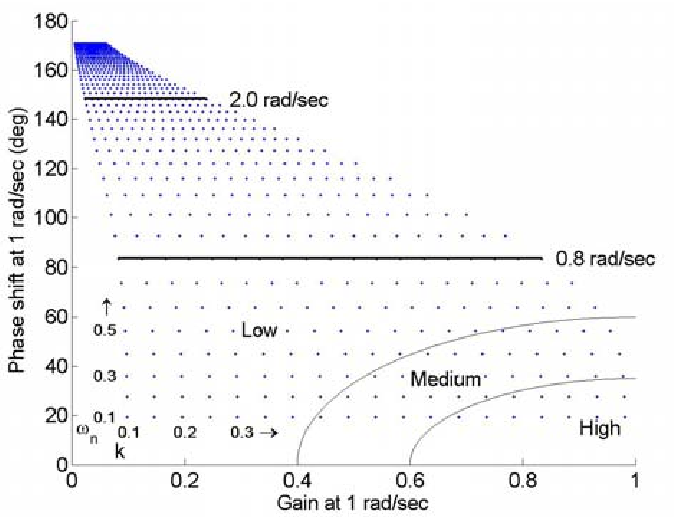

Figure 2-13: Available motion space boundaries, [26].

For each point in blue, it was checked if the simulator stayed inside its workspace for three maneuvers. It can be seen that for a more aggressive maneuver, the achieved boundary line lies at a high phase difference and lower gain. This indicates that for higher specific forces and rotational accelerations, the achievable fidelity is lower.

2-3-2 Objective Motion Cueing Test

In 2006, an objective assessment technique for the motion cueing fidelity was proposed by Advani and Hosman in [5], since the Royal Aeronautical Society started revision of the ICAO simulator document that year. Three research centers performed the proposed objective motion cueing test and results were published in [7]. It was found that between the three research institutes: UTIAS, JAXA and TsAGI, there were significant differences between the dynamic characteristics of the motion cueing system. This was considered remarkable since two of the three research institutes are renowned for their research into motion cueing. After this, the proposed test was amended in Attachment F of the ICAO manual 9625, [4]. In 2009 the OMCT was published furthermore in the fourth edition of the Aeroplane Flight Simulation Training Device Evaluation Handbook, by the Royal Aeronautical Society [27].

To further evaluate the OMCT, 7 more research facilities participated and performed the OMCT on their simulator. Results have been published in [8]. In [8], an attempt was made to asses if a criterion could be possible to judge simulator motion cueing fidelity based on the OMCT. It was found that the Sinacori Schroeder criterion, [28] does not cover the entire frequency range of the OMCT and that a larger requirement is both possible and necessary.

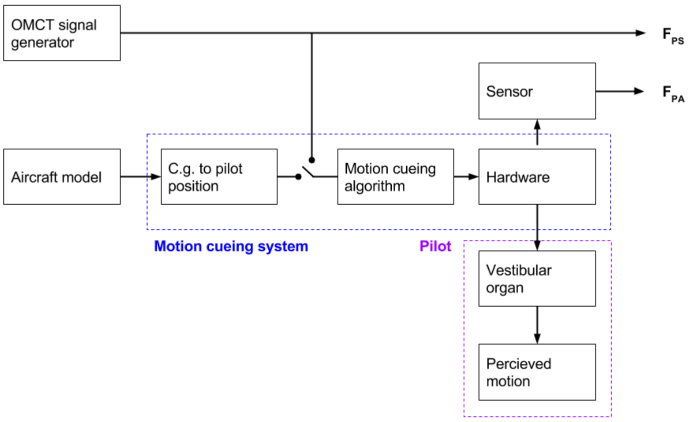

Figure 2-14: Generic flowchart of the motion cueing system for pilot-in-the-loop simulation and for the OMCT.

Input axis of aircraft	Output axis of simulator					
	Roll (P)	Pitch (Q)	Yaw (R)	Surge (X)	Sway (Y)	Heave (Z)
Roll (P)	3				4	
Pitch (Q)		1		2		
Yaw (R)			5			
Surge (X)		7		6		
Sway (Y)	9				8	
Heave (Z)						10

Figure 2-15: OMCT input and output channels as specified in [8].

Besides looking at the differences between the outcome of the OMCT for different simulators and confirming the need for of the OMCT by pointing out differences between respectable simulators, an attempt was made by Hagiwara in 2008, [29], to evaluate the OMCT by comparing it to the gain and phase margins for a series of pilot in the loop experiments for different settings of the motion filter. It was found that the phase margin was indeed influenced by the test set-up, but the phase margin could not be correlated to the OMCT results sufficiently.

The OMCT is intended as end-to-end test, meaning that it studies the difference between cockpit motion and simulator motion at the position of the pilot in the simulated aircraft in the frequency domain. Figure 2-14 shows a generic flowchart of the OMCT.

In the OMCT, the motion at the cockpit of the aircraft is replaced by a set of artificial sinusoids from a signal generator. The simulator motion is then measured directly form the cockpit by means of a sensor, and compared in frequency domain to the original signal from the OMCT signal generator, [9]. For every axis (6 for a generic 6 DOF hexapod MCS), there are 12 sinusoids prescribed, with a specific amplitude and frequency, ranging from 0.1 [rad/s] to 15.8 [rad/s].

These input signals are then used as input for different simulator axes. It was chosen to test 10 combinations, according to Figure 2-15. It can be seen that tests on the diagonal of Figure 2-15 show single axis response of simulator motion. However, there are also present four test which test the simulator motion cueing for cross-talk between the surge and sway channels and the pitch and roll channels respectively. The result of the OMCT is a frequency response plot, in the form of Bode- or a Nyquist diagram.

The main advantage of the OMCT is that is repeatable, meaning no pilot judgment is needed. Furthermore the test is relatively easy to set up, since it is an end-to-end test. However, there can be identified some drawbacks:

- Firstly and most importantly, the OMCT assumes that the motion input is similar for all maneuvers/aircraft types. However, motion cueing depends on the specific aircraft and task element to be simulated, according to subjective pilot ratings, [30].
- No requirements exist for acceptable and unacceptable differences between simulator output and input exist, [8]. However, an effort is made to bundle results from the evaluation of industry and research simulators to come up with a 'best practice'.
- The input signals for the OMCT make assumptions on the aircraft motion.
  - Decoupling of the input of specific forces and accelerations is assumed, expect for the cross-coupling between pitch and surge and sway and roll, which are testing in test 2, 7 and 4, 9 respectively.
  - The amplitude of the OMCT signals is assumed to be 1 $[m/s^2]$ for the specific forces and 1 [rad/s] for the rotational velocities.
  - There is a limited range of frequencies, being 0.1 [rad/s] to 15.8 [rad/s]. Especially for rotorcraft, vibrations higher than 15.8 [rad/s] are to be expected. These vibration are important for pilot experience and the recognition of certain events, e.g. blade stall or buffer limits. However, vibrations in this frequency range are not directly used for controlling the state of the aircraft. The influence of this assumption is therefore unclear.
  - Based on fixed-wing aircraft dynamics, an uncoordinated pitch and a coordinated roll is assumed. The practical implementation of this assumptions is that for test 1 and 2, not only the pitch axis is driven, also an input according to the gravity, $g \sin \theta$, is fed into the surge axis.
- The data processing to convert time data into frequency domain data is prone to errors. An example is that leakage can occur if the simulation time is not properly adjusted to the frequency of the input sinusoid.

2-3-3 Pilot Fidelity Ratings

Another option would be let pilots fly in the simulator, and let them evaluate the motion cueing subjectively [13]. One of the first **pilot rating scales** was based on the Cooper-Harper rating scale for workload, the **Handling Quality Rating (HQR)** scale, [31].

The HQR is basically a flow chart which results in a handling quality metric. The basic idea behind this rating scale, is that if the simulator handles similarly to the real aircraft, the simulator resembles the aircraft closely and has therefore a good fidelity. Figure 2-16 shows a handling quality rating scale.

Evaluating the simulator requires the pilot to fill out two forms, leaving the simulator engineer to make a comparison. Hodge therfore developed a rating scale to assess fidelity of simulators directly, the Motion Fidelity Rating scale or **MFR**. As shown in Figure 2-17, This rating scale directly results in a metric assessing simulator fidelity [32].

A problem with the reasoning of both the HQR and the MFR, is that the HQR only evaluates fitness-for-purpose as if the simulator was an actual aircraft. However, the purpose of the simulator is often very different.

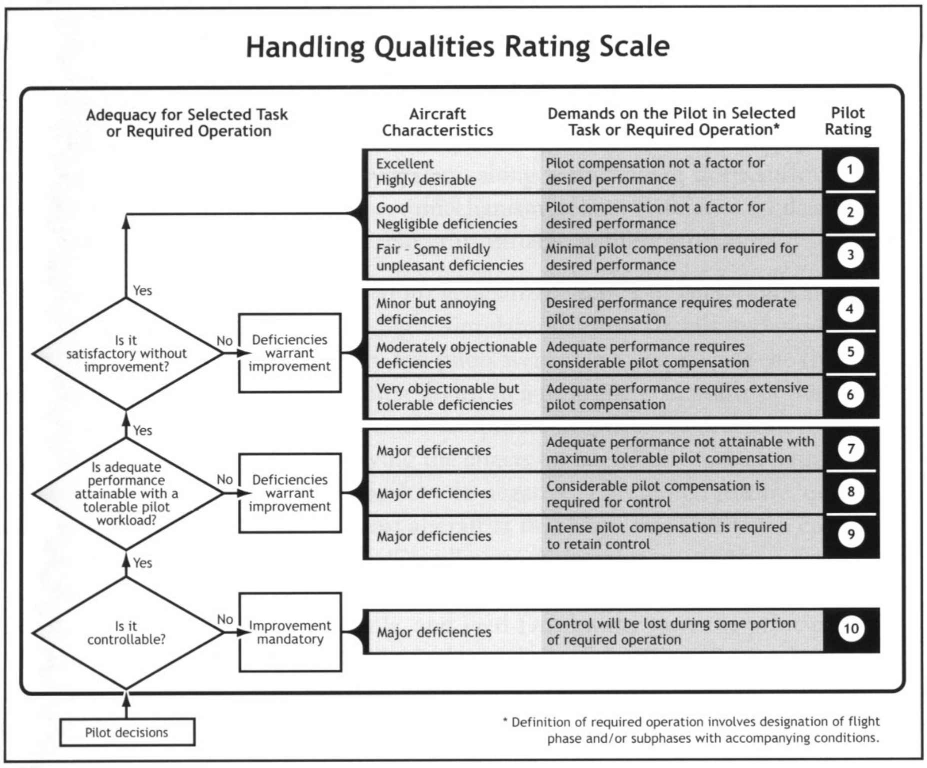

Figure 2-16: Handling Quality Ratings as defined by Cooper and Harper, [31].

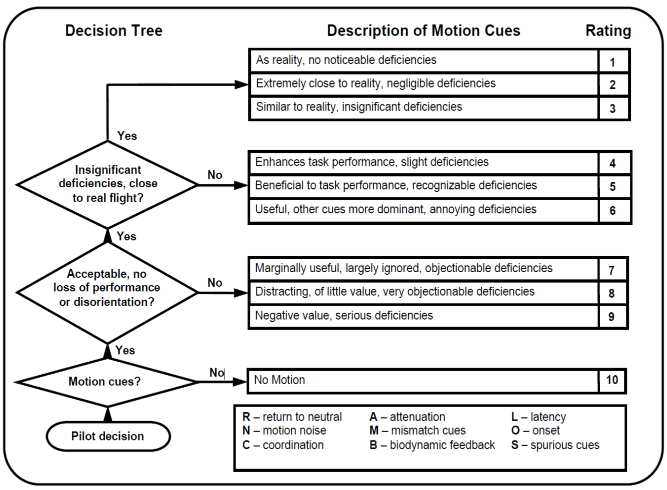

Figure 2-17: Motion Fidelity Rating Scale developed by the University of Liverpool, [32].

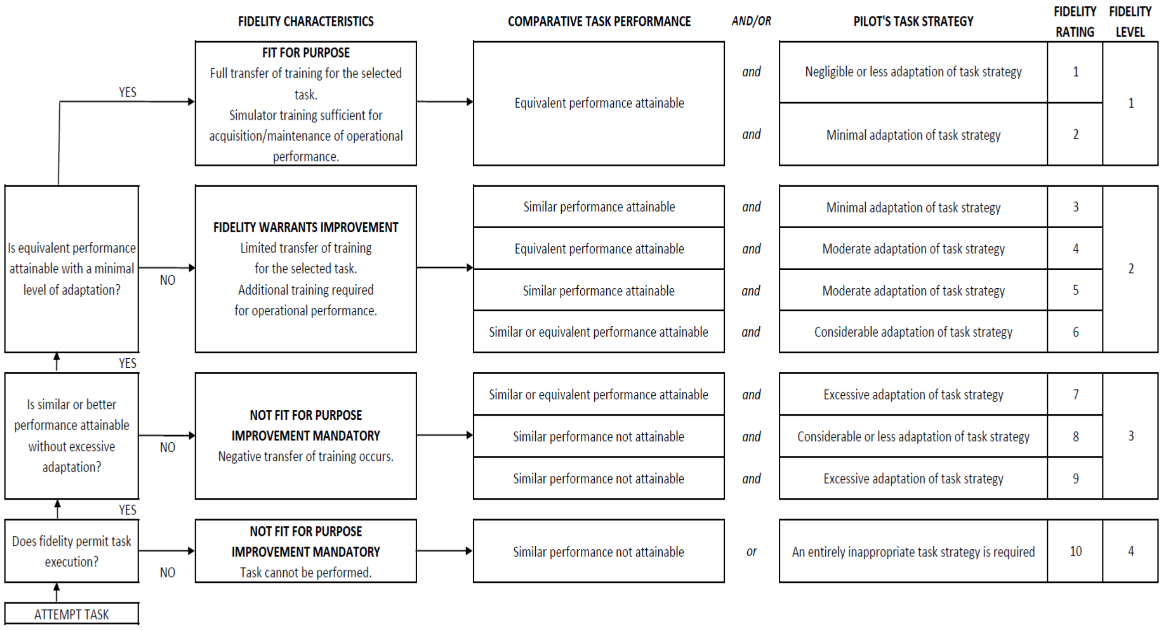

Figure 2-18: Simulator Fidelity Rating scale, [34]

An attempt was made, during the lifting standards project, [33], to develop a subjective metric with a better distinction between fidelity and fitness-for-purpose. The result was a metric shown in Figure 2-18.

From Figure 2-18, it can be seen that there are indeed two separate questions for the fidelity and the task performance of the pilot in the simulator. However, it does not distinguish between fidelity and fitness-for-purpose, it actually makes a dubious connection between the two .

Advocates of subjective assessment state that this form of fidelity assessment has key advantages over objective analysis. Firstly, subjective assessment uses knowledge of the experienced pilot. Since the interaction between the pilot and the system is of a very complex nature this knowledge is an advantage when evaluating fidelity. Secondly, subjective ratings help determine thresholds of acceptable and unacceptable fidelity levels.

2-3-4 Control Input Analysis

Behavior fidelity can be measured by studied the pilot control input to the system and by looking at the psycho-physiological response. A good example of the pilot psychological response is the **workload.** Measuring workload is usually done by means of a Cooper-Harper Workload rating scale. It is therefore a subjective assessment.

Secondly the **control input** of the pilot can be studied. Padfield et al. formulated a method in the time domain analysis the control input in 1994, [35]. The **Control Attack** method uses the total number of control deflections per maneuver, the average of the control rate per deflection and average of the amplitude per deflection as variables to quantify the pilot behavior. Some studies show that these metrics are in agreement with pilot opinion, [36].

Wiskemann e.a. found in 2014 however, that the control attack method was not always in agreement with pilot opinion [37]. Moreover, no criteria exist to judge differences in control behavior.

2-3-5 Modeling the Pilot

Besides objective fidelity, perceptual fidelity is also of large importance to this discussion. Since most simulators are for training purposed, the motion 'feel' is of great importance in simulator industry. A way to assess perceptual fidelity is by modeling the pilot. This way, the control strategy of the pilot can be evaluated. If the control strategy of the pilot is similar to that of a pilot in the simulator, than motion fidelity is assumed high.

The groundwork for modeling the pilot was done by McRuer in 1974, with the development of the crossover model, [38]. However, pilot models were first used to assess fidelity by Hess and colleagues in 1991, [39]. They used a **Structural Pilot Model** to identify problems in motion fidelity by investigating a bob-up and side-step maneuver. An advantage of this approach, is that difference in the motion cueing system are taken into account objectively:

It is not the differences [differences between the nominal and simulated vehicle dynamics]themselves, but their effect on piloting technique and pilot/vehicle performance that determines fidelity in such cases.[39]

The structural model however, does not take into account that for the inner control loop, motion can also be perceived visually. This is a downside of this approach. Furthermore, in real life, pilot control strategy changes based state variable of the aircraft, and is not constant in a single maneuver.

In an attempt take into account the latter drawback, Padfield developed the **Adaptive Pilot Model** in 2005 [40]. For this investigation, a rudimentary helicopter model was used to fly an acceleration/deceleration task, with a simplified model of the pilot. However, the parameters of the model were made dependent on the time to close on surfaces. The main drawback however, is that the adaptation of the model is highly dependent on the mission task. The adaptive pilot model is therefore hard to generalize.

More recently a **cybernetic approach** was used for assessing simulator fidelity by modeling the pilot. Figure 2-19 shows the general set-up of the pilot-vehicle model as used in the cybernetic approach.

As can be seen from Figure 2-19, the pilot model consist of a visual channel and a motion channel and is based on the pilot model devised by McRuer in 1974, [38]. The cybernetic approach determines the coefficients of this pilot model by a pilot-in-the-loop experiment using a steady-state tracking task. By comparing coefficients from simulator experiments to coefficients measured in real flight, as was done by Daan Pool in [18], pilot behavior in the simulator can be compared to pilot behavior in the real aircraft. A big advantage of the cybernetic approach is that it is an objective way to assess fidelity. However, the cybernetic approach has several drawbacks [17]. The cybernetic approach can only be used for steady-state tracking tasks, not for short-duration transient maneuvers. Also, the cybernetic approach does not model higher-loop control tasks as effectively as lower loop control tasks.

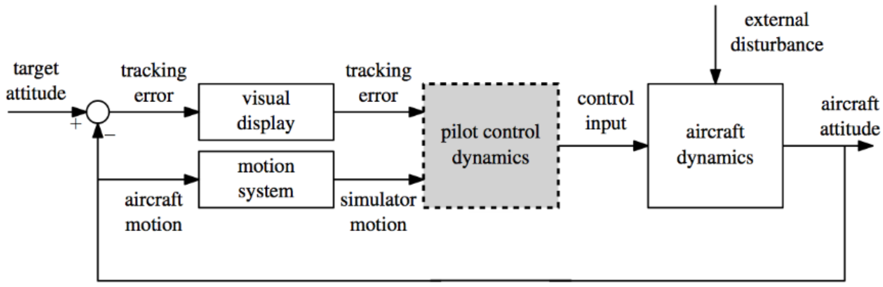

Figure 2-19: Flow chart of the simulated-pilot-in-the-loop structure for a manual tracking task, [17].

Nevertheless, identification methods have improved to allow for more realistic tracking tasks. The following drawbacks still remain:

- There are a limited amount of Degrees of Freedom that can be used.
- The pilot has limited freedom to select actual missions and task strategy.
- Lastly, during real flight, the pilot is able to look out of the window and acquire additional cues for the aircraft motion and attitude. The cybernetic approach does not provide a way to model these cues.

2-3-6 Task Performance

Finally, error fidelity can be used to evaluate total simulator performance. The reasoning behind this is that if the pilot is not able to achieve comparable performance in the simulator, the utility of the training device is in question. Two methods for evaluating error fidelity are identified.

Firstly, **Handling Qualities** are defined in ADS-33E-PRF, rotorcraft handling qualities for the american air force. ADS-33E-PRF prescribes requirements of aircraft responses to standard inputs: E.g.: step, doublet or frequency sweep. The handling qualities can also be applied to simulator performance. This way the simulator performance can be compared through a fixed set of rules to aircraft performance.

Secondly, task performance can be used to measure fidelity. Task performance is described accurately in ADS-33 for different **Mission Task Elements** (MTE's), [13]. An MTE consist of a prescribed maneuver, e.g. bob-up or acceleration/deceleration, coupled performance indicators. Two categories are identified: 'adequate performance' and 'desired performance'. If a pilot has the same level of performance in the simulator as he has in the aircraft, then the error fidelity is considered good.

The main advantage of MTE's and Handling Qualities is that they are used for aircraft certification and are therefore very well defined. However, The following disadvantages can be identified:

- No limits on acceptable/unacceptable differences in performance between the simulator and the aircraft exist.
- MTE were developed to evaluate A/C therefore they may be aggressive than training/-operational tasks.

- There are also many cases where simulator deficiencies lead to better task performance. E.g.: performing a task will scaled motion cues may lead to less disorientation than in the real aircraft. The pilot may be able to better concentrate on the mission task element.
- However, the main problem with this approach is that the simulator may have a different purpose than the real aircraft. This means that by using handeling qualities, fitness-for-purpose and fidelity are confused.

2-4 Certification of Helicopter Simulators

With different fidelity metrics according to academia explained and classified, it is now time to make the link to the simulator industry. To make this link, the following question is posed:

> What is the current process of the qualification and certification of the motion of Flight Simulator Training Devices (FSTD's)?

To answer this question, two aspect are important. Firstly a certification basis needs to be found. What are the necessary characteristics for an Flight Simulator Training Device (FSTD). Secondly, how does the aviation authority check if these criteria are met? What process is used? Furthermore it is interesting to view some of the challenges that are specific to the helicopter simulator industry. Therefore, the following subquestions are identified:

> - What are the specific challenges in the helicopter simulator industry?
> - What are the requirements posed on on different levels of simulator fidelity?
> - What process is used to verify stated requirements?

2-4-1 Helicopter Simulation Fidelity

The development of the market for full flight simulators for rotorcraft is somewhat lagging behind the development of the fixed-wing market. Whereas many fixed-wing simulators are being designed and produced, it is very rare for a helicopter type to have a fully certified level D FFS. The reason for this can be found in four categories,[41].

1. Firstly the regulations for helicopter simulators are not up-to-date/
2. Secondly, the cost of designing and operating an FFS is too much for many helicopter operators.
3. Thirdly, helicopters pose specific technical challenges to simulators. These challenges boil down to three categories, which are still relevant today.
   (a) **Helicopter Dynamics**
   Firstly, helicopter dynamics require more complicated models, than their fixed-wing counter parts. Is is mainly due to the complexity of the rotor. A more complex model means more computing power is required. However, with the acces of cheap computing power due to the rise of the personal computer, this problem has become less critical in the past decade.
   (b) **Motion System**
   Secondly, the the traditional 6 DOF motion system developed for fixed wing aircraft

is not ideal for rotorcraft use. The classical 6 DOF hexapod does not cue the high frequency sustained vibrations that are characteristic for helicopter movement. However, is this a problem for helicopter simulations? It seems at this point, the inevitable motion-no motion question should be treated, as was already touched upon briefly in subsection 2-1-1.
There has been done a lot of research about motion in helicopter simulation. McCauley stated in 2006 after an extensive literature study to assess the need for motion platforms in military helicopter pilot training[16], that there is no evidence to support the effectiveness of motion platforms for training. However, motion does contribute to the realism and thus to the pilot acceptance of the simulator. Based on this last point civil regulations do mandate a motion platform for training simulators in the helicopter industry in [42], as will be discussed in section 2-4.

(c) **Visual System**
Lastly there is the technical challenge of the visual system. Helicopter cockpits offer a larger field of view that fixed-wing aircraft. This field of view is also frequently used, especially in low velocity hover and maneuvering tasks. Large dome-like structures offer the desired field of view, but are costly and hard to combine with a motion platform. A possible solution is to rotate the dome with respect to the cockpit to give the pilot flying more field of view, as was done for the Helicopter Pilot Station (HPS) at the Netherlands Aerospace Centre (NLR).

4. Finally, training practices do not keep in mind daily operations of the helicopter fleet well enough.

2-4-2 Qualification Basis

In Europe, certification and qualification of Helicopter simulator is regulated in the Certification Standard for Helicopter Flight Simulation Training Devices, CS-FSTD(H) [24]. In the United states, simulator certification is regulated in Advisory Circular (AC) 120-40b [43] for fixed-wind aircraft and AC 120-63 [44]. In the CS-FSTD(H), requirements for all subsystems are given, as well as integrated requirements. Since this literature study focuses primarily on the European market, the following analysis will be focused on EASA regulations.

CS-FSTD(H) consists of two books: the certification specifications and the acceptable means of compliance. In terms of qualification, EASE distinguishes 3 types of Flight Simulator Training Devices (FSTD's), given here in order of increasing fidelity:

- **Flight Navigation Procedures Trainer (FNTP)**
  An FNTP is a training device which represents part of the flight deck/cockpit with accompanying compute. Category: I, II, III and MCC.
- **Flight Training Device (FTD)**
  An FTD is a is a training device which has a full size replica of the flight deck/cockpit, but does not require a visual or motion cueing system. Category: 1, 2 and 3.
- **Full Flight Simulator (FFS)**
  An FFS is a training device which has a full size replica of the flight deck/cockpit and a visual system to provide visual cueing of the outside world to the pilot. An FFS also requires a motion cueing system to provide vestibular feedback to the pilot. Category A, B, C and D.

Table 2-2: AMC1 FSTD(H).300

Testnumber	**Test name**	**Tolerance**	**A**	**B**	**C**	**D**
4.a.(1)(i)	Pitch Displacement	20 deg	x	x		
		25 deg			x	x
4.a.(1)(ii)	Pitch Velocity	15 deg/s	x	x		
		20 deg/s			x	x
4.a.(1)(iii)	Pitch Acceleration	75deg/s2	x	x		
		100 deg/s2			x	x
4.a.(2)(i)	Roll Displacement	20 deg	x	x		
		25 deg			x	x
4.a.(2)(ii)	Roll Velocity	15deg/s	x	x		
		20 deg/s			x	x
4.a.(2)(iii)	Roll Acceleration	75 deg/s2	x	x		
		100 deg/s2			x	x
4.a.(3)(i)	Yaw Displacement	25 deg		x	x	x
4.a.(3)(ii)	Yaw Velocity	15 deg/s	x	x		
⋮	⋮	⋮	⋮	⋮	⋮	⋮

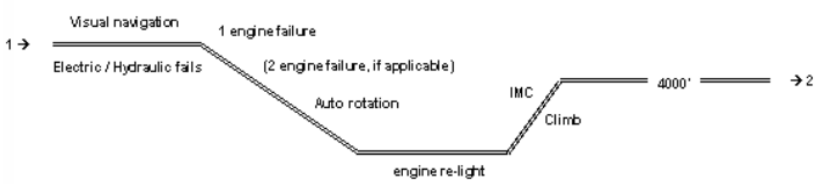

Figure 2-20: Example of a characteristic mission for the subjective evaluation of a FFS.

In subpart C of the first book of AMC1 FSTD(H).300 the requirements are given per subsystem. Requirements for the mathematical model and hardware subsystems are pooled together. However, requirements are divided over performance, handling qualities, atmospheric models, motion systems, visual system and FSTD Systems.

Table 2-2 shows the first five requirements for the motion system. It can be seen that they pose physical limits to the actuation system, but not necessarily consider the motion cueing algorithm.

2-4-3 Evaluation Procedure

The evaluation procedure of these requirements is however documented in subpart FSTD of the Annex to ED Decision 2012/006/R. This document describes how the requirement should be tested and is therefore more interesting for the purposes of this literature study. It basically consist of two parts of evaluation of FSTD qualification. Firstly the certification basis, based on objective tests, as was given in Table 2-2. These test are conducted in several stages. Interestingly, the test guide does mention anything about tuning, or the methods that can be used to achieve satisfactionary motion cueing characteristics.

Within Book 2 about the subjective assessment methods, FSTD(H) states the following: *When evaluating functions and subjective tests, the fidelity of simulation required for the highest level of qualification should be very close to the aircraft. However, for the lower levels of qualification the degree of fidelity may be required in accordance with the criteria contained.* There exists therefore currently no technique or method to assess the overall fidelity of a helicopter simulator other than letting an experienced pilot fly in the simulator and let him 'check' if the fidelity of simulator is very close to the real aircraft.

2-5 Discussion & Conclusions

From the preceding literature review, it can be seen that there are many kinds of fidelity and that there are subsequently many different ways to interpret the simulator motion fidelity. In general, the field can be divided in subjective evaluation methods, like pilot rating scales or measuring workload and objective methods such as searching a way to model to pilot or objectively evaluation the motion cueing system.

In general, the main advantages of objective assessment is repeatability, that is, results about simulator performance are not subject to pilot opinion. However, objective methods such as pilot models are model and task specific. Generalized applicability is therefore limited. Furthermore, there exist few criteria for the allowable difference between the simulator and the aircraft for these metrics.

Subjective assessment on the other hand has the advantage that a clear distinction is made between sufficient and insufficient simulator performance. Moreover, subjective ratings can be applied regardless of the aircraft type or MTE and have therefore a more generalized applicability.

The 'holy grail' is the field of simulator motion fidelity is therefore to find a way to objectively evaluate fidelity that is broad enough to cover the whole envelope of daily simulator operations. The OMCT has been proven to find discrepancies between certified simulators and is therefore a step towards this goal. However, the OMCT does not take into account the specific characteristics of the aircraft type and Mission Task Elements. Furthermore the OMCT is makes assumptions based on the input signal. To increase the applicability, these aspects need to investigated. Furthermore, still no criteria or performance metric exist for the OMCT.

This literature study was carried out to find an answer to the following research question:

> What is the present state of research in the field of **simulator motion fidelity** and can an **Objective Motion Cueing Test** contribute to an improvement of simulator fidelity evaluation in the **helicopter domain?**

In light of the result section, the following observations have been made.

- There exist many initiatives to improve the evaluation of motion fidelity. However, in the foreseeable future the academic world agrees that subjective evaluational will be necessary.
- The Objective Motion Cueing Test provides an end-to-end test to evaluate the motion cueing system and was developed for fixed-wing simulators. However, a close look

should be taken at the assumptions made on the input signals and their validity in the helicopter domain.

In conclusion, it can be stated that the Objective Motion Cueing Test can therefore contribute to an improvement of simulator fidelity evaluation in the helicopter domain.

Chapter 3

Simulation of two Helicopter Mission Task Elements

In this chapter the simulation of two helicopter Mission Task Elements (MTEs) is discussed. A closed loop simulation structure will be used, illustrated in Figure 3-1.

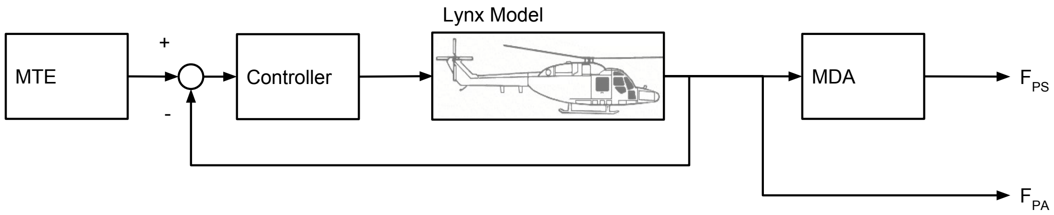

Figure 3-1: Schematic representation of the closed loop simulation of two Mission Task Elements.

As can be seen, a mathematical helicopter model will be implemented, controlled by a non-human controller, to fly an MTE. Furthermore, a time trace of these mission task elements will be fed into the motion filter of the SRS studying the cueing characteristics in the time domain.

This chapter is structured as follows. Firstly the mathematical helicopter model in discussed in section 3-1. Thereafter this model is trimmed, linearized and verified in section 3-2 and section 3-3 respectively. Thereafter the loop is closed for the first MTE in section 3-6. A second MTE is studied in section 3-5. Lastly, the time trace of the MTE is converted to the frequency domain for use in the proceeding analysis in section 3-7.

3-1 3DOF Lynx Helicopter Model

In this section, the implementation of a three Degrees of Freedom (DOF), longitudinal helicopter model is discussed. This model is based on the description of a helicopter model given by Th. van Holten and J. A. Melkert in [45]. For this model numerical values will be based on the DRA (RAE) research Lynx, ZD559, [12].

Figure 3-2 shows a schematic of the non-linear, 3DOF, longitudinal helicopter model.

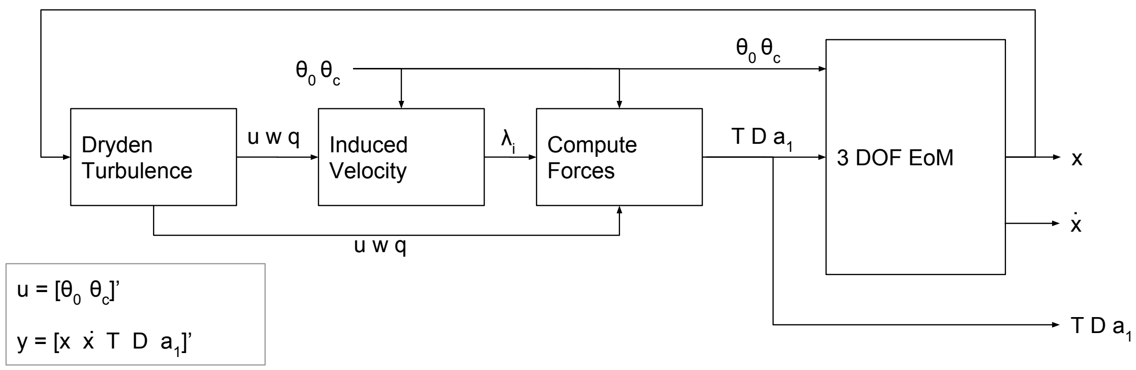

Figure 3-2: Schematic representation the computation architecture of the helicopter model.

From Figure 3-2, it can be seen that there are four computational blocks: the Equations of Motion, the computation of forces, the iterative solver for the induced velocity and a Dryden turbulence model. In subsection 3-1-1 to subsection 3-1-4 these blocks will be discussed respectively.

3-1-1 The Equations of Motion

Just as for the dynamics of fixed-wing aircraft, the equations of motion are one of the most important tools to model and predict rotorcraft behavior. For this research the following assumptions were made on the aircraft body:

- Any coupling between the symmetric and asymmetric motion is not taken into account.
- There are no aerodynamic moments acting on the fuselage, but a drag force. This also means that the aerodynamic forces of the tail-plane are neglected.
- The center of the rotor hub is positioned directly above the center of gravity of the aircraft.
- Only the moment of inertia about the Y-axis is taken into account.
- H-forces in rotor plane are neglected (i.e. no "Amer-effect"), thrust T normal to tip path plane.

The result of these assumptions is there are only acting three forces on the simulated helicopter body. In Figure 3-3, a Free Body Diagram (FBD) is given including the total drag force on the helicopter D, the weight W and the thrust from the main rotor T.

Expressing stated forces in the appropriate directions results in a set of 3 equations, given by Equation 3-1. Furthermore, to complete the longitudinal equations, one extra equation gives the kinematic relation between the rotational pitch velocity and the pitch angle.

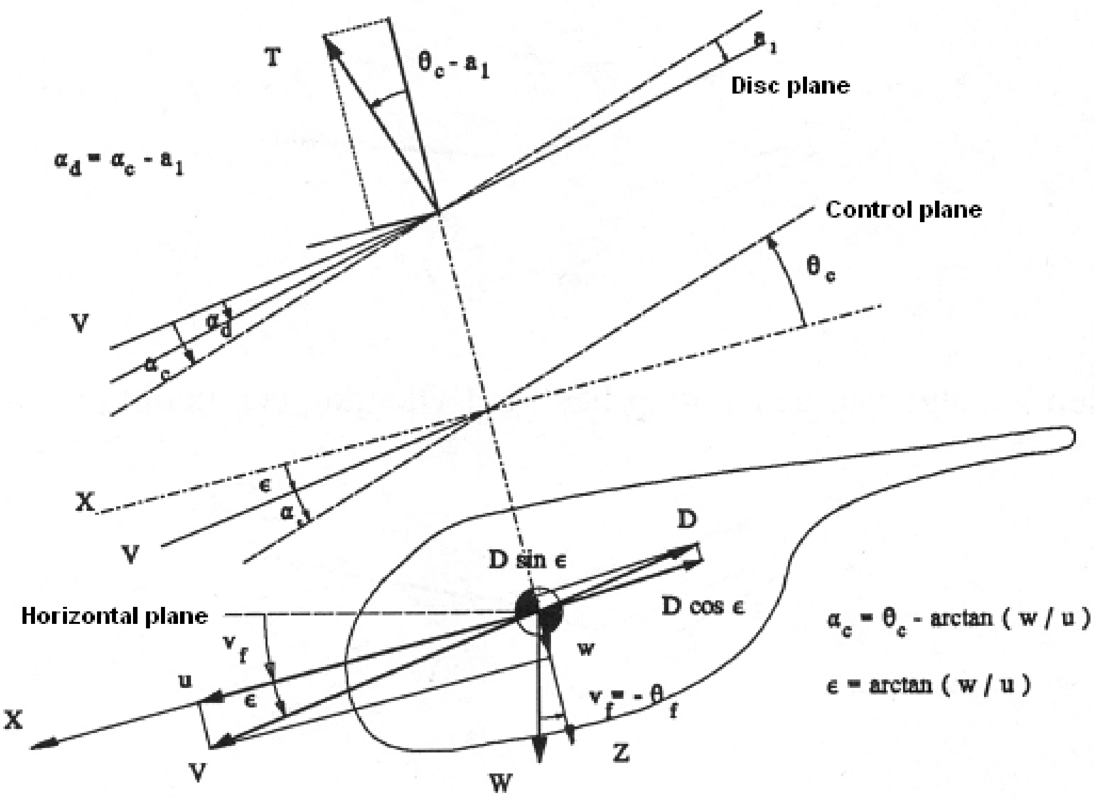

Figure 3-3: Schematic Free Body Diagram, displaying relevant relevant angles of the main rotor disk, [45].

$$\dot{u} = -g\sin\theta_f - \frac{D}{m}\cos(\theta_f) + \frac{T}{m}\sin(\theta_{1c} - a_1) - qw \tag{3-1a}$$

$$\dot{w} = g\cos\theta_f - \frac{D}{m}\sin(\theta_f) - \frac{T}{m}\sin(\theta_{1c} - a_1) + qu \tag{3-1b}$$

$$\dot{q} = -\frac{T}{I_y}\sin(\theta_{1c} - a_1) \tag{3-1c}$$

$$\dot{\theta}_f = q \tag{3-1d}$$

3-1-2 The Computation of Forces acting on the Helicopter Body

Considering the assumptions stated in subsection 3-1-1, an estimate of the three forces acting on the body can be found, using the equations shown in Equation 3-2.

$$T = C_T \rho (\Omega R)^2 \pi R^2 \tag{3-2a}$$
$$D = C_D \frac{1}{2} \rho V^2 S \tag{3-2b}$$
$$W = M_a g \tag{3-2c}$$

The drag coefficient C_D was a single values for both the main rotor and the body, taken 0.08, [12] for this simulation. Other numerical values used are given in Appendix B.

However, the thrust coefficient C_T is not easily found. For fixed wing aircraft, lift can directly be computed from the aerodynamics on the main wing. However, for rotorcraft, it is not possible to compute the thrust force directly from the aerodynamics on a rotor blade. First, it must be taken into account that the blade is free to flap around a hinge. The ability for helicopter to do so is critical, since it firstly enables the blade to automatically equalize the difference in lift force on the advancing and retreating blades of the rotor, [12]. Secondly, a flapping blade enable the tilt of the rotor disk and thus control over the thrust force.

For more information on the dynamics of the rotor blade, the interested reader is referred to Appendix A, where a rudimentary form of the flapping equation is derived and discussed. Furthermore, if the reader is unfamiliar with the symbols used in this chapter, it is also recommended to read Appendix A, as clear definitions are given here.

As was stated, the model implemented is largely based on the 3DOF longitudinal model presented by van Holten and Melkert in 2002, [45]. They derive a form of the flapping equation equal to Equation 3-3, which forms the basis for the model presented. Equation 3-3 is an extension of the equation presented in Appendix A, Equation A-18, that includes the influence of a forward velocity, μ, on the aerodynamic forces of the flapping equation. Equation 3-3 is not derived in this report, but taken from [45].

$$\begin{aligned}\ddot{\beta} + \frac{\gamma}{8}\Big(1 + \frac{4}{3}\mu \sin\psi\Big)\dot{\beta} + \big(1 + \frac{\gamma}{6}\mu\cos\psi + \frac{\gamma}{8}\mu^2 \sin(2\psi)\Big)\beta = \\ -2\frac{q}{\Omega}\sin\psi + \frac{\gamma}{8}\Big(\theta_0(1+\mu^2) - \frac{4}{3}(\lambda_c + \lambda_i) + \mu(\frac{8}{3}\theta_0 - 2(\lambda_c + \lambda_i))\sin\psi \\ + \frac{q}{\Omega}\cos\psi + \frac{4}{3}\frac{q}{\Omega}\mu\sin(2\psi) - \theta_0\mu^2\cos(2\psi)\Big)\end{aligned} \tag{3-3}$$

For Equation 3-3, the following assumptions on the dynamics of the main rotor blades were made:

- A spring-less, non-eccentric flapping hinge and an infinitely stiff blade are assumed. Therefore, no moments are generated on the rotor hub.
- There is no coupling between the flapping and the feathering motion of the blade. Therefore there is no δ_3-effect.
- Blades with no twist and constant chord are assumed.
- Flapping angles are small, with linear aerodynamics and have no stall nor dynamic stall.
- Quasi-steady flapping dynamics and inflow velocity are assumed.
- A constant RPM is assumed: the engine is assumed to deliver the power required without delay.

Considering these assumptions, the solution of the flapping equation has the form of $\beta = a_0 + a_1 \sin(\psi) + b_1 \cos(\psi)$. Coefficients a_0, a_1 and b_1 are given with respect to the hub plane, according to Equation 3-4, [45].

$$\begin{aligned} a_0 &= \frac{\gamma}{8}\theta_0(1+\mu^2) - \frac{\gamma}{6}(\lambda_c + \lambda_i) \\ a_1 &= \frac{\frac{8}{3}\mu\theta_0 - 2\mu(\lambda_c+\lambda_i) - \frac{16}{\gamma}\frac{q}{\Omega}}{1-\frac{1}{2}\mu^2} \\ b_1 &= \frac{\frac{4}{3}\mu a_0 - \frac{q}{\Omega}}{1+\frac{1}{2}\mu^2} \end{aligned} \tag{3-4}$$

With the homogeneous solution for a_1, an estimate for the thrust coefficient can now be found by solving for the induced velocity of the airflow going through the main rotor, according to Equation 3-5. The physical meaning of coefficient a_1, is the longitudinal angle of the disk plane, visualized in Figure 3-3.

$$a_1 = \frac{\frac{8}{3}\mu\theta_0 - 2\mu(\lambda_c+\lambda_i) - \frac{16}{\gamma}\frac{q}{\Omega}}{1-\frac{1}{2}\mu^2} \tag{3-5a}$$

$$CT_{BEM} = \frac{1}{4}a_0\sigma\big(\frac{2}{3}\theta_0(1+\frac{3}{2}\mu^2) - (\lambda_c+\lambda_i)\big) \tag{3-5b}$$

$$CT_{GLA} = 2\lambda_i\sqrt{\Big(\frac{V}{\Omega R}\cos(\alpha_c - a_1)\Big)^2 + \Big(\frac{V}{\Omega R}\sin(\alpha_c - a_1) + \lambda_i\Big)^2} \tag{3-5c}$$

(3-5d)

Equation 3-5 gives two relations for the thrust coefficient. Firstly there is the thrust coefficient according to Blade Element theory, Equation 3-5c. Secondly, Glauert provides a relation that estimates the C_T coefficient based upon the airflow. The variables V, α_c, λ_i and μ are non-dimensional coefficients for the state of the aircraft and were determined using the relations described in Equation 3-6.

$$V = \sqrt{u^2 + w^2} \tag{3-6a}$$

$$\alpha_c = \theta_{1c} - \tan^{-1}\frac{w}{u} \tag{3-6b}$$

$$\mu = V\frac{\cos\alpha_c}{\Omega R} \tag{3-6c}$$

$$\lambda_c = V\frac{\sin\alpha_c}{\Omega R} \tag{3-6d}$$

The variable λ_i, or the induced velocity of the rotor inflow, is not known. However, since both Glauert and Blade Element Theory provide an equation for the thrust coefficient, there is a system of two equations and two unknowns. To solve this system, a Newton-Raphson solver was implemented.

3-1-3 Newton-Raphson Iterative Solver

To solve for the induced velocity, the thrust coefficient according the the blade element method and the thrust coefficient according to Glauert need to be similar, or $CT_{BEM} = CT_{GLA}$. Therefore, a λ_i can be found for which $CT_{BEM} - CT_{GLA} = 0$. Substituting equations Equation 3-5c and Equation 3-5d gives Equation 3-7.

$$\begin{aligned} f(\lambda_i) =& \frac{1}{4} a_0 \sigma \big(\frac{2}{3}\theta_0 (1 + \frac{3}{2}\mu^2) - (\lambda_c + \lambda_i) \big) \\ & - 2\lambda_i \sqrt{(\frac{V}{\Omega R}\cos\alpha_c - a_1)^2 + (\frac{V}{\Omega R}\sin\alpha_c - a_1 + \lambda_i)^2} \end{aligned} \tag{3-7}$$

Equation 3-7 was solved by means of a Newton-Raphson method, [46]. This method finds where a function intersects the x-axis by using the derivative to make an estimate for the new iteration, $x_{i+1} = x_i + \frac{\dot{f}(x_i)}{f(x_i)}$ A schematic overview of this method is given in Figure 3-4.

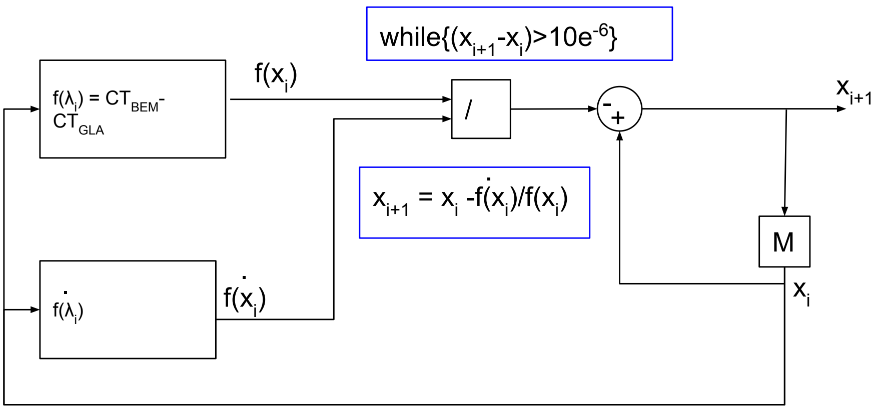

Figure 3-4: Flowchart of the computation scheme used to solve equation Equation 3-7.

The derivative of equation Equation 3-7 was found analytically, shown in Equation 3-8,

$$\dot{f}(\lambda_i) = -\frac{a_0\,\sigma}{4} - \sqrt{\frac{(V\,\sin Z + \Omega\,R\,\lambda_i)^2}{\Omega^2\,R^2} + \frac{V^2\cos Z^2}{\Omega^2\,R^2}} - \frac{\lambda_i\left(2\,\lambda_i + \frac{2\,V\,\sin Z}{\Omega\,R} - \frac{8\,V\,\lambda_i\,\mu\,\cos Z}{\Omega\,R\,(\mu^2-2)}\right)}{2\sqrt{\frac{(V\,\sin Z+\Omega\,R\,\lambda_i)^2}{\Omega^2\,R^2} + \frac{V^2\cos Z^2}{\Omega^2\,R^2}}} \tag{3-8}$$

where coefficient Z is given by the expression from Equation 3-9.

$$Z = \left(\alpha_c - \frac{2\,\mu\,(\lambda_c + \lambda_i) - \frac{8\,\mu\,\theta_0}{3} + \frac{16\,q}{\Omega\,\gamma}}{\frac{\mu^2}{2} - 1}\right) \tag{3-9}$$

After solving for the induced velocity, the thrust coefficient can be computed and in turn the total thrust force. With the thrust force, all forces are now known.

3-1-4 Turbulence model

The basic model set-up is now complete. However, in real-life simulation atmospheric disturbances excite the mathematical mode, on top of pilot input. Therefore an extra block was added to the dynamics. This block models the dynamics of atmospheric turbulence by means of a Dryden model, [47]. This model uses two filters to filter white noise inputs on the vertical and horizontal body axes. The transfer function of the filters for the x- and z-axis are given in Equation 3-10 respectively.

$$H_{\bar{u}w_1}(s) = \sigma_{\bar{u}}\sqrt{2\frac{L_u}{V}}\frac{1}{\frac{L_u}{V}s+1} \tag{3-10a}$$

$$H_{\bar{w}w_3}(s) = \sigma_{\bar{w}}\sqrt{\frac{L_w}{V}}\frac{1+\sqrt{3}\frac{L_w}{V}s}{(\frac{L_w}{V}s+1)^2} \tag{3-10b}$$

In Equation 3-10, w_1 and w_3 give the white noise inputs for u and w respectively. It was assumed that no rotational component is present in the turbulence.

A Dryden gust model relies on velocity of the aircraft, V to generate variations in the wind speed. For the use in hover, this model will therefore not generate any turbulence. However, it was considered outside the scope of this project to investigate more complex turbulence model such as the Mixer Equivalent Turbulence Simulations (METS) or Simulation of Rotor Blade Element Turbulence (SORBET) models, as described by Lusardi in [48]. Therefore it was decided to use a Dryden turbulence spectrum to generate deviations from the horizontal and vertical aircraft body speeds using fictive fixed airspeed of 90 [kts] or 45 [m/s], representing a category A fixed-wing aircraft at approach, at 500 [ft].

The parameters for the turbulence model were then set according to military specification MIL-F-8287C, [49]. Longitudinal turbulence scale L_u was set according to $L_u = \frac{h}{(0.177+0.000823h)^{1.2}}$, where h is the altitude in feet. Vertical turbulence scale L_w was set according to $L_w = \frac{h}{2}$. Turbulence intensity σ_u was set to 2.5, corresponding to light turbulence, [49]. Finally vertical turbulence intensity was set to $\sigma_w = \frac{\sigma_u}{2.5}$. Coefficients for the Dryden model are summarized in to Table 3-1.

Table 3-1: Chosen values for the Dryden turbulence model.

$V[m/s]$	$L_u[-]$	$L_w[-]$	$\sigma_u[-]$	$\sigma_w[-]$
45	944.7	250	2.5	1

Figure 3-5 shows a time-trace for 100 [s] of simulated turbulence, for both the longitudinal and vertical component.

3-2 Trim

Before any simulation can be run with the constructed model, the aircraft needs to be trimmed according to the airspeed. This process boils down essentially to the computation of control

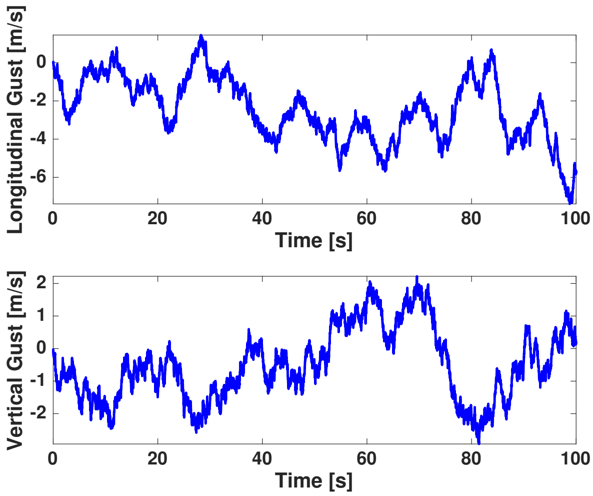

Figure 3-5: Visualization of on on the seeds for the longitudinal and vertical gust speeds.

inputs, for which the aircraft maintains its wanted velocity. Implicitly this means that it is assumed that $\dot{u} = \dot{w} = \dot{q} = 0$. To simplify the trim computations for the purpose of this simulation even further, also zero pitch velocity is assumed, $q = \dot{\theta}_f = 0$.

The stated assumptions result in a Free Body Diagram with forces indicated in blue in Figure 3-6. Moreover, the forward velocity is indicated in red.

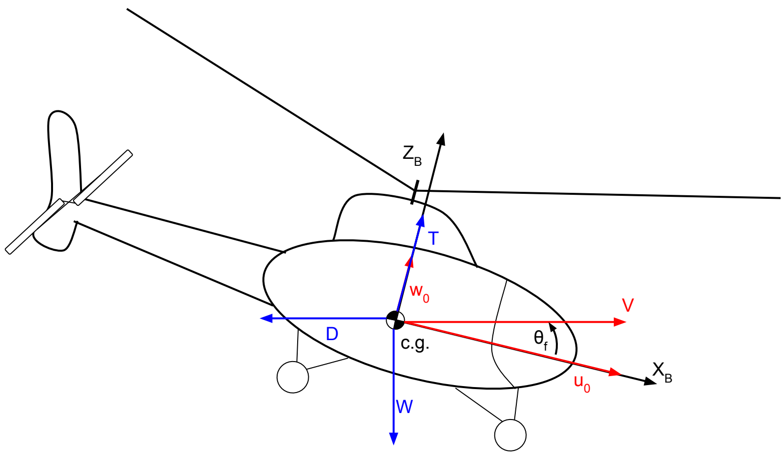

Figure 3-6: Free Body Diagram and Kinetic Diagram of a helicopter in steady forward flight.

The first step to computing the control inputs is to compute the forces indicated in the FBD in Figure 3-6. Weight and drag are computed readily from aircraft parameters, according to Equation 3-11a and Equation 3-11b. The thrust can then be estimated with the aircraft pitch angle, making use of the assumption there is no angle of attack, and that the thrust force is in-line with the aircraft z-body axis,

$$D = C_D \frac{1}{2} \rho V_0^2 S \tag{3-11a}$$
$$W_0 = M_a g \tag{3-11b}$$
$$\theta_{f_0} = -\tan^{-1}(\frac{D}{W}) \tag{3-11c}$$
$$T_0 = W_0 \cos(\theta_{f_0}) - D_0 \sin(\theta_{f_0}) \tag{3-11d}$$

where the pitch angle was found using the computed weight and drag forces, according to Equation 3-11c. The only variably left that is needed for the computation of the initial control input is the inflow velocity of the rotor. However, the thrust coefficient at this point can be computed according Equation 3-12b and can be used directly to determine λ_i, without the use of the blade-element method, directly from the Glauert equation, Equation 3-12b.

$$CT_0 = \frac{T_0}{\rho(\Omega R)^2 S)} \tag{3-12a}$$
$$CT_0 = 2\lambda_{i_0} \sqrt{\Big(\frac{V_0}{\Omega R} \cos(\tan^{-1}\Big(\frac{D_0}{W_0}\Big))\Big)^2 + (\frac{V_0}{\Omega R} \sin(\tan^{-1}\Big(\frac{D_0}{W_0}\Big)) + \lambda_{i_0}\Big)^2} \tag{3-12b}$$
$$\mu_0 = \frac{V_0}{\Omega R} \tag{3-12c}$$

As can be seen from Equation 3-12b, use has been made from the fact that, since the thrust is assumed to be in line with the z-direction of the body reference frame, the disk angle is assumed to be equal to the pitch angle, given in Equation 3-13.

$$\alpha_d = \alpha_c - a_1 = -\theta_{f_0} = \tan^{-1}(\frac{D}{W}) \tag{3-13}$$

Control inputs can now be found by using the equation for the thrust coefficient according to blade element theory, and the solution for coefficient a_1 of the flapping equation. For convenience these equations are repeated in Equation 3-14.

$$a_1 = \frac{\frac{8}{3}\mu\theta_0 - 2\mu(\lambda_c + \lambda_i) - \frac{16}{\gamma}\frac{q}{\Omega}}{1 - \frac{1}{2}\mu^2} \tag{3-14a}$$
$$CT_{BEM} = \frac{1}{4} a_0 \sigma \big(\frac{2}{3}\theta_0(1 + \frac{3}{2}\mu^2) - (\lambda_c + \lambda_i)\big) \tag{3-14b}$$

The induced inflow due to flight velocity can now be substituted by an expression, derived using Equation 3-13.

$$\lambda_{c_0} = \frac{V}{\Omega R} \sin \alpha_c \tag{3-15a}$$
$$= \frac{V}{\Omega R} \sin(\alpha_d + a_1) \tag{3-15b}$$
$$= \frac{V}{\Omega R} \sin(\tan^{-1}(\frac{D}{W}) + a_1) \tag{3-15c}$$
$$= \mu_0 a_1 + \mu_0 \frac{D}{W} \tag{3-15d}$$

Furthermore, for a trimmed aircraft, the rotor pitch angle θ_{1c} is equal to the solution for a_1 of the flapping equation. Since an infinitely stiff blade was assumed for this model, in this case the thrust vector for this particular model is in line with the vertical z-axis, as can be seen from Figure 3-3. Substituting $\theta_{1c} = a_1$ and $\$lambda_{c_0} = \mu_0 a_1 + \mu_0 \frac{D}{W}$ into Equation 3-14, Equation 3-16 is obtained. Furthermore it should be noted that $\dot{q}$ is assumed to be zero.

$$\theta_{1c} = \frac{\frac{8}{3}\mu\theta_0 - 2\mu(\mu\theta_{1c} + \mu\frac{D}{W} + \lambda_i)}{1 - \frac{1}{2}\mu^2} \tag{3-16a}$$

$$CT = \frac{1}{4}a_0\sigma\left(\frac{2}{3}\theta_0(1 + \frac{3}{2}\mu^2) - (\mu\theta_{1c} + \mu\frac{D}{W} + \lambda_i)\right) \tag{3-16b}$$

Equation 3-16 can now be rewritten in a matrix form equal to that of Equation 3-17 and used to solve for control inputs θ_{1c} and θ_0.

$$\begin{bmatrix} \theta_{1c_0} \\ \theta_{0_0} \end{bmatrix} = \begin{bmatrix} 1 + \frac{3}{2}\mu^2 & -\frac{8}{3}\mu \\ -\mu & \frac{2}{3} + \mu^2 \end{bmatrix}^{-1} \begin{bmatrix} -2\mu^2\frac{D_0}{W_0} - 2\mu\lambda_{i_0} \\ \frac{4}{\sigma}\frac{CT_0}{a_0} + \mu\frac{D_0}{W_0} + \lambda_{i_0} \end{bmatrix} \tag{3-17}$$

To verify the outcome of the trim procedure the aircraft was trimmed for a range of velocities, up to $\mu = 0.3$. This corresponds to roughly 70 [m/s]. The control inputs needed for a trimmed aircraft are given in Figure 3-7.

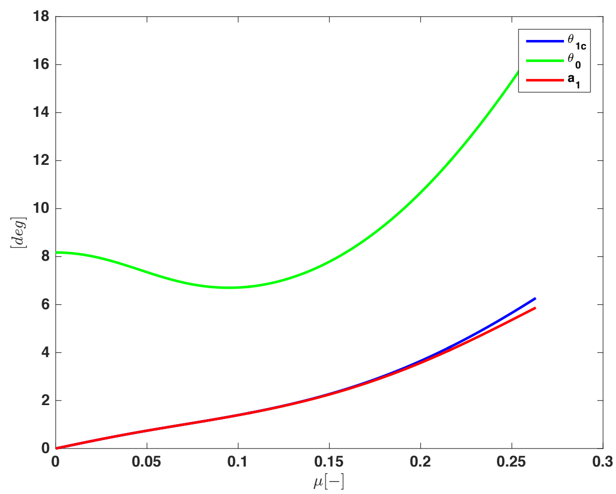

Figure 3-7: Trimmed control inputs vs. initial velocity, expressed in $\mu = \frac{V}{\Omega R}$.

As can be seen that collective blade pitch initially decreases when the initial velocity is increased. However, thereafter it is increased. The longitudinal blade pitch gradually increases up to 4 [deg], indicating a forward cyclic input. Furthermore, coefficient of the flapping angle a_1 is also given. It can be seen that up to $\mu = 0.2$, a_1 is roughly equal to θ_{1c}. However after $\mu = 0.2$ the blue and red line start deviating, indicating that thrust vector is not fully in line with the aircraft z-axis. This is due to the fact that small angle approximations used for Equation 3-15 no longer hold for large velocities.

In order to verify if the aircraft is indeed trimmed at $t = 0$, forces and moments were computed for the resulting control inputs. Figure 3-8 shows the specific forces and rotational acceleration at $t = 0$. Also indicated are the boundaries for the vestibular system. These boundaries are used, since the primary use of this model is an application in a motion cueing research.

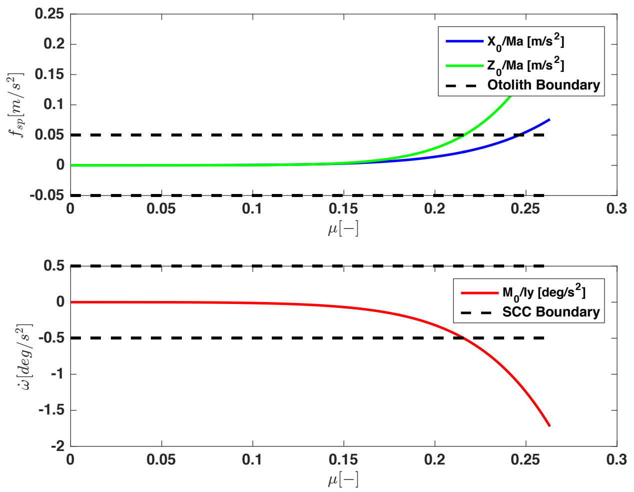

Figure 3-8: Initial specific forces and rotational acceleration vs. initial velocity.

As can be seen, up to $\mu = 0.2$, specific forces f_{x0} and f_{z0} are below the boundary of the vestibular system. Thereafter however, initial forces and moments are not zeros and above the boundaries of the vestibular system. Therefore the model is considered trimmed up to 70 [m/s]. Mathematically there could be found a way trim the aircraft at higher speeds. However, this is considered outside of the scope of this research.

3-3 Verification

To verify if the mathematical model is correctly implemented, two steps have been undertaken.

- Firstly the eigenvalues and motions were studied by linearizing the model, and comparing the output to the implemented non-linear model.
- Secondly, the linearized model is compared to data from a more complex model simulating the lynx, given by Padfield [12].

3-3-1 Eigenmotions

The model was linearized analytically using the following procedure.

As can be seen from Figure 3-9, after trimming the model for a particular initial condition, the initial forces are computed. Thereafter, the states and inputs perturbed, indicated by Δ, one by one. The resulting differences in forces and rotational moments were subsequently computed, as is shown in the equation in Figure 3-9.

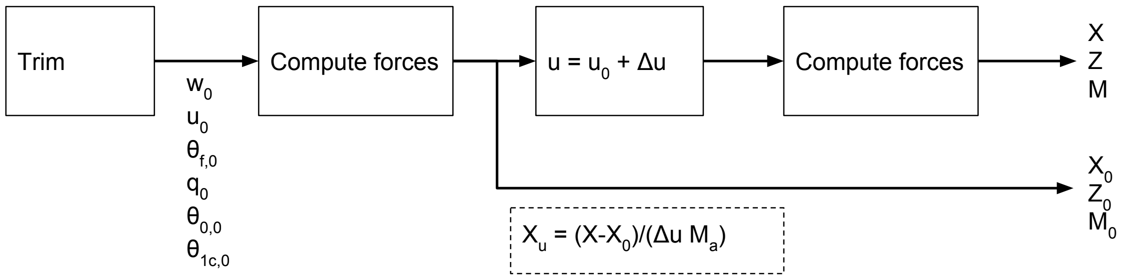

Figure 3-9: Schematic flowchart of the lenearisation procedure.

Stability and control derivatives were computed to construct a state space system according to Equation 3-18.

$$\begin{bmatrix} \Delta\dot{u} \\ \Delta\dot{w} \\ \Delta\dot{\theta}_f \\ \Delta q \end{bmatrix} = \begin{bmatrix} X_u & X_w & X_{\theta_f} - W\cos(\theta_{f_0}) & X_q - mw_0 \\ Z_u & Z_w & Z_{\theta_f} - W\sin(\theta_{f_0}) & Z_q + mu_0 \\ 0 & 0 & 0 & 1 \\ M_u & M_w & M_{\theta_f} & M_q \end{bmatrix} \begin{bmatrix} \Delta u \\ \Delta w \\ \Delta\theta_f \\ \Delta q \end{bmatrix} + \begin{bmatrix} X_{\theta_0} & X_{\theta_{1c}} \\ Z_{\theta_0} & Z_{\theta_{1c}} \\ 0 & 0 \\ M_{\theta_0} & M_{\theta_{1c}} \end{bmatrix} \begin{bmatrix} \Delta\theta_0 \\ \Delta\theta_{1c} \end{bmatrix} \tag{3-18}$$

In Equation 3-18, gravity is added in the X and Z equation. Moreover, rational components mu_0 and $-mw_0$ are also taken into account. Eigenvalues were subsequently computed and are visualized in Figure 3-10.

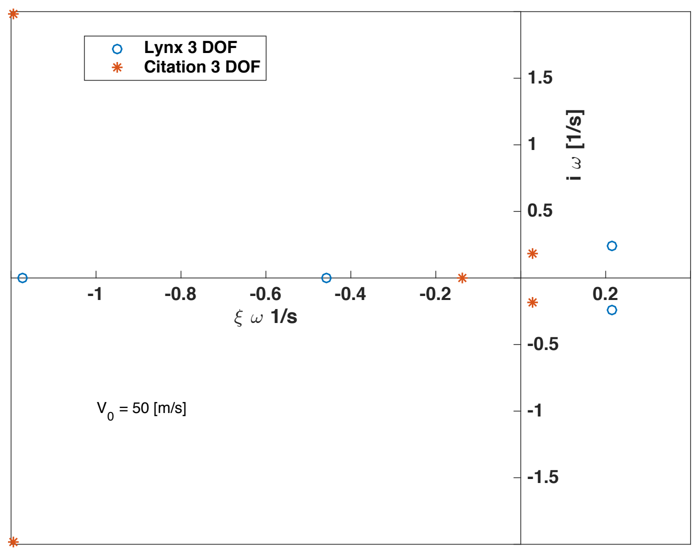

Figure 3-10: A comparison of eigenvalues to a fixed-wing example, the Cessna Citation II PH-LAB.

As can be seen from Figure 3-10, also eigenvalues for the Cessna Citation II PH-LAB at cruise speed are given. It can be seen that the the Citation has 5 eigenvalues. The two most right eigenvalues correspond to a phugoid motion, which is unstable in this case. The most left pair of eigenvalues correspond to a short period, which is periodic and stable. Lastly there is an eigenvalue corresponding to a heave motion, which aperiodic and stable.

The helicopter model however, has 4 eigenvalues. The corresponding eigemotions were found using the eigenvectors. Similarly to the Citation, there is an unstable pair corresponding to a phugoid. Secondly, there are two real eigenvalues in the left side of the plot. The most negative eigenvalue corresponds to the short period, which in this case is an aperiodic exponential function. The last eigenvalue is linked with heave motion and is also aperiodic and stable.

The most interesting eigenmotion is this case is the phugoid, since it is highly unstable. To visualize the response of the phugoid motion, the helicopter was trimmed in hover. Thereafter a block input was given on the cyclic, as is represented in Figure 3-11a. For both the linearized and the non-linear model the response was then computed and given in Figure 3-11b.

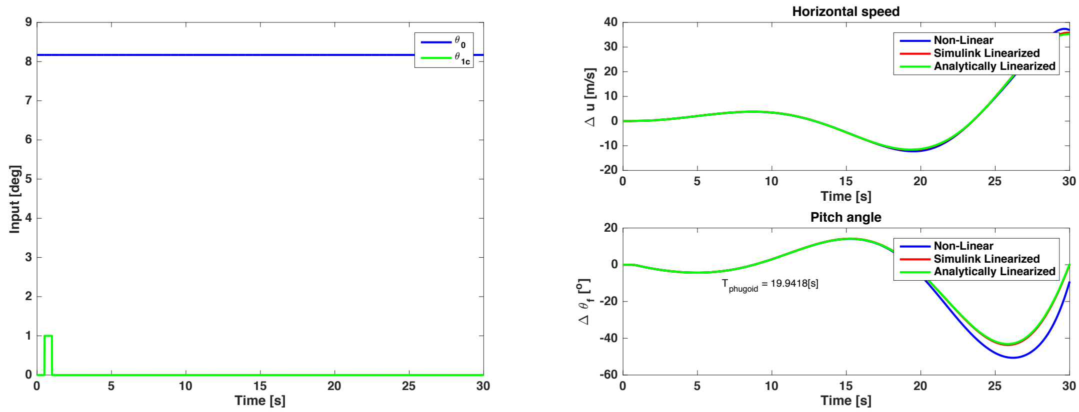

(a) Control inputs for the simulation of a phughoid motion.

(b) Horizontal speed and pitch angle computed from the non-linear model and an analytical lenearisation.

Figure 3-11: Visualization of the phugoid eigenmotion.

As can be seen, up to 20 [s] the non-linear and linear models predict horizontal speed and pitch angles similarly. However after 20 [s], the pitch angle exceeds -20 [deg]. At large difference from the initial condition the assumption of linearity is no longer valid. The linear and non-linear model therefore no longer overlap.

3-3-2 Comparison to Padfield

To further verify that the model output is as expected of a rudimentary helicopter model, stability and control derivatives were compared to those of a more advanced helicopter model of the lynx. Table 3-2 shows stability derivatives of the linearized model and a lynx 6 DOF model given by Padfield for an initial condition of 0 [kts].

Table 3-2: Stability Derivatives for the Lynx helicopter at 0 [kts].

	X_u	X_w	X_q	Z_u	Z_w	Z_q	M_u	M_w	M_q
Padfield	-0,02	0,02	0,8	0	-0,3	0	0,05	0,005	-2
Linearized	-0,015	0	0,62	0	-0,27	0	0,006	0	-0,25

The differences in stability derivatives are discussed subsequently:

- It can be seen that the force in x-direction is affected less by the linearized model than by the model by Padfield. X_w is not even taken into account. The main reason for this is thought to originate in the fact that it was assumed that there are no H-forces acting on the rotor. With no in-plane forces acting on the rotor, X_u is only affected by the drag force of the body. A similar explanation can be sought for the difference in X_q.
- The main contribution to Z_w is the rotor inflow, which was modeled by the Newton-Raphson iterator. As can be seen, this gives a good estimate.
- Since it was assumed that aerodynamic moments on the fuselage are neglected, contributions to M are all due to the main rotor thrust force. Therefore M_u, M_w and M_q are all smaller for the linearized model than for the more complex model by Padfield. Furthermore, there is no offset from the rotor hub to the centre of gravity. This might also explain the large difference in M_u.

Table 3-3 shows the control derivatives of the linearized model and a lynx 6 DOF model given by Padfield for an initial condition of 0 [kts].

Table 3-3: Control Derivatives for the Lynx helicopter at 0 [kts].

	X_{θ_0}	$X_{\theta_{1c}}$	Z_{θ_0}	$Z_{\theta_{1c}}$	M_{θ_0}	$M_{\theta_{1c}}$
Padfield	7	2	-95	-0,5	1	-6
Linearized	0	9,81	-95,2	0,09	0	-3,88

Control derivatives are discussed subsequently:

- For the lynx helicopter, the rotor hub is not directly positioned above the c.g. Therefore in hover, the rotor is tilted slightly forward. An input on the collective will result therefore directly in an increade in the force in x-direction. X_{θ_0} is not affected by a collective input in the linearized model, but is severely affected by Padfield. Secondly, $X_{\theta_{1c}}$ is affected more for the linearized model than the model according to Padfield. Since an infinitely stiff rotor is assumes a change in cyclic pitch will result directly in a change of aircraft pitch angle. The contribution to X is equal to g.
- Forces in z-direction also differ. It can be seen that Z_{θ_0} is of similar magnitude but that $Z_{\theta_{1c}}$ is of opposite sign. $Z_{\theta_{1c}}$ for the linearized model is positive since a positive change in θ_{1c} will result in a decrease in lift. Therefore, force in direction will become more positive(Z_B positive down). A typographical error is suspected in in the sign of this control derivative in Padfield.
- M_{θ_0} is zero for the linearized model since it assumed that the rotor is positioned directly above the centre of gravity. Therefore a change in collective does not result in a pitch moment. M_{θ_0}

Summarizing from the preceding, to assumptions with the most effect on the helicopter model fidelity are:

- No aerodynamic moments acting on the body (no tailplane).
- The rotor is positioned directly above the c.g.
- No H-forces acting on the main rotor.

For improvement of the model, the first two assumptions can be relatively easily implemented. To incorporate the H-forces, requires more work. At this point, these improvement are considered outside of the scope of this project, since focus is put on the performance of the motion cueing system. However, if during pilot trials it is found that the model in its current form has insuficient fidelity, it is recommended to incorporate stated improvements.

3-4 Validation

No actual data of the Lynx helicopter was provided for this project. Therefore no validation work was performed. However, the model was verified with a different model which was validated by Padfield e.a. Although numerous differences were found, the model is thought to capture the most rudimentary dynamic characteristics of rotorcraft. Since the focus of this project is on motion cueing performance the model in its current form is therefore considered sufficient to continue to the next step, the simulation of two mission task elements.

3-5 Mission Task Element I: Take-Off Abort

The first mission task element was chosen to explore coupling between the pitch motion and the surge motion, focusing mainly on the low-frequency response of the mathematical model. No turbulence was used for this task. It was therefore decided to choose the take-off and abort task from ADS-33, [13]. For a complete description the interested reader is referred to Appendix C.

Figure 3-12 shows a schematic representation of the maneuver. The maneuver is initiated from hover, pushing the cyclic forward until a velocity of 40 [kts] is reached. Thereafter the pilot immediately decelerates the aircraft to a hover again, simulating an aborted take-off.

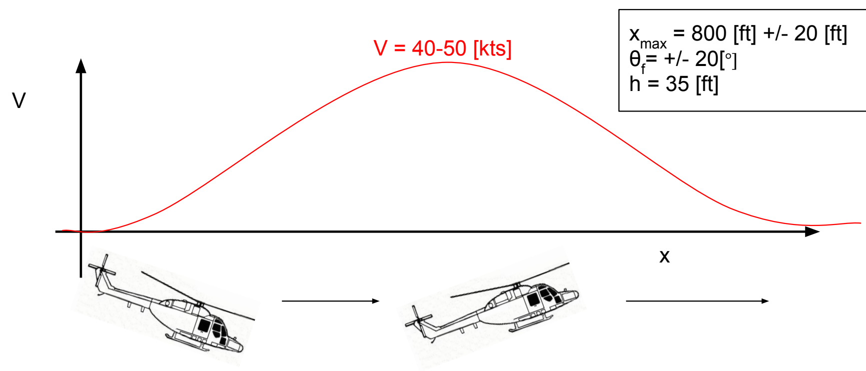

Figure 3-12: Schematic representation of the Take-Off/Abort MTE.

The box in Figure 3-12 indicates desired performance criteria from ADS-33. The total distance traveled should be 800 ft. Furthermore, the maneuver should be flown at an altitude of 35 [ft] and the maximum pitch angle should be approximately +/- 20 [deg].

3-5-1 Controller

A controller was designed to fly the model for this MTE. It consist of three parts. Firstly, the collective was used to keep the altitude to a constant value by means of proportional and derivative control. Secondly the cyclic was used to control the pitch angle of the aircraft and in turn the velocity. Figure 3-13 shows a flowchart of the designed structure.

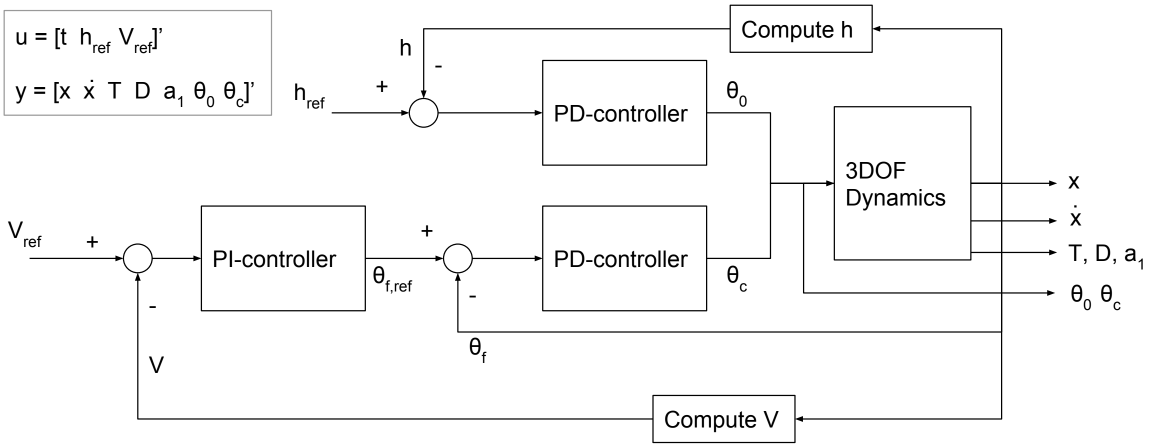

Figure 3-13: Flowchart of the controller built to fly the TO-Abort mission task element.

Subsequently the three proposed controllers were tuned to achieve a desirable tracking performance. Table 3-4 shows the gains that were used.

Table 3-4: Gains used to fly the TO-Abort MTE.

	K_h	$K_{\dot{h}}$	K_θ	K_q	K_u	K_x
TO-Abort	0.3	0.1	-5	-0.25	-0.12	-0.01

3-5-2 Results

This section will show and discuss the state, input and output characteristic of the closed loop simulation.

Firstly, the desired input for the controllers and the actual states of the aircraft is given in Figure 3-14a. As can be seen, there is some overshoot present in the velocity controller, where the aircraft state represented by the green lines lags behind the desired input represented by the blue line. The aircraft reaches a maximum velocity of 23.3 [m/s], which is desired performance for this maneuver.

At first glance it can be seen that the tracking performance of the altitude controller looks bad. However, considering the scale, it can be seen that it does not deviate by more than 0.3 [m], which is considered sufficient for this maneuver.

Figure 3-14b shows the accompanying input for the collective and cyclic inputs. It can be seen that there are no high frequent components or sudden jumps in the input. Therefore at this stage, the input is considered of sufficient quality to continue the analysis.

Besides the input and tracking performance, the states in the model were also studied. Firstly the thrust and drag forces have been plotted in Figure 3-15a. Furthermore, it is interesting

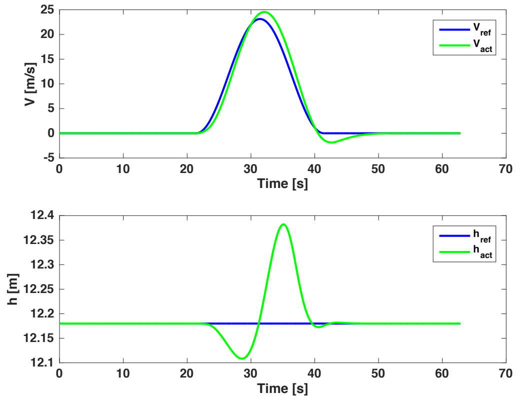

(a) Tracking performance of the Velocity controller (TOP) and altitude controller (BOTTOM).

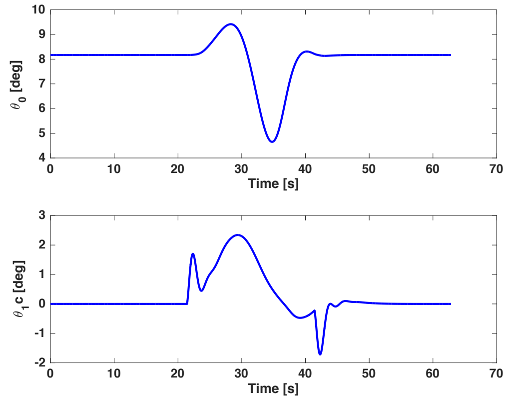

(b) Input of the collective (TOP) and cyclic (BOTTOM).

Figure 3-14: Controller performance for MTE I: TO and Abort.

to look at the level of coordination of the maneuver. From literature it was seen that the OMCT assumes a uncoordinated pitch-surge motion. In other words, the OMCT assumes that when pitching, there is a $gsin\theta$ component on the surge axis.

Figure 3-15b shows the acceleration on the surge axis and the contribution of the gravity vector in the same figure. For a coordinated maneuver, it would be expected that the two lines would overlap. If the acceleration on the surge axis is equal to the contribution of the gravity vector, then the specific force is equal to zero, and the motion is coordinated.

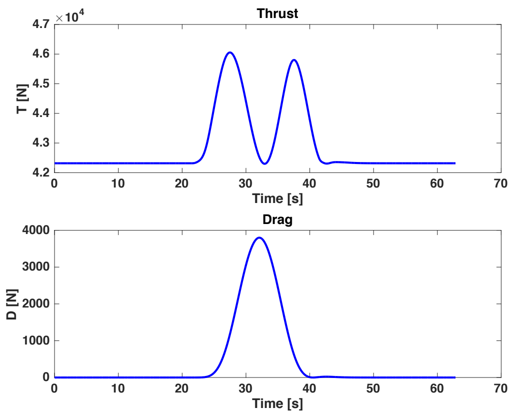

(a) Thrust and drag during the TO-Abort MTE.

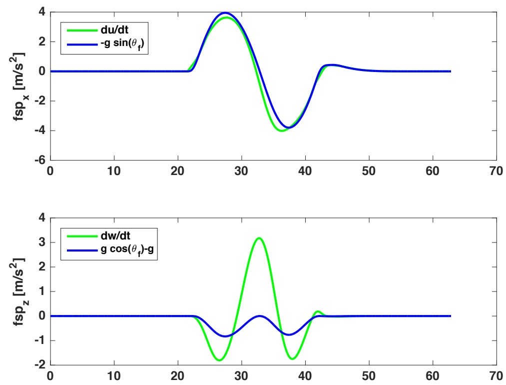

(b) Acceleration of on the x-axis (TOP) and on the z-axis (BOTTOM) and gravity components.

Figure 3-15: Forces and states for MTE I: TO and Abort.

Looking at Figure 3-15b, it can be seen that for the surge direction, gravity and linear acceleration mostly overlap, indicated that the maneuver is mostly coordinated.

3-5-3 Simulator Response

The next step is to connect the output of the 3 DOF model to the motion cueing algorithm. To do so however, the states firstly have to be converted into specific forces and rotational accelerations. This is done according to Equation 3-19.

$$f_{sp_x} = \dot{u} + g\sin(\theta_f) + wq \tag{3-19a}$$
$$f_{sp_z} = \dot{w} - g\cos(\theta_f) - uq \tag{3-19b}$$
$$\omega_{sp_y} = \dot{q} \tag{3-19c}$$

The specific forces and rotational acceleration were subsequently fed into the motion cueing algorithm of the SRS. As a test, similar parameter setting as the sensitivity analysis of the OMCT were used. The interested reader is referred to Table 4-2.

Figure 3-16 shows a time domain trace of the specific force in x an z-direction, together with the rotational acceleration.

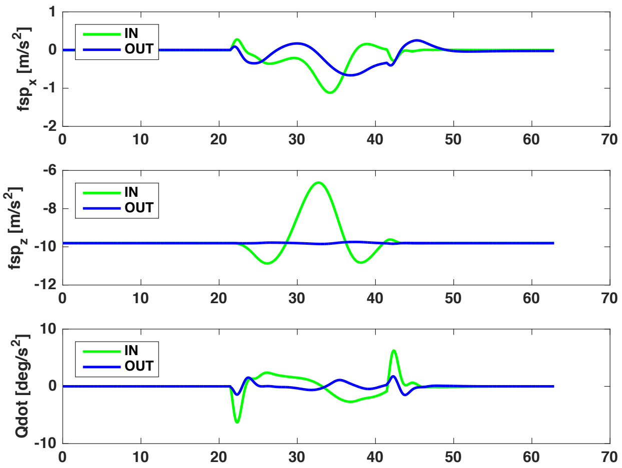

Figure 3-16: Specific forces of the aircraft (IN) and the simulator response (OUT).

Some general remarks on Figure 3-16:

- As can be seen, the performance on the heave axis is very poor. There a is large high pass break frequency on the heave axis needed since there is a limited workspace of the simulator. Low-frequency content is therefore filter out of the aircraft motion. Pilots often refer to this as the lack of response of the motion system to the collective. No 'collective dip' is felt. This is typical for helicopter simulations.
- High-frequency content is filtered out of the pitch acceleration by the cueing algorithm. Secondly, it can be seen that sustained pitch accelerations are 'washed out' by the filter on the pitch channel.

- On the surge channel, a similar response can be seen. Moreover, it can be seen that the high-frequency content is exited earlier. This is due to the lead generated by the high-pass filter.
- Lastly, from Figure 3-16 the presence of tilt coordination can be seen in the form of a bump at around 35 [s] in the pitch acceleration output of the simulator. This bump is the result of sustained surge acceleration of the aircraft at that time.

3-6 Mission Task Element II: Hover

To excite the higher frequencies more, it was decided to simulate a second mission task element, included turbulence. Turbulence settings were chosen as explained in subsection 3-1-4. It was chosen to simulate a hover motion, since it requires more precision from the pilot.

The task is initiated with a small forward velocity of 6 [kts]. The goal is the stabilized the aircraft in hover within 3 [s] and keep it at the same position +/- 3 [ft] for an extra 30 seconds.

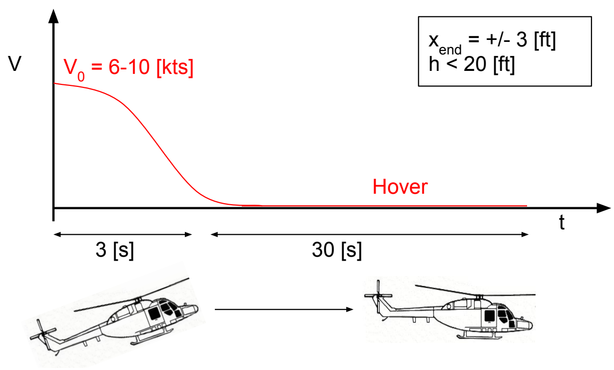

Figure 3-17: Schematic representation of the hover MTE.

Figure 3-17 shows a schematic representation of the maneuver. Notice the desired performance in the black square. For more information about the task, the reader is referred to Appendix C.

3-6-1 Controller

A similar control strategy was applied as for the Take-Off and Abort task. The collective was used to control the altitude and the Cyclic was used to control the pitch altitude and in turn the velocity. Figure 3-18 shows a schematic representation of the control scheme used for this task.

Table 3-5 shows the gains used for the controller.

Table 3-5: Gains used to fly the hover MTE.

	K_h	$K_{\dot{h}}$	K_θ	K_q	K_u	K_x
Hover	0.3	0.1	-2.5	-0.25	-0.1	-0.03

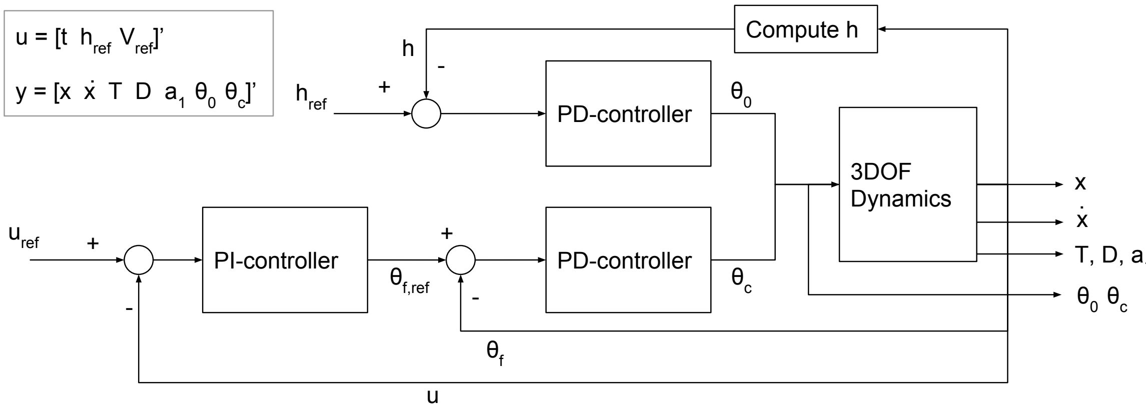

Figure 3-18: Schematic representation of the simulation of two basic MTE's.

From Table 3-5 it can be seen that K_x is higher that for the take-off abort maneuver. This is to ensure a better tracking of the position in hover. Secondly, the gain on the pitch angle K_θ is slightly relaxed, 2.5 instead of 5. This is to cope with the turbulence.

3-6-2 Results

The results of the simulation will be discussed here in a similar fashion as was done for the Take-Off and Abort MTE.

Figure 3-19a shows the performance of the altitude and velocity controllers. Figure 3-19b shows the accompanying input for the collective and the cyclic inputs.

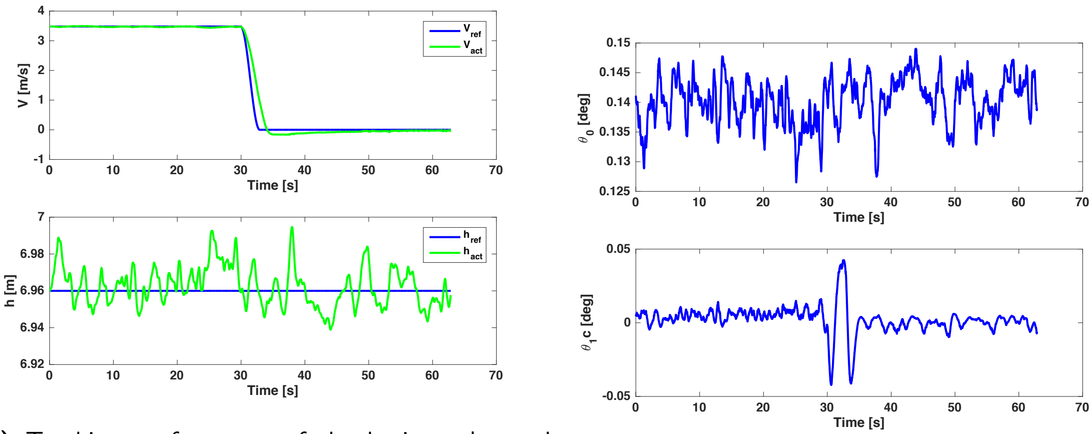

(a) Tracking performance of the horizontal speed controller (TOP) and altitude controller (BOTTOM).

(b) Input of the collective (TOP) and cyclic (BOTTOM).

Figure 3-19: Controller performance for MTE II: Hover.

It can be seen that the actual altitude and horizontal speed of the aircraft are signals with some power at the higher frequencies. Furthermore, it is seen that the helicopter does not stabilize in hover in under 3 seconds, but takes somewhat more, about 5 [s]. Due to the severity of the turbulence, a less aggressive controller was implemented.

Figure 3-20a shows the thrust and drag for this maneuver. It can be seen that the forces shows the characteristics of the turbulence, since both are directly related due to the inflow.

Figure 3-20b shows the acceleration along the body axes and compares it to the appropriate gravitational component. It can be seen that the acceleration along the z-axis is especially effected by the turbulence. This is to be expected, since this acceleration is directly coupled with thrust, which affected by the induced flow of the rotor. The horizontal velocity is affected less, since drag is less sensitive to the turbulence.

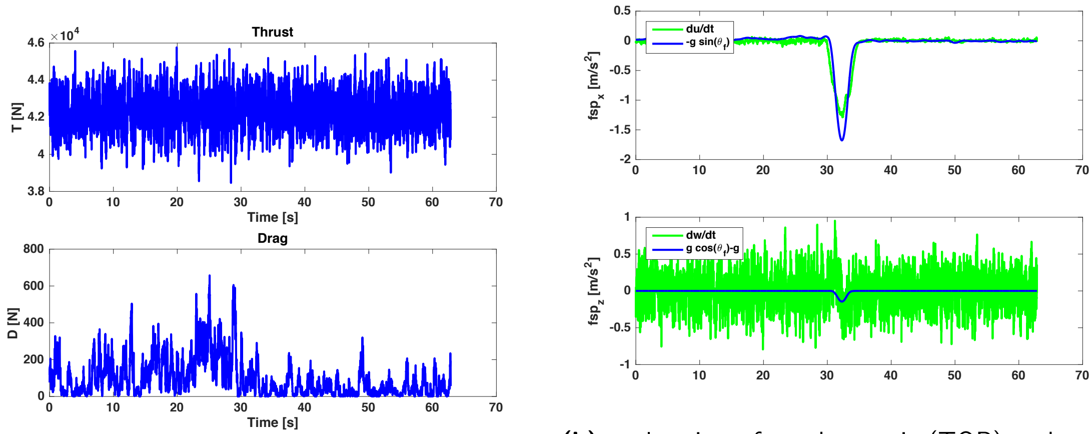

(a) Thrust and drag during the Hover MTE.

(b) cceleration of on the x-axis (TOP) and on the z-axis (BOTTOM) and gravity components.

Figure 3-20: Forces and states for MTE II: Hover.

3-6-3 Simulator Response

Similarly to the Take-off and Abort maneuver, the specific forces and rotational accelerations were computed and fed into the SRS motion cueing algorithm, according to Equation 3-19. Figure 3-21 shows the input and output of the cueing algorithm.

Several observations can be made about Figure 3-21:

- Firstly the motion in heave direction has more high-frequency content than for the take-off and abort MTE. This high frequency content is cued better.
- Not much pitch and surge input from the aircraft are present for this task, except for the deceleration at around 30 [s]. During this deceleration, similar cueing characteristics can be seen as during the take-off and abort task.

3-7 Frequency Domain

For the OMCT, it is of interest what the characteristics of these two maneuvers are in the frequency domain, such that they can be compared to set of input signals as described by the

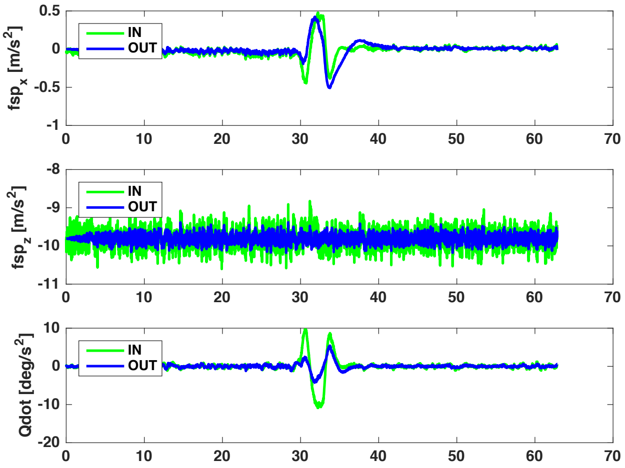

Figure 3-21: Specific forces of the aircraft (IN) and the simulator response (OUT).

OMCT. Therefore the fast fourier transform routine of matlab, *fft.m* was applied to the time domain traces of both maneuvers. No windowing was used. It is expected that two distinct areas are visible. A region at low frequencies with high power for the take-off and abort MTE and a region at high frequencies with power for the hover MTE. Figure 3-22 shows the amplitude and phase spectrum of the rotational acceleration for both maneuvers.

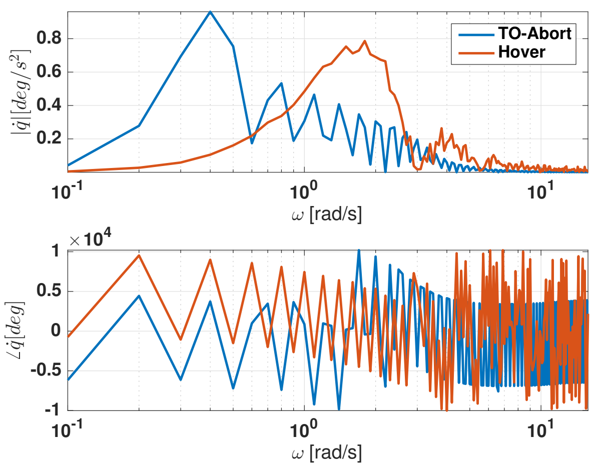

Figure 3-22: Amplitude and phase spectrum for the rotational acceleration of the Take-Off and Abort and Hover task.

It can be seen from Figure 3-22, that for the rotational acceleration indeed there are two distinct regia. Note however, that the power at these signals low compared to the original OMCT, around 0.01 [rad/s2]. Furthermore it can be seen that the phase shifts 180 degrees for every consecutive data point. This is due to the fact that the time traces of the signal resemble a sinc function. The Fourier transform of a sinc function has a phase that shift 180 [deg], to make the sinusoids damp each other out.

Figure 3-23a and Figure 3-23b show the same plots for the specific force in x-direction and z-direction respectively.

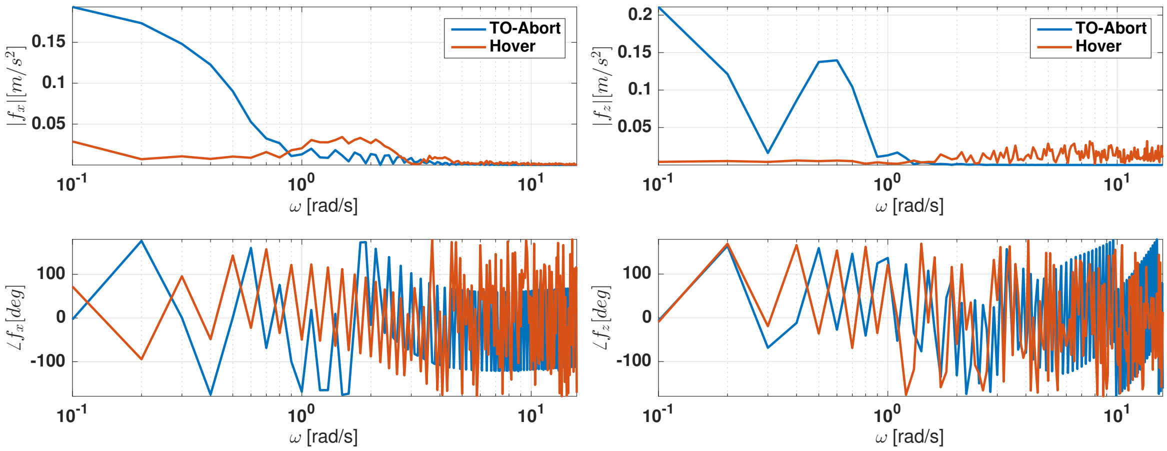

(a) Amplitude and phase spectrum for the specific force in x-direction of the Take-Off and Abort and Hover task.

(b) Amplitude and phase spectrum for the specific force in z-direction of the Take-Off and Abort and Hover task.

Figure 3-23: Frequency domain output for two MTEs.

It can be seen that for both surge and heave, at low frequencies, $\omega < 1[rad/s]$, take-off and abort has a high amplitude. Power for the hover motion is low throughout the amplitude spectrum.

Chapter 4

OMCT Sensitivity Analysis

This chapter discusses an off line implementation of the Objective Motion Cueing Test in its current form, together with a thorough sensitivity analysis. section 4-1 discusses the practical implementation of an OMCT on the motion drive algorithm of the SRS. This procedure is then verified in by comparing results to literature in section 4-2.

After an OMCT routine has been established, the sensitivity of two aspects is investigated.

- Firstly the shape of the OMCT plots is explained by performing a sensitivity study of the OMCT to parameters of the classic washout algorithm in section 4-3. Some remarks on the usefulness of the OMCT for tuning are furthermore discussed.
- In section 2-3, it was seen that the OMCT makes assumptions on the input spectrum about the aircraft dynamics. The influence of these assumptions on the frequency response function of the OCMT is therefore studied. section 4-4 studies the sensitivity of the OMCT to linearity of the input spectrum. Secondly the influence of coupling between input signals of different degrees of freedom is studied.

4-1 Off-line Implementation of the OMCT

The OMCT was published in Attachment F of amendment 3 of the ICAO manual 9625, [4]. This document offers guidance on the OMCT in terms of set-up, specified input signals and presentation of results. For this analysis, this will be the leading source of information.

The core of this off line OMCT is a `simulink` file with the MDA as is in used by the SRS, represented by the block *Motion Cueing Algorithm* in Figure 4-1. Around this script, a `matlab` file was built to run the MDA with different inputs. Figure 4-1 shows the process illustrated in a flow chart. As can be seen, the simulation consists of a signal generator, the `simulink` model and a post-simulation data processing part.

From Figure 4-1, it can be seen that several steps are taken towards the computation of different frequency response functions of the MCS. For every frequency specified, the following steps were repeated:

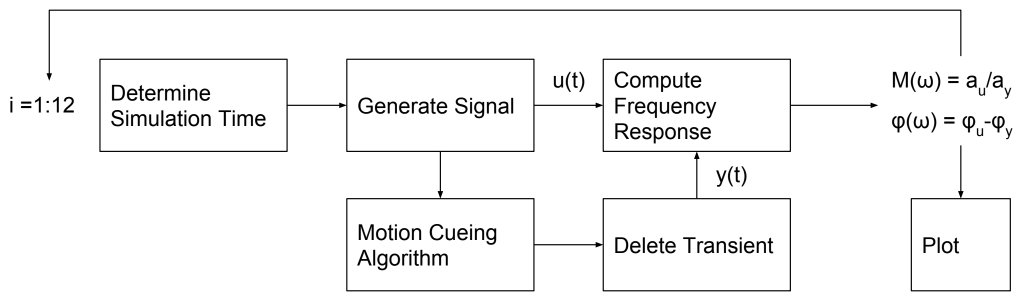

Figure 4-1: Flowchart of the off line OMCT simulation.

- In the first block, the simulation time is adjusted for every frequency input. This is done for two reasons. Firstly it was seen that the SRS has a transient period of approximately 10 [s]. This transient response of the simulator needs to be excluded in the frequency analysis that follows, since MCA contains a fade-in to ensure a smooth start-up of the hardware. Secondly, the simulation time needs to be adjusted such that the input an output sinusoid fit an integer number of periods in the simulation time. This is to minimize any leakage effects in the Fast Fourier Transform that will be used to analyze the frequency characteristics of the signals. The total simulation time T is therefore computed by Equation 4-1.
$$T = (n_1 + n_2)\frac{2\pi}{\omega} \tag{4-1}$$
Where n_1 is the total number of vibrations that fit inside the transient, rounded upwards, according to Equation 4-2, and n_2 is the total amount of vibrations used for this simulation. To keep computation time small for low frequency input signals, the number of vibrations was set to 10, $n_2 = 10$.
$$n_1 = ceil(t_0\frac{\omega}{2\pi}) \tag{4-2}$$
Where t_0 for this simulation has been chosen to be 10 [s].
- Secondly the signal generator generates an input according to Equation 4-3. Note however, that for some tests, there is also an input on other axes. For every axis (6 for a generic 6 DOF hexapod MCS), there are 12 sinusoids prescribed in the form of Equation 4-3.
$$u = A\sin\omega t \tag{4-3}$$
Where u is the input signal on the specific channel, A is the amplitude and ω one of the twelve frequencies. A and ω are specified in Table 4-1.
As can be seen, the specified amplitude for the input signals of the translational channels is always equal to 1. Furthermore, signal 6 represents the Sinacori Schroeder criterion, which is the frequency and phase response at 1 $[rad/s]$ and 1 $[m/s^2]$. These input signals are then used as input signals for different channels in combination with different output channels. 12 combinations were tested, according to Figure 2-15
- The Motion Cueing Algorithm is a `simulink` file with a loaded parameter in use for the SRS. It uses 9 inputs, according to Equation 4-4. For this simulation however,

Table 4-1: OMCT input signals as specified in [4].

Frequency Number	Frequency	Translational Amplitude	Rotational Amplitude
[-]	ω $[rad/s]$	$A[m/s^2]$	$A[deg/s2]$
1	0.060	1.0	0.060
2	0.150	1.0	0.150
3	0.251	1.0	0.251
4	0.398	1.0	0.398
5	0.631	1.0	0.631
6	1.000	1.0	1.000
7	1.585	1.0	1.585
8	2.512	1.0	2.512
9	3.981	1.0	3.981
10	6.310	1.0	6.310
11	10.000	1.0	10.000
12	15.849	1.0	10.000

the simulator will not be driven by angular rates P, Q an R, but only by angular accelerations.

$$u = \begin{bmatrix} f_{sp_{x,y,z}} \\ P,Q,R \\ \dot{P},\dot{Q},\dot{R} \end{bmatrix} \begin{matrix} [m/s^2] \\ [rad/s] \\ [rad/s^2] \end{matrix} \tag{4-4}$$

As output the `simulink` model gives the specific forces of the simulator, angular accelerations and actuator position of the six hydraulic pistons, according to Equation 4-5

$$y = \begin{bmatrix} f_{sp_{x,y,z}} \\ \dot{P},\dot{Q},\dot{R} \\ FUD_{1-6} \end{bmatrix} \begin{matrix} [m/s^2] \\ [rad/s^2] \\ [m] \end{matrix} \tag{4-5}$$

- Thereafter, the transient response of the output is deleted from the time domain measurements, by deleting $n_1\frac{2\pi}{\omega}$ from the dataset, as is illustrated in Figure 4-2.

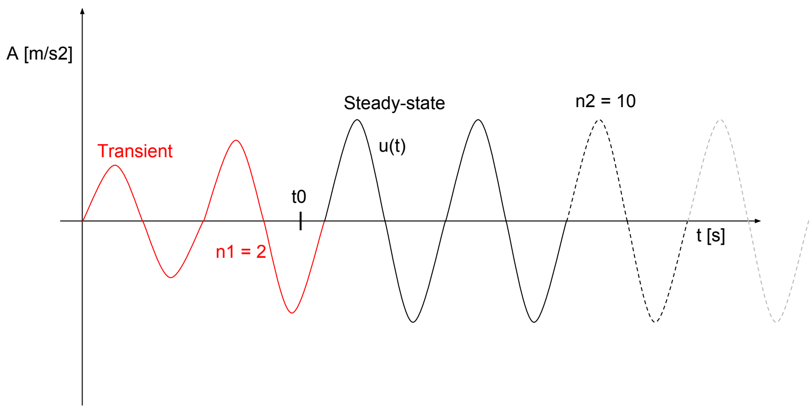

Figure 4-2: Illustration of a typical output signal of the MDA. As can be seen, for this perticular example there fit two periods of the ouput sine inside transient period. The Fast Fourier Transform will therefore by conducted on t=$[n_1\frac{2\pi}{\omega}$ - $10\frac{2\pi}{\omega}]$.

- In the time domain, the input and output signals will look for example like the illustration in Figure 4-3.

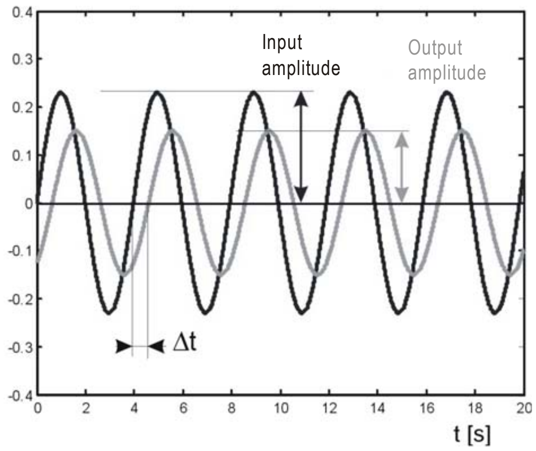

Figure 4-3: Illustration of and exemplary input and output signal from the MDA.

These signals were converted to the frequency domain using the Fast Fourier Transform, (FFT), routine in `matlab`. Note that it was chosen to both use the FFT on the output and input signal. This was done because potential leakage would affect both the amplitude of $y(\omega)$ and $u(\omega)$, which would therefore be minimized in the division to compute the modulus.

- Thereafter the modulus and phase difference were computed according to Equation 4-6 and Equation 4-7 respectively.

$$|H(\omega)| = \frac{|y|}{|u|} \tag{4-6}$$

$$\angle H(\omega) = \angle y - \angle u \tag{4-7}$$

- Finally, the resulting points in frequency domain were plotted using a Bode plot.

4-2 Verification

To verify the explained process, test results for test 1-10 were reproduced and compared with data from an OMCT conducted on the SRS, [9]. For the sake of brevity, the result of this verification process is not given here, but put into Appendix D.

4-3 Sensitivity to MDA Settings

This Section discusses the sensitivity of the OMCT to changes in the MDA settings. The insights gained in this section are also useful for tuning. A basic set of parameters was used for the verification of the algorithm, shows here in Table 4-2. Four specific parameters were changed subsequently, after which the effect was measured on the OMCT sub tests.

Table 4-2: Reference settings of the SRS motion cueing system.

	Gain [-]	2nd Order High-Pass Break Frequency ω_n $[rad/s]$	2nd Order High-Pass Damping ζ [-]	1st Order Break Frequency ω_b $[rad/s]$	2nd Order Low-Pass Break Frequency ω_{nLP} $[rad/s]$
Roll	0.6	0.8	1.0	-	-
pitch	0.7	0.8	1.0	-	-
Yaw	0.6	1.0	1.0	-	-
Surge	0.7	1.0	1.0	-	2.0
Sway	0.6	1.0	1.0	-	2.0
Heave	0.5	2.5	1.0	0.2	-

Since the model developed in the proceeding has only three degrees of freedom, focus will be put on heave, surge and pitch. This reduces the OMCT to test 1, 2, 6, 7 and 10, where 1, 6 and 10 are tests on a single axis. Test 2 and 7 display the cross tests. Considering the classical washout algorithm, there are four filters that influence the longitudinal motion of the simulator, as can be seen in Figure 4-4.

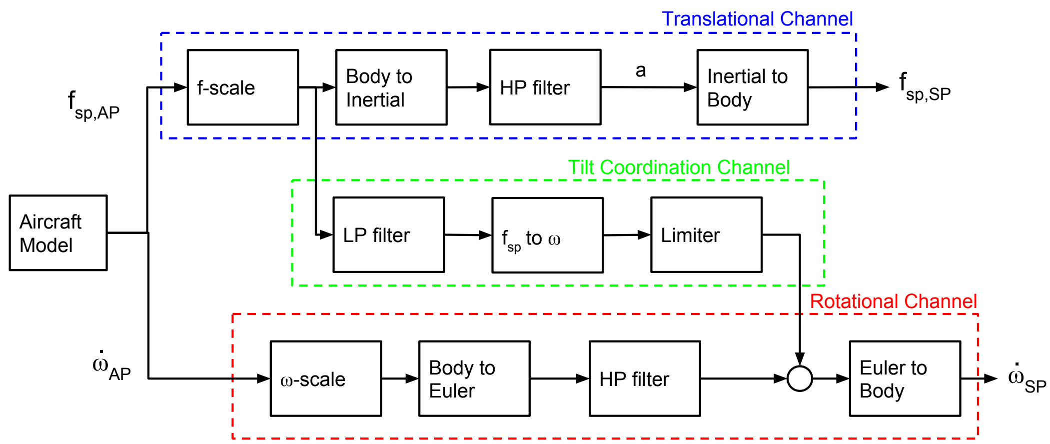

Figure 4-4: Schematic representation of the classical washout motion drive algorithm.

The filter that affect longitudinal simulator motion are:

- The high-pass filter in the surge translational channel, represented by its break frequency ω_{nx}.
- The high-pass filter in the heave translational channel, represented by its break frequency ω_{nz},
- The high-pass filter in the pitch rotational channel, represented by its break frequency $\omega_{n\theta}$.
- The low-pass filter in the surge tilt coordination channel, represented by its break frequency ω_{nLPx}.

For a complete single axis analysis therefore, 20 plots are required. However, if the dynamics of the simulator are considered decoupled, heave is only affected by ω_{nz}, surge is only affected by ω_{nx} and ω_{nLPx} and pitch only by $\omega_{n\theta}$. However, the OMCT also includes a surge input for test 1 and 2. Therefore those test are also influenced by ω_{nx}.

The resulting sensitivity analysis consists of 8 plots, 2 for $\omega_{n\theta}$, 4 for ω_{nLPx}, 1 for ω_{nx} and 1 for ω_{nz}. The information these plots give about the classical washout algorithm is apparent. For practical purposes not all plots will be given here. They are present however, in Appendix E.

However, to illustrate that the OMCT gives meaningful information about the motion cueing performance, one plot is shown here. Figure 4-5 shows the sensitivity of test 6, the direct frequency response function of the surge axis, to changes in the high-pass break frequency on the surge channel, ω_{nx}.

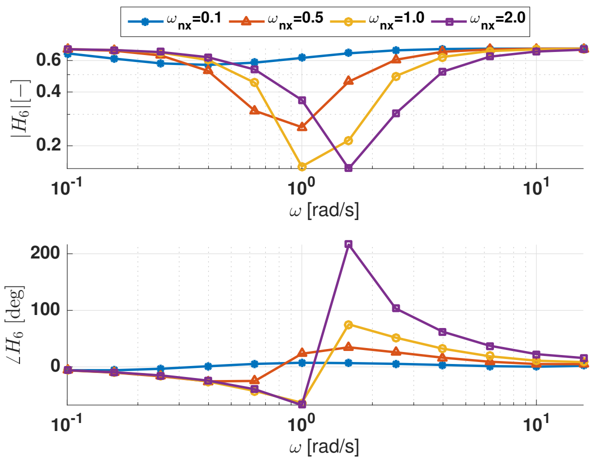

Figure 4-5: Sensitivity of Test 6:surge-surge to change in ω_{nx}.

It can be seen that the 'dip' in gain around 1 [rad/s] is shifting to the left and is gradually smoothened out when decreasing the break frequency on the surge channel. This is to be expected, since more surge is passed through by the high-pass channel at low frequencies. Therefore, according to this plot, the performance of the motion filter becomes better when decreasing the high-pass break frequency on the surge channel, since the modulus of the transfer function is closer to 1 on this frequency range. However, when decreasing ω_{nx}, the simulator will eat up more workspace. For the purpose of tuning, additional information might be needed for Figure 4-5.

4-3-1 Tuning

Tuning on a single axis with the OMCT is a straightforward procedure, and will be explored briefly in this section. To find appropriate values for gain and break frequencies, two pieces of information can be added to the sensitivity plots made in section 4-3, to make them more insightful.

1. Firstly, the **workspace** of the simulator needs to be taken into account. Some tuning settings will cause the simulator actuators to extend more than their limits, given an unworkable tuning setting. Therefore it is important to calculate the actuator lengths at any given time during the simulation.
   The actuator lengths are calculated by computing the positions of the gimbal points in the lower frame, indicated by $\bar{l}_i$, and subtracting them from the gimbal points in the

upper frame of the simulator. The interested reader is referred to Appendix F, where the geometry of the SRS, including the positioning of gimbal points is described. i ranges from 1 to 6 for the hexapod system. Equation 4-8, shows the computation of actuator lengths.

$$l_{act_i} = \sqrt{(l_{i_x} - u_{i_x})^2 + (l_{i_y} - u_{i_y})^2 + (l_{i_z} - u_{i_z})^2} \tag{4-8}$$

$\bar{l}_i$ was computed readily from the geometry of the SRS as described in Appendix F. $\bar{u}_i$ however also includes to movement of the simulator, according to Equation 4-9.

$$\begin{aligned} u_i = &\begin{bmatrix} x_{UGP} \\ y_{UGP} \\ z_{UGP} \end{bmatrix} + \\ &\begin{bmatrix} \cos\theta\cos\psi & \sin\phi\sin\theta\cos\psi - \cos\phi\sin\psi & \cos\phi\sin\theta\cos\psi + \sin\phi\sin\psi \\ \cos\theta\sin\psi & \sin\phi\sin\theta\sin\psi + \cos\phi\cos\psi & \cos\phi\sin\theta\sin\psi - \sin\phi\cos\psi \\ -\sin\theta & \sin\phi\cos\theta & \cos\phi\cos\theta \end{bmatrix} \bar{u}_{i_M} \end{aligned} \tag{4-9}$$

Equation 4-9 is the transformation of the simulator body frame to the inertial reference frame, where x_{UGP},y_{UGP} and z_{UGP} are the translations from the classical washout algorithm and ϕ,θ and ψ are the rotations. In rest, stated values have the following properties: $(x_{UGP}, y_{UGP}, z_{UGP}, \phi, \theta, \psi) = (0, 0, 2.446[m], 0, 0, 0)$, [14].
To verify the computation of the actuator lengths, for different input positions and rotations, the actuator lengths were computed and checked against the actuator stroke limits from Appendix F. Figure 4-6a shows these limits in the surge-heave plane in green. In Figure 4-6a also the single axis simulator limits have been plotted, as calculated by Gouverneur, [26]. A similar computation was made in Figure 4-6b, where the pitch angle is varied instead of the heave position.

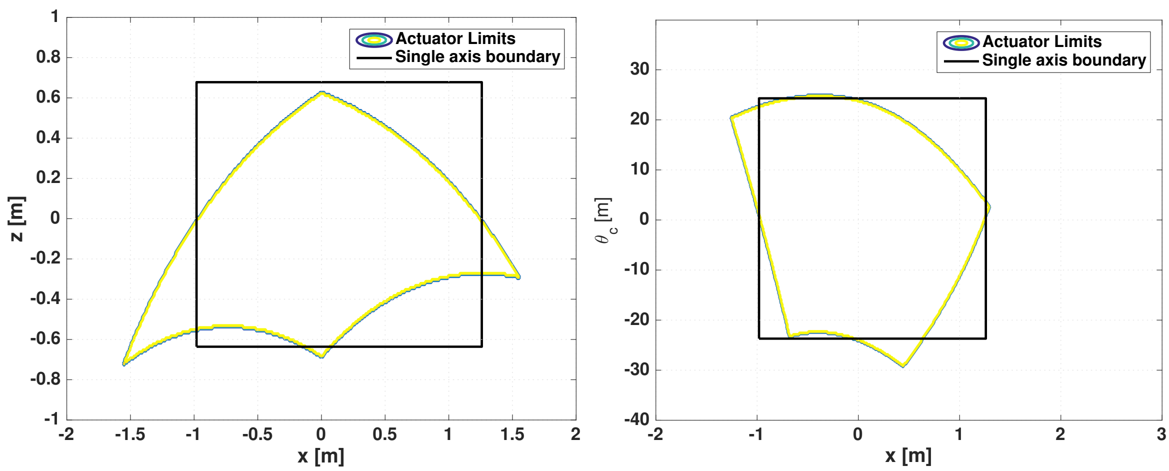

(a) Motion space surge vs. heave.

(b) Motion space surge vs. pitch.

Figure 4-6: Visualization of the motion space for the SRS.

It is expected that for both plots, at $x = 0$, $z = 0$ or $\theta = 0$ the green and the black limits will intersect. When the simulator is constrained to one axis, actuator stroke limits are

expected to be similar to the single axis limits. For for $z = 0$ and $\theta = 0$ this is the case. However for $x = 0$, there is a discrepancy. This is due to the fact that the neutral position z_{UGP_0} taken from Advani[14] is slightly different Gouverneur uses in his work, [26].
A time trace of the flight data is fed into the MDA with a particular cueing setting. The output of this is a required translational and rotational acceleration of the simulator. With this information an estimate can subsequently be made about the required actuator lengths, using the model stated above.

2. Secondly, some knowledge is needed about which frequencies are most important when flying a specific type of aircraft, mission or task. By combining knowledge from the two simulated Mission Tasks Elements, an estimate can be made as to which frequencies are more important. With this knowledge, the tuning engineer can focus his attention on that specific region of the plot. These important frequencies from now on will be referred to as **dominant frequencies**.
To find the dominant frequencies for both Mission Task Elements, the PSDs from section 3-7 were compared to the sensitivity analysis given in Appendix E. The amplitude from the PSDs was plotted over the gain from the frequency response function. However, since the amplitude is not of the same magnitude as the gain in most frequency functions, the amplitude from the PSDs for pitch surge and heave was normalized and scaled, according to Equation 4-10,

$$|\dot{q}|_{adj} = K_q \frac{|\dot{q}| - |\dot{q}|_{min}}{|\dot{q}|_{max} - |\dot{q}|_{min}} \tag{4-10a}$$

$$|f_x|_{adj} = K_x \frac{|f_x| - |f_x|_{min}}{|f_x|_{max} - |f_x|_{min}} \tag{4-10b}$$

$$|f_z|_{adj} = K_z \frac{|f_z| - |f_z|_{min}}{|f_z|_{max} - |f_z|_{min}} \tag{4-10c}$$

where $|\dot{q}|_{adj}$, $|f_x|_{adj}$ and $|f_z|_{adj}$ are the adjusted amplitudes computed from $|\dot{q}|$, $|f_x|$ and $|f_z|$ and K_q, K_x and K_z are gains from the classical washout algorithm given in Table 4-2.

With the flight data provided by the simulation of two mission task elements, the dominant frequencies and the workspace analysis can both be visualized in one plot. Doing so, results in 8 new plots for the sensitivity analysis using the take-off and abort MTE and 8 new plots for the hover MTE. For the sake of brevity, they are included in Appendix G. Figure 4-7 shows an example of this analysis done on test 6 of the OMCT, using the time domain trace of the take-off and abort MTE.

From Figure 4-7, it can be seen that for some filter settings ($\omega_{nx} = 0.1, 0.5$), the OMCT plot is a dotted line, indicating it exceed the workspace boundary for one or more actuators for the take-off and abort MTE.

The blue line displayed in top of the OMCT shows the frequency domain data from the take-off and abort MTE. It can be seen that for this particular model and this particular controller, the helicopter motion has most of it power at low frequencies, ($\omega < 1[rad/s]$).

An engineer tuning a new simulator might think that the ω_{nx} would have to be as low as possible, without violating the motion space. However, if shown this plot he would see that,

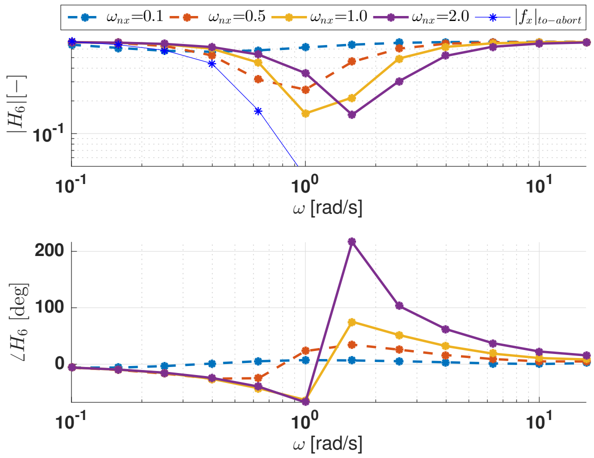

Figure 4-7: Sensitivity of test 6 to changes in the high-pass break frequency of the surge translational channel, values ranging from $\omega_{nx} = 0.1$ to $\omega_{nx} = 2.0$

since the dominant frequencies are below 1 [rad/s], it might also be a good idea to go for a larger high-pass break frequency, e.g. $\omega_{nx} = 2.0$.

4-4 Sensitivity to the OMCT Assumptions

From literature, it was seen that the OMCT makes 3 assumptions on the input of the motion from a mathematical model of the aircraft. Firstly, there is a limited frequency range. This assumption is considered valid, since the region for manual control lies between 0.5 - 5 [rad/s]. Secondly however, the OMCT assumes a constant amplitude of ingoing sinusoids. Thirdly, the OMCT studies only cases were one axis at a time is driven (except for test 1 and 2). The question therefore arises, what is the influence of the last two assumptions? subsection 4-4-1 discusses the size of the ingoing sinusoids, whereas subsection 4-4-2 studies driving multiple axes simultaneously.

4-4-1 Amplitude Spectrum

Besides looking at the OMCT sensitivity to the classical washout algorithm, it is also important to see it's sensitivity to the input amplitude of the ingoing sinusoids.

For all longitudinal tests, the input spectrum was varied from 0.1 to 2.0 $[m/s^2]$ on the heave and surge input channels and from 0.5 to 10 $[deg/s^2]$ on the pitch input channel. Note that the amplitude for the rotational channel of the OMCT is a ramp function, therefore the constant amplitude spectrum used for this sensitivity analysis in test 1 and test 2 differs significantly from the OMCT. Figure 4-8, shows the result for test 6. It can be seen that for high frequencies of the spectrum, little difference is seen in the OMCT. However, for the low frequencies of the spectrum, the difference is apparent.

Similarly to test 6, tests 1, 2, 7 and 10 were studied. Once again, for the sake of brevity, the results have been put in an appendix, Appendix H.

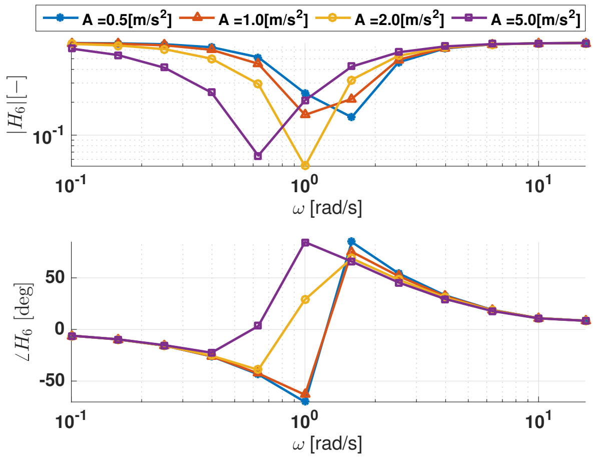

Figure 4-8: Sensitivity of test 6 to changes in the amplitude of the input sinusoids.

It was seen that the OMCT is sensitive to non-linear effects is the simulator motion cueing, most apparent among which was the rate limiter in the tilt coordination channel. The rate limiter is present, to make sure that any rotations caused by the tilt coordination channel stay below vestibular thresholds. Looking at Figure 4-8, it is seen that for low amplitudes of the input spectrum, the OMCT lines are similar. However, after $A = 1.0$, the 'dip' in test 6 starts moving left and becomes deeper. At higher amplitudes of the surge input signal, especially at low frequencies, the pitch rate asked to achieve desired sustained surge accelerations exceeds vestibular boundaries. Here, the rate limiter reduces the pitch rate, but in turn also affects the simulated surge accelerations.

4-4-2 Coupling of Input Signals

Crosstalk from Surge to Pitch

The most important form of coupling in the cueing algorithm is crosstalk from surge to pitch. Sustained surge motion is simulated by tilting the simulator through a low-pass filter in the tilt coordination channel. This form of crosstalk is studied by the OMCT in 2 tests. Firstly the surge axis is excited and the output on the pitch axis is studied. Figure 4-9 shows a pitch frequency response function due to an input on surge.

A typical tuning purpose of this test would be to determine the low-pass break frequency of the tilt coordination channel. As can be seen from figure 4-9, a higher break frequency will result in more cross coupling from surge to pitch. However, it is hard tune the algorithm based on this plot. It is is not clear which combination of gain and phase results in a simulation with the high predicted motion fidelity. Crosstalk from surge to pitch is not a false cue since it is needed for tilt coordination. Therefore the gain of test 7 should not be as low as possible. However, a too large gain might result in unwanted pitch acceleration.

A second test that studies crosstalk from surge to pitch is the pitch frequency response function using both surge and pitch input. Since for fixed-wing aircraft it is assumed that there is an uncoordinated motion between pitch and surge, also a signal is fed into the simulator on surge: $f_x = gsin(\theta)$. Figure 4-10 shows test 1 of the OMCT.

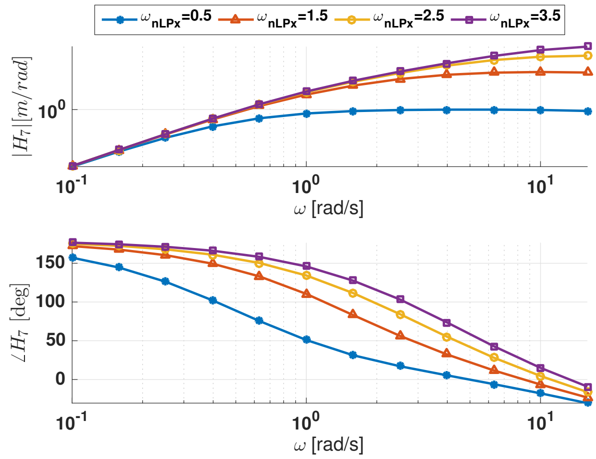

Figure 4-9: Pitch frequency response function for a surge input, test 7 of the OMCT.

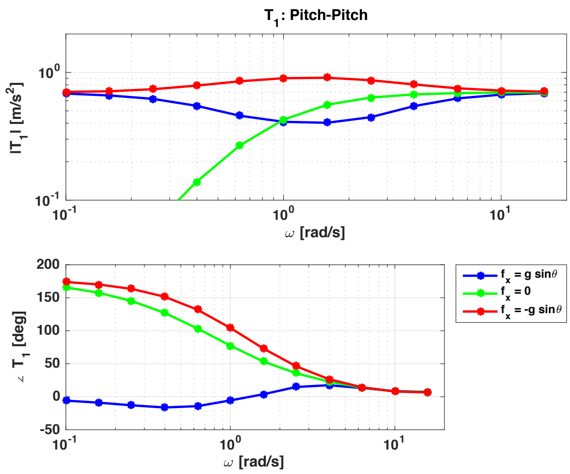

Figure 4-10: Pitch frequency response computed with an input on pitch and surge axes, test 1 of the OMCT

In figure 4-10 three situations are depicted. Firstly a frequency response function from the current OMCT is depicted, indicated by $f_x = g\sin\theta$. Helicopter motion is mostly coordinated, which is a common assumption for helicopter dynamics in simulator fidelity research, used for example in [50] and [37]. This is an indication that during a regular helicopter task, $f_x = \dot{u} - g\sin(\theta) \cong 0$. In figure 4-10 this scenario is represented by $f_x = 0$. Thirdly a test is shown were instead of $f_x = g\sin(\theta)$, $f_x = -gsin(\theta)$ is cued.

It can be seen that the assumption of uncoordinated pitch-surge motion significantly influences the motion characteristics, especially at low frequencies.

Crosstalk from Pitch to Surge

Crosstalk from pitch to surge originates from the transformation between the aircraft body frame of reference and the simulator inertial frame, indicated in figure 4-4. In the longitudinal plane this transformation reduces to the addition of $g \sin\theta$. θ in this case is the filtered pitch angle of the simulator. The OMCT studies this crosstalk by means of test number 2. Figure 4-11 shows a surge frequency response function due to an input on the pitch and surge channels.

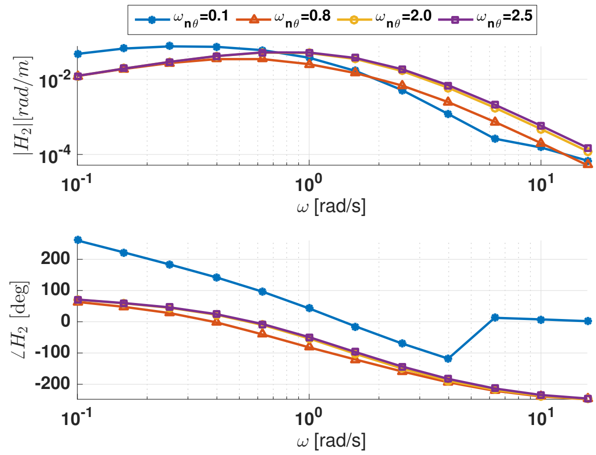

Figure 4-11: Surge frequency response function due to pitch input, test 2 of the OMCT.

A typical tuning purpose of this test would be to determine the high-pass break frequency of the pitch channel. As can be seen from figure 4-11, a higher break frequency will result in more cross coupling from pitch to surge. However, as was the case for figure 4-9, the results from figure 4-11 are hard to interpret.

- As for test 1 displayed in figure 4-10, both an input on pitch axis and on the surge axis is used for this test. Therefore, not only is pitch-surge coupling is included, but also surge-pitch coupling.
- Furthermore, surge acceleration a_x, not specific force f_x is taken as the output for this test.
- Cross talk from pitch to surge is a false cue but, especially due to the presence of tilt coordination not entirely unavoidable, as was discussed in [50]. Similar to figure 4-9, it is therefore it is hard to judge the motion characteristics, since it is unclear what combination of gain and phase gives a high predicted motion fidelity.

Crosstalk from Pitch to Heave

Thirdly there is crosstalk from pitch to heave. In a similar way as crosstalk from pitch to surge, this form of crosstalk originates in the fact that input from the mathematical model has to be transformed to the inertial frame of reference of the simulator, indicated in figure 4-4. In the longitudinal plane this transformation reduces to the addition of $g \cos\theta$ for a longitudinal simulation. The OMCT does not provide a test to study this type of cross talk. However, since pitch simulator angles are small daily helicopter simulation, this form of crosstalk is not expected to influence the motion characteristics significantly.

4-5 Conclusion

In this chapter the sensitivity of the OMCT was studied in two ways.

- Firstly the influence of MDA settings was investigated. It was seen that meaningful information can be obtained about motion cueing characteristics when performing a single axis sensitivity analysis OMCT. However, for effective tuning, firstly the motion space needs to be taken into account and secondly, the characteristics of aircraft motion from the mathematical model.
- Secondly the influence two assumptions of the current set of input signals of the OMCT on the frequency response functions were put to the test. It was seen firstly that there is a large sensitivity to rate limiting in the tilt coordination channel. Secondly, it was seen that surge-pitch coupling is represented incorrectly in the direct pitch frequency response function, figure 4-10. Finally the results from cross coupling tests 2 and 7, given by figure 4-11 and figure 4-9 respectively, are hard to interpret.

The sensitivity of the OMCT to the set of input signals essentially boils down to to the fact that the OMCT might not incorporate knowledge about the physical motion of the aircraft sufficiently. Therefore, a possible next would be to investigate whether a set of input signals can be found that potentially better represent helicopter motion in the longitudinal plane.

Chapter 5

A Tailored OMCT

At this point the OMCT has been investigated and the the characteristics of rudimentary helicopter motion have been simulated and converted to the frequency domain. From the sensitivity analysis conducted with the original OMCT, it was seen that the amplitude of the input spectrum and coupling inputs on different axes influences the outcome of the plots greatly. In this chapter therefore an attempt is made to use the knowledge gained and design a new set of input signals for the OMCT. By making use of the amplitude and phase spectra given in section 3-7, options for new inputs signals will be explored.

The envisioned test has the following requirements, stated in order of their importance.

1. The set of input signals has to be as close as possible to the actual motion of the helicopter in the simulated Mission Task Elements.
2. The test should yield meaningful information about the motion cueing system.
3. The test should be easily implementable in practice, this means test duration should be limited and that inputs should be of a magnitude high enough not to cause any problems with signal to noise ratio for an IMU in a possible on-line OMCT.

Before a design was proposed, several design options have been explored. Figure 5-1 shows a design option tree, containing 4 design options for a tailored OMCT.

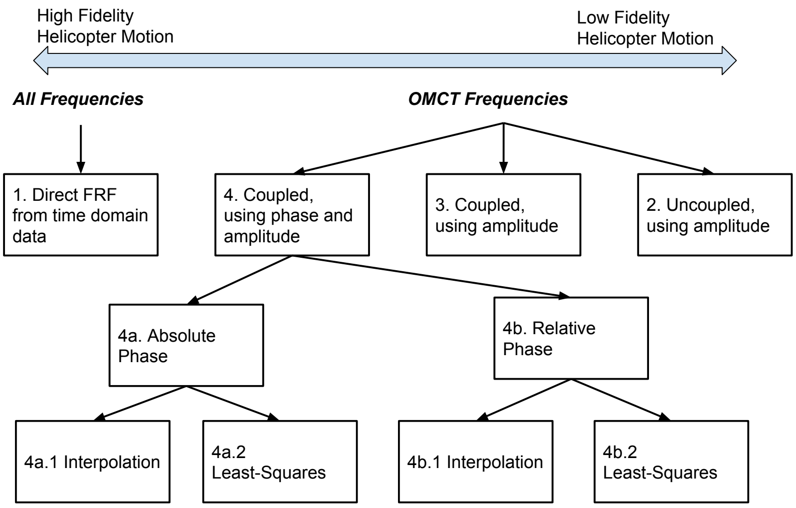

Figure 5-1: Design Option Tree of different options to tailor an OMCT on specific MTE data. Options on the left are more close to real helicopter motion, option on the right contain helicopter motion of a lower fidelity.

The following design options were identified:

1. **Direct Frequency Response Function**
It is hypothesized that a frequency response function can be constructed by transforming time domain data from the MTEs directly to the frequency domain. Instead of using sinusoidal input signals on certain designated frequencies, an estimate of the frequency response functions is constructed from the available time domain data in the simulation. This is a quick way to make an estimate of the frequency response of the Motion Drive Algorithm. However, this method is at the same time less attractive from a signal processing point of view, since known problems with the FFT, such as windowing and leakage, might affect the frequency response more.
2. **Uncoupled, tailored amplitude**
In chapter 4, it was seen that the OMCT is influenced by changes to the amplitude of the input spectrum. Therefore a next logical step in the analysis could be to tailor the amplitude of the input sinusoids to the two simulated Mission Task Elements. However, in real helicopter simulation multiple axes are excited simultaneously, which makes a difference for the frequency response functions computed by the OMCT.
Therefore, to make a realistic Objective Motion Cueing Test, there should be an input on all axes simultaneously. An uncoupled OMCT with only a tailored amplitude will therefore not yield a level fidelity of the input signals that is sought. This design option is therefore discarded.
3. **Coupled, tailored amplitude**
Design option 3, proposes to include inputs on 3 different axis simultaneously. However there exist a problem when doing so. Consider again the first test of the classic OMCT, illustrated in Figure 4-10. It of importance if the pitch-surge motion is cued with the same phase, with a term $g \sin\theta$ or maybe in the opposite direction $-g\sin\theta$.
It can be seen that when using a term of $-g\sin\theta$, or in other words with a phase shift of 180 degrees, the sinusoids are added through the tilt coordination in the area around 1

[rad/s], instead of being subtracted. It can be concluded therefore that the phase is also of importance when designing a set of input signal that resembles helicopter dynamics. Design option 3 is therefore also discarded from this point on.

4. **Coupled, tailored amplitude and phase**
   A fourth design option is to use a set of input signals for the OMCT that have not only the same amplitude as the FFT data on all axes, but also have the same phase relative to other degrees of freedom.
   There can be distinguished however two different ways to extract a good estimate of the amplitude and phase spectra on the OMCT frequency points. One can use the absolute phase of the signals or the relative phase difference. These two options will be explored in the proceeding.

After a preliminary analysis, two options are left from the design option tree. Firstly there is a direct FRF. In section 5-1 this option will be evaluated. Secondly, coupled test using both amplitude and phase information will be studied in section 5-2. Based in this analysis a final design will be chosen in subsection 5-2-3. Thereafter a sensitivity analysis with this adapted OMCT will be conducted and discussed in section 5-3.

5-1 Direct Frequency Response Function

A direct frequency response function of the motion cueing system can be computed intuitively by transforming the time domain data indicated in Figure 5-2 by F_{PS} and F_{PA} to the frequency domain. This process yields two sets of complex numbers. A frequency response

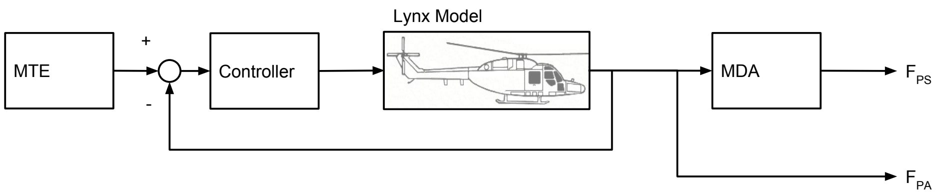

Figure 5-2: Schematic representation of the simulation of two Mission Task Elements.

function is then constructed by finding the relative amplitude $|H| = \frac{A_{out}}{A_{in}}$ and the phase $\angle H = \theta_{out} - \theta_{in}$ for the 3 degrees of freedom.

This computation yields 3 FRFs for the Take-Off and Abort maneuver and 3 FRFs for the hover task. For the sake of brevity, not all are displayed here. However, to illustrate the characteristics of the method, Figure 5-3a shows the direct FRF for the surge axis of the Take-Off and Abort Task. Figure 5-3b shows a similar figure for the hover task.

The following observation were made about these FRFs.

- Both Figure 5-3b and Figure 5-3a do not shows the characteristic dip at 1 [rad/s], clearly visible in Figure 4-8. Figure 5-3a does show however some fluctuation around this region. There is a dip just before 1 [rad/s] with upswing before and after. Therefore expected characteristics of the motion cueing are not visible.
- Secondly, both tasks have little amplitude at higher frequencies. Especially the take-off and abort maneuver shows noise at higher frequencies.

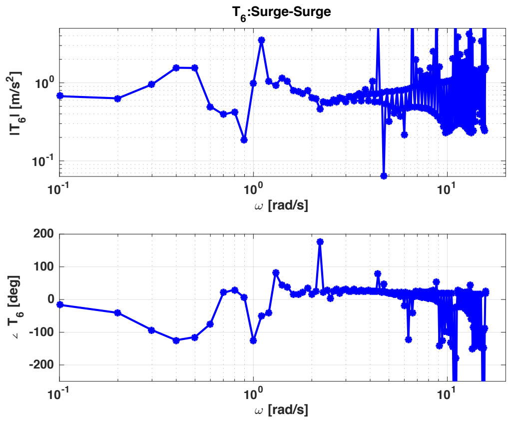

(a) A direct transfer fuction computed for the Take-Off and Abort task for test 6, surge to surge.

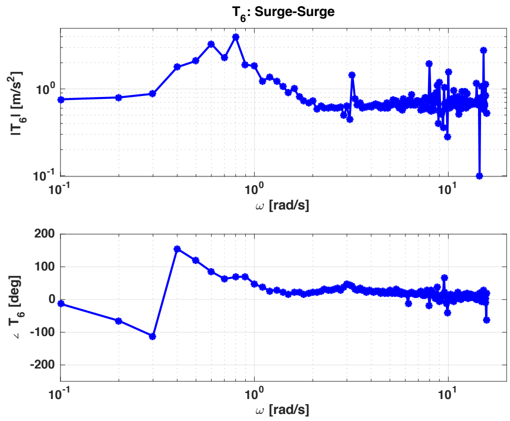

(b) A direct transfer fuction computed for the hover maneuver for test 6, surge to surge.

Figure 5-3: Test 6 of the OMCT.

Considering the observations mentioned above, using a direct FRF as an OMCT would have the following advantages and disadvantages.

- An advantage of this method would be that also for frequencies between the prescribed OMCT points there is an FFT reconstruction of the motion characteristics of the cueing system.
- However, this method would require a pilot-in-the-loop simulation. Considering that the results are expected to be very dependent on the precise time traces of the task, this would make this method hard to repeat.
- Noise is present at higher frequencies in the FRFs. This noise is present due to windowing in FFT process. Therefore, it is hard to distinguish what characteristics are caused by the dynamics of the cueing system and what characteristics of the FRFs are caused by the noise.

5-2 Coupled, Tailored Amplitude and Phase

Option 4 from Figure 5-1 indicates 4 different sub-choices. Phase information can be used directly, but also relative to a different degree of freedom.

Furthermore, two ways of estimating the amplitude and phase at the precise OMCT frequencies are distinguished. Firstly it is possible to do an interpolation to the nearest point, yielding design options 4a.1 and 4b.1. Secondly it is possible to make a least square model of the amplitude and phase. This choice yields design options 4a.2 and 4b.2.

From these 4 options, only 2 were explored however. Due to the jumps of 180 degrees in phase, modeling the absolute phase would be a difficult process. A least square fit would simply take the average of these jumps of 180 degrees, which is wrong. Option 4a.2 is therefore discarded.

In theory, an OMCT with absolute phase and relative phase should yield exactly the same results. Interpolation to the nearest point will therefore give the same results for design option 4a.1 and 4b.1. Therefore it was chosen to only study the absolute phase with interpolation, since it does not require the extra computational step of determining the relative phase. Design option 4b.1 is discarded.

5-2-1 Design Option 4a.1

Frequencies response functions are expected the differ for different axes, tasks and aircraft model. A least-square fit is often sensitive to the characteristics of the data needing fitting. Therefore it is anticipated that a least square model will need tuning before implementation. It would be simpler therefore to use an interpolation to get an estimate of the FFT on OMCT frequencies.

Therefore, an interpolation to the nearest point was performed on the amplitude and phase data directly taken from section 3-7, using the matlab routine `interp1.m`. The amplitude and phase at the frequencies specified by the OMCT were found.

5-2-2 Design Option 4b.2

To model the amplitude and phase, firstly the relative phase was computed. The phase of the pitch input was set to zero, and the relative phase for surge and heave was used as input to those axes. Equation 5-1 shows the resulting phase used for computing the frequency responses of the motion cueing system.

$$\angle f_x = \angle \dot{q} - \angle f_x \tag{5-1a}$$
$$\angle f_z = \angle \dot{q} - \angle f_z \tag{5-1b}$$
$$\angle \dot{q} = 0 \tag{5-1c}$$

To model the resulting amplitude and phase information, univariate splines were used. The interval [0.1 - 15.8] was divided into 100 sections. For all those sections a least squares fit was performed using a polynomial of order 2, $d = 2$. Furthermore a continuity between splines of degree 1, $r = 1$, was used. Figure 5-4 show the amplitude and relative phase for the longitudinal axes to illustrate the model fit.

From Figure 5-4 it can be seen that the model captures the most important trends of the amplitude and phase spectrum. A similar fit was performed for the hover MTE in Figure 5-5.

It is also important to note that, instead of a phase signal that has 180 [deg] jumps, the relative phase seems the be constant towards 100 [deg] at low frequencies and relatively constant at 180 [deg] for higher frequencies. At high frequencies, a positive pitch rotational acceleration will result in a negative surge acceleration, as is expected from the helicopter model.

5-2-3 Final Design

Now that the three design options have been evaluated, a trade-off can be made with respect to the proposed requirements. In the following, the design options will be discussed per requirement.

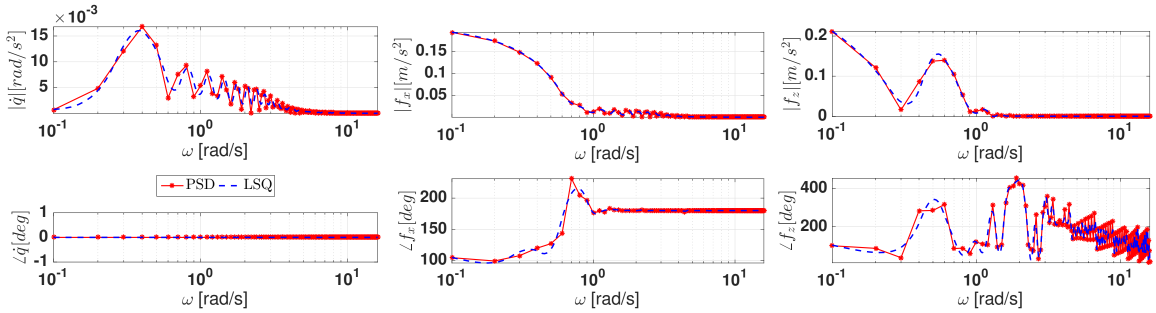

(a) Pitch. **(b)** Surge. **(c)** Heave.

Figure 5-4: Input spectra for a tailored OMCT based on the take-off and abort task, using design option 4b.2.

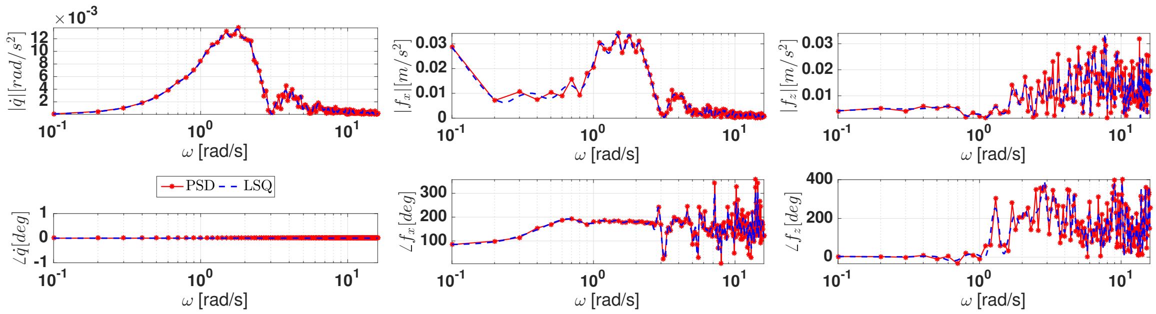

(a) Pitch. **(b)** Surge. **(c)** Heave.

Figure 5-5: Input spectra for a tailored OMCT based on the hover task, using design option 4b.2.

1. **Accurate Helicopter Motion**
Since a direct frequency response function is computed directly from the MTE PSDs, it is not bound by the respecified OMCT frequencies. It has therefore a better resolution and is considered to better represent helicopter motion. For a good comparison however, the direct frequency response function are compared to design options 4a.1 and 4b.2. An OMCT with the interpolated and modeled spectra was constructed. In these tailored tests, all axes were excited *simultaneously*. Since all axes are driven simultaneously, cross test are no longer studied. Figure 5-7 shows the outcome for test 1, test 6 and test 10 for the hover MTE.
As can be seen from Figure 5-6, the OMCT based on the Least-Squares model represents the direct FRF more closely than a direct interpolation. The cause for this can be sought in two factors:
    - At low frequencies there are less data points available than at high frequencies, since the `fft.m` data is not evenly spaced on a logarithmic scale. Therefore, the distance to the nearest data point is relatively large at low frequencies for the interpolated OMCT. A LSQ estimates in between the data points and will therefore possibly provide a more accurate estimation.
    - When interpolating, outliers in the FFT due to signal processing can be included in the OMCT. The LSQ fit will not be affected as much by outliers however.

For completeness, Figure 5-7 shows the outcome for test 1, test 6 and test 10 for the

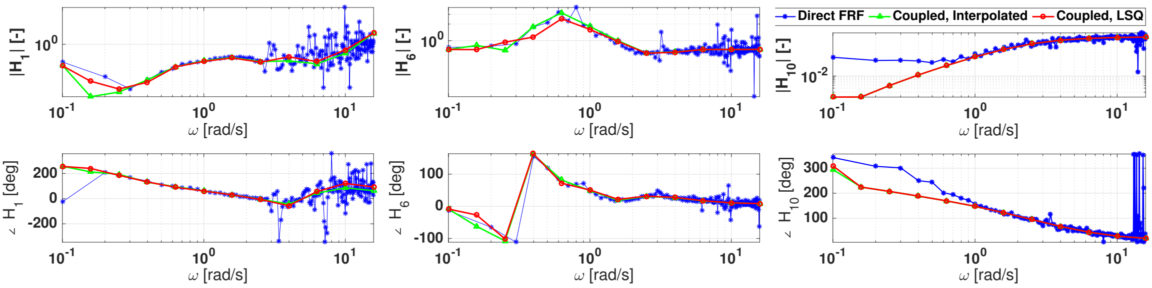

(a) Pitch. **(b)** Surge. **(c)** Heave.

Figure 5-6: Frequency response functions from pitch, surge and heave for 3 different OMCT design options for the hover MTE.

take-off and abort MTE.

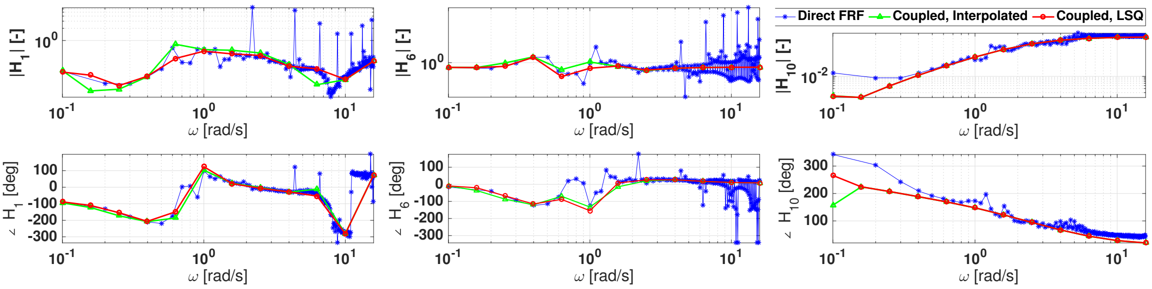

(a) Pitch. **(b)** Surge. **(c)** Heave.

Figure 5-7: Frequency response functions from pitch, surge and heave for 3 different OMCT design options for the take-off and abort MTE.

2. **Meaningful Information about the MCA**
From section 5-1, it was seen that there was noise present in the direct FRF, especially at high frequencies. Therefore the information that can be obtained about the MCA is limited in this region. By looking at individual frequencies this problem is less pronounced. Therefore more meaningful information about the MCA can be obtained with these two design options.
3. **Practical Implementation**
A direct FRF is badly repeatable since a pilot-in-the-loop simulation is required. A direct FRF scores badly on this requirement, since a goal of objective motion cueing is to eliminate the pilot from the evaluation process. The coupled OMCT however, can be repeated easily on different simulators. It is hypothesized that it is possible to create *standardized* MTE spectra that are generalizable in-between pilots.
Moreover, all tests proposed here have the advantage that the tests do not have to be repeated for every degree of freedom. Instead, data for all FRF can be obtained by one sweep of the OMCT frequencies.
However, a check is needed to see if the proposed amplitudes for both the interpolation and the LSQ are sufficiently high to ensure a good signal to noise ratio for any sensors measuring the motion of the simulator in real life. For a typical IMU, like the Xsens MTi 10-series, [51] the noise density for the gyroscope is 0.03 $[deg/s/\sqrt{Hz}]$ and the noise

density for the accelerometer is specified as 80 $[\mu g]$. The variance of the measurement depends on the sampling rate of the output for the sensor, Δt, according to Equation 5-2,

$$\sigma_w = \frac{N_0}{\sqrt{\Delta t}} \tag{5-2}$$

where σ_w is the white noise standard deviation of the output measurement and N_0 is the noise density. For the purpose of a tailored OMCT, frequencies bigger than 15.8 $[rad/s]$ are not of interest, giving a minimal sampling time of $\Delta t \cong 0.3[s]$. Substituting the values for the Xsens MTi 10-series gives a $\sigma_q = 0.055[deg/s]$ and $\sigma_{fx} = \sigma_{fz} = 0.0015[m/s^2]$. Figure 5-8 shows the input signals for both MTEs, plotted together with twice the compute standard deviations for the linear and rotational accelerations.

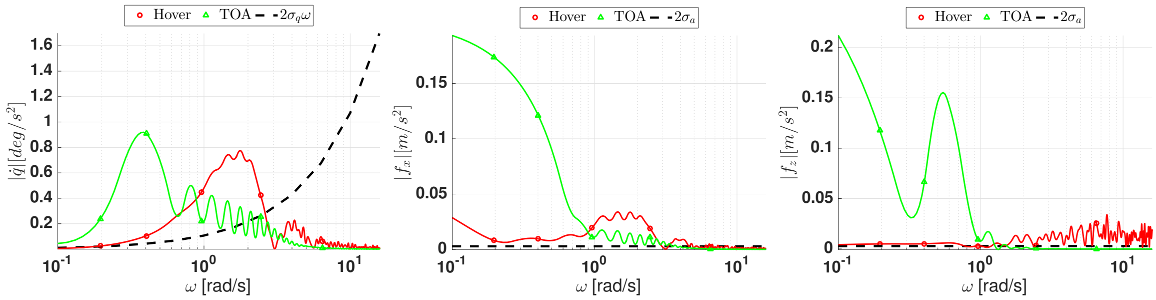

(a) Pitch. **(b)** Surge. **(c)** Heave.

Figure 5-8: Input signals for the hover and take-off and abort MTE, plotted together with reference IMU noise standard deviations.

Since the IMU specs are given in $[deg/s]$ for the gyroscope, the threshold for the acceleration depends on $\sigma_q \omega$. From Figure 5-8 it can be seen that at some areas the input signals are below two times the standard deviation of noise levels given by the IMU. This is considered a problem for practical implementation.

The preceding remarks have been summarized in a trade-off table given in Figure 5-9.

	Direct TF	LSQ	Interpolation
1. Accurate Helicopter motion	++	+	+/-
2. Meaningfull Information about MCS	-	+/-	+/-
3. Practical Implementation	--	+	+

Figure 5-9: Trade-off table containing 3 requirements and 3 design options.

As can be seen the direct FRF scores well on the accuracy of helicopter motion and badly on the practical implementation. The interpolation method and the LSQ score equally well on the information gained and the practical implementation. However, the LSQ method scores better at its ability to accurately portray the motion of the aircraft. This is because this method seems to capture the amplitude and phase information contained in the MTE signals more accurately than the interpolation method. The input spectra of the LSQ fit using relative phase are therefore chosen to continue the analysis.

5-3 Sensitivity to MDA Settings

Now that a new design for an OMCT is acquired with a set of input signals that more accurately represent the motion of rotor craft, it is time to put it to the test. The important question is, does this test make a different prediction about the fidelity of certain parameter settings of the classical washout algorithm of the SRS?

To answer this question, a sensitivity analysis was performed in a similar fashion as was done in section 4-3. The effect of four different filters was studied: the high pass filters on the translational channel: surge ω_{nx} and heave ω_{nz}, the high pass filter of the rotational channel: pitch ω_{nq} and the low pass filter of the tilt coordination channel, ω_{nLPx}.

It is important to note that since all axes are driven simultaneously for this test, the FRFs between different degrees of freedom lose their significance. Every direct test is essentially already a cross test. The following sections shows the results per axis.

It should be noted that here for the sake of brevity, only the most important results for the hover MTE are displayed here. For all sensitivity plots and the analysis for the take-off and abort maneuver, the interested reader is referred to Appendix I.

5-3-1 Pitch

The FRF of test 1 was influenced by ω_{nq}, shown in Figure 5-10a, and by ω_{nx}, shown in Figure 5-10b.

From Figure 5-10a it can be seen that for low frequencies the performance is poor, with an amplitude of $|H_1| = 0.1$. This is an expected characteristics of a high-pass filter. Little pitch is excited due to the tilt coordination channel, since the frequency response function resembles a high-pass filter at low frequencies. This means that helicopter motion might be more coordinated at low frequencies low frequencies then the classic OMCT assumes. This is an confirmation of the result from the OMCT sensitivity analysis. Furthermore it can be seen that as expected, decreasing ω_{nq} gives favorable motion characteristics of the pitch channel.

From Figure 5-10b, cross talk between the surge axis and the pitch axis is clearly visible. When tilt coordination is done for only low frequencies, $\omega_{nLPx} = 0.5$, test 1 resembles a high pass filter. However, when tilt coordination is also done for higher frequencies, upswing in test 1 becomes visible for $\omega > 2.0$. This is a false cue induced on the pitch channel by the surge channel.

5-3-2 Surge

For the surge axis it was seen that the bode plot is influenced by three filters, ω_{nx}, ω_{nx} and ω_{nq}.

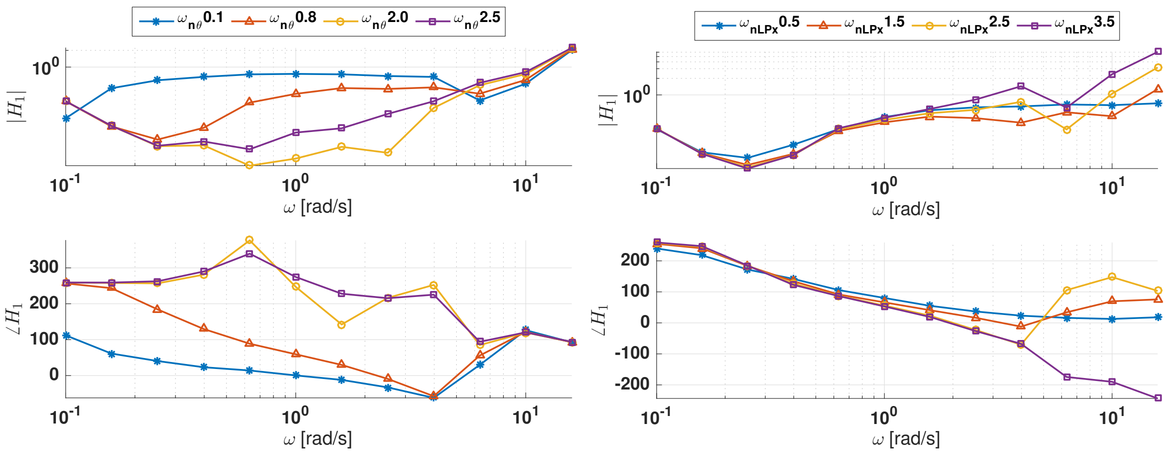

(a) Sensitivity of test 1 to the break frequency of the high pass filter of the pitch channel.

(b) Sensitivity of test 1 to the break frequency of the low pass filter of the surge channel.

Figure 5-10: Test 1, sensitivity analysis to MDA settings.

Figure 5-11a shows the influence of ω_{nx}. Figure 5-11b shows the influence of the tilt coordination on the performance in surge direction, ω_{nx}.

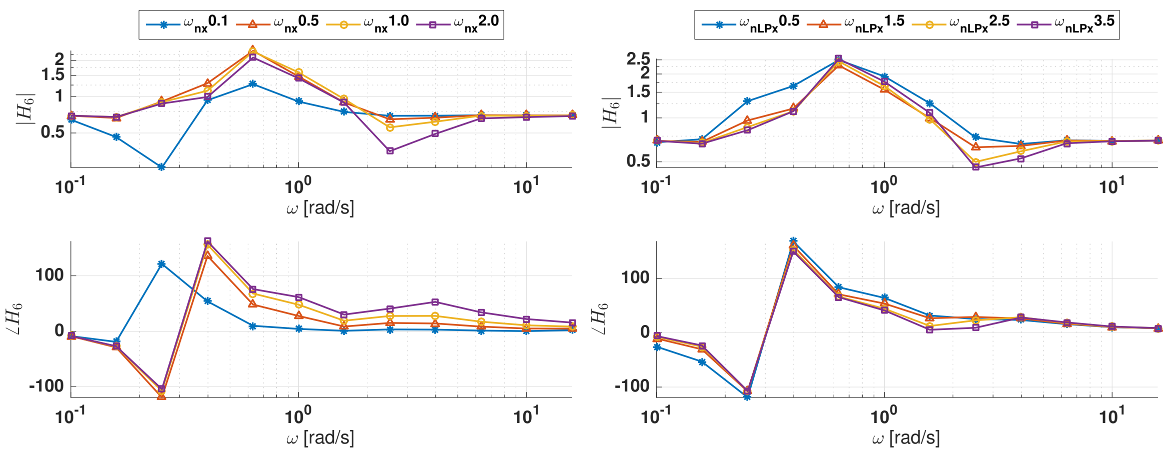

(a) Sensitivity of test 6 to the break frequency of the high pass filter of the surge channel.

(b) Sensitivity of test 6 to the break frequency of the low pass filter of the tilt coordinated channel channel.

Figure 5-11: Test 6, sensitivity analysis to MCA settings.

Firstly it can be seen that, as was seen in Figure 5-3a and Figure 5-3b, the characteristic dip of the classic OMCT is not visible for test 6. Instead, the amplitude firstly shows upswing, then a dip to 0.4 and thereafter again upswing. This can be explained by the fact that this plot is actually a visualization of the 'battle' between the pitch channel, represented by false cues of the surge channel, and the tilt coordination. The high pass break frequency of the surge channel therefore has little effect on the shape of Figure 5-11a.

However, at $\omega_{nx} = 0.1$, a cliff-like phenomenon is visible. The simulator goes out of its workspace, and the performance is severely degraded.

Interestingly however, this FRF is also greatly influenced by the pitch channel. Figure 5-12 shows a large influence of ω_{nq} in the FRFs.

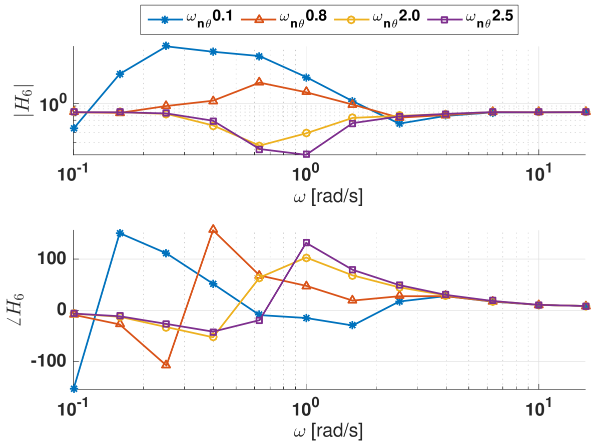

Figure 5-12: Sensitivity of test 6 to the break frequency of the high pass filter of the pitch channel.

It can be seen that for a very high ω_{nq} of 2.2, the FRF includes little false cues from the pitch channel and resembles more the original non-coupled OMCT. When decreasing ω_{nq}, a large upswing is visible at $\omega < 2.0$.

5-3-3 Heave

It was found that the FRF of heave was only influenced by ω_{nz}. This confirms the hypothesis that the heave motion is mostly uncoupled from other degrees of freedom. Figure 5-13 shows the influence of ω_{nz} on test 10.

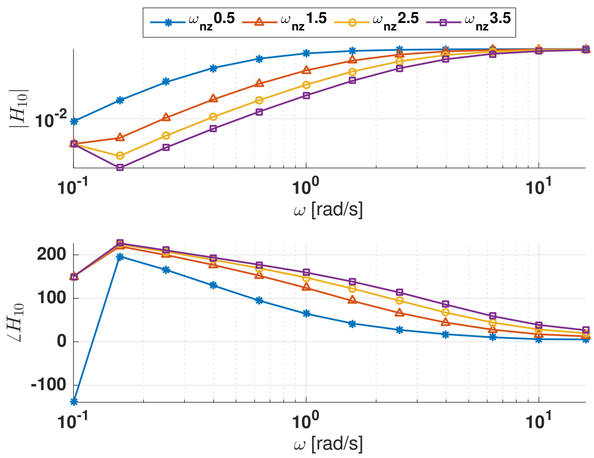

Figure 5-13: Sensitivity of test 10 to the break frequency of the high pass filter of the heave channel.

From Figure 5-13 it can be seen that the motion cueing system resembles a high pass filter, as is expected from the classical washout algorithm. This result is similar to that of the original OMCT.

5-4 Conclusion

In this chapter it was hypothesized that an OMCT where all axes are excited simultaneously can provide a more representative test to evaluate motion characteristics. This hypothesis was put to the test by designing a coupled OMCT, making use of the frequency spectra obtained from time traces of the two MTEs simulated.

Three sets of input signals were designed and fed into the MDA, driving surge, pitch and heave simultaneously. It was seen that a direct frequency response function gives a detailed picture of motion cueing characteristics, however pilot-in-the-loop simulation would be necessary for every OMCT. Two other methods were proposed, firstly an OMCT using a tailored set of input signals found by interpolation and secondly a set of input signals found by means of a least-square model. It was seen that a tailored set of input signals using a least-squares model better represented the characteristics found from a direct frequency response function. Therefore this method was chosen as a final design.

Finally, a similar sensitivity analysis was conducted as for the standard OMCT. From this sensitivity analysis it was found a set of input signals is tailored to MTEs has the following advantages.

- With this methodology, notable differences in the motion cueing characteristics were identified for the pitch and surge axes. Most importantly it was seen that coupling between pitch and surge are directly visible in the frequency response plots Figure 5-10b and Figure 5-12, as an addition to frequency response functions from the original OMCT.
- Since the test is coupled, all information about the cueing system can be obtained by doing a single sweep through the OMCT frequencies, as opposed to doing 10 individual tests for the original OMCT.

However the following drawbacks were found.

- Since all axes are driven simultaneously, the shape of the bode plots can be less intuitively related to the classical washout motion filter.
- Practical implementation of such a test would be hindered by the fact for some areas the amplitude of the input signals is low enough to case problems with IMU signals to noise ratios.
- The tailored OMCT outcome is very sensitive to the signal-processing of the amplitude and relative phase spectra. It was seen that this least-squares fit is very sensitive to the degree of polynomial and amount of splines used.

For actual pilot-in-the-loop simulation, the human controller will influence the control input of the model and therefore the characteristics of the helicopter motion. A limitation of the preceding analysis is therefore that the amplitude and relative phase of different degrees of freedom are not only influenced by the dynamics and Mission Task Element, but also by pilot control behavior.

Part III

Revised Appendices to the Preliminary Report

Appendix A

Derivation of a Flapping Equation

In this appendix, a form of the flapping equation is derived to gain understanding of the fundamental dynamics of the rotor system. The derivation if performed by formulating the Lagrangian for a moving mass on an axis, according to Figure A-1. Figure A-1 shows a schematic of a moving blade on an axis, indicated in grey. It can be seen that there are two relevant axes systems for this derivation. Firstly there is body axis of the aircraft and

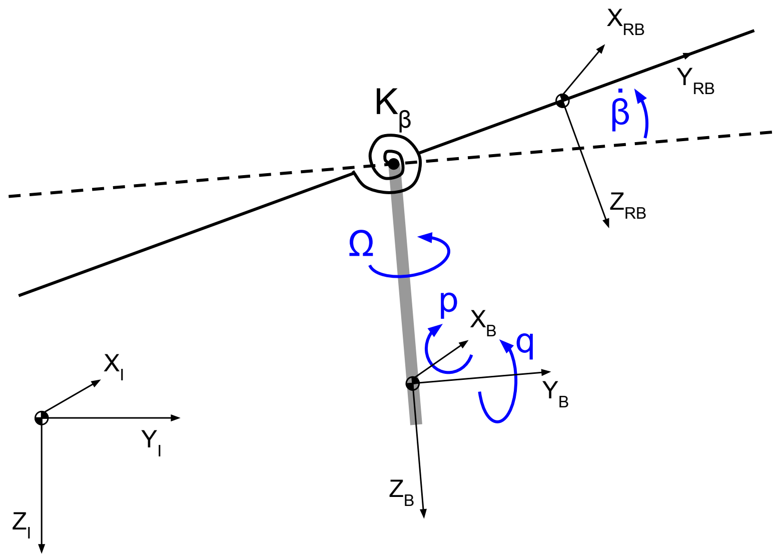

Figure A-1: Schematic indicating the two relevant axis systems and rotational rates for the simplified flapping equation.

secondly there is the rotating axis of the rotor blade, indicate with the subscript RB. To transform rotations from the body frame to the rotor blade frame, first the reference frame is rotated CCW around the Z_B axis with and angle of ψ, ψ_0 being defined at $\{E_B\}_X$, which convention. Furthermore, there is an extra rotation of $\frac{1}{2}\pi$ needed to put the Y-axis in the direction of the blade instead of the X-axis. Equation A-1 shows the transformation between $\{E_B\}$ and $\{E_{RB}\}$.

$$\{E_{RB}\} = [-\psi + \frac{1}{2}\pi][-\beta]\{E_B\} \tag{A-1}$$

Secondly the reference frame is rotated with an angle of β around the X_B axis. Equation A-2 and Equation A-3 show the transformation matrices for ψ and β respectivaly.

$$[-\beta] = \begin{bmatrix} 1 & 0 & 0 \\ 0 & \cos(\beta) & -\sin(\beta) \\ 0 & \sin(\beta) & \cos(\beta) \end{bmatrix} \tag{A-2}$$

$$[-\psi + \frac{1}{2}\pi] = \begin{bmatrix} \sin(psi) & \cos(\psi) & 0 \\ -cos(\psi) & \sin(\psi) & 0 \\ 0 & 0 & 1 \end{bmatrix} \tag{A-3}$$

The total rotational rate for a blade will therefore be equal to Equation A-4.

$$\begin{aligned} \omega_{RB} =& (p, q, -\Omega)[-\psi + \frac{1}{2}\pi][-\beta]\{E_B\} + (-\dot{\beta}, 0, 0)\{E_{RB}\} \\ \omega_{RB} =& \big(p\sin(\psi) - q\cos(psi) - \dot{\beta}, \\ & p\cos(\beta)\cos(\psi) - \Omega\sin(\beta) + q\cos(\beta)\sin(\psi), \\ & -\Omega\cos(\beta) - p\cos(\psi)\sin(\beta) - q\sin(\beta)\sin(\psi)\big) \end{aligned} \tag{A-4}$$

The Lagrangian is now computed using the potential and kinetic energy of the blade, according to Equation A-5.

$$\frac{d}{dt}\Big(\frac{\partial T}{\partial \dot{\beta}}\Big) - \frac{\partial V}{\partial \beta} + \frac{\partial V}{\partial \beta} = Q_\beta \tag{A-5}$$

Where the kinetic energy T is equal to Equation A-6,

$$T = \frac{1}{2}T_\beta \omega_{RB}^2 \tag{A-6}$$

and the potential energy V only depends on the spring constant at the hub, which is equal to Equation A-7,

$$V = \frac{1}{2}K_\beta \beta^2 \tag{A-7}$$

and the residual Q_β is equal to the aerodynamic moment M_a. And integrate over the entire length of the rotor:

$$K_\beta \beta = -\int_0^R rm(r)\{r\ddot{\beta} + r\Omega^2\beta\}dr \tag{A-8}$$

Now rearrange and substitute the moment of inertia for the rotor $I_\beta = \int_0^R m(r)r^2dr$:

$$\begin{aligned} K_\beta \beta &= I_\beta\{-\ddot{\beta} + \Omega^2\beta\} \\ K_\beta \beta &= -I_\beta\ddot{\beta} - I_\beta\Omega^2\beta \\ I_\beta\ddot{\beta} + \{K_\beta + I_\beta\Omega^2\}\beta &= 0 \\ \ddot{\beta} + \{\frac{K_\beta}{I_\beta} + \Omega^2\}\beta &= 0 \\ \ddot{\beta} + \lambda_\beta^2\beta &= 0 \end{aligned} \tag{A-9}$$

Working out the terms, a rudimentary flapping equation is found. After collecting the term for β, the flapping equation has the form of Equation A-10.

$$\ddot{\beta} + \lambda_\beta^2 \beta = \frac{2}{\Omega}(p\cos\psi - q\sin\psi) + \frac{M_a}{I_\beta} \tag{A-10}$$

It can be seen that Equation A-10 is second order ODE, where λ_β^2 is the flapping frequency ratio, given by Equation A-11.

$$\lambda_\beta^2 = \frac{K_\beta}{I_\beta} + \Omega^2 = \frac{K_\beta}{I_\beta \Omega^2} + 1 \tag{A-11}$$

A flapping frequency ratio of 1 means no damping is present at the hub, or $K_\beta = 0$. The result of Equation A-10 then becomes an oscillation of frequency Ω. However, if there is damping present, then $\lambda_\beta^2 > 1$, and the result to Equation A-9 will be an oscillation with a frequency faster than Ω.

Due to a pitch velocity or roll velocity, the rotating mass of the rotor is susceptible to gyroscopic accelerations, which are represented by $\frac{2}{\Omega}(p\cos\psi - q\sin\psi)$ in the flapping equation. It can be seen that a roll rate is effective at $\cos\psi$ meaning at the longitudinal axis. Similarly, the pitch rate is only effective at $\sin\psi$, the lateral axis. This is an early indication the longitudinal and lateral dynamics are therefore highly coupled for rotorcraft. This fact will be discussed in greater detail in section A-3.

A-1 Aerodynamics Forces

Equation A-10 already gives some valuable insight in the rotor mechanics. However, the control inputs θ_0, θ_c and θ_s, representing the collective, longitudinal and lateral cyclic inputs respectively, have not yet been represented in this equation. To do so, let's look at the aerodynamic forces. For this example, only the lift force will be considered. Figure A-2 depicts the lift on a rotorblade as a function of the inflow angel ϕ and the pitch angle θ.

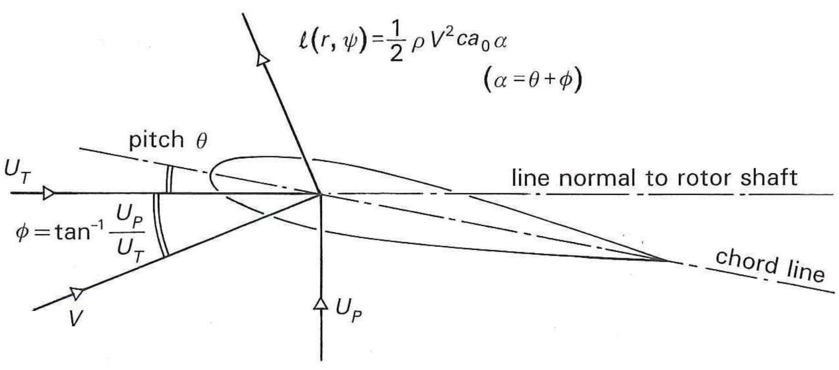

Figure A-2: Lift as a function of the inflow velocity and pitch angle, taken from [12].

For the equation of motion, the moment around the flapping hinge d.t. the lift force is of interest. This is computed by computing the local lift, multiplying with the local radius and integrating over the total span of the rotor blade, as is shown in Equation A-12.

$$M_a = \int_0^R l(r,\psi) r dr \tag{A-12}$$

Equation A-12 can be expanded by substituting the local lift and adding the insight that the effective angle of attack $\alpha = \phi + \theta$ and $\phi = \tan^{-1} \frac{U_P}{U_T} \sim \frac{U_P}{U_T}$.

$$M_a = \int_0^R \frac{1}{2} \rho V^2 c_{\alpha_0} (\frac{U_P}{U_T} + \theta) r dr \tag{A-13}$$

In Equation A-13 the tangential velocity is made up by the rotor speed and the total velocity V is estimated to be approximately equal to the tangential velocity. Furthermore, the upward speed U_P is given by the rotor upwash ν_i, flapping velocity $\dot{\beta}$ and two terms caused by gyroscopic acceleration. Expressions for V, U_P and U_T are given in Equation A-14.

$$\begin{aligned} V &= \Omega r \\ U_T &= \Omega r \\ U_P &= -\nu_i + \dot{\beta} r + q r \cos\psi + p r \sin\psi \end{aligned} \tag{A-14}$$

Equation A-14 can now be substituted to evaluate the integral given in Equation A-13. Equation A-15 shows the outcome of this evaluation.

$$\begin{aligned} M_a &= \int_0^R \frac{1}{2} \rho (U_T)^2 c_{\alpha_0} (\frac{U_P}{U_T} + \theta) r dr \\ M_a &= \int_0^R \frac{1}{2} \rho c_{\alpha_0} (U_P U_T + (U_T)^2 \theta) r dr \\ \frac{M_a}{I_\beta} &= \frac{\rho c_{\alpha_0}}{2 I_\beta} \int_0^R (-\nu_i + \dot{\beta} r + q r \cos\psi + p r \sin\psi (\Omega r) + \Omega^2 r^2 \theta) r dr \\ \frac{M_a}{I_\beta} &= \frac{\rho c_{\alpha_0}}{2 I_\beta} \Big(-\frac{1}{3} \Omega \nu_i R^3 - \frac{1}{4} \Omega \dot{\beta} R^4 + \frac{1}{4} \Omega (q \cos\psi + p \sin\psi) R^4 + \frac{1}{4} \Omega^2 \theta R^4 \Big) \\ \frac{M_a}{I_\beta} &= \frac{\rho c_{\alpha_0} R^4}{2 I_\beta} \Big(-\frac{1}{3R} \Omega \nu_i - \frac{1}{4} \Omega \dot{\beta} + \frac{1}{4} \Omega (q \cos\psi + p \sin\psi) + \frac{1}{4} \Omega^2 \theta \Big) \end{aligned} \tag{A-15}$$

At this point it can be identified that the terms outside the brackets is an important parameter, being effectively the ratio between the aerodynamic forces and the inertial forces. This ratio is called the Lock parameter and is described in Equation A-16.

$$\gamma = \frac{\rho c a_0 R^4}{I_\beta} \tag{A-16}$$

A heavy blade will result therefore in a lower Lock number, which in turn will lower the effective forced acceleration for the flapping equation. When substituted, the Lock number will transform Equation A-15 to Equation A-17.

$$\begin{aligned} \frac{M_a}{I_\beta} &= \frac{\gamma}{2} \Big(-\frac{\nu_i \Omega}{3R} - \frac{\Omega}{4} \dot{\beta} + \frac{\Omega}{4} (q \cos\psi + p \sin\psi) + \frac{\Omega^2}{4} \theta \Big) \\ \frac{M_a}{I_\beta} &= -\frac{\gamma \Omega}{8} \dot{\beta} - \frac{\gamma \Omega^2}{6} \lambda_i + \frac{\gamma \Omega}{8} (q \cos\psi + p \sin\psi) + \frac{\gamma \Omega^2}{8} \theta \end{aligned} \tag{A-17}$$

Substituting Equation A-17 back into Equation A-10, gives a workable result.

$$\ddot{\beta}+\frac{\gamma\Omega}{8}\dot{\beta}+\lambda_\beta^2\Omega^2\beta=2\Omega(p\cos\psi-q\sin\psi)+\frac{\gamma\Omega^2}{8}\Big(\theta-\frac{4}{3}\lambda_i+\frac{q}{\Omega}\cos\psi+\frac{p}{\Omega}\sin\psi\Big) \quad \text{(A-18)}$$

Equation A-18 is a simplification of the general flapping equation. However at this stage it is sufficient to connect collective and cyclic inputs to a flapping angle, taking into account the following considerations.

- The flapping equation in this form takes into account the induced velocity, the rotational velocity of the blade element, the flapping velocity and the pitch and roll motion of the aircraft
- However, forward velocity is not taken into account.
- Drag on the rotor blade is not taken into account.

A-2 A Solution to the Flapping Equation

An attempt will now be made to find a solution to the linear, non-homogeneous, second order differential equation Equation A-18. To do so, the method of undetermined coefficients is used. Firstly, a steady state solution is assumed to be of the form according to Equation A-19.

$$\begin{aligned}\beta &= \beta_0+\beta_{1_c}\cos\psi+\beta_{1_s}\sin\psi\\ \dot{\beta} &= -\beta_{1_c}\Omega\sin\psi+\beta_{1_s}\Omega\cos\psi\\ \ddot{\beta} &= -\beta_{1_c}\Omega^2\cos\psi-\beta_{1_s}\Omega^2\sin\psi\end{aligned} \quad \text{(A-19)}$$

Physically, the form of Equation A-19 corresponds to three angles, displayed in Figure A-3. β_0 is the coning angle and β_{1_c} and β_{1_s} or longitudinal and lateral flapping respectively.

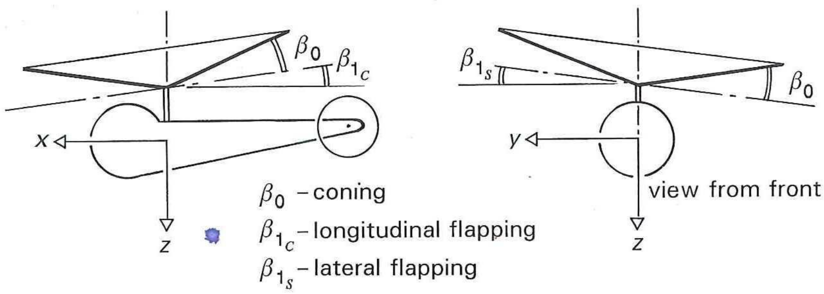

Figure A-3: Physical representation of β_0, β_{1_c} and β_{1_s}, taken from [12].

Equation A-19 is substituted into Equation A-18, giving Equation A-20aand Equation A-20b. For clarity, the equation is split into the left half of flap equation Equation A-18, indicated with (a) and the right half of the flap equation, indicated with (b).

$$\Big(-\beta_{1_c}\Omega^2\cos\psi-\beta_{1_s}\Omega^2\sin\psi\Big)+\frac{\gamma\Omega}{8}\Big(-\beta_{1_c}\Omega\sin\psi+\beta_{1_s}\Omega\cos\psi\Big)+\lambda_\beta^2\Omega^2\Big(\beta_0+\beta_{1_c}\cos\psi+\beta_{1_s}\sin\psi\Big) \tag{A-20a}$$

$$2\Omega(p\cos\psi-q\sin\psi)+\frac{\gamma\Omega^2}{8}\Big(\big(\theta_0+\theta_{1_c}\cos\psi+\theta_{1_s}\sin\psi\big)-\frac{4}{3}\lambda_i+\frac{q}{\Omega}\cos\psi+\frac{p}{\Omega}\sin\psi\Big) \tag{A-20b}$$

Furthermore, the pitch angle input, θ is split into the collective pitch θ_0, and the longitudinal and lateral cyclic, θ_{1c} and θ_{1c} respectively. The total pitch angle is than formed by Equation A-21.

$$\theta=\theta_0+\theta_{1_c}\cos\psi+\theta_{1_s}\sin\psi \tag{A-21}$$

To solve for coefficients β_0, β_{1c} and β_{1s}, firstly the terms have to be rearranged, to collect all terms with $\sin\psi$ and $\cos\psi$ separately.

$$\Big(-\beta_{1_c}\Omega^2+\beta_{1_s}\frac{\gamma\Omega^2}{8}+\beta_{1_c}\lambda_\beta^2\Omega^2\Big)\cos\psi+\Big(-\beta_{1_s}\Omega^2-\beta_{1_c}\frac{\gamma\Omega^2}{8}+\beta_{1_s}\lambda_\beta^2\Omega^2\Big)\sin\psi+\beta_0\lambda_\beta^2\Omega^2 \tag{A-22a}$$

$$\Big(2\Omega p+\frac{\gamma\Omega^2}{8}\theta_{1c}+\frac{\gamma\Omega^2 q}{8\Omega}\Big)\cos\psi+\Big(-2\Omega q+\frac{\gamma\Omega^2}{8}\theta_{1s}+\frac{\gamma\Omega^2 p}{8\Omega}\Big)\sin\psi+\frac{\gamma\Omega^2}{8}\big(\theta_0-\frac{4}{3}\lambda_i\big) \tag{A-22b}$$

From Equation A-22a and Equation A-22b, there can be distinguished three equations with three unknowns, β_0, β_{1c} and β_{1s}. The cone angle β_0, is derived first in Equation A-23.

$$\begin{aligned}\beta_0\lambda_\beta^2\Omega^2&=\frac{\gamma\Omega^2}{8}\big(\theta_0-\frac{4}{3}\lambda_i\big)\\ \beta_0&=\frac{\gamma}{8\lambda_\beta^2}\big(\theta_0-\frac{4}{3}\lambda_i\big)\end{aligned} \tag{A-23}$$

Thereafter, the terms using $\cos\psi$ are given in Equation A-24a and terms using $\sin\psi$ are given in Equation A-24b

$$-\beta_{1_c}\Omega^2+\beta_{1_s}\frac{\gamma\Omega^2}{8}+\beta_{1_c}\lambda_\beta^2\Omega^2=2\Omega p+\frac{\gamma\Omega^2}{8}\theta_{1c}+\frac{\gamma\Omega^2 q}{8\Omega} \tag{A-24a}$$

$$-\beta_{1_s}\Omega^2-\beta_{1_c}\frac{\gamma\Omega^2}{8}+\beta_{1_s}\lambda_\beta^2\Omega^2=-2\Omega q+\frac{\gamma\Omega^2}{8}\theta_{1s}+\frac{\gamma\Omega^2 p}{8\Omega} \tag{A-24b}$$

Rewriting Equation A-24a to collect terms containing β_{1c} and β_{1s}, dividing by Ω^2 and substituting $\bar{p}=\frac{p}{\Omega}$ and $\bar{q}=\frac{q}{\Omega}$gives:

$$\beta_{1s}+S_\beta\beta_{1c}=\theta_{1c}+\bar{q}+\frac{16}{\gamma}\bar{p} \tag{A-25a}$$

$$-\beta_{1c}+S_\beta\beta_{1s}=\theta_{1s}+\bar{p}-\frac{16}{\gamma}\bar{q} \tag{A-25b}$$

Where use has been made of the fact that $\frac{8(\lambda_\beta^2-1)}{\gamma} = S_\beta$, which is the stiffness number, a ratio of hub stiffness to aerodynamic moments. After expressing β_{1s} as a function of β_{1c} and substituting, the following equation for coefficient β_{1c} was found.

$$\beta_{1_c} = \frac{1}{1+S_\beta^2}\Big(S_\beta\theta_{1c} - \theta_{1s} + \bar{p}(S_\beta\frac{16}{\gamma} - 1) + \bar{q}(S_\beta + \frac{16}{\gamma})\Big) \tag{A-26}$$

In a similar way, an equation for β_{1_s} can be derived.

$$\beta_{1_s} = \frac{1}{1+S_\beta^2}\Big(S_\beta\theta_{1s} + \theta_{1c} + \bar{p}(S_\beta + \frac{16}{\gamma}) - \bar{q}(S_\beta\frac{16}{\gamma} - 1)\Big) \tag{A-27}$$

Equation A-23, Equation A-26 and Equation A-27 now form a workable solution to the flapping equation.

A-3 Interpretation

To make sense of the solution presented in section A-2, consider an infinitely stiff rotor blade, $S_\beta = 0$. This this simplifies Equation A-26 and Equation A-27 into Equation A-28 and Equation A-29.

$$\beta_{1_c} = -\theta_{1s} - \frac{p}{\Omega} + \frac{16}{\gamma}\frac{q}{\Omega} \tag{A-28}$$

$$\beta_{1_s} = \theta_{1c} + \frac{q}{\Omega} + \frac{16}{\gamma}\frac{p}{\Omega} \tag{A-29}$$

This simplification gives an important insight into the coupling of the longitudinal and lateral axes of the main rotor of rotorcraft, since the flap angles are directly coupled to lateral and longitudinal moment of the aircraft. The roll and pitch moment on the aircraft due to the rotor can now be estimated using the flap deflection and the spring stiffness at the hub according to Equation A-30 and Equation A-31 respectively.

$$M = -N_b\frac{K_\beta}{2}\beta_{1_c} \tag{A-30}$$

$$L = -N_b\frac{K_\beta}{2}\beta_{1_s} \tag{A-31}$$

Where, N_b is the number of rotor blades.

- Firstly it can be seen that a change in lateral blade pitch θ_{1s} influences the longitudinal flap angle and therefore the longitudinal dynamics. Similarly, a change in longitudinal blade pitch θ_{1c} influences the lateral flap angle. This effect is called *the Fundamental 90° Phase Shift.*
- Secondly the terms indicated in green are coupling terms between lateral motion and longitudinal motion of the aircraft, d.t. gyroscopic accelerations These terms are an important reason why there exists a strong coupling between symmetric and asymmetric motions for rotorcraft.
- Thidly it can be seen that terms highlighted in dark blue, rotation of the rotor due to an in-plane rotational velocity of the aircraft. It can be seen that the tip lags the rotation of the control plane in this case, meaning that these terms give *damping* to aircraft motions.

Appendix B

The DRA (RAE) Research Lynx, ZD559

This appendix shows the numerical values used for the rudimentary mathematical helicopter model as presented in section 3-1. Figure B-1 shows important numerical values, whereas Figure B-1 shows the general lay-out of the DRA (RAE) Lynx.

a_0	6.0/rad	I_{zz}	12 208.8 kg m ^{2}	x_{cg}	−0.0198
a_{0T}	6.0/rad	K_β	166 352 N m/rad	δ_0	0.009
α_{tp0}	−0.0175 rad	l_{fn}	7.48 m	δ_2	37.983
β_{fn0}	−0.0524 rad	l_{tp}	7.66 m	δ_3	−45°
c	0.391 m	l_T	7.66 m	δ_{T0}	0.008
g_T	5.8	M_a	4313.7 kg	δ_{T2}	5.334
h_R	1.274 m	N_b	4		
h_T	1.146 m	R	6.4 m	γ	7.12
I_β	678.14 kg m ^{2}	R_T	1.106 m	γ_s	0.0698 rad
I_{xx}	2767.1 kg m ^{2}	S_{fn}	1.107 m ^{2}	λ_β^2	1.193
I_{xz}	2034.8 kg m ^{2}	S_{tp}	1.197 m ^{2}	θ_{tw}	−0.14 rad
I_{yy}	13 904.5 kg m ^{2}	s_T	0.208	Ω_{idle}	35.63 rad/s

Figure B-1: Specifications for the Lynx research helicopter, [12].

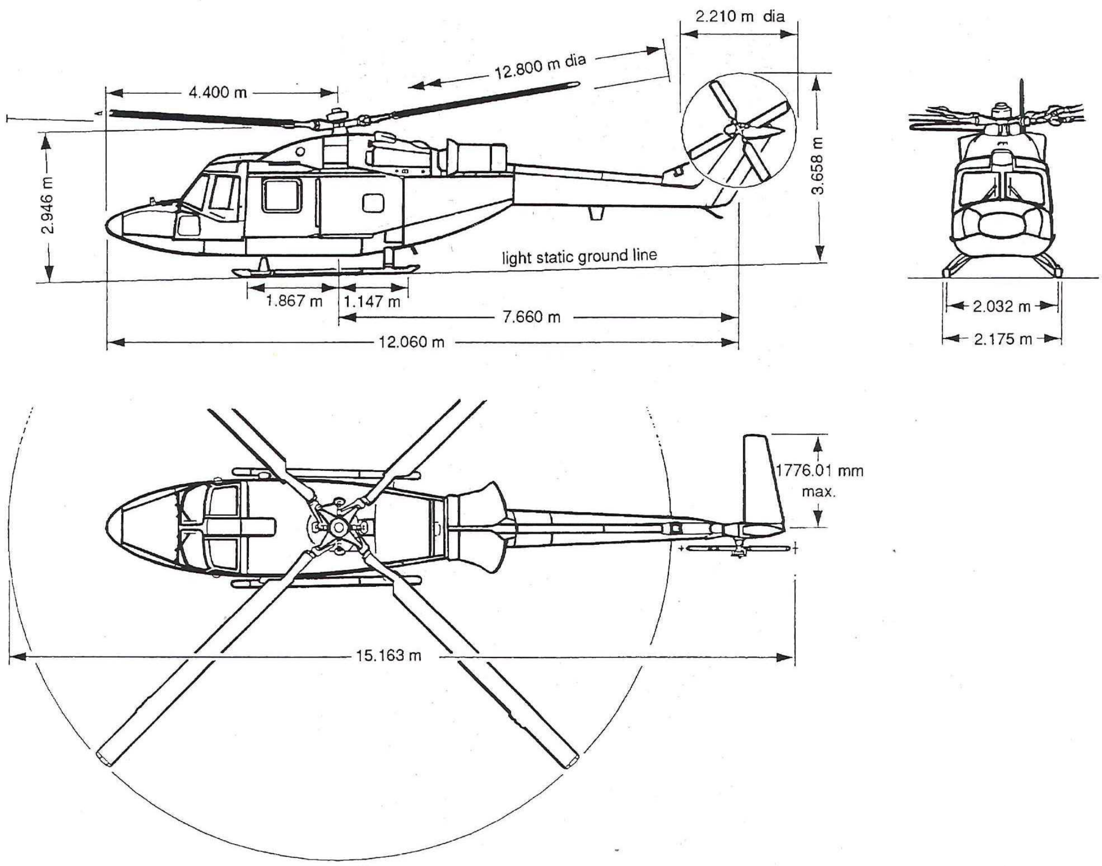

Figure B-2: Lay-out of the Lynx research helicopter, [12].

Appendix C

MTE Description and Performance Standards

3.11.7 Depart/Abort

a. Objectives.

- Check pitch axis and heave axis handling qualities during moderately aggressive maneuvering.
- Check for undesirable coupling between the longitudinal and lateral-directional axes.
- Check for harmony between the pitch axis and heave axis controllers
- Check for overly complex power management requirements.
- Check for ability to re-establish hover after changing trim
- With an external load, check for dynamic problems resulting from the external load configuration.

b. Description of maneuver. From a stabilized hover at 35 ft wheel height (or no greater than 35 ft external load height) and 800 ft from the intended endpoint, initiate a longitudinal acceleration to perform a normal departure. At 40 to 50 knots groundspeed, abort the departure and decelerate to a hover such that at the termination of the maneuver, the cockpit shall be within 20 ft of the intended endpoint. It is not permissible to overshoot the intended endpoint and move back. If the rotorcraft stopped short, the maneuver is not complete until it is within 20 ft of the intended endpoint. The acceleration and deceleration phases shall be accomplished in a single smooth maneuver. For rotorcraft that use changes in pitch attitude for airspeed control, a target of approximately 20 degrees of pitch attitude should be used for the acceleration and deceleration. The maneuver is complete when control motions have subsided to those necessary to maintain a stable hover.

c. Description of test course. The test course shall consist of at least a reference line on the ground indicating the desired track during the acceleration and deceleration, and markers to denote the starting and endpoint of the maneuver. The course should also include reference lines or markers parallel to the course reference line to allow the pilot and observers to perceive the desired and adequate longitudinal tracking performance, such as the example shown in Figure 27.

d. Performance standards.

Performance –Depart/Abort

	Cargo/Utility		**Externally Slung Load**	
	GVE	DVE	GVE	DVE
DESIRED PERFORMANCE				
• Maintain lateral track within ±X ft:	10 ft	10 ft	10 ft	10 ft
• Maintain radar altitude below X ft:	50 ft	50 ft	50 ft*	50 ft*
• Maintain heading within ±X deg:	10 deg	10 deg	10 deg	10 deg
• Time to complete maneuver:	25 sec	25 sec	30 sec	30 sec
• Maintain rotor speed within:	OFE	OFE	OFE	OFE
ADEQUATE PERFORMANCE				
• Maintain lateral track within ±X ft:	20 ft	20 ft	20 ft	20 ft
• Maintain radar altitude below X ft:	75 ft	75 ft	75 ft*	75 ft*
• Maintain heading within ±X deg:	15 deg	15 deg	15 deg	15 deg
• Time to complete maneuver:	30 sec	30 sec	35 sec	35 sec
• Maintain rotor speed within:	SFE	SFE	SFE	SFE

* Altitudes refer to height of external load, measured at hover

3.11.1 Hover

a. Objectives.

• Check ability to transition from translating flight to a stabilized hover with precision and a reasonable amount of aggressiveness.

• Check ability to maintain precise position, heading, and altitude in the presence of a moderate wind from the most critical direction in the GVE; and with calm winds allowed in the DVE.

b. Description of maneuver. Initiate the maneuver at a ground speed of between 6 and 10 knots, at an altitude less than 20 ft. For rotorcraft carrying external loads, the altitude will have to be adjusted to provide a 10 ft load clearance. The target hover point shall be oriented approximately 45 degrees relative to the heading of the rotorcraft. The target hover point is a repeatable, ground-referenced point from which rotorcraft deviations are measured. The ground track should be such that the rotorcraft will arrive over the target hover point (see illustration in Figure 24). In the GVE, the maneuver shall be accomplished in calm winds and in moderate winds from the most critical direction. If a critical direction has not been defined, the hover shall be accomplished with the wind blowing directly from the rear of the rotorcraft.

c. Description of test course. The suggested test course for this maneuver is shown in Figure 24. Note that the hover altitude depends on the height of the hover sight and the distance between the sight, the hover target, and the rotorcraft. These dimensions may be adjusted to achieve a desired hover altitude.

d. Performance standards. Accomplish the transition to hover in one smooth maneuver. It is not acceptable to accomplish most of the deceleration well before the hover point and then to creep up to the final position.

Performance – Hover

	Scout/Attack		Cargo/Utility		Externally Slung Load	
	GVE	DVE	GVE	DVE	GVE	DVE
DESIRED PERFORMANCE						
• Attain a stabilized hover within X seconds of initiation of deceleration:	3 sec	10 sec	5 sec	10 sec	10 sec	13 sec
• Maintain a stabilized hover for at least:	30 sec	30 sec	30 sec	30 sec	30 sec	30 sec
• Maintain the longitudinal and lateral position within ±X ft of a point on the ground:	3 ft	3 ft	3 ft	3 ft	3 ft	3 ft
• Maintain altitude within ±X ft:	2 ft	2 ft	2 ft	2 ft	4 ft	4 ft
• Maintain heading within ±X deg:	5 deg	5 deg	5 deg	5 deg	5 deg	5 deg
• There shall be no objectionable oscillations in any axis either during the transition to hover or the stabilized hover	✓*	✓	✓	✓	✓	NA*
ADEQUATE PERFORMANCE						
• Attain a stabilized hover within X seconds of initiation of deceleration:	8 sec	20 sec	8 sec	15 sec	15 sec	18 sec
• Maintain a stabilized hover for at least:	30 sec	30 sec	30 sec	30 sec	30 sec	30 sec
• Maintain the longitudinal and lateral position within ±X ft of a point on the ground:	6 ft	8 ft	6 ft	6 ft	6 ft	6 ft
• Maintain altitude within ±X ft:	4 ft	4 ft	4 ft	4 ft	6 ft	6 ft
• Maintain heading within ±X deg:	10 deg	10 deg	10 deg	10 deg	10 deg	10 deg

*Note: For all tables, ✓ = performance standard applies; NA = performance standard not applicable

Appendix D

OMCT Verfication

In this appendix, the developed algorithm will compared to OMCT measurement data from the SRS, as was presented in [9]. This data is from an online experiment using the SRS, with a dummy parameter set for motion filter gains. Comparing the offline simulation to this online simulation will provide two important insights. Firstly, since the MDA used for both the online and offline simulation data is similar, the online simulation data provides a way verify the offline OMCT algorithm. Secondly, since the hardware characteristics of the SRS are incorporated in the online simulation, a comparison to the offline simulation provides some insight in the hardware dynamics of the SRS motion system.

The parameters used for the verification are dummy filter setting according to Table 4-2. The parameter set as depicted in Table 4-2 was used to computed all frequency responses for test 1- 10, on de axes described in Figure 2-15. The following subsections will discus results for the 6 input axes respectively.

Table D-1: Transfer function for test 1-10 presented in tabular form.

			Output				
		Roll	Pitch	Yaw	Surge	Sway	Heave
	Roll	$\frac{\dot{P}_{PS}}{\dot{P}_{PA}}(\omega)$				$\frac{f_{x_{PS}}}{\dot{P}_{PA}}(\omega)$	
	Pitch		$\frac{\dot{Q}_{PS}}{\dot{Q}_{PA}}(\omega)$		$\frac{a_{x_{PS}}}{\dot{Q}_{PA}}(\omega)$		
Input	Yaw			$\frac{\dot{R}_{PS}}{\dot{R}_{PA}}(\omega)$			
	Surge		$\frac{\dot{Q}_{PS}}{f_{x_{PA}}}(\omega)$		$\frac{f_{x_{PS}}}{f_{x_{PA}}}(\omega)$		
	Sway	$\frac{\dot{P}_{PS}}{f_{y_{PA}}}(\omega)$				$\frac{f_{y_{PS}}}{f_{y_{PA}}}(\omega)$	
	Heave						$\frac{f_{z_{PS}}}{f_{z_{PA}}}(\omega)$

D-1 Pitch

The first and second test of the OMCT study pitch and surge response of the classical washout algorithm due to to a pitch input signal respectively. These tests differ from test 3 and 4 for a roll input, in the sense that they require an coupled pitch maneuver.

For civil aviation aircraft, when there is a change in pitch angle, in most maneuvers there is also a change in forward speed. This means that for the input cues of the simulator, a pitch acceleration is in most cases combined with a surge acceleration. Pitch acceleration and surge acceleration are therefore coupled and tested at the same time in test 1. It is assumed that the required surge acceleration is dependent on the pitch angle θ. θ can be found by differentiating the $\ddot{\theta}$ input twice, according to Equation D-1.

$$\theta = -\frac{A}{\omega^2} \sin \omega t \tag{D-1}$$

The surge input will then become according to Equation D-2

$$f_{sp_x} = -g \sin \theta = -g \sin \left(\frac{-A}{\omega^2} \sin \omega t \right) \tag{D-2}$$

Following the same logic there is also a small change in input on the heave acceleration channel. The total input will therefore be according to Equation D-3. Figure D-1 shows the amplitude response of the MDA for three conditions.

$$u = \begin{bmatrix} -g \sin \left(\frac{-A}{\omega^2} \sin \omega t \right) \\ 0 \\ -g \cos \left(\frac{-A}{\omega^2} \sin \omega t \right) \\ 0 \\ 0 \\ 0 \\ 0 \\ A \sin \omega t \\ 0 \end{bmatrix} \tag{D-3}$$

The frequency response for the first test was computed according to Equation D-4.

$$H_1(\omega) = \frac{\dot{q}_{PS}}{\dot{q}_{PA}}(\omega) \tag{D-4}$$

Firstly an uncoupled OMCT was performed, meaning only a pitch acceleration was used as input. It can be seen that the frequency response is the one of a high pass filter, as would be expected from angular acceleration channel of the classical washout algorithm. Secondly, the test was conducted with only a signal on the surge channel. As can be seen, the response due to only a surge channel resembles a low pass filter, as is also to be expected form the classical washout algorithm ,Figure 2-10. The coupled response is then the addition of the first two curves. Figure D-2 shows than the offline OMCT bode plot, together with the online data from the SRS, indicated by $p5$, as this was the fifth parameter set that was tested. It can be seen that for low frequencies the two curves overlap. However, at high frequencies the

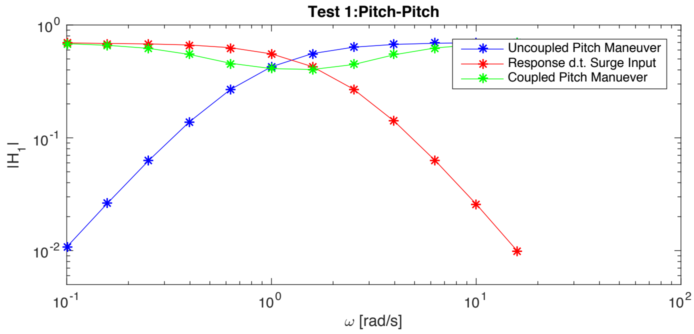

Figure D-1: Amplitude response for three different configurations of test 1.

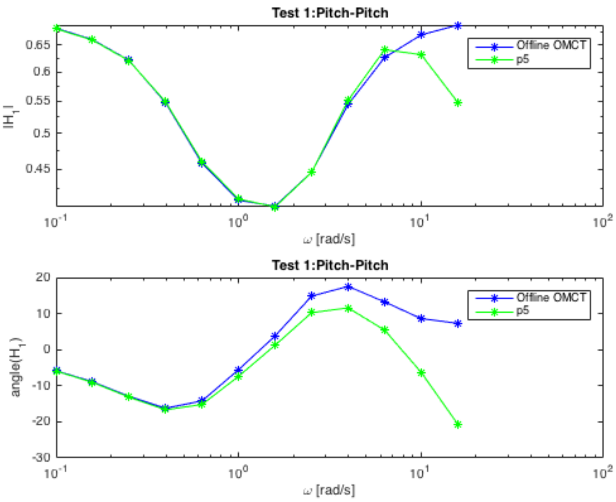

Figure D-2: Verification plot of test 1, pitch acceleration input and pitch acceleration output.

hardware is not able to follow the software input, and the amplitude is less then predicted. This also shows in the phase plot, where more lag is generated at high frequencies.

For the second test, pitch input was compared to surge output. For this test as well, a coupled surge input was considered. Therefore the same input was used as Equation D-3.

$$H_2(\omega) = \frac{a_{x_{PS}}}{\dot{q}_{PA}}(\omega) \tag{D-5}$$

Moreover, it can be seen that instead of specific force, the acceleration without the effect of tilt coordination is considered, which is computed according to Equation D-6.

$$a_{x_{PS}} = f_{sp_x} - g\sin(\theta) \tag{D-6}$$

This is because test 2 is interested in spurious surge cues due to pitch acceleration. In theory, such cues could not be possible, since there exists no communication from angular rate channel to the specific forces channel in the classical washout algorithm. However, since a coupled pitch-surge input is considered, the two channels are still connected via the tilt coordination, which is driven by the pitch angle. The transfer function will therefore resemble a low pass

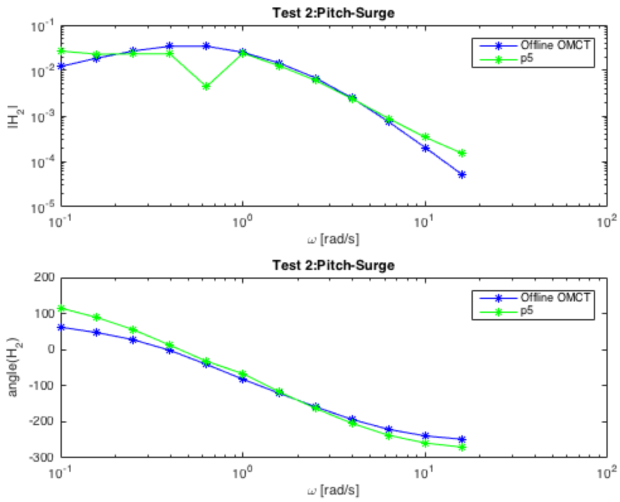

Figure D-3: Verification plot of test 2, pitch acceleration input and surge acceleration output.

filter, due to the tilt coordination, as is confirmed by Figure D-3. It can be seen that the commanded signal resembles the hardware response in the middle, but underestimates at low frequencies and very high frequencies. Furthermore there is a dip in amplitude response of the hardware signal around 0.6 $[rad/s]$. Therefore more cross talk between the pitch and surge channel found in the SRS than this offline simulation predicted. At this point, no clear explanation is found for these differences.

D-2 Roll

Contrary to pitch acceleration, a change in roll angle is in most maneuvers not combined with a change in sideward speed, because for civil aviation aircraft most turns are coordinated. A coordinated turn means that there is no side-slip and thus no lateral acceleration. This means that the input cues on roll acceleration are usually not combined with a sway input. Therefore test 3 and 4 use only a roll input to test the frequency response for this axis. Equation D-7 gives the equation to compute the frequency response for test 3 of the OMCT.

$$H_3 = \frac{\dot{P}_{PS}}{\dot{P}_{PA}}(\omega) \tag{D-7}$$

As can be seen test 3 measures the frequency response of roll due to roll. Equation D-8 gives than the equation to compute the frequency response for test 4 of the OMCT.

$$H_4 = \frac{f_{x_{PS}}}{\dot{P}_{PA}}(\omega) \tag{D-8}$$

As can be seen test 4 compares the specific force to a roll input. Figure D-4 shows a verification plot using data from the SRS. It can be seen that test 4 represents a high-pass filter, which is to be expected from the rotational channel. It can be seen that at high frequencies the plot shows some upswing, meaning that the amplitude of the roll motion is higher than expected.

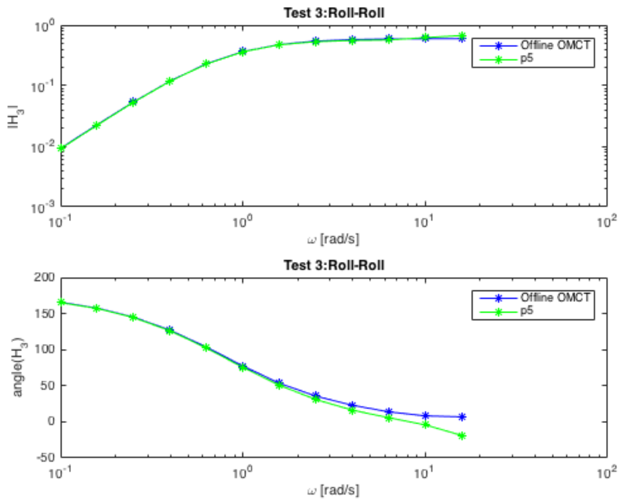

Figure D-4: Verification plot of test 3, roll acceleration input and roll acceleration output.

This combined with a slight phase lag, meaning that the hardware is unable the following software input at high frequencies. Figure D-5 shows the cross channel test for roll input and sway acceleration output. As can be seen, at low frequencies, the roll input causes a sway

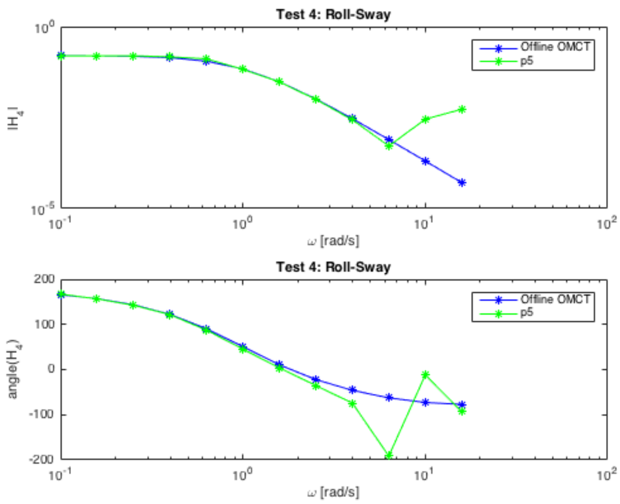

Figure D-5: Verification plot of test 2, roll acceleration input and sway acceleration output.

acceleration due to tilt coordination. This is to be expected. The OMCT does not prescribe to subtract the gravity component in this case, unlike test 2. The reason for this is unclear. For the purpose of understanding, Figure D-6 shows test 4 without the gravity component added. As can be seen from Figure D-6, H_4 shows a similar trend to test 2, Figure D-3.

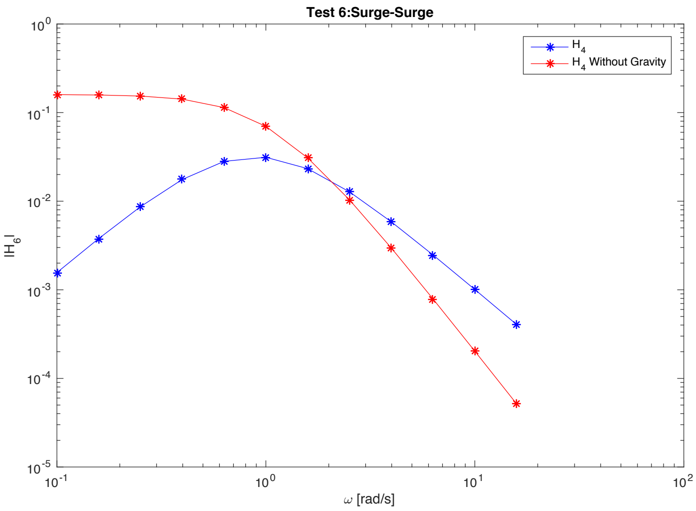

Figure D-6: Alternative test 4, similar to test 2. Gravity component added and neglected.

D-3 Yaw

The next test, test 5, looks at the frequency response of yaw due to a yaw input. From theory it expected that the frequency response will resemble a high pass filter, according to the rotational channel of the classical washout algorithm. Figure D-7 shows a comparison of the offline OMCT to the SRS data. It can be seen that the yaw response indeed resembles a

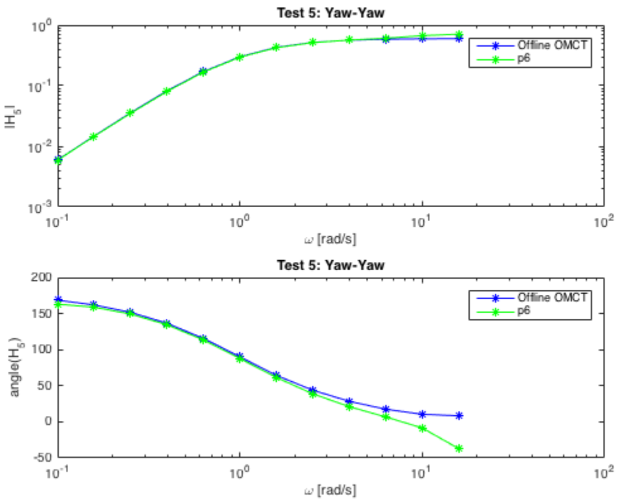

Figure D-7: Verification plot of test 5, yaw acceleration input and yaw acceleration output.

high pass filter. However, similarly to the roll response, there is some upswing and phase lag occurring at high frequencies.

D-4 Surge

The frequency response due to sway is characterized by test 6 and test 7. Equation D-9 shows the tranfer function for test 6.

$$H_6 = \frac{f_{xPS}}{f_{xPA}}(\omega) \tag{D-9}$$

It can be seen that test 6 is focussed on specific force. The surge specific force is formed two channels in the classical washout algorithm: the translational channel which is a high pass filter and the tilt coordination which is a low pass filter. Figure D-8 shows the response of both channels and the total modulus of surge. Figure D-9 shows the comparison to the SRS data.

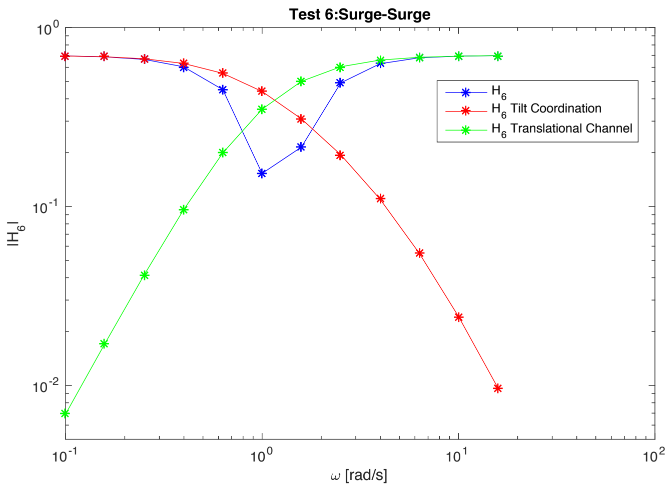

Figure D-8: Breakdown of filter contribution to the modulus response of test 6.

It can be seen that the initial drop in modulus is steeper for the real simulator. The reason

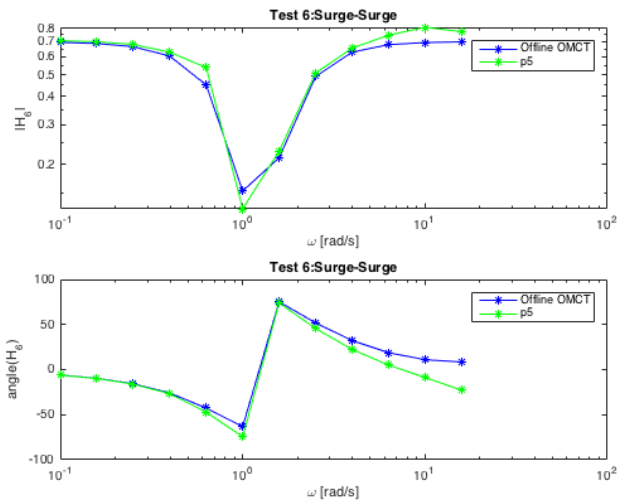

Figure D-9: Verification plot of test 6, surge acceleration input and surge acceleration output.

for this is unclear. It should be said however, that in order to make a good comparison in this region, the frequency points of the OMCT should be positioned closer together. Furthermore, the upswing and phase lag is also present for this channel at high frequencies.

The pitch response due to a surge input is measured in Equation D-10.

$$H_7 = \frac{\dot{Q}_{PS}}{f_{x_{PA}}}(\omega) \tag{D-10}$$

Theoretically this plot should resemble only the tilt coordinated channel and therefore the green line in Figure D-8. However, as can be seen from Figure D-10, H_7 resembles a high pass

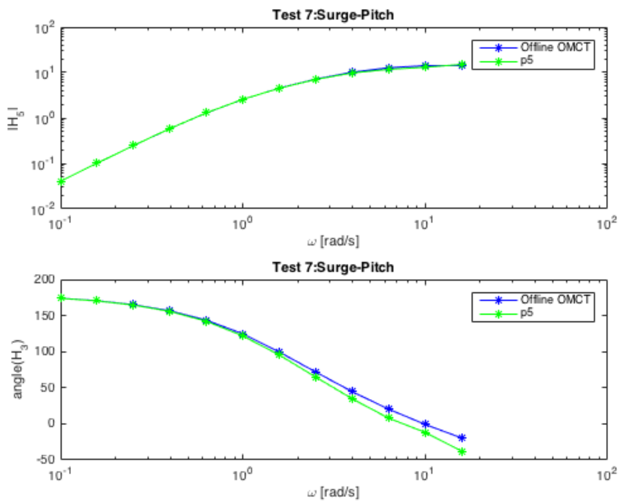

Figure D-10: Verification plot of test 7, surge acceleration input and pitch acceleration output.

filter, instead of a low pass filter, which is to be expected from the tilt coordination channel of the classical washout algorithm. This can be explained by the fact that we are look at the pitch response, and not the pitch acceleration response. If a low pass filter is integrated twice(from pitch acceleration to pitch) then it becomes a high pass filter. This is was test 7 resembles a high pass filter.

D-5 Sway

The frequency response for a sway acceleration input is for a hexapod motion cueing system very similar to the surge input, and will therefore be discussed only briefly in the subsection. Equation D-10 and Equation D-11 give the transfer functions for sway to sway and for sway to roll respectivaly.

$$H_8 = \frac{f_{y_{PS}}}{f_{y_{PA}}}(\omega) \tag{D-11}$$

$$H_9 = \frac{\dot{P}_{PS}}{f_{y_{PA}}}(\omega) \tag{D-12}$$

Figure D-11 and Figure D-12 show the verification plots for the transfer function H_8 and H_9 respectively. Similarly to transfer function H_7, Figure D-12 shows the trend of a high pass filter.

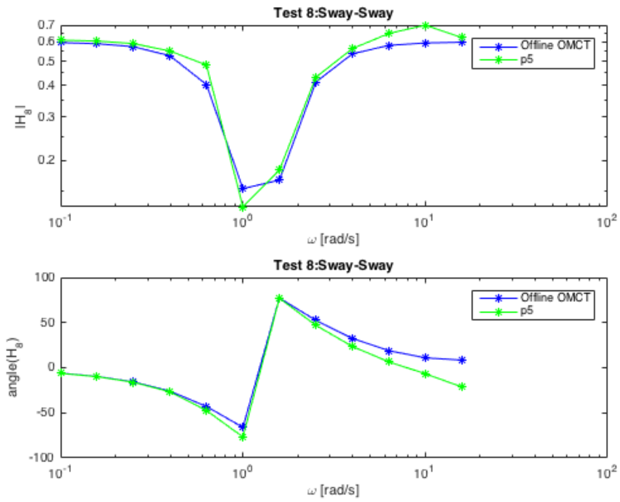

Figure D-11: Verification plot of test 8, sway acceleration input and sway acceleration output.

D-6 Heave

Finally, the frequency response due to an input for heave was investigated in test 10, according to a transfer function specified in Equation D-13.

$$H_10 = \frac{f_{z_{PS}}}{f_{z_{PA}}}(\omega) \tag{D-13}$$

The heave acceleration was also verified using the SRS data. Figure D-13 shows a bode plot for H_10. As can be seen from Figure D-13, there is upswing and phase lag present at high frequencies due to hardware characteristics.

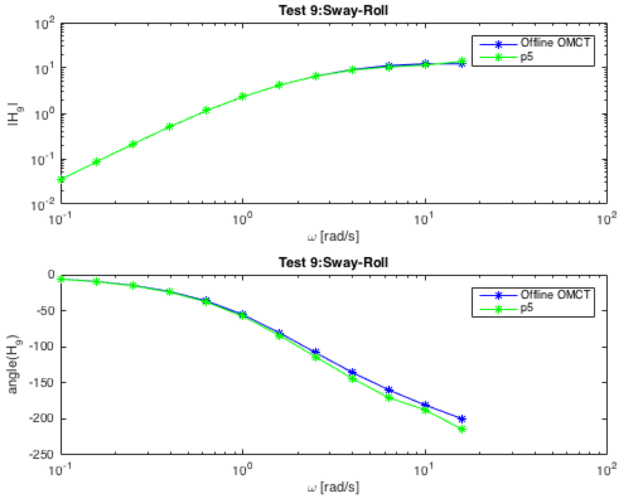

Figure D-12: Verification plot of test 9, sway acceleration input and roll acceleration output.

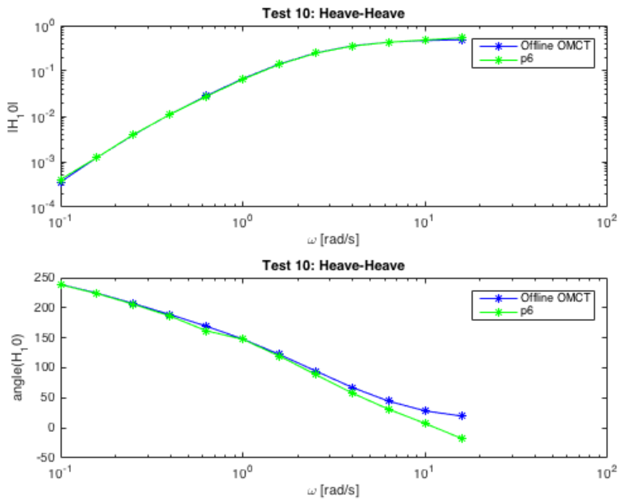

Figure D-13: Verification plot of test 10, heave acceleration input and heave acceleration output.

Appendix E

OMCT Sensitivity to MDA Settings

In this appendix, results are presented from the sensitivity analysis conducted in chapter 4, to investigate the influence of different break frequencies in the classical washout algorithm on the OMCT. Figure E-1 shows the influence of $\omega_{n\theta}$ on test 1 and test 2. Figure E-2 shows the influence of ω_{nLPx} on test 1, 2, 6 and 7. Finally, Figure E-3 shows the influence of ω_{nx} on test 6 and the influence of ω_{nz} on test 10.

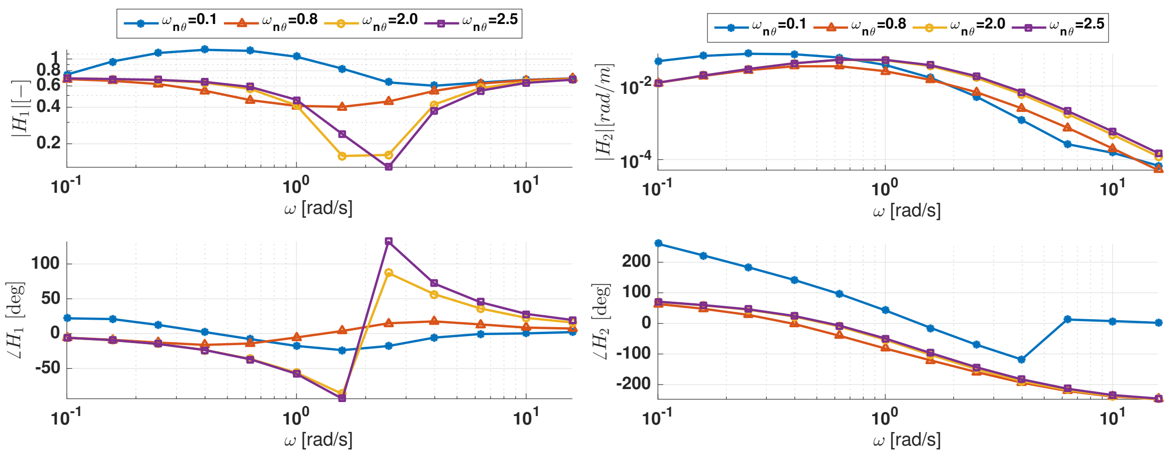

(a) Pitch frequency response function, test 1. **(b)** Surge frequency response function, test 2.

Figure E-1: Influence of $\omega_{n\theta}$.

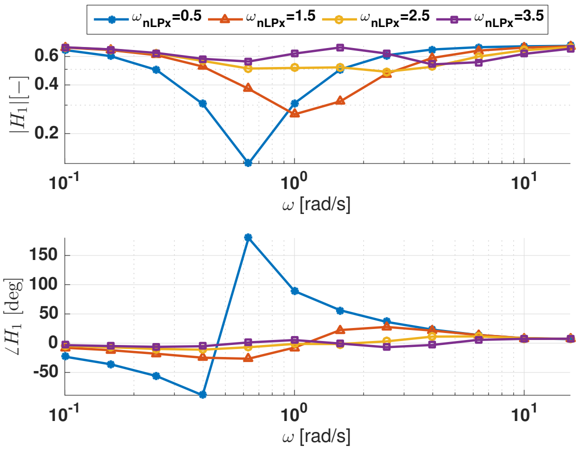

(a) Pitch frequency response function, test 1.

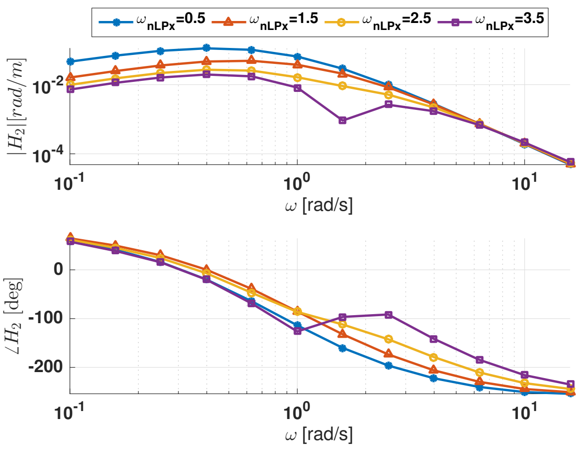

(b) Surge frequency response function, test 2.

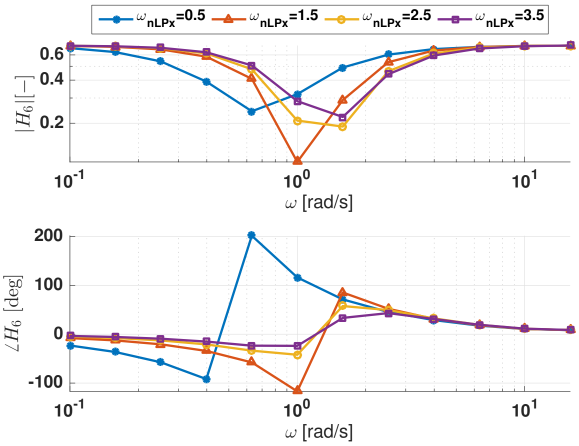

(c) Surge frequency response function, test 6.

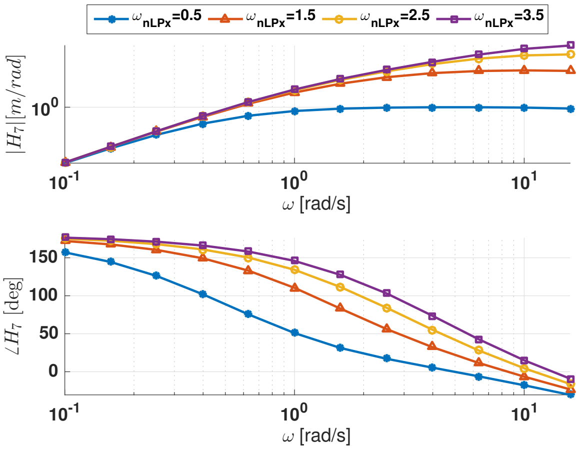

(d) Pitch frequency response function, test 7.

Figure E-2: Influence of ω_{nLPx}.

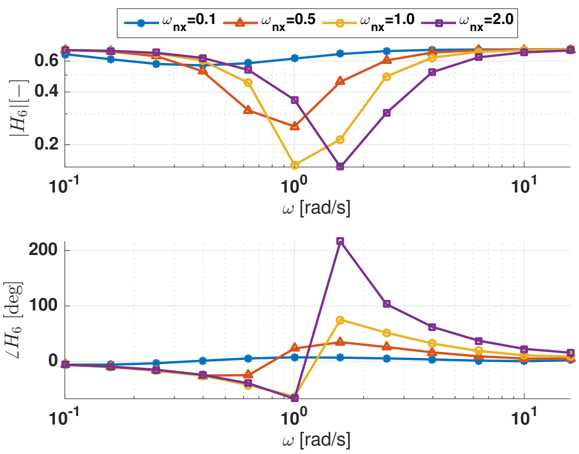

(a) Surge frequency response function, test 6.

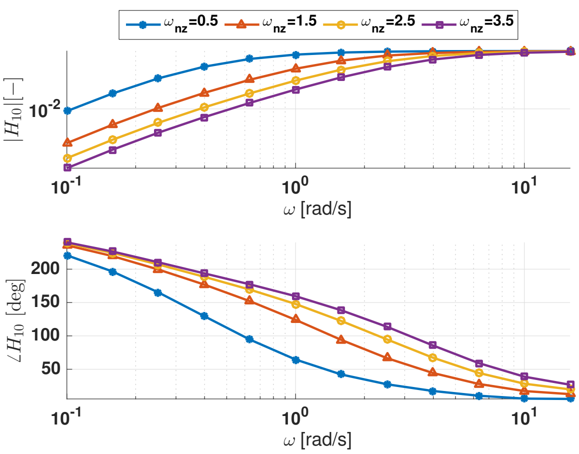

(b) Heave frequency response function, test 10.

Figure E-3: Influence of ω_{nx} on test 6 and influence of ω_{nz} on test 10.

Appendix F

SRS Geometry

This appendix shows the geometry of the Simona Research Simulator, for the computation of required actuator lengths. Figure F-1b shows a schematic top view of the SRS, where the Upper Gimbal Circle (indicated with UGC) and the Lower Gimbal Circle (LGC) are visible. Figure F-1a shows numerical values for important geometrical parameters in Figure F-1b.

Platform Property	Standard Notation	Value in millimetres
Upper Circle Radius	Ar	1600
Lower Circle Radius	Br	1650
Upper Gimbal Spacing	2P	200
Lower Gimbal Spacing	2D	600
Actuator Property	**Standard Notation**	**Value in millimetres**
Retracted Length	Lmin	2081
Maximum Length	Lmax	3331
Stroke (absolute total)	S	1250
Lower Buffers	Bl	50
Upper Buffers	Bu	50
Maximum Operational Length	Lmax,o	3281
Minimum Operational Length	Lmin,o	2131
Operational Stroke	So	1150

(a) Important geometric parameters of the SRS.

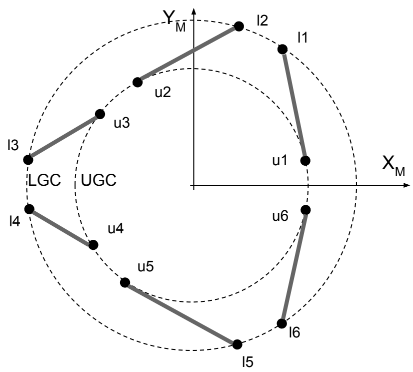

(b) Schematic top view of the SRS.

Figure F-1: SRS geometry.

Appendix G

OMCT Sensitivity to MDA Settings: Tuning

In this appendix, results are presented from the sensitivity analysis conducted in chapter 4, to investigate how tuning might be accomplished using the OMCT. Figure G-1 and Figure G-4 show the influence of ω_{n_θ} on test 1 and test 2. Figure G-2 and Figure G-5 show the influence of ω_{nLPx} on test 1, 2, 6 and 7. Finally, Figure G-3 and Figure G-6 show the influence of ω_{nx} on test 6 and the influence of ω_{nz} on test 10.

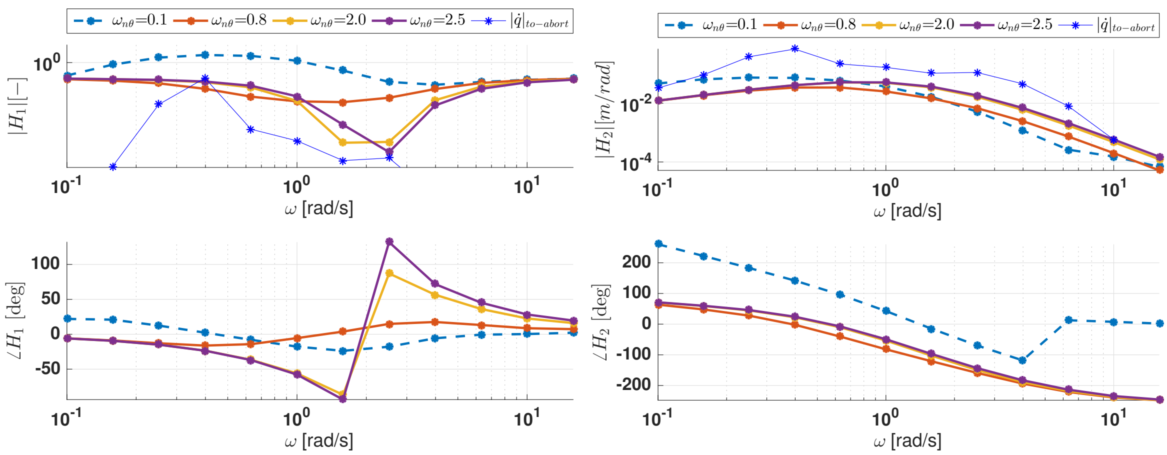

(a) Pitch frequency response function, test 1.

(b) Surge frequency response function, test 2.

Figure G-1: Influence of $\omega_{n\theta}$ with added information from the take-off and abort MTE.

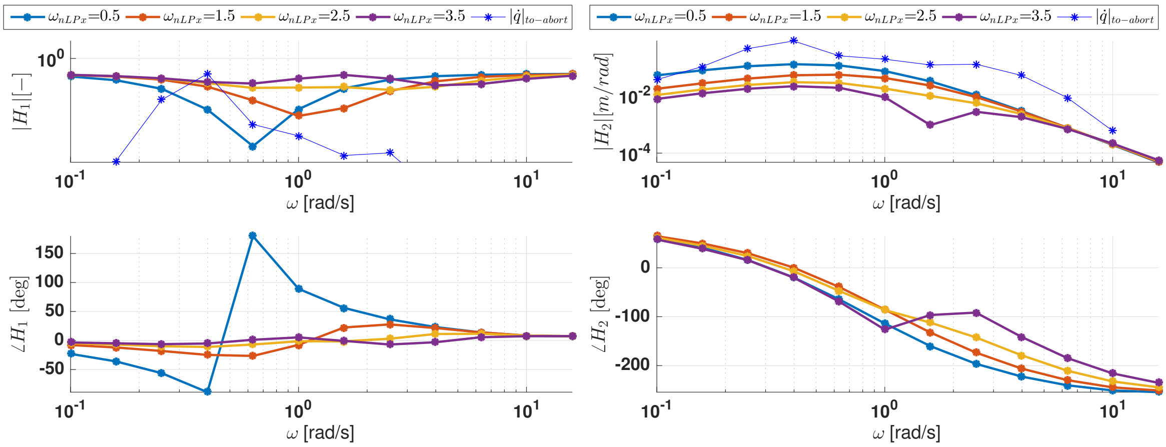

(a) Pitch frequency response function, test 1.

(b) Surge frequency response function, test 2.

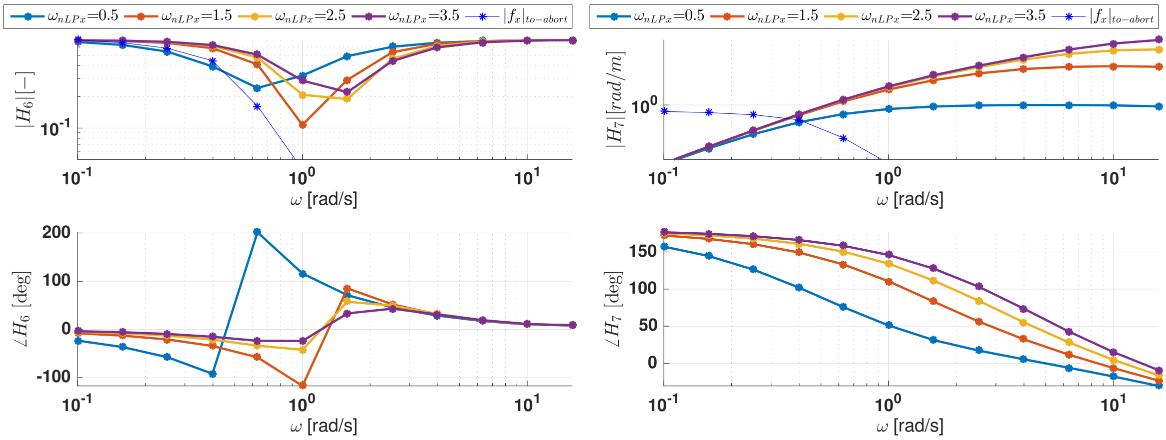

(c) Surge frequency response function, test 6.

(d) Pitch frequency response function, test 7.

Figure G-2: Influence of ω_{nLPx} with added information from the take-off and abort MTE.

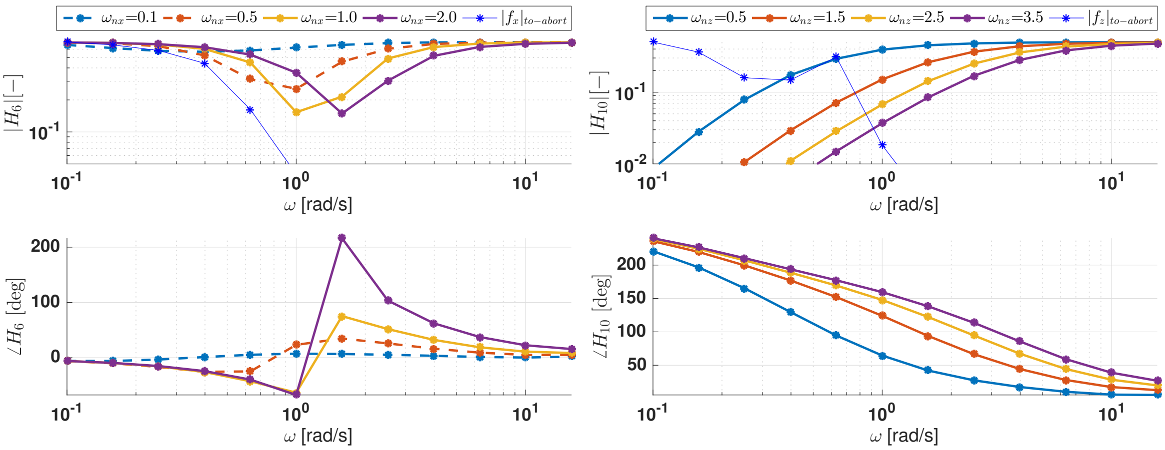

(a) Surge frequency response function, test 6.

(b) Heave frequency response function, test 10.

Figure G-3: Influence of ω_{nx} and influence of ω_{nz}, with added information from the take-off and abort MTE.

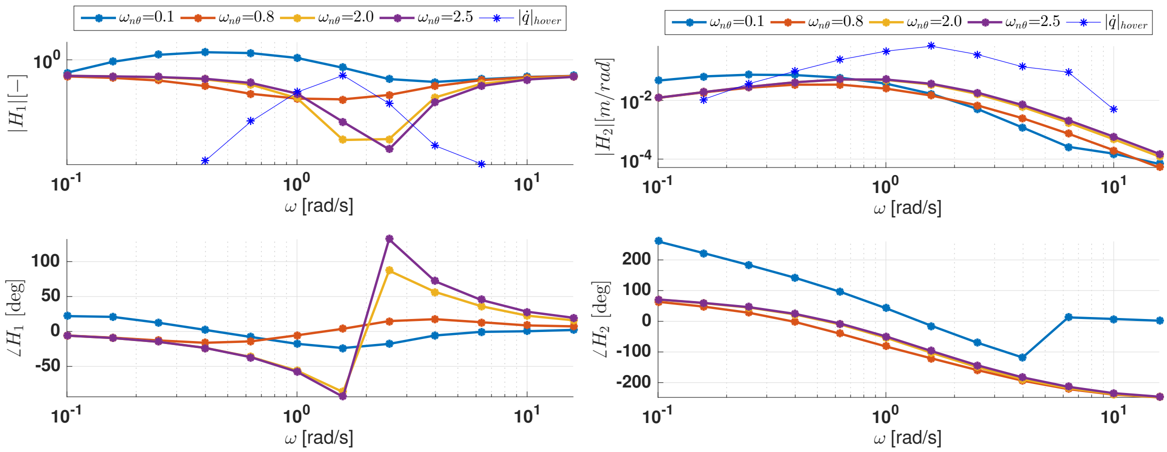

(a) Pitch frequency response function, test 1. **(b)** Surge frequency response function, test 2.

Figure G-4: Influence of $\omega_{n\theta}$ with added information from the hover MTE.

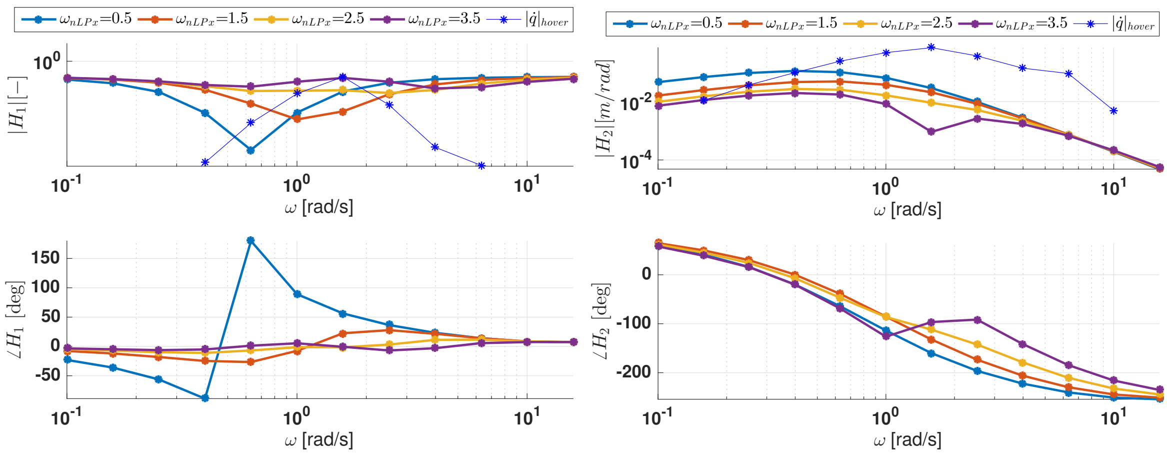

(a) Pitch frequency response function, test 1. **(b)** Surge frequency response function, test 2.

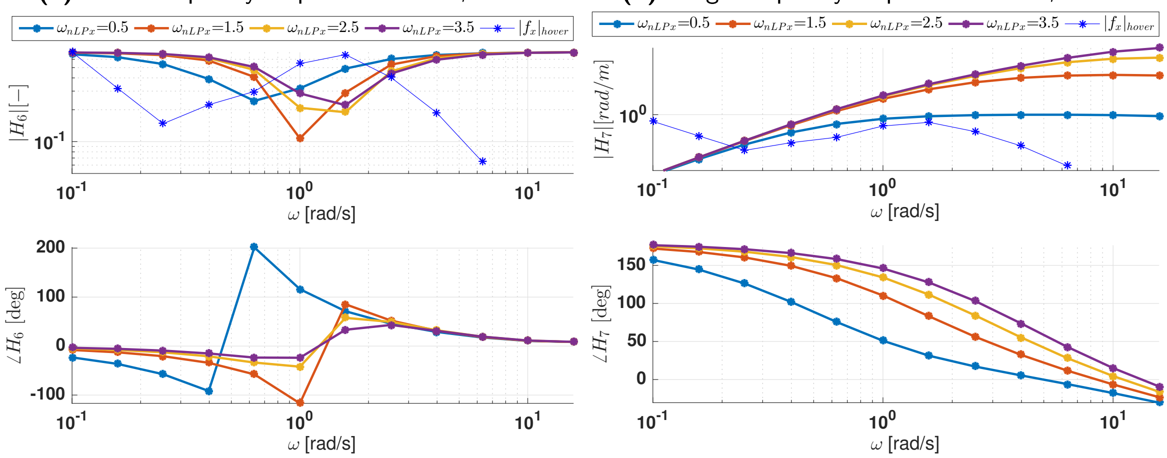

(c) Surge frequency response function, test 6. **(d)** Pitch frequency response function, test 7.

Figure G-5: Influence of ω_{nLPx} with added information from the hover MTE.

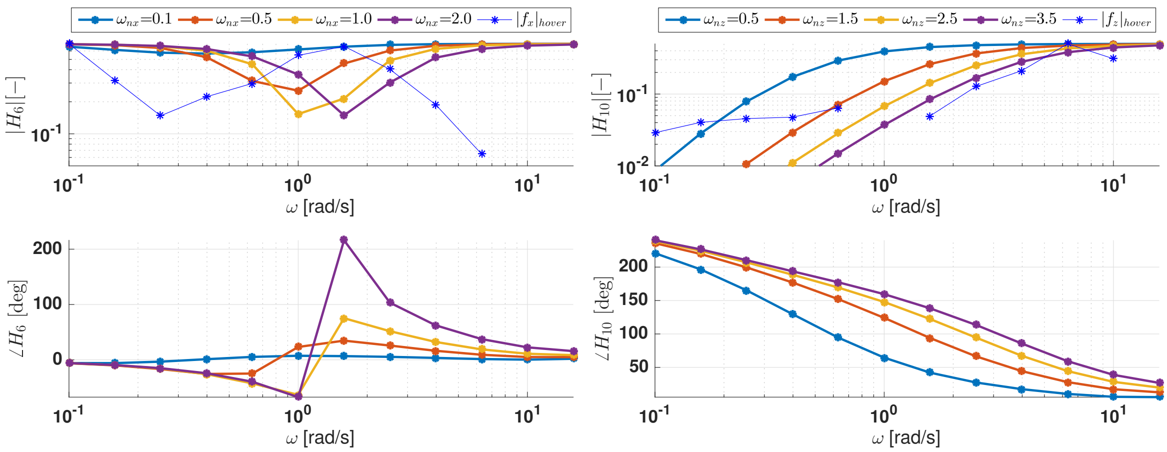

(a) Surge frequency response function, test 6. **(b)** Heave frequency response function, test 10.

Figure G-6: Influence of ω_{nx} and influence of ω_{nz}, with added information from the hover MTE.

Appendix H

OMCT Sensitivity to Input Signals

In this appendix, results are presented from the sensitivity analysis conducted in chapter 4, to investigate the influence of the size of the input signals on the OMCT. Figure H-1 shows the result for test 1 and test 2. Figure H-2 and Figure H-3 show the results for test 6, 7 and 10 respectively.

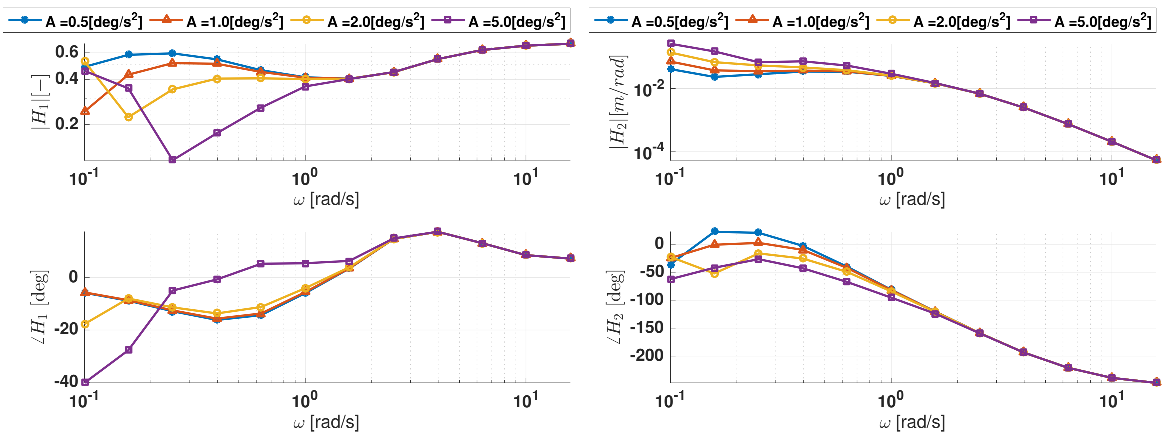

(a) Pitch frequency response function, test 1. **(b)** Surge frequency response function, test 2.

Figure H-1: Influence of the input spectrum on the frequency response functions.

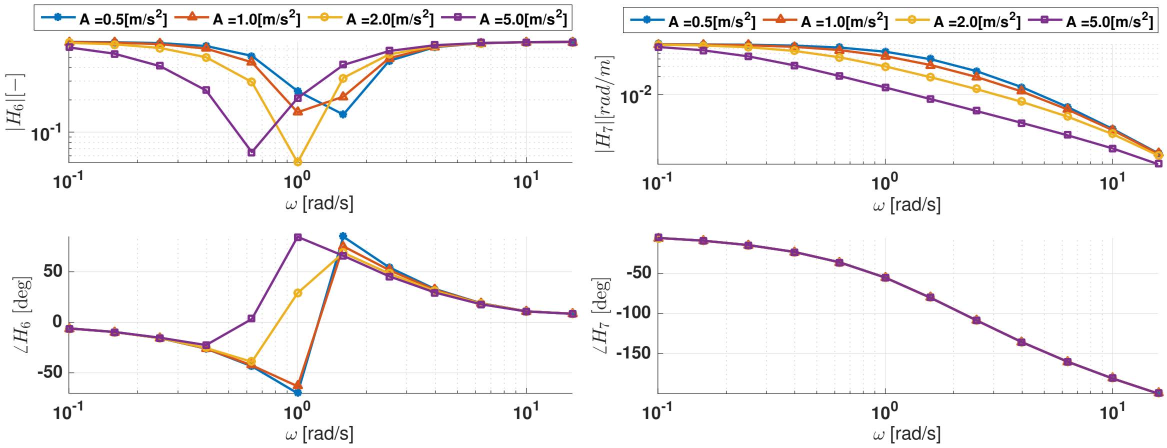

(a) Surge frequency response function, test 6.

(b) Pitch frequency response function, test 7.

Figure H-2: Influence of the input spectrum on the frequency response functions.

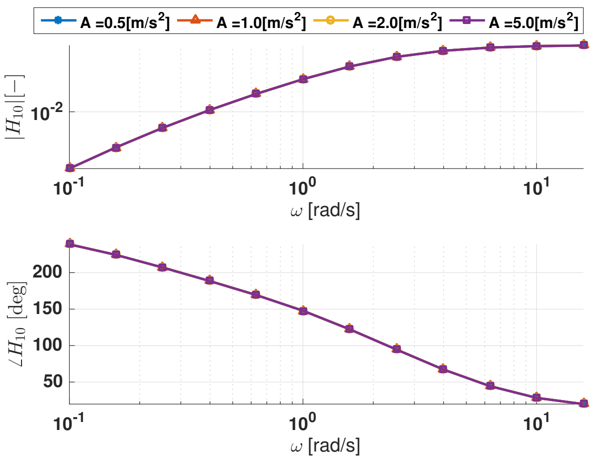

Figure H-3: Influence of the input spectrum on the heave frequency response functions, test 10.

Appendix I

Tailored OMCT Sensitivity to MDA Settings

THis appendix gives results of a sensitivity analysis conducted with input spectra of a tailored OMCT based on the two Mission Task Elements separately. Figures are structured per test. Figure I-1, Figure I-2 and Figure I-3 give the sensitivity of a tailored OMCT based on TO and Abort data for test 1, 6 and 10 respectively. Figure I-4, Figure I-5 and Figure I-6 give the sensitivity of a tailored OMCT based on hover data for test 1, 6 and 10 respectively.

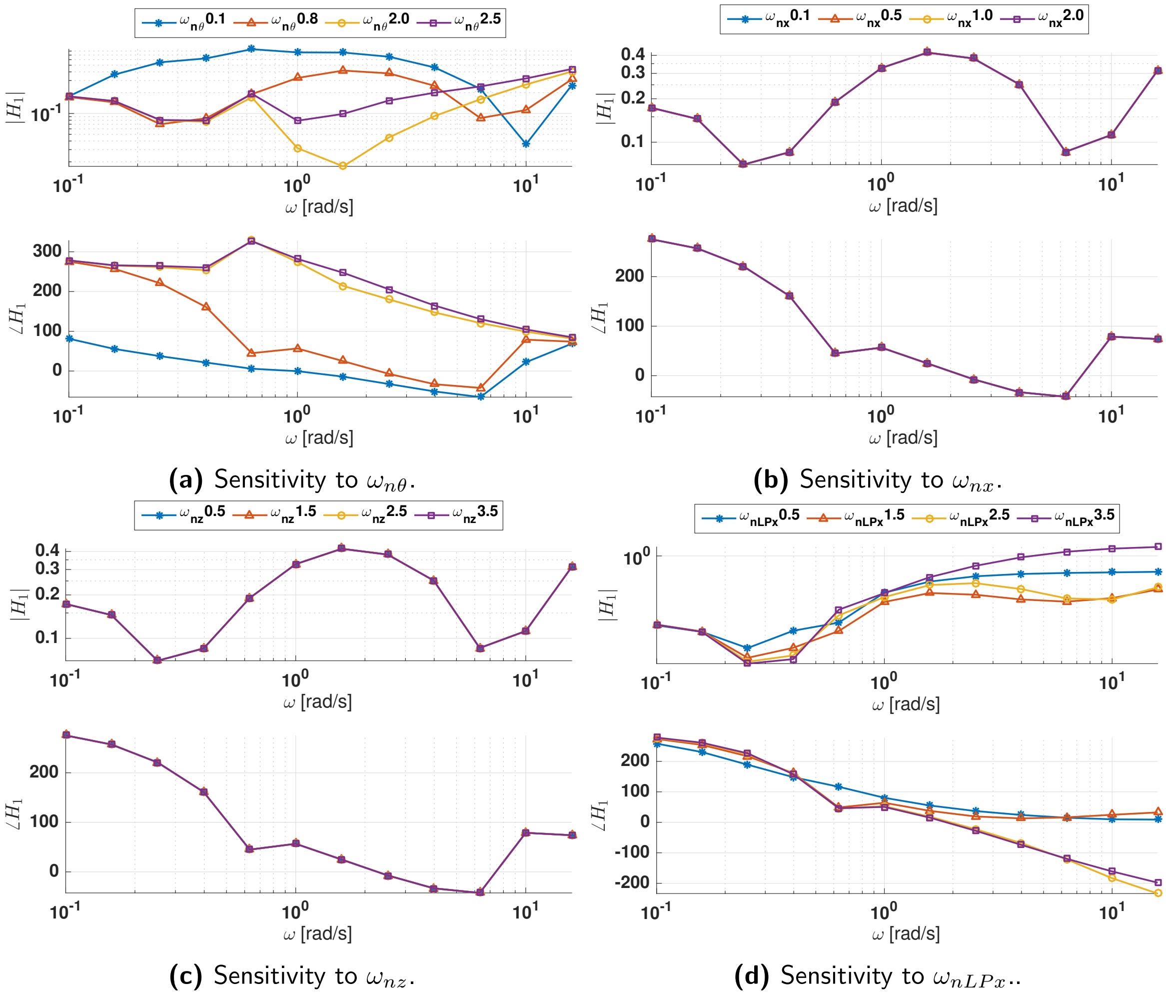

(a) Sensitivity to $\omega_{n\theta}$.

(b) Sensitivity to ω_{nx}.

(c) Sensitivity to ω_{nz}.

(d) Sensitivity to ω_{nLPx}..

Figure I-1: Sensitivity of a tailored OMCT to the take-off and abort MTE - Test 1.

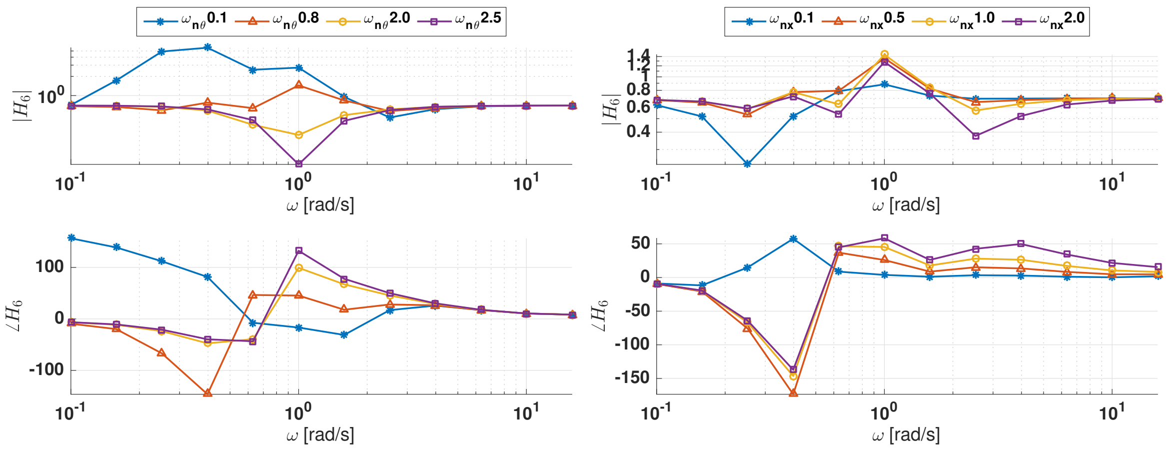

(a) Sensitivity to $\omega_{n\theta}$.

(b) Sensitivity to ω_{nx}.

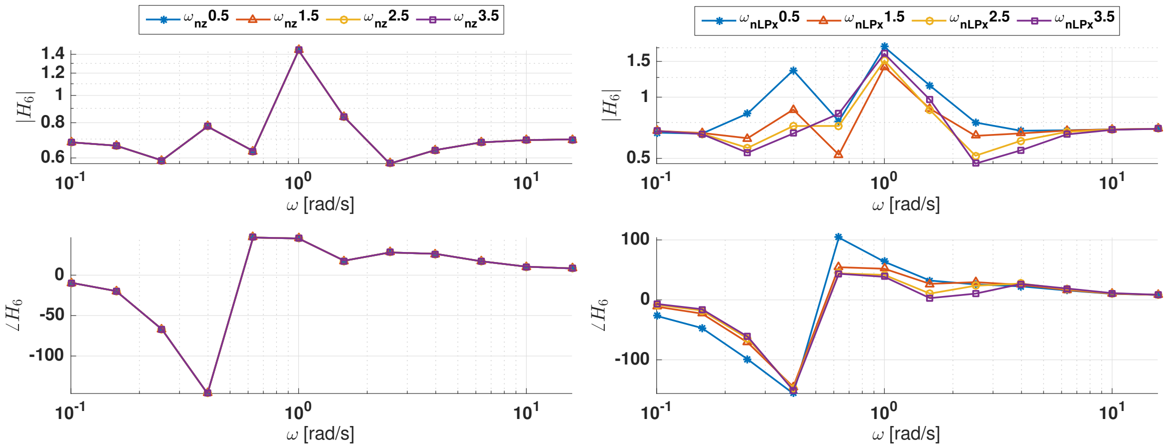

(c) Sensitivity to ω_{nz}.

(d) Sensitivity to ω_{nLPx}..

Figure I-2: Sensitivity of a tailored OMCT to the take-off and abort MTE - Test 6.

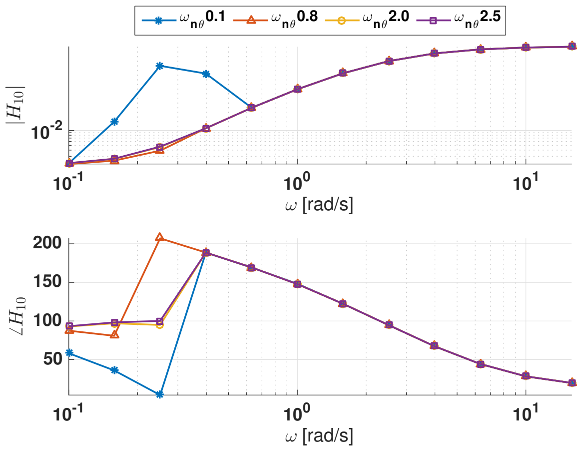

(a) Sensitivity to $\omega_{n\theta}$.

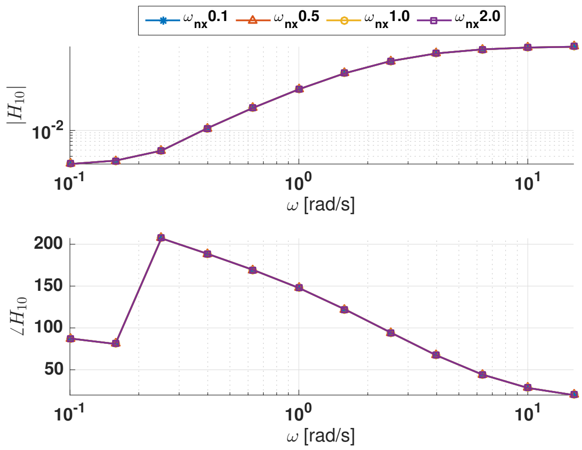

(b) Sensitivity to ω_{nx}.

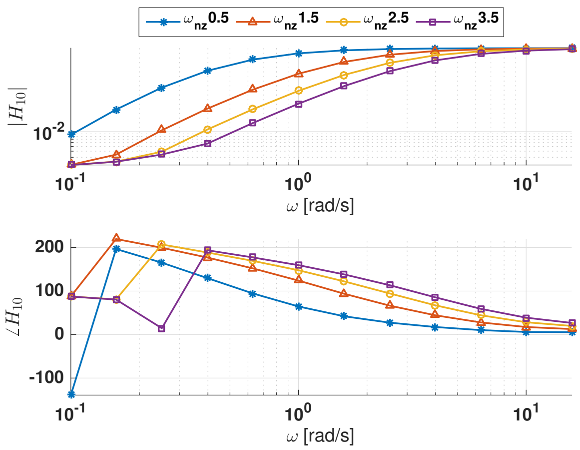

(c) Sensitivity to ω_{nz}.

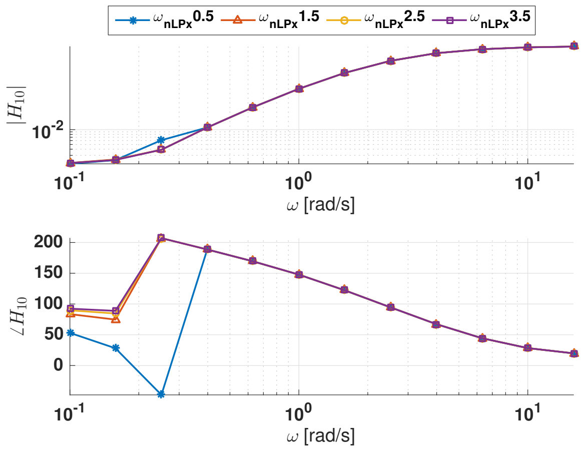

(d) Sensitivity to ω_{nLPx}..

Figure I-3: Sensitivity of a tailored OMCT to the take-off and abort MTE - Test 10.

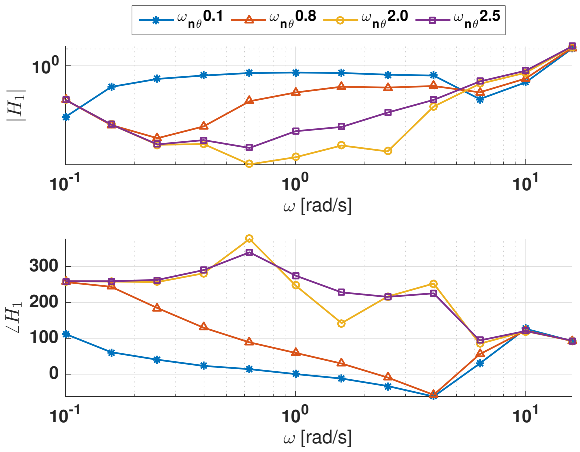

(a) Sensitivity to $\omega_{n\theta}$.

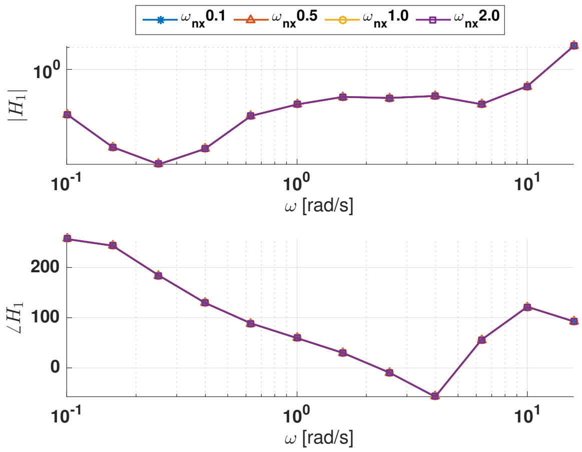

(b) Sensitivity to ω_{nx}.

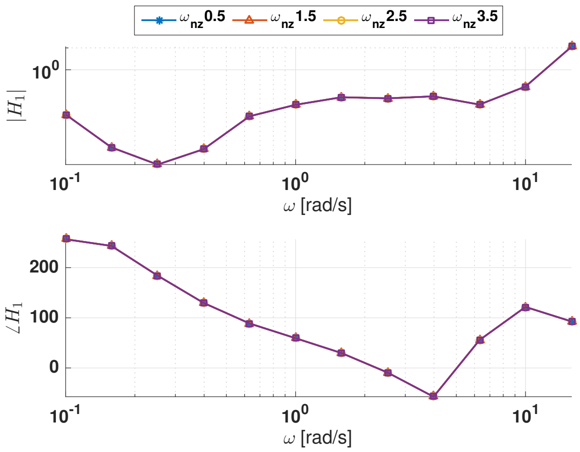

(c) Sensitivity to ω_{nz}.

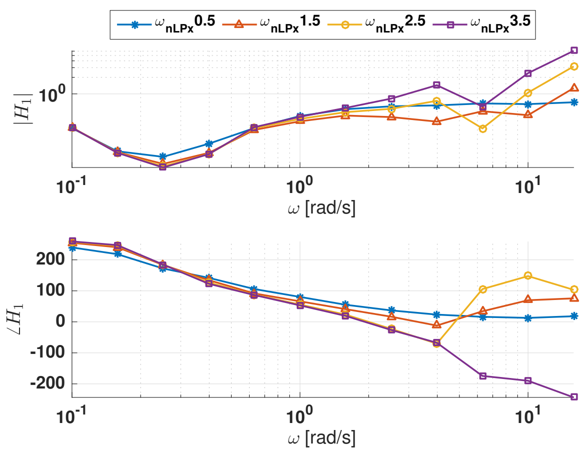

(d) Sensitivity to ω_{nLPx}..

Figure I-4: Sensitivity of a tailored OMCT to the hover MTE - Test 1.

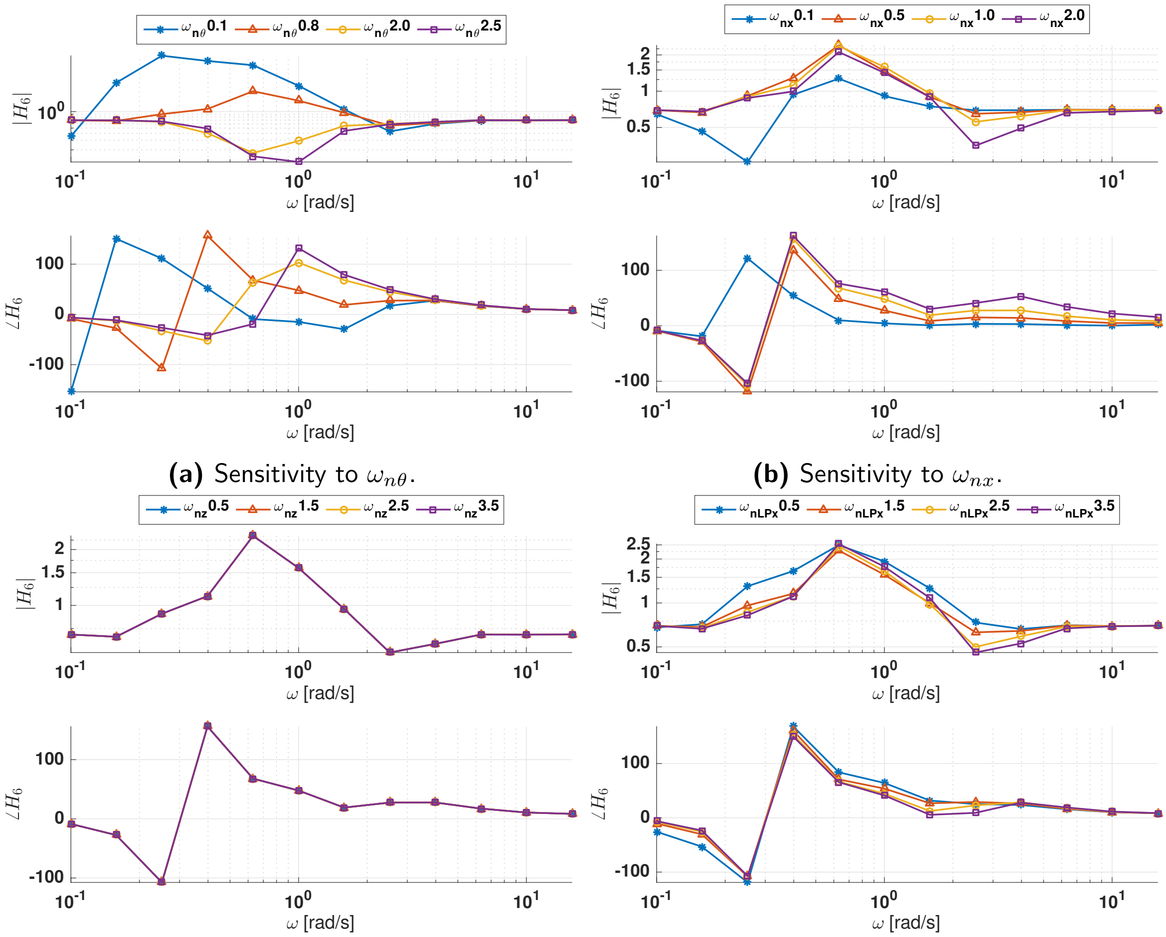

(a) Sensitivity to $\omega_{n\theta}$.

(b) Sensitivity to ω_{nx}.

(c) Sensitivity to ω_{nz}.

(d) Sensitivity to ω_{nLPx}..

Figure I-5: Sensitivity of a tailored OMCT to the hover MTE - Test 6.

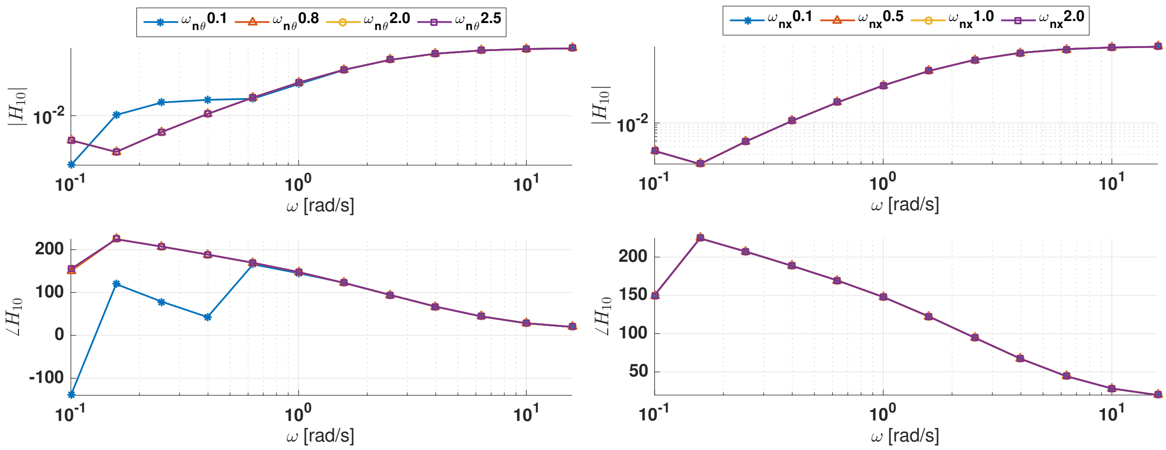

(a) Sensitivity to $\omega_{n\theta}$. **(b)** Sensitivity to ω_{nx}.

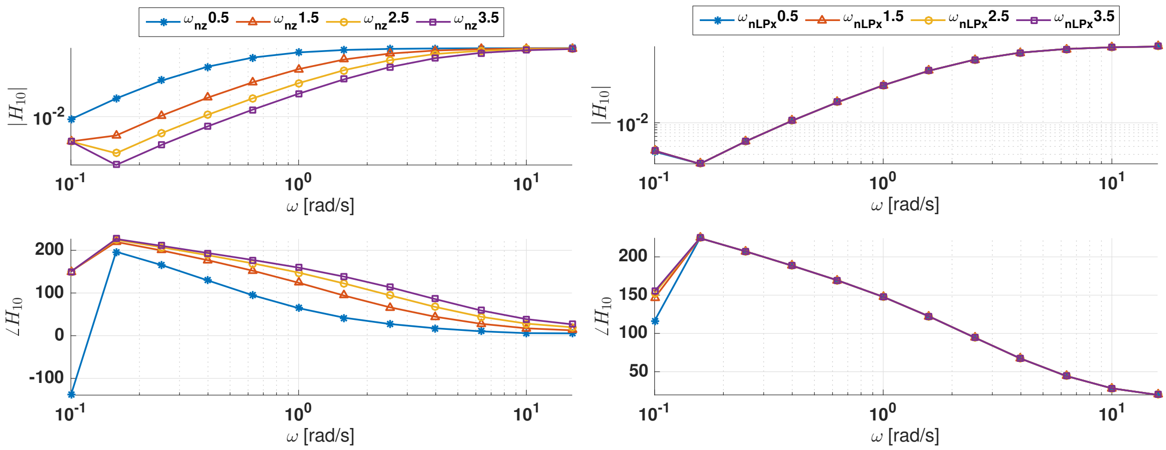

(c) Sensitivity to ω_{nz}. **(d)** Sensitivity to ω_{nLPx}..

Figure I-6: Sensitivity of a tailored OMCT to the hover MTE - Test 10.

Part IV

Appendices to the Paper for the 73rd Annual Forum of the American Helicopter Society

Appendix J

Time-domain Data

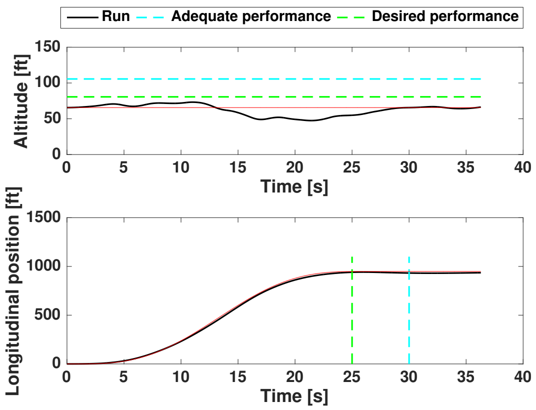

(a) Performance.

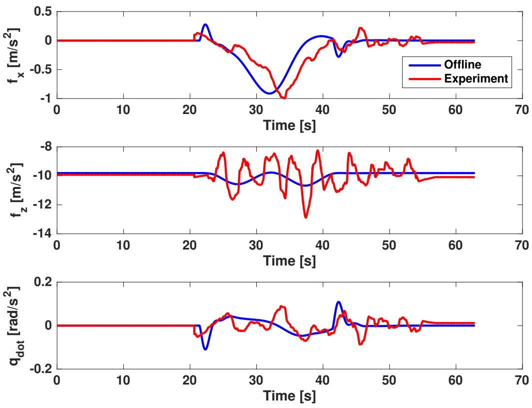

(b) Motion Outputs.

Figure J-1: Example of a run with good performance, take-off and abort MTE, run 47, subject 1, $\omega_{n\theta} = 0.8$.

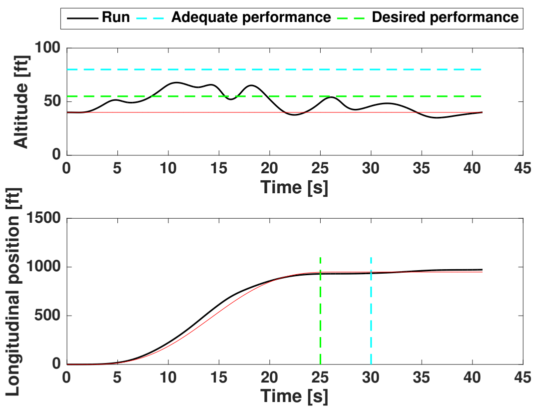

(a) Performance.

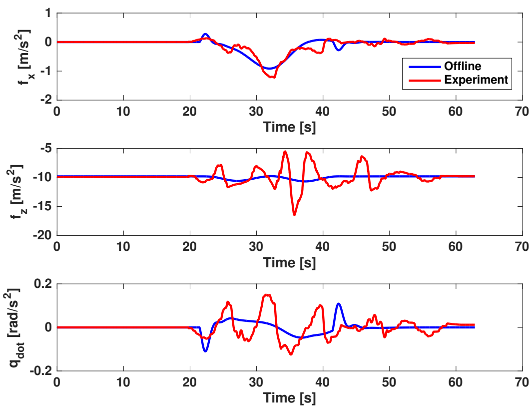

(b) Motion outputs.

Figure J-2: Example of a run with average performance, take-off and abort MTE, run 69, subject 3, $\omega_{n\theta} = 1.2$.

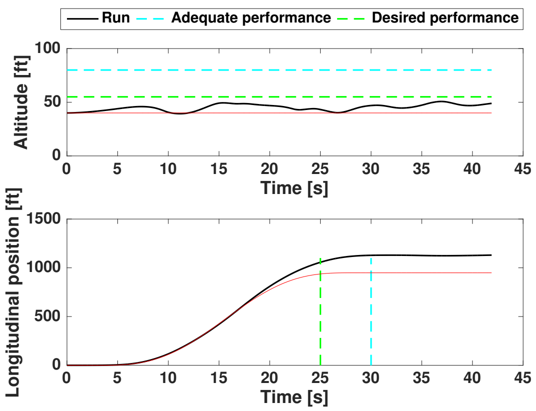

(a) Performance.

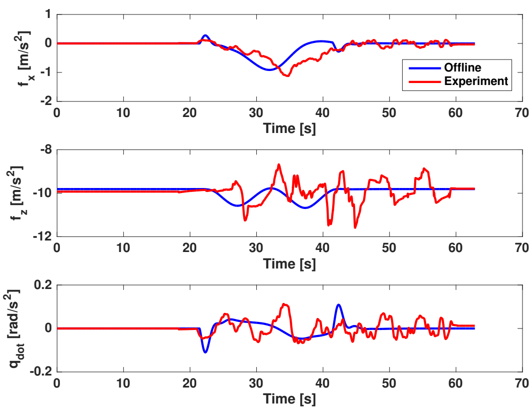

(b) Motion outputs.

Figure J-3: Example of a run with bad performance, take-off and abort MTE, run 36, subject 2, $\omega_{n\theta} = 1.2$.

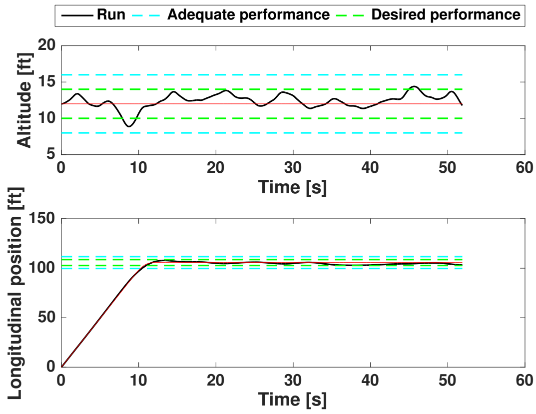

(a) Performance.

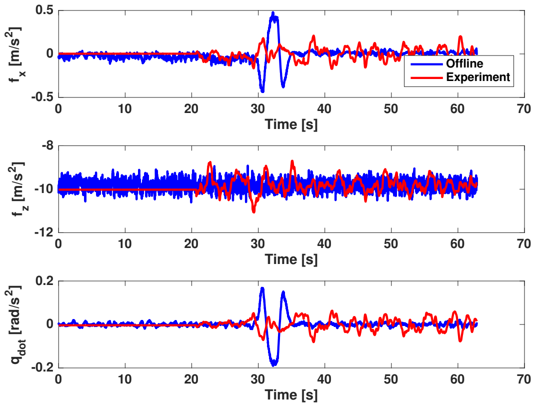

(b) Motion outputs.

Figure J-4: Example of a run with good performance, hover MTE, run 19, subject 2, $\omega_{n\theta} = 1.2$.

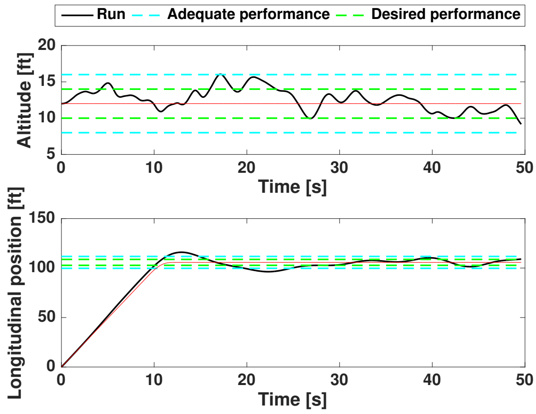

(a) Performance.

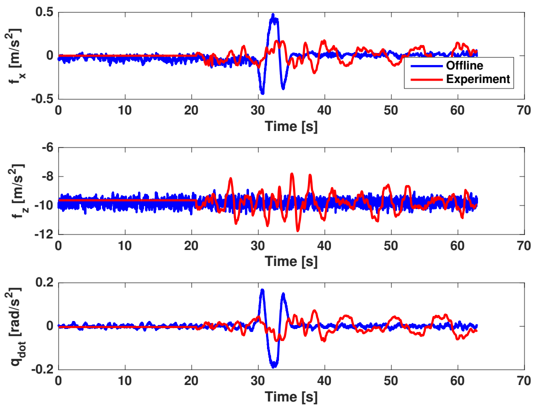

(b) Motion outputs.

Figure J-5: Example of a run with average performance, hover MTE, run 47, subject 3, $\omega_{n\theta} = 1.2$.

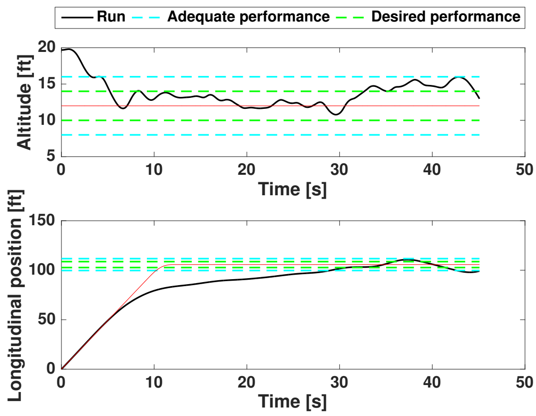

(a) Performance.

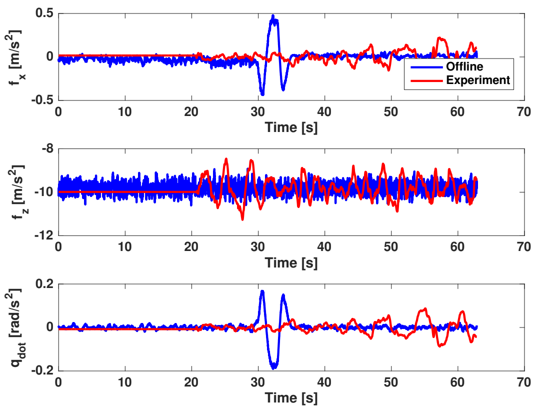

(b) Motion outputs.

Figure J-6: Example of a run with bad performance, hover MTE, run 26, subject 1, $\omega_{n\theta} = 0.8$.

Appendix K

Frequency-domain Data

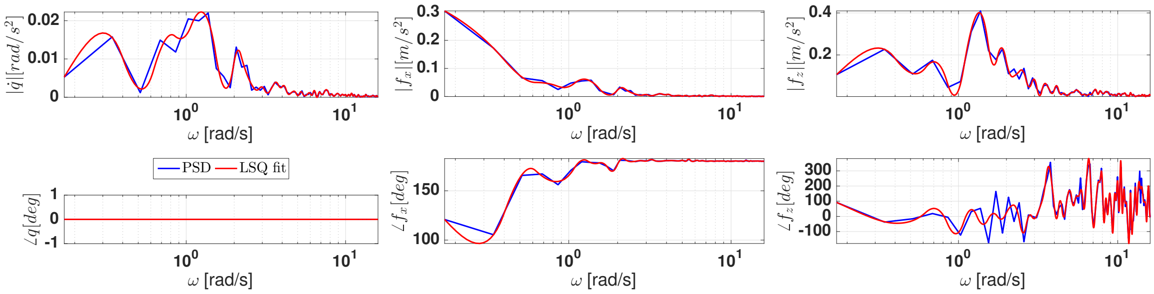

(a) $\dot{q}$. **(b)** f_x. **(c)** f_z.

Figure K-1: Example of a run with good performance, take-off and abort MTE, run 47, subject 1, $\omega_{n\theta} = 0.8$.

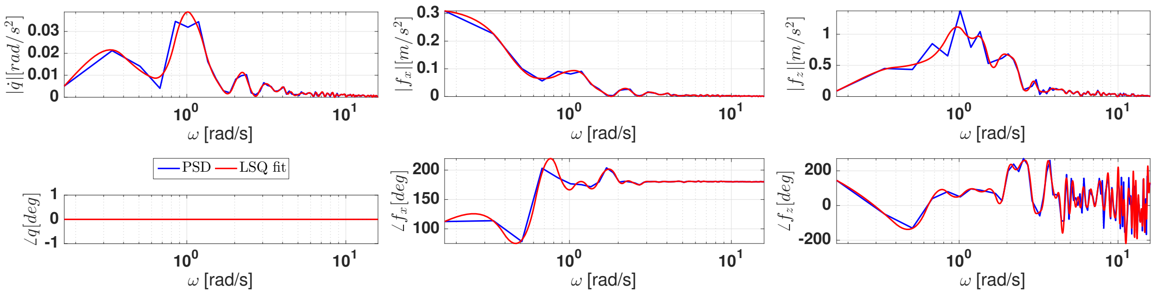

(a) $\dot{q}$. **(b)** f_x. **(c)** f_z.

Figure K-2: Example of a run with average performance, take-off and abort MTE, run 69, subject 3, $\omega_{n\theta} = 1.2$.

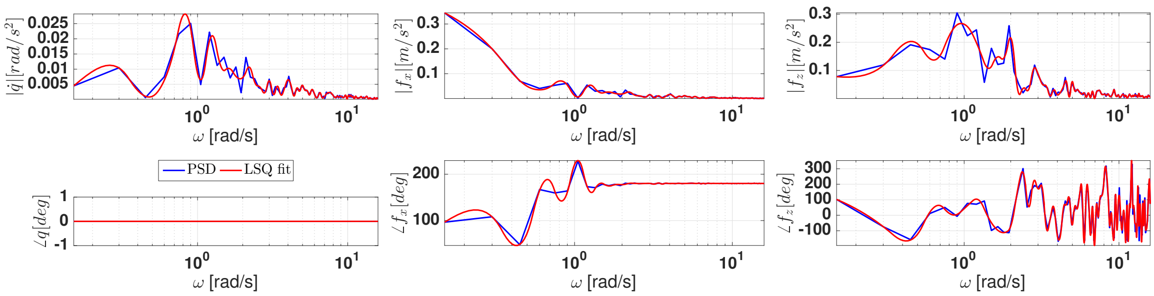

(a) $\dot{q}$. **(b)** f_x. **(c)** f_z.

Figure K-3: Example of a run with bad performance, take-off and abort MTE, run 36, subject 2, $\omega_{n\theta} = 1.2$.

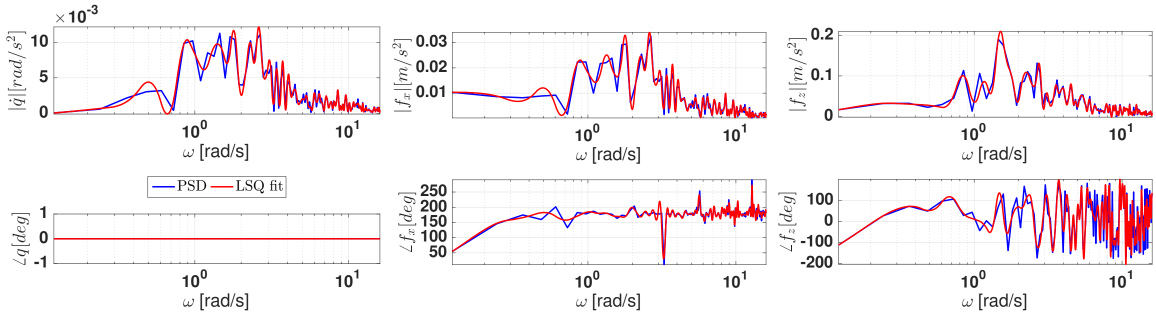

(a) $\dot{q}$. **(b)** f_x. **(c)** f_z.

Figure K-4: Example of a run with good performance, hover MTE, run 19, subject 2, $\omega_{n\theta} = 1.2$.

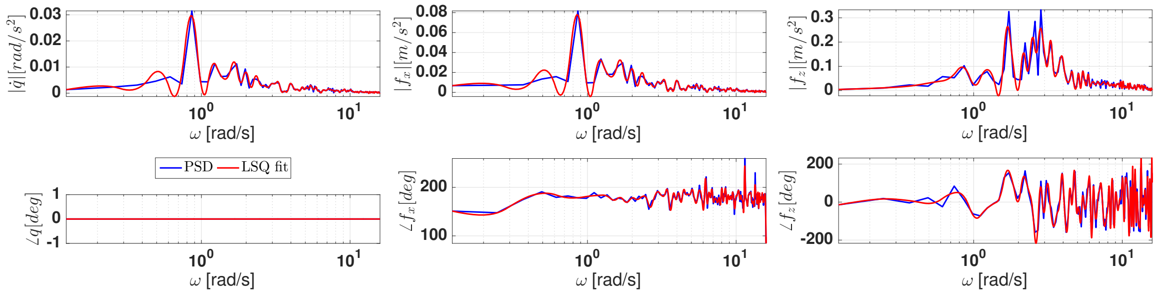

(a) $\dot{q}$. **(b)** f_x. **(c)** f_z.

Figure K-5: Example of a run with average performance, hover MTE, run 47, subject 3, $\omega_{n\theta} = 1.2$.

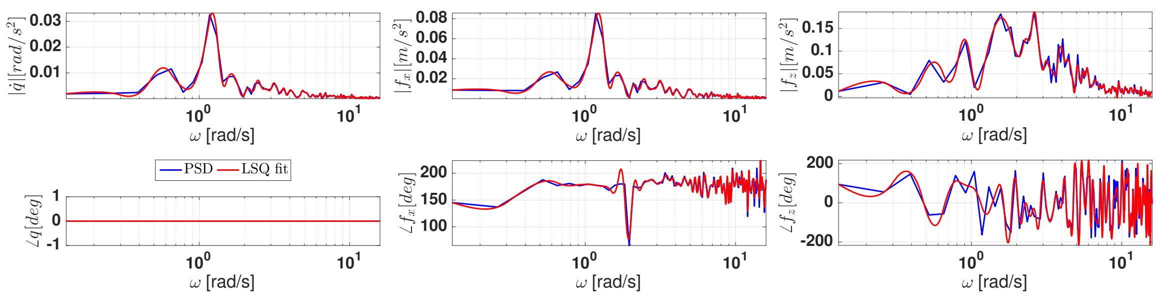

(a) $\dot{q}$. **(b)** f_x. **(c)** f_z.

Figure K-6: Example of a run with bad performance, hover MTE, run 26, subject 1, $\omega_{n\theta} = 0.8$.

Appendix L

Tailored OMCT Input Signals

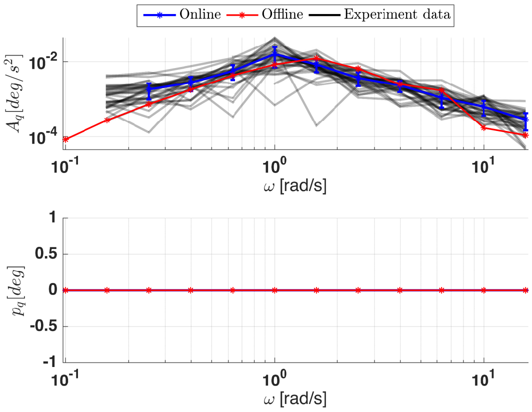

(a) $\dot{q}$ for the hover task.

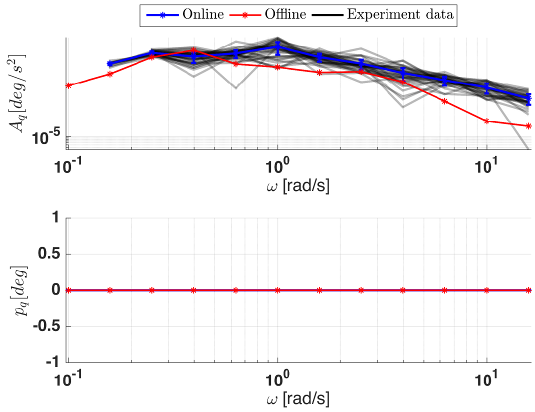

(b) $\dot{q}$ for the take-off and abort task.

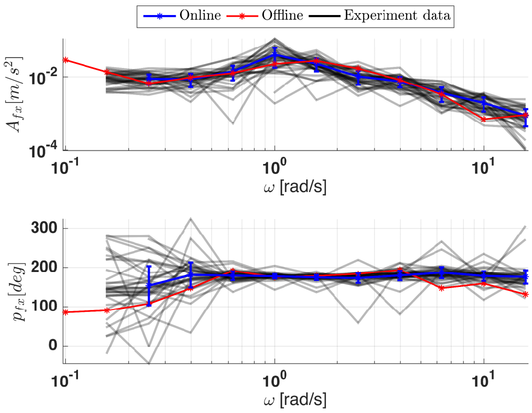

(c) f_x for the hover task.

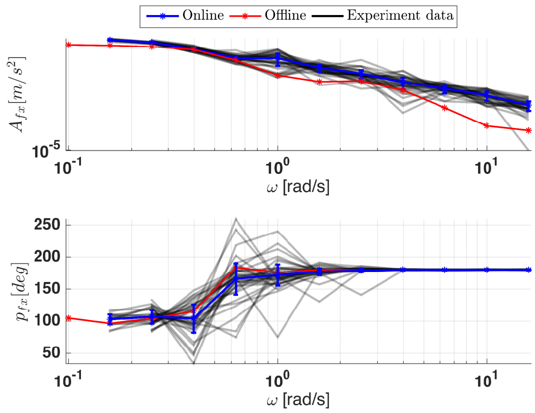

(d) f_x for the take-off and abort task.

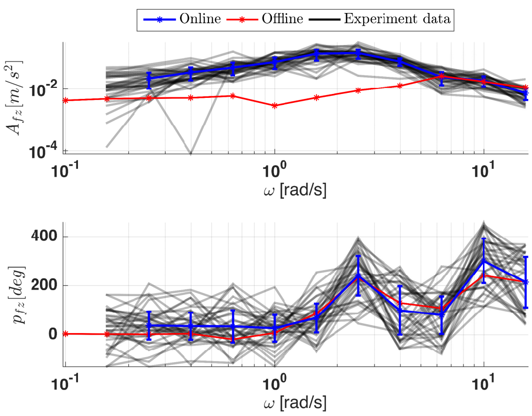

(e) f_z for the hover task.

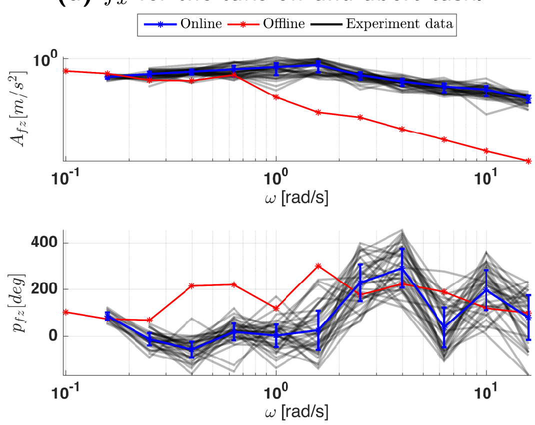

(f) f_z for the take-off and abort task.

Figure L-1: Tailored OMCT input signals, given for all test conditions and all participants.

Appendix M

Tailored OMCTs

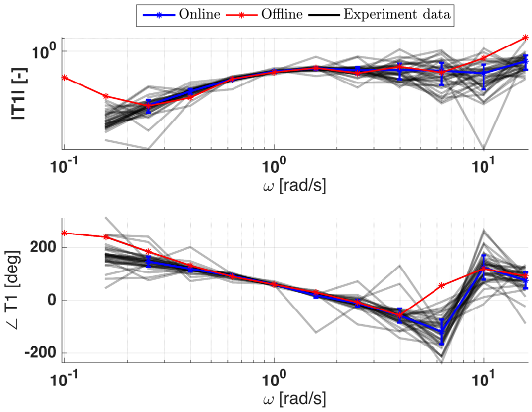

(a) Pitch frequency response for the hover task.

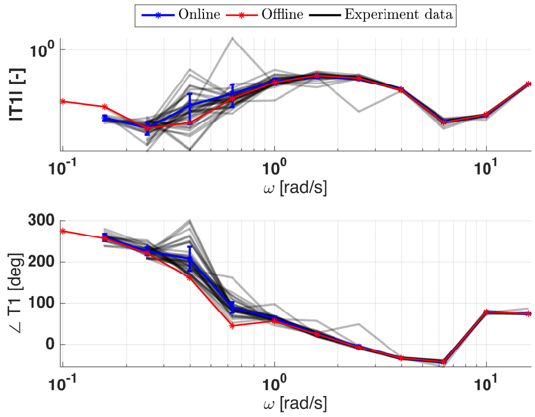

(b) Pitch frequency response for the take-off and abort task.

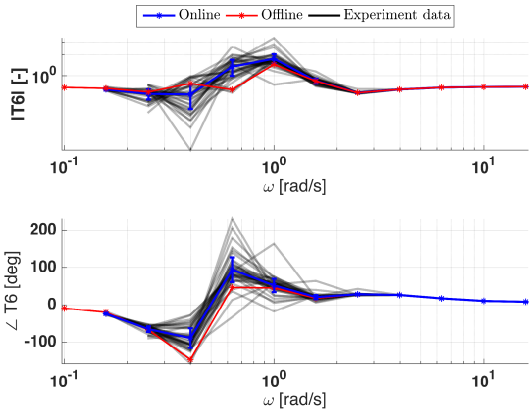

(c) Surge frequency response for the hover task.

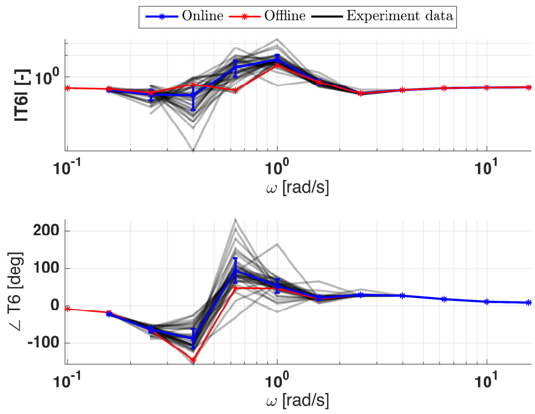

(d) Surge frequency response for the take-off and abort task.

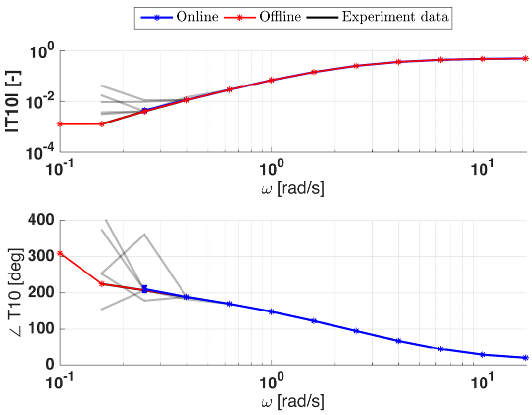

(e) Heave frequency response for the hover task.

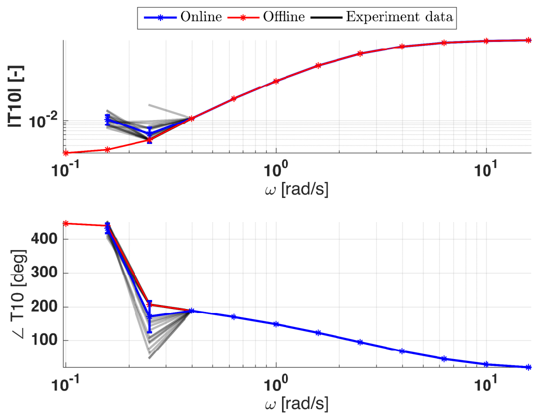

(f) Heave frequency response for the take-off and abort task.

Figure M-1: Tailored OMCT motion characteristics, given for all test conditions and all participants.

Appendix N

Input Analysis

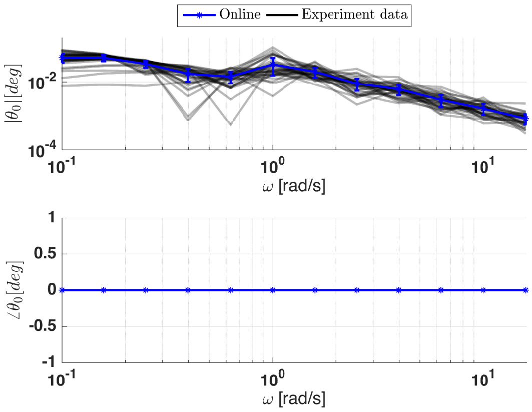

(a) $\dot{q}$ for the hover task.

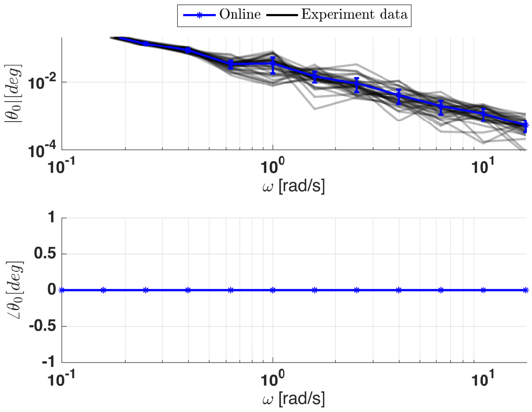

(b) $\dot{q}$ for the take-off and abort task.

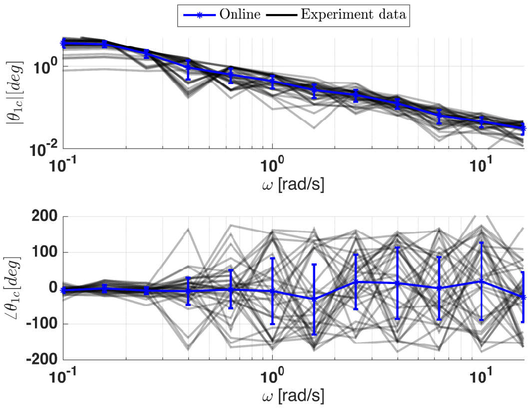

(c) f_x for the hover task.

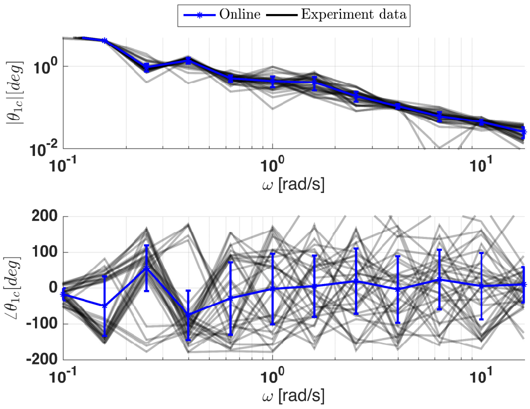

(d) f_x for the take-off and abort task.

Figure N-1: Tailored OMCT input signals, given for all test conditions and all participants.

Appendix O

Pilot Feedback

Lynx3DOFSim SIMONA Experiment

Pilot Questionnaires

Set #1

Subject Name: ....

Subject number: 1

Wouter Dalmeijer

September 2016

Awarded Simulation Fidelity Rating Scales

Task	Conditions #	SFR	Comments
Practice	Practice	7	"vaste stick uitslagen" "veel kracht op stick" motion niet opgevallen.
Hover	Condition 1 t1	2	heel secuur bewegen -> veel nadenken "motion wordt gebruikt voor PID visual primair motion secundair"
Hover	Condition 2 t3	2	"Motion vinden goed." "heave minder minder intuïtief dan de vorige" focus light op heave.
Hover	Condition 3 t2	2	"Meer rotatie meer sense of the parts versus vorige. heel vinden op eerste vlucht
Hover	Condition 4 t4	2	meer surge, beïnvloedt mijn strategie niet.

Awarded Simulation Fidelity Rating Scales

Task	Conditions #	SFR	Comments
Take-Off and Abort	Condition 1 t3	2	"Hij merkt niet heel veel in longitudinale as." weinig pitch. voel ik niet veel van → surge.
Take-Off and Abort	Condition 2 t1	2	weinig verschil met de vorige set. → gebruikt alleen visueel. om de voorwaarts-acc. snelheid vergelijken.
Take-Off and Abort	Condition 3 t4	6	"weinig pitch voelbaar" i.v.m. echte vlucht. pitch = surge. "attitude is herkenbaar"
Take-Off and Abort	Condition 4 t2	2	het voelde beter "hangen in banden"

Final Questionnaire

Indicate the realism of the experienced visual cues.

Landscape	◯ very realistic ◯ realistic ☒ rather realistic ◯ not very realistic ◯ not realistic ◯ not realistic at all	Comments
MTE Attributes	◯ very realistic ☒ realistic ◯ rather realistic ◯ not very realistic ◯ not realistic ◯ not realistic at all	Comments
Airport Attribute	◯ very realistic ☒ realistic ◯ rather realistic ◯ not very realistic ◯ not realistic ◯ not realistic at all	Comments
Cockpit Instruments	☒ very realistic ◯ realistic ◯ rather realistic ◯ not very realistic ◯ not realistic ◯ not realistic at all	Comments

Indicate the realism of the helicopter model.

Collective response	○ very realistic ○ realistic ☒ rather realistic ○ not very realistic ○ not realistic ○ not realistic at all	Comments
Cyclic Pitch Response	○ very realistic ○ realistic ○ rather realistic ○ not very realistic ☒ not realistic ○ not realistic at all	Comments Zeer grote/grove uit-slagen nodig voor effect.
Hover	○ very realistic ○ realistic ○ rather realistic ☒ not very realistic ○ not realistic ○ not realistic at all	Comments Zie cyclic. kom snel in pilot induced oscillation.
Forward flight	○ very realistic ☒ realistic ○ rather realistic ○ not very realistic ○ not realistic ○ not realistic at all	Comments
Trim	○ very realistic ☒ realistic ○ rather realistic ○ not very realistic ○ not realistic ○ not realistic at all	Comments

Please answer the following questions.

What is your experience flying helicopters?
TH67, OH58, CH47D/F
Do you have any experience with simulator training?
Yes
What motions did you find exaggerated?
None
What motions did you find emphasized too little?
pitch during acceleration
Describe the difference between different motion conditions as you perceived it.
Very hard to perceive changes, trained to ignore the motions
Were the tasks at hand sufficient to judge the motion cueing system?
Yes, although still hard. See last point.
If you were allowed to make one change in the motion cuing setting (description in words is sufficient), what would it be?
Pitch, I would emphasize this more
What would be the optimal way to test the motion cueing settings according to your opinion?
I reckon just forward flight (120 kts) with large bank angles would make judgement easier

Lynx3DOFSim SIMONA Experiment

Pilot Questionnaires

Set #2

Subject Name: ....

Subject number: 2

Wouter Dalmeijer

September 2016

Awarded Simulation Fidelity Rating Scales

Task	Conditions #	SFR	Comments
Practice	Practice	0	Adaptatie van verwachtingen → ik moet er wel wat voor doen →
Hover	Condition 1	~~1~~	- nose-up tilt goed voelbaar "pitch rotatie" - heave motion responsief. -
Hover	Condition 2	2	→ turbulentie leek "soep." → verticale beweging wel gedempt. → pitch niet zo goed gevoeld
Hover	Condition 3	1	→ pitch erg goed → heave minder dan conditie 1
Hover	Condition 4	1	→ "goede combinatie tussen ~~[illegible]~~ cond 1 en ~~[illegible]~~ cond. 3

"[illegible]"

"worst"

"intermediate"

"best"

Awarded Simulation Fidelity Rating Scales

Task	Conditions #	SFR	Comments
Take-Off and Abort	Condition 1	4/5	→ "meer handvatten weinig dan normaal." → ~~tog~~ zie nu - stable.
Take-Off and Abort	Condition 2	3	→ pitch initieel beter 20° nose-down uit of voelscan → longitudinaal versnelling beter.
Take-Off and Abort	Condition 3	2	→ hoort dichtersbij werkelijkheid → verticaal vlak geen "progressive sim" → pitch beter → acceleratie beter & daarna ①
Take-Off and Abort	Condition 4	2	→ initiële pitch voelscan / stabiele pitch with voelscan. speerpunt accel/decel.

1 & 4 vergelijkbaar op het verticale vlak.

3 - gaat ~~waar~~ voor beste resultaten.

Final Questionnaire

Indicate the realism of the experienced visual cues.

Landscape	○ very realistic ⊗ realistic ○ rather realistic ○ not very realistic ○ not realistic ○ not realistic at all	Comments
MTE Attributes	○ very realistic ⊗ realistic ○ rather realistic ○ not very realistic ○ not realistic ○ not realistic at all	Comments
Airport Attribute	○ very realistic ⊗ realistic ○ rather realistic ○ not very realistic ○ not realistic ○ not realistic at all	Comments
Cockpit Instruments	⊗ very realistic ○ realistic ○ rather realistic ○ not very realistic ○ not realistic ○ not realistic at all	Comments

Indicate the realism of the helicopter model.

Collective response	◯ very realistic ⊗ realistic ◯ rather realistic ◯ not very realistic ◯ not realistic ◯ not realistic at all	Comments
Cyclic Pitch Response	◯ very realistic ◯ realistic ⊗ rather realistic ◯ not very realistic ◯ not realistic ◯ not realistic at all	Comments CYCLIC HEEFT MEER TRAVEL NODIG DAN ACTUAL. (GROTERE INPUTS BENODIGD)
Hover	◯ very realistic ◯ realistic ⊗ rather realistic ◯ not very realistic ◯ not realistic ◯ not realistic at all	Comments ZIE HIERBOVEN
Forward flight	◯ very realistic ◯ realistic ⊗ rather realistic ◯ not very realistic ◯ not realistic ◯ not realistic at all	Comments MIS ACCELERATIE GEVOEL, MAAR GOED GENOEG BRUIKBAAR
Trim	◯ very realistic ⊗ realistic ◯ rather realistic ◯ not very realistic ◯ not realistic ◯ not realistic at all	Comments

Please answer the following questions.

What is your experience flying helicopters?
7 YEARS / 1000 HRS CHINOOK
Do you have any experience with simulator training?
YES 250 HRS
What motions did you find exaggerated?
NONE
What motions did you find emphasized too little?
ACCELERATON
Describe the difference between different motion conditions as you perceived it.
1/ HVR: LONGITUDINAL GOOD FWD: NOT CLOSE TO REALITY 2/ HVR: NOT CLOSE TO REALITY FWD: " " " " 3/ HOVER: PITCH GOOD FWD: BEST EQUAL OF REALITY 4/ HVR: GOOD COMBINATION BTW PITCH & LONGT. FWD: MISSES ACCEL, GOOD PITCH
Were the tasks at hand sufficient to judge the motion cueing system?
YES
If you were allowed to make one change in the motion cuing setting (description in words is sufficient), what would it be?
MAKE INPUTS MORE PROGRESIVE/AGRESSIVE.
What would be the optimal way to test the motion cueing settings according to your opinion?
START IN HVR CONDITION WITH HIGHER SPEED.

Lynx3DOFSim SIMONA Experiment

Pilot Questionnaires

Set #3

Subject Name: ....

Subject number: 5.

Wouter Dalmeijer

September 2016

Awarded Simulation Fidelity Rating Scales

Task	Conditions #	SFR	Comments
Practice	Practice		
Hover	Condition 1	6 ~~5~~	~~staart uitslagen. (groter~~ "vertraging" ~~dan gewend)~~ daardoor ga je overcompenseren → pitch/swing
Hover	Condition 2	2	→ directly voor a echte (swing set, subject indicated confused movement)
Hover	Condition 3	1	→ directer dan Cougar/Alouette → soms vertraging (nu niet) positie, (vóór/naar achteren)
Hover	Condition 4	1	nóg beter dan vorige. "gevoel" "nog directer."

subject had het gevoel dat de beste performance was bij condition 3

Awarded Simulation Fidelity Rating Scales

Task	Conditions #	SFR	Comments
Take-Off and Abort	Condition 1	2	in de → pitch wat oriënteren →
Take-Off and Abort	Condition 2	1	→ oriënteren door vorige → stuur inputs wel preciezer.
Take-Off and Abort	Condition 3	5	Stuuruitslagen, daardoor 5 weinig verschil in motion. → iets trager.
Take-Off and Abort	Condition 4	6	→ forse pitch bewegingen.

Final Questionnaire

Indicate the realism of the experienced visual cues.

Landscape	◯ very realistic ☑ realistic ◯ rather realistic ◯ not very realistic ◯ not realistic ◯ not realistic at all	Comments
MTE Attributes	☑ very realistic ◯ realistic ◯ rather realistic ◯ not very realistic ◯ not realistic ◯ not realistic at all	Comments very helpfull
Airport Attribute	◯ very realistic ☑ realistic ◯ rather realistic ◯ not very realistic ◯ not realistic ◯ not realistic at all	Comments
Cockpit Instruments	◯ very realistic ◯ realistic ☑ rather realistic ◯ not very realistic ◯ not realistic ◯ not realistic at all	Comments

Indicate the realism of the helicopter model.

Collective response	○ very realistic ○ realistic ☒ rather realistic ○ not very realistic ○ not realistic ○ not realistic at all	Comments soms grote uitslagen nodig
Cyclic Pitch Response	○ very realistic ☒ realistic ○ rather realistic ○ not very realistic ○ not realistic ○ not realistic at all	Comments
Hover	○ very realistic ☒ realistic ○ rather realistic ○ not very realistic ○ not realistic ○ not realistic at all	Comments
Forward flight	○ very realistic ☒ realistic ○ rather realistic ○ not very realistic ○ not realistic ○ not realistic at all	Comments
Trim	○ very realistic ☒ realistic ○ rather realistic ○ not very realistic ○ not realistic ○ not realistic at all	Comments erg bruikbaar

Please answer the following questions.

What is your experience flying helicopters?
over 4000 hrs
Do you have any experience with simulator training?
yes super puma and cougar
What motions did you find exaggerated?
none
What motions did you find emphasized too little?
some setting
Describe the difference between different motion conditions as you perceived it.
some too sloppy
Were the tasks at hand sufficient to judge the motion cueing system?
yes
If you were allowed to make one change in the motion cuing setting (description in words is sufficient), what would it be?
more direct
What would be the optimal way to test the motion cueing settings according to your opinion?
fly the different tasks several times as we did.

Bibliography

[1] L. D. Allen, "Evolution of Flight Simulation," in *Proceedings of the Modeling and Simulation Technologies Conference*, (Monterey, CA), AIAA, 1993.

[2] D. J. Allerton, "The Impact of Flight Simulation in Aerospace," *Aeronautical Journal*, vol. 114, no. 1162, pp. 747–756, 2010.

[3] R. J. A. W. Hosman, S. K. Advani, and J. Takats, "Status of the ICAO Objective Motion Cueing Test," in *Flight Simulation Research, New Frontiers, Conference Proceedings*, (London, UK), Royal Aeronautical Society, 2012.

[4] Anon, "Attachment F. Frequency-domain Motion Cueing System Performance Test," in *Doc 9625, Manual of Criteria for the Qualification of Flight Simulators*, vol. I - Aeropl, ICAO, third ed., 2009.

[5] S. K. Advani and R. J. A. W. Hosman, "Revising Civil Simulator Standards - An Opportunity for Technological Pull," in *Proceedings of the Modeling and Simulation Technologies Conference*, (Keystone, CO), AIAA, 2006.

[6] J. B. Sinacori, "The Determination of Some Requirements for a Helicopter Flight Research Simulation Facility," tech. rep., NASA Ames Research Center, Moffet Field, CA, 1977.

[7] S. K. Advani, R. J. A. W. Hosman, and M. Potter, "Objective Motion Fidelity Qualification in Flight Training Simulators," in *Proceedings of the Modeling and Simulation Technologies Conference*, (Hilton Head, SC), pp. 1–13, AIAA, 2007.

[8] R. J. A. W. Hosman and S. K. Advani, "Are Criteria for Motion Cueing and Time Delays Possible ? Part 2 . Manual of Criteria for the Qualification and Testing of Flight Simulation Training," in *Proceedings of the Modeling and Simulation Technologies Conference*, (Boston, MA), AIAA, 2013.

[9] O. Stroosma, "Applying the Objective Motion Cueing Test to a Classical Washout Algorithm," in *Proceedings of the Modeling and Simulation Technologies Conference*, (Boston, MA), AIAA, 2013.

[10] C. Seehof, U. Durak, and H. Duda, "Objective Motion Cueing Test - Experiences of a New User," in *Proceedings of the Modeling and Simulation Technologies Conference*, (Atlanta, GA), AIAA, 2014.

[11] W. H. Dalmeijer, "Motion Fidelity Assessment for Helicopter Simulations - Preliminary Simulations," tech. rep., Delft University of Technology, Delft, 2016.

[12] G. D. Padfield, *Helicopter Flight Dynamics : The Theory and Application of Flying Qualities and Simulation Modeling.* Washington, DC: John Wiley & Sons., 2007.

[13] Anon, *ADS-33E-PRF, Aeronautical Design Standard Performance Specification Handling Qualities Requirements for Military Rotorcraft.* Redstone Arsenal, Alabama: United States Army, 2000.

[14] S. K. Advani, *Kinematic Design of Flight Simulator Motion-Bases.* PhD thesis, Delft University of Technology, Delft, 1998.

[15] R. E. Jones, R. T. Hennessy, and S. Deutsch, *Human Factors Aspects of Simulation.* Washington, D. C.: National Academy Press, 1985.

[16] M. E. Mccauley, "Do Army Helicopter Training Simulators Need Motion Bases?," Tech. Rep. February, U.S. Army Research Institute for the Behavioral and Social Sciences, Arlington, VA, 2006.

[17] M. Mulder, P. M. T. Zaal, D. M. Pool, H. J. Damveld, and M. M. van Paassen, "A Cybernetic Approach to Assess Simulator Fidelity: Looking back and looking forward," in *Proceedings of the Modeling and Simulation Technologies Conference*, (Boston, MA), AIAA, 2013.

[18] D. M. Pool, *Objective Evaluation of Flight Simulator Motion Cueing Fidelity Through a Cybernetic Approach.* Phd thesis, Delft University of Technology, Delft, 2012.

[19] J. Burki-Cohen, N. N. Soja, and T. Longridge, "Simulator Platform Motion-The Need Revisited," *The International Journal of Aviation Psychology*, vol. 8, no. 3, pp. 197–208, 1998.

[20] J. Burki-Cohen, J. Burki-Cohen, T. Go, T. Go, W. Chung, and W. Chung, "Simulator fidelity requirements for airline pilot training and evaluation continued: An update on motion requirements research," *Proceedings of the 12th ...*, no. April, pp. 1–8, 2003.

[21] D. M. Pool, G. A. Harder, and M. M. van Paassen, "Effects of Simulator Motion Feedback on Training of Skill-Based Control Behavior," *Journal of Guidence, Control and Dynamics*, 2016.

[22] D. J. Allerton, *Principles of Flight Simulation.* No. 1, Chichester, UK: John Wiley & Sons, 2014.

[23] L. D. Reid and M. A. Nahon, "Flight Simulation Motion-base Drive Algorithimns: Part 1-Developing and Testing the Equations," Tech. Rep. 296, UTIAS, Toronto, 1985.

[24] Anon, *Certification Specifications for Helicopter Flight Simulation FSTD (H).* EASA, 2012.

[25] J. A. Schroeder, “Flight Simulation Motion Platform Requirements,” Tech. Rep. July, NASA Ames Research Center, Moffet Field, CA, 1999.

[26] B. Gouverneur, J. A. Mulder, M. M. van Paassen, O. Stroosma, and M. Field, “Optimisation of the Simona Research Simulators Motion Filter Setting for Handling Qualities Experiments,” in *Proceedings of the Modeling and Simulation Technologies Conference*, (Austin, TX), AIAA, 2003.

[27] Anon, *Aeroplane Flight Simulator Evaluation Handbook*. London: Royal Aeronautical Society, third ed., 2009.

[28] J. A. Schroeder, “Evaluation of Simulation Motion Fidelity Criteria in the Vertical and Di- rectional Axes,” *Journal of American Helicopter Society*, vol. 41, no. 2, pp. 44–57, 1996.

[29] T. Hagiwara, S. K. Advani, K. Funabiki, K. Wakairo, K. Muraoka, T. Nojima, and A. Notations, “Evaluating an objective method for motion cueing fidelity,” in *Proceedings of the Modeling and Simulation Technologies Conference*, (Honolulu, HA), AIAA, 2008.

[30] S. Manso, M. D. White, and S. J. Hodge, “An Investigation of Task Specific Motion Cues for Rotorcraft Simulators,” in *Proceedings of the Modeling and Simulation Technologies Conference*, (San Diego, CA), AIAA, 2016.

[31] G. E. Cooper and R. P. J. Harper, “The Use of Pilot Rating in the Evaluation of Aircraft Handling Qualities,” tech. rep., NASA Ames Research Center, Moffet Field, CA, 1969.

[32] S. J. Hodge, P. Perfect, G. D. Padfield, and M. D. White, “Optimising the Vestibular Cues Available from a Short Stroke Hexapod Motion Platform,” in *Proceedings of the 67th American Helicopter Society International Annual Forum*, (Virginia Beach, VA), 2011.

[33] M. D. White, P. Perfect, G. D. Padfield, A. W. Gubbels, and A. Berryman, “Acceptance Testing of a Rotorcraft Flight Simulator for Research and Teaching : the Importance of Unified Metrics,” in *Proceedings of the 35th European Rotorcraft Forum*, (Hamburg, Germany), 2009.

[34] P. Perfect, M. D. White, G. D. Padfield, R. Erdos, and A. W. Gubbels, “A Rating Scale for the Subjective Assessment of Simulation Fidelity,” *The Aeronautical Journal*, vol. 118, no. 1206, pp. 953–974, 2014.

[35] G. D. Padfield, M. T. Charlton, J. P. Jones, and R. Bradley, “Where Does the Workload go When Pilots Attack Manoeuvres?,” in *Proceedings of the 20th European Rotorcraft Forum*, (Amsterdam, the Netherlands), 1994.

[36] P. Perfect, M. D. White, G. D. Padfield, and A. W. Gubbels, “Rotorcraft Simulation Fidelity: New Methods for Quantification and Assessment,” *Aeronautical Journal*, vol. 117, no. 1189, pp. 235–282, 2013.

[37] C. M. Wiskemann, F. M. Drop, D. M. Pool, M. M. van Paassen, M. Mulder, and H. H. Bülthoff, “Subjective and Objective Metrics for the Evaluation of Motion Cueing Fidelity for a Roll-Lateral Reposition Maneuver,” in *Proceedings of the 70th American Helicopter Society International Annual Forum*, (Montréal, Québec, Canada), pp. 1706–1720, 2014.

[38] D. T. McRuer, “Mathematical Models of Human Pilot Behavior,” Tech. Rep. January, Advisory Group for Aerospace Research and Development, Paris, France, 1974.

[39] R. Hess and T. Malsbury, “Closed-loop Assessment of Flight Simulator Fidelity,” *Journal of Guidence, Control and Dynamics*, vol. 14, no. Jan-Feb, pp. 191–197, 1991.

[40] G. D. Padfield and M. D. White, “Measuring Simulation Fidelity Through an Adaptive Pilot Model,” *Aerospace Science and Technology Journal*, no. 9, pp. 400–408, 2005.

[41] B. Hampson, “The Use of Full Flight Simulators and Synthetic Training Devices in the Fields of Helicopter Training, Testing and Checking,” in *Proceedings of the Modeling and Simulation Technologies Conference*, (Denver, CO), AIAA, 2000.

[42] Anon, *Acceptable Means of Compliance (AMC) and Guidance Material (GM) to part -ORO*. EASA, 2014.

[43] Anon, *Advisory Circular 120-63 - Helicopter Simulator Qualification*. FAA, 1994.

[44] Anon, *Advisory Circular 120-40 - Airplane Simulator Qualification*. FAA, 1991.

[45] T. van Holten and J. Melkert, “Helicopter Performance, Stability, and Control,” tech. rep., Delft Universitty of Technology, Delft, 2002.

[46] P. Deuflhard, *Newton Methods for Nonlinear Problems, Affine Invariance and Adaptive Algorithms*. Berlin: Springer, 2004.

[47] F. M. Hoblit, *Gust Loads on Aircraft: Concepts and Applications*. Washington, DC: AIAA, 1988.

[48] J. A. Lusardi, C. L. Blanken, and M. B. Tischler, “Piloted Evaluation of a UH-60 Mixer Equivalent Turbulence Simulation Model,” in *Proceedings of the 53th American Helicopter Society International Annual Forum*, (Phoenix, AZ), pp. 309–320, 2003.

[49] Anon, *Military Specification MIL-F-8785C, Flying Qualities of Piloted Airplanes*. Washington, D. C.: United States Army, 1980.

[50] S. J. Hodge and M. D. White, “Challenges in Roll-Sway Motion Cueing Fidelity : A View from Academia,” in *Royal Aeronautical Society Flight Simulation Group Conference on ”Challenges in Flight Simulation”*, (London, UK), 2015.

[51] Anon, *MTi User Manual*. Enschede, the Netherlands: xsens, 2016.